

Exploring functional heteromeric interactions of the human P2X4 receptor

Anna Fortuny i Gómez



A thesis submitted for the degree of Doctor of Philosophy
University of East Anglia
School of Biological Sciences

May 2023

© This copy of this thesis has been supplied on condition that anyone who consults it is understood to recognise that its copyright rests with the author and that use of any information derived therefrom must be in accordance with current UK Copyright Law.

In addition, any quotation or extract must include full attribution.

Declaration

I verify that the work presented in this thesis is my own original work and has not been previously submitted for a degree at this or any other university. Where work by other authors has been included, their work has been fully cited and referenced.

In line with the regulations for submission for a degree of Doctor of Philosophy at the University of East Anglia, this thesis has a word count of approximately 75,100 words, which includes the references list but excludes the appendices, which consist of approximately 620 words.

Abstract

P2X receptors are non-selective ATP-gated ion channels. ATP can act as a neurotransmitter and activate P2X receptors, allowing the passage of small cations into the cell, causing membrane depolarisation and ultimately increasing intracellular calcium levels. Functional P2X receptors are trimeric, formed by the association of three subunits around a common pore. Seven pore-forming subunits have been cloned and characterised in mammals, named P2X1-P2X7. Amongst them, the P2X4 receptor subtype is involved in numerous biological responses, contributing to ATP-mediated neurotransmission, neuroinflammation, and other inflammatory responses. P2X4 receptors can also modulate normal function and disease development in various organs, namely the heart, lungs, kidneys, and liver. Hence, P2X4 receptors have remarkable therapeutic potential for the treatment of neuropathic pain and cardiovascular disease, for example. Over the past fifteen years, there has been a growing interest in identifying possible heteromeric P2X subunit arrangements, combining different P2X subunits to constitute a functional channel pore. While the existence of heteromeric P2X2/3 receptors is well established, the composition of other P2X heteromers and the interaction between distinct trimeric receptors remains controversial.

This project aims to gain biochemical and functional evidence of human P2X4 subunit interactions. To do so, we developed a novel experimental strategy that combined functional calcium mobilisation assays to assess the effects of human P2X ‘dead receptor’ tools (i.e., double lysine-to-alanine mutants that generate a non-functional human P2X subunit) on the human P2X4 receptor activity, and Western blotting and co-immunoprecipitation assays to verify physical protein-protein interactions.

Our data revealed that human P2X1, P2X5, and P2X6 dead receptor tools exert a dominant negative effect on the human P2X4 receptor ATP-evoked calcium responses, compromising the ATP binding pocket and indicating that functional subunit interactions occurred. Analysis of protein expression and co-immunoprecipitation assays also suggested the formation of functional interactions between human P2X4 subunits and P2X1, P2X5, and P2X6 subunits. These data revealed that functional human P2X1/4, P2X4/5, and P2X4/6 heteromeric receptors can exist in this heterologous system. Human P2X2 dead receptor tools did not affect the human P2X4 ATP-evoked calcium responses, yet protein data showed a positive interaction between P2X2 and P2X4 subunits. These results supported interaction between homomeric P2X2 and P2X4 receptors rather than between subunits. Human P2X3 dead receptor tools did not affect the human P2X4 receptor ATP-evoked calcium responses and did not co-immunoprecipitate with P2X4 subunits, indicating that no functional heteromeric interactions occurred and that a heteromeric P2X3/4 receptor is unlikely. Human P2X4 receptor ATP-evoked calcium responses were affected when co-expressed with human P2X7 dead receptor tools due to a reduction in P2X4 receptor cell surface expression. Furthermore, human P2X4 and P2X7 subunits did not co-immunoprecipitate. These results indicate that a functional human P2X4/7 heteromer is unlikely, although their expression patterns seem to be intertwined.

This thesis has contributed to the understanding of novel functional interactions of the human P2X4 receptor and critically interpreted previous and current P2X4 heteromerisation studies. However, further research is required to decipher whether human P2X4 subunits form functional interactions between subunits and/or trimeric receptors. Unravelling the multimeric organisation of human P2X4 receptors will deepen our understanding of ATP signalling in health and disease and open new routes for the development of more selective therapeutics.

Access Condition and Agreement

Each deposit in UEA Digital Repository is protected by copyright and other intellectual property rights, and duplication or sale of all or part of any of the Data Collections is not permitted, except that material may be duplicated by you for your research use or for educational purposes in electronic or print form. You must obtain permission from the copyright holder, usually the author, for any other use. Exceptions only apply where a deposit may be explicitly provided under a stated licence, such as a Creative Commons licence or Open Government licence.

Electronic or print copies may not be offered, whether for sale or otherwise to anyone, unless explicitly stated under a Creative Commons or Open Government license. Unauthorised reproduction, editing or reformatting for resale purposes is explicitly prohibited (except where approved by the copyright holder themselves) and UEA reserves the right to take immediate 'take down' action on behalf of the copyright and/or rights holder if this Access condition of the UEA Digital Repository is breached. Any material in this database has been supplied on the understanding that it is copyright material and that no quotation from the material may be published without proper acknowledgement.

Table of contents

<i>Declaration</i>	2
<i>Abstract</i>	3
<i>List of Figures</i>	7
<i>List of Tables</i>	11
<i>Abbreviations</i>	12
<i>Acknowledgements</i>	15
<i>Chapter 1. Introduction</i>	17
1.1 Ion channels.....	18
1.1.1 Mechanically-gated ion channels.....	19
1.1.2 Voltage-gated ion channels	19
1.1.3 Ligand-gated ion channels	20
1.2 Purinergic signalling: ATP as a neurotransmitter.....	21
1.2.1 P1 receptors	22
1.2.2 P2 receptors	22
1.3 P2X4 receptors.....	27
1.3.1 P2X4 receptor structure and ATP binding site	27
1.3.2 P2X4 receptor activation and gating mechanism.....	32
1.3.3 P2X4 receptor pharmacology	38
1.3.4 Physiological roles of the P2X4 receptor	40
1.4 Aim and objectives	46
<i>Chapter 2. Materials and methods</i>	48
2.1 Materials and reagents.....	49
2.2 Cell culture.....	50
2.2.1 Human 1321N1 astrocytoma cells	50
2.3 DNA constructs	51
2.3.1 Generation of P2X double mutant receptors	54
2.4 High-efficiency transformation of plasmid	56
2.4.1 Generation of <i>Escherichia coli</i> competent cells	56
2.4.2 LB broth and agar preparation	57
2.5 Preparation of glycerol stocks, DNA extraction, and sequencing.....	57
2.6 Transient transfection of parental 1321N1 astrocytoma cells	58
2.6.1 TurboFect.....	59

2.6.2	X-tremeGENE.....	59
2.6.3	Lipofectamine 2000	59
2.7	Transient co-transfection of 1321N1 parental astrocytoma cells	60
2.7.1	Scaled-up transient co-transfection of 1321N1 parental astrocytoma cells	61
2.8	Calcium mobilisation assay	62
2.8.1	Calcium mobilisation buffers	62
2.8.2	Intracellular calcium measurements.....	63
2.9	Western blotting	63
2.9.1	Protein extraction and sample preparation.....	64
2.9.2	SDS polyacrylamide gel electrophoresis and membrane transference	64
2.9.3	Membrane blocking, protein detection, and visualisation	64
2.10	Biotinylation assay.....	65
2.11	Co-immunoprecipitation assay	65
2.12	Immunocytochemistry.....	66
2.13	Data and statistical analysis	68
2.13.1	Calcium mobilisation assay data analysis	68
2.13.2	Western blot image data analysis.....	69
3	<i>The hypothesis of the dead receptor and validation of the experimental system</i>	71
3.1	Introduction	72
3.1.1	Aim and objectives.....	77
3.2	Results	78
3.2.1	Transient transfection and expression of the human P2X4 receptor in a heterologous system	78
3.2.2	Pharmacological characterisation of the human P2X4 receptor in a heterologous system	91
3.2.3	The hypothesis of the dead receptor and validation of the experimental system	111
3.3	Discussion	143
3.3.1	Successful transient transfection of 1321N1 parental astrocytoma cells with the human P2X4 receptor	143
3.3.2	Heterologously expressed human P2X4 receptor accurately reflected its specific pharmacological properties	145
3.3.3	The use of dead receptor tools as a reliable experimental system to evidence functional homo- and hetero-oligomeric human P2X subunit interactions.....	150
4	<i>Exploring functional heteromeric interactions of the human P2X4 receptor</i>	159
4.1	Introduction	160
4.1.1	Aim and objectives.....	167
4.2	Results	168
4.2.1	Probing functional interactions of the human P2X4 receptor for ATP	168

4.2.2 Potential impacts of co-expressing human P2X4 wild-type subunits with other P2X wild-type subunits on its pharmacological properties	204
4.3 Discussion	212
4.3.1 Human P2X4 subunits functionally interacted with human P2X1 subunits	214
4.3.2 Human P2X2 subunits formed interaction complexes with human P2X4 subunits but did not alter their receptor function	216
4.3.3 Human P2X4 subunits did not functionally interact with human P2X3 subunits	218
4.3.4 Human P2X4 subunits functionally interacted with human P2X5 subunits containing exon 10	219
4.3.5 Human P2X4 subunits functionally interacted with human P2X6 subunits.....	220
4.3.6 Human P2X7 subunits did not form interaction complexes with human P2X4 subunits but altered their receptor function	222
5 General discussion.....	225
5.1 Key findings and concluding remarks	226
5.2 Future directions	229
References.....	232
Appendix 1	253
Appendix 2	260

List of Figures

Chapter 1

Fig 1.1	ATP-permeable ion channels and transporters.	24
Fig 1.2	General structure of nucleosides, nucleotides, and nucleobases.	25
Fig 1.3	Schematic representation of P1, P2X, and P2Y receptors, and their intracellular signalling pathways.	26
Fig 1.4	Crystal structure of the truncated zebrafish P2X4 receptor in an ATP-bound state.	29
Fig 1.5	The P2X4 receptor ATP-binding pocket and key residues involved in ligand recognition.	31
Fig 1.6	Schematic representation of the P2X receptor gating cycle.	34
Fig 1.7	Cell surface and subcellular trafficking of P2X4 receptors.	37
Fig 1.8	Pleiotropic effects of P2X4 receptor-mediated signalling.	41

Chapter 2

Fig 2.1	Map of a pcDNA 3.1 (+) vector encoding the human P2X4 gene with a C-terminus HA epitope.	52
----------------	--	----

Chapter 3

Fig 3.1	Visual representation of the dead receptor hypothesis.	75
Fig 3.2	Clustal-Omega Multiple Sequence Alignment of rat P2X2 and human P2X1-7 receptors.	76
Fig 3.3	Human 1321N1 parental astrocytoma cells are poor transfection hosts.	80
Fig 3.4	The effect of passage on the magnitude of 30 μ M ATP-evoked calcium response in human P2X4 stable and transiently transfected 1321N1 astrocytoma cells.	81
Fig 3.5	TurboFect was not a suitable reagent for transient transfection of human P2X4 WT in 1321N1 parental astrocytoma cells.	82
Fig 3.6	X-tremeGENE reagent had low success rates for transient transfection of human P2X4 WT in 1321N1 parental astrocytoma cells.	83
Fig 3.7	Changes in initial cell density and transfection complex incubation times did not improve the transfection efficiency and success rates of X-tremeGENE.	84
Fig 3.8	Successful transient transfection of human P2X4 WT in 1321N1 parental astrocytoma cells using Lipofectamine 2000 reagent.	86
Fig 3.9	Optimisation of human P2X4 WT transient transfection protocol in 1321N1 parental astrocytoma cells using Lipofectamine 2000 reagent.	87
Fig 3.10	Whole-cell and cell surface expression levels of human P2X4 WT FLAG-tagged subunits in transiently transfected 1321N1 parental astrocytoma cells.	88

Fig 3.11	ATP mediated a Ca^{2+} response in human P2X4 1321N1 stable astrocytoma cells in a concentration-dependent manner.	92
Fig 3.12	ATP did not cause an endogenous Ca^{2+} response in 1321N1 parental astrocytoma cells.	93
Fig 3.13	Pharmacological characterisation of the human P2X4 receptor in 1321N1 stable astrocytoma cells.	96-97
Fig 3.14	Application of ATP- γ -S and AP4A did not induce Ca^{2+} responses in 1321N1 astrocytoma cells stably expressing human P2X4 receptors.	98
Fig 3.15	Broad-spectrum P2X receptor antagonists inhibited the Ca^{2+} response to ATP in 1321N1 astrocytoma cells stably expressing human P2X4 receptors.	100
Fig 3.16	Broad-spectrum P2X receptor antagonist Suramin did not affect the ATP-mediated Ca^{2+} response in 1321N1 cells stably expressing human P2X4 receptors.	101
Fig 3.17	Inhibitory effects on ATP-induced Ca^{2+} responses after treatment with TNP-ATP and PPADS in 1321N1 astrocytoma cells stably expressing human P2X4 receptors.	102
Fig 3.18	30-minute incubation with the organic solvent DMSO did not affect human P2X4 receptor sensitivity to ATP in stable 1321N1 astrocytoma cells.	105
Fig 3.19	Selective antagonism of the human P2X4 receptor inhibited the Ca^{2+} response to ATP in 1321N1 stable astrocytoma cells.	106-107
Fig 3.20	Inhibitory effects on ATP-evoked Ca^{2+} responses after treatment with various selective human P2X4 receptor antagonists in 1321N1 stable astrocytoma cells.	108-109
Fig 3.21	Whole-cell and cell surface expression levels of human P2X4 [K67A, K313A] transiently transfected in human P2X4 WT stable 1321N1 astrocytoma cells.	113
Fig 3.22	Mutations of conserved ectodomain lysine residues caused a minor loss of function at human P2X4 receptors.	114
Fig 3.23	Determination of the maximal amount of plasmid DNA for successful transient co-transfection of 1321N1 parental astrocytoma cells using Lipofectamine 2000.	116
Fig 3.24	Mutations of conserved ectodomain lysine residues caused a significant loss of function at human P2X4 receptors.	117
Fig 3.25	Determination of antibody specificity and protein titration in 1321N1 astrocytoma cells stably expressing human P2X4 WT receptors.	120
Fig 3.26	Lack of specificity for Ms α -P2X4 C-terminus (C-term) and Ms α -P2X4 extracellular (EC) antibodies in 1321N1 astrocytoma cells transiently transfected with human P2X4 WT EE-tagged receptors.	121
Fig 3.27	Determination of antibody specificity and protein titration in 1321N1 astrocytoma cells transiently expressing human P2X4 WT HA-tagged receptors.	122
Fig 3.28	ATP evoked Ca^{2+} responses via human P2X4 WT receptors transiently transfected in 1321N1 parental astrocytoma cells in a concentration-dependent manner.	123
Fig 3.29	Common HRP-conjugated secondary antibodies detecting heavy and light antibody chains were not a good choice for co-immunoprecipitation studies in transiently co-transfected 1321N1 parental astrocytoma cells.	126
Fig 3.30	Determination of which secondary antibodies to use for co-immunoprecipitation studies in transiently co-transfected 1321N1 parental astrocytoma cells.	128

Fig 3.31	Homomeric interaction of human P2X4 WT subunits in transiently co-transfected 1321N1 parental astrocytoma cells.	131
Fig 3.32	Whole-cell and cell surface expression levels of human P2X4 WT and human P2X4 [K67A, K313A] subunits in transiently co-transfected 1321N1 parental astrocytoma cells.	134
Fig 3.33	The human P2X4 [K67A, K313A] dead subunit had a dominant negative effect on human P2X4 WT ATP-induced Ca^{2+} responses in transiently co-transfected 1321N1 parental astrocytoma cells.	135
Fig 3.34	Human P2X4 WT subunits interacted with human P2X4 [K67A, K313A] dead subunits in transiently co-transfected 1321N1 parental cells.	136
Fig 3.35	Whole-cell and cell surface expression levels of human P2X3 WT, human P2X2 WT, and human P2X2 [K81A, K319A] subunits in transiently co-transfected 1321N1 parental astrocytoma cells.	139
Fig 3.36	Validation of the dead receptor hypothesis as a good tool to probe for functional human P2X heteromeric interactions.	140
Fig 3.37	Positive interaction between human P2X2 WT and human P2X3 WT subunits in transiently co-transfected 1321N1 parental astrocytoma cells.	142

Chapter 4

Fig 4.1	Whole-cell and cell surface expression levels of human P2X dead subunits in transiently co-transfected 1321N1 parental astrocytoma cells.	169-170
Fig 4.2	The human P2X1 [K68A, K309A] dead subunit had a dominant negative effect on human P2X4 WT ATP-evoked Ca^{2+} responses in transiently co-transfected 1321N1 parental astrocytoma cells.	174
Fig 4.3	Whole-cell and cell surface expression levels of human P2X4 WT and human P2X1 [K68A, K309A] subunits in transiently co-transfected 1321N1 parental astrocytoma cells.	175
Fig 4.4	Human P2X4 WT subunits co-immunoprecipitated with human P2X1 WT subunits when transiently co-transfected in 1321N1 parental astrocytoma cells.	176
Fig 4.5	Human P2X4 WT subunits co-immunoprecipitated with human P2X1 [K68A, K309A] subunits when transiently co-transfected in 1321N1 parental astrocytoma cells.	177
Fig 4.6	The human P2X6 [K78A, K315A] dead subunit had a dominant negative effect on human P2X4 WT ATP-evoked Ca^{2+} responses in transiently co-transfected 1321N1 parental astrocytoma cells.	180
Fig 4.7	Human P2X4 WT subunits co-immunoprecipitated with human P2X6 WT subunits when transiently co-transfected in 1321N1 parental astrocytoma cells.	181
Fig 4.8	The human P2X2 [K81A, K319A] dead subunit did not affect the human P2X4 WT ATP-evoked Ca^{2+} responses in transiently co-transfected 1321N1 parental astrocytoma cells.	185
Fig 4.9	The human P2X3 [K63A, K299A] dead subunit did not affect the human P2X4 WT ATP-evoked Ca^{2+} responses in transiently co-transfected 1321N1 parental astrocytoma cells.	186
Fig 4.10	Effects of human P2X2 [K81A, K319A] and human P2X3 [K63A, K299A] dead subunits on the human P2X4 WT desensitisation phase in transiently co-transfected 1321N1 parental astrocytoma cells.	187

Fig 4.11	Human P2X4 WT subunits co-immunoprecipitated with human P2X2 WT subunits when transiently co-transfected in 1321N1 parental astrocytoma cells.	188
Fig 4.12	Human P2X4 WT subunits did not co-immunoprecipitate with human P2X3 WT subunits when transiently co-transfected in 1321N1 parental astrocytoma cells.	189
Fig 4.13	The human P2X5 [K69A, K314A] dead subunit had a dominant negative effect on human P2X4 WT ATP-evoked Ca^{2+} responses in transiently co-transfected 1321N1 parental astrocytoma cells.	193
Fig 4.14	Whole-cell and cell surface expression levels of human P2X4 WT and human P2X5 [K69A, K314A] subunits in transiently co-transfected 1321N1 parental astrocytoma cells.	194
Fig 4.15	Human P2X4 WT subunits co-immunoprecipitated with human P2X5 WT subunits when transiently co-transfected in 1321N1 parental astrocytoma cells.	195
Fig 4.16	Human P2X4 WT subunits co-immunoprecipitated with human P2X5 [K69A, K314A] subunits when transiently co-transfected in 1321N1 parental astrocytoma cells.	196
Fig 4.17	The human P2X7 [K64A, K311A] dead subunit had a dominant negative effect on human P2X4 WT ATP-evoked Ca^{2+} responses in transiently co-transfected 1321N1 parental astrocytoma cells.	200
Fig 4.18	Whole-cell and cell surface expression levels of human P2X4 WT and human P2X7 [K64A, K311A] subunits in transiently co-transfected 1321N1 parental astrocytoma cells.	201
Fig 4.19	Human P2X4 WT subunits did not co-immunoprecipitate with human P2X7 WT subunits when transiently co-transfected in 1321N1 parental astrocytoma cells.	202
Fig 4.20	Human P2X4 WT subunits did not co-immunoprecipitate with human P2X7 [K64A, K311A] subunits when transiently co-transfected in 1321N1 parental astrocytoma cells.	203
Fig 4.21	Whole-cell expression levels of human P2X1-7 WT subunits in transiently co-transfected 1321N1 parental astrocytoma cells.	207
Fig 4.22	The human P2X4 WT FLAG-tagged subunit had no effect on human P2X4 WT HA-tagged ATP-evoked Ca^{2+} responses in transiently co-transfected 1321N1 parental astrocytoma cells.	208
Fig 4.23	Human P2X1, P2X3 and P2X5 WT subunits had no effect on human P2X4 WT ATP-evoked Ca^{2+} responses in transiently co-transfected 1321N1 parental astrocytoma cells.	209
Fig 4.24	Effects of human P2X2 WT subunit co-transfection on the human P2X4 WT ATP-evoked Ca^{2+} responses in transiently co-transfected 1321N1 parental astrocytoma cells.	210
Fig 4.25	Human P2X6 and P2X7 WT subunits had an inhibitory effect on human P2X4 WT ATP-evoked Ca^{2+} responses in transiently co-transfected 1321N1 parental astrocytoma cells.	211

Chapter 5

Fig 5.1	Structure modelling of a potential human P2X1/4 heteromeric receptor in the apo state.	231
----------------	--	-----

List of Tables

Chapter 2

Table 2.1	List of exogenous nucleotides and ligands.	49
Table 2.2	List of broad-spectrum purinergic receptor antagonists.	49
Table 2.3	List of human P2X4 selective antagonists.	49
Table 2.4	List of gene constructs purchased.	53
Table 2.5	Numbering of human P2X1-7 lysine (K) to alanine (A) substitutions and their respective AAG codon positions (bp). Detailed sequences for each mutagenic primer set and the annealing temperatures used for PCR.	55
Table 2.6	Optimised protocol outline for transient transfection and co-transfection of human 1321N1 parental astrocytoma cells.	61
Table 2.7	List of primary antibodies used for immunocytochemistry and Western blotting.	67
Table 2.8	List of secondary antibodies used for immunocytochemistry and Western blotting.	67

Chapter 3

Table 3.1	Summary of the conditions used to transiently transfet human 1321N1 parental astrocytoma cells using Turbofect and X-tremeGENE reagents.	89
Table 3.2	Summary of the conditions used to transiently transfet human 1321N1 parental astrocytoma cells using the Lipofectamine 2000 reagent.	90
Table 3.3	Summary of agonist-evoked responses via human P2X4 receptors stably expressed in 1321N1 astrocytoma cells.	95
Table 3.4	Effects of broad-spectrum antagonists on the ATP-evoked responses via human P2X4 receptors stably expressed in 1321N1 astrocytoma cells.	110
Table 3.5	Effects of human P2X4 selective antagonists on the ATP-evoked responses in stable 1321N1 astrocytoma cells.	110

Chapter 4

Table 4.1	Current biochemical and functional evidence for P2X receptor heteromerisation.	164
Table 4.2	Summary of the effects of human P2X dead subunits on the human P2X4 WT 30 μ M ATP-evoked calcium responses and co-immunoprecipitation data.	213

Abbreviations

2-MeSATP	2-(methylthio)adenosine 5'-triphosphate
5-BDBD	5-(3-bromophenyl)-1,3-dihydro-2H-benzofuro[3,2-e]-1,4-diazepin-2-one
ADP	Adenosine 5'-diphosphate
ADP	Adenosine 5'-diphosphate
AFM	Atomic Force Microscopy
AKI	Acute kidney injury
AM	Acetoxymethyl
AMP	Adenosine 5'-monophosphate
AP4A	Di-adenosine tetraphosphate
APS	Ammonium persulphate
ASIC	Acid-sensing ion channel
ATP	Adenosine 5'-triphosphate
ATP-γ-S	Adenosine-5'-O-(3-thio-triphosphate)
AUC	Area under the curve
BAY-1797	N-[4-(3-chlorophenoxy)-3-sulfamoylphenyl]-2-phenylacetamide
BDNF	Brain-derived neurotrophic factor
bGH	Bovine growth hormone
BiFC	Bimolecular Fluorescence Complementation
BRET	Bioluminescence Resonance Energy Transfer
BSA	Bovine serum albumin
BzATP	2'(3')-O-(4-benzoylbenzoyl)adenosine 5'-triphosphate
C-term	Carboxy-terminus
Ca ²⁺	Calcium ions
CaCl ₂	Calcium chloride
cAMP	Cyclic adenosine monophosphate
Carbachol	Carbamylcholine
Cav-1	Caveolin-1
CHO	Chinese hamster ovary
CNS	Central Nervous System
CO ₂	Carbon dioxide
CoIP	Co-immunoprecipitation
CTP	Cytidine 5'-triphosphate
CVD	Cardiovascular disease
DAMP	Danger-associated molecular patterns
DAPI	4',6-diamidino-2-phenylindole
DMEM	Dulbecco's Modified Eagle Media
DMSO	Dimethyl sulfoxide
dNTP	Deoxynucleoside triphosphate
DTT	Dithiothreitol
<i>E. coli</i>	<i>Escherichia coli</i>
ELISA	Enzyme-linked immunosorbent assay
ENaC	Epithelial sodium channel
eNOS	Endothelial nitric oxide synthase
FBS	Foetal bovine serum

FRET	Fluorescence Resonance Energy Transfer
Fura-2 AM LB	Fura 2-AM Loading Buffer
GABA	γ -aminobutyric acid receptors
GPCR	G-protein coupled receptor
HCl	Hydrogen chloride
HEPES	4-(2-hydroxyethyl)-1-piperazineethanesulfonic acid
hP2XR	Human P2X receptor
HRP	Horseradish peroxidase
IVM	Ivermectin
K ⁺	Potassium ions
KCC2	Potassium-chloride co-transporter 2
KCl	Potassium chloride
KLD	Kinase, ligase and DpnI enzyme mix
KO	Knockout
LB	Luria Bertani
LGIC	Ligand-gated ion channel
LPS	Bacterial lipopolysaccharides
MCS	Multiple Cloning Site
Mg ²⁺	Magnesium ions
MgCl ₂	Magnesium chloride
N-term	Amino-terminus
Na ⁺	Sodium ions
nAChR	Nicotinic acetylcholine receptor
NaCl	Sodium chloride
NaOH	Sodium hydroxide
NDP	Nucleoside 5'-diphosphate
NF- κ B	Nuclear factor kappa-light-chain-enhancer of activated B cells
NLRP3	NLR family pyrin domain containing 3
NMP	Nucleoside 5'-monophosphate
NO	Nitric oxide
NRK	Normal rat kidney cells
NTP	Nucleoside 5'-triphosphate
O/N	Overnight
ori	Origin of replication
P2XR	P2X receptor
P2YR	P2Y receptor
PAM	Positive allosteric modulator
PAMP	Pathogen-associated molecular pattern
PBS	Phosphate-buffered saline
PCR	Polymerase Chain Reaction
Pen/Strep	Penicillin/streptomycin antibiotic solution
PFA	Paraformaldehyde
PLC- β	Phospholipase C- β
PPADS	Pyridoxalphosphate-6-azophenyl-2',4'-disulfonic acid
PRR	Pattern-recognition receptor
PSB-12054	N-(benzyloxycarbonyl)phenoxazine
PSB-12062	N-(p-methylphenylsulfonyl)phenoxazine

PVDF	Polyvinylidene difluoride
RA	Rheumatoid arthritis
rP2XR	Rat P2X receptor
rpm	Revolutions per minute
RT	Room temperature
SBS	Salt-buffered saline
SDS	Sodium Dodecyl Sulphate
SDS-PAGE	SDS polyacrylamide gel electrophoresis
SNARE	Soluble N-ethylmaleimide-sensitive factor attachment protein receptors
SNP	Single nucleotide polymorphism
SOC	Super optimal broth with catabolite repression outgrowth media
TEMED	Tetramethylethylenediamine
TGN	trans-Golgi network
TM	Transmembrane domain
TNP-ATP	2',3'-O-(2,4,6- trinitrophenyl)-ATP
Tris	Tris(hydroxymethyl)aminomethane
UDP	Uridine 5'-diphosphate
UDP-glucose	Uridine 5'-diphosphate-glucose
UTP	Uridine 5'-triphosphate
WT	Wild-type
zfP2XR	Zebrafish P2X receptor
$\alpha\beta$ -MeATP	α,β -methyleneadenosine 5'-triphosphate
γ -imidoATP	Adenosine-5'-[γ -(propargyl)-imido]triphosphate

Acknowledgements

During my journey as a PhD student, I thought about what I would list in the thesis acknowledgements. So, of course, I would write something upbeat, possibly ending with an ode to coffee, dark chocolate, and Birra Moretti. Instead, I find myself a few days away from the submission deadline, and those who know me can imagine I started welling up as soon as I started typing.

Firstly, I thank my supervisors, Prof Samuel Fountain and Dr Leanne Stokes. Sam, you have supported and inspired me from the start. You have reassured me and pushed me to be the researcher I am today. With Leanne, you have guided me throughout this journey, discussed project ideas and imagined future next steps. Despite the numerous setbacks and difficulties, I always found the help I needed in you. Secondly, I would like to thank the BBSRC Doctoral Training Partnership for funding my research project and the University of East Anglia for offering me many teaching opportunities and letting me be part of three promotional videos. Many thanks to Cambridge Cancer Genomics, who welcomed me for three months during the Covid-19 outbreak. Especially to my CCG supervisors, Dr Nirmesh Patel and Olivia Edwards, who always allowed me to embark on all the projects I wanted to. Also, thanks to my examiners, Dr Mark Young and Prof Ian Clark, for your advice and for agreeing to be some of the people who will ever read my thesis.

More than ever, I want to thank my partners in crime, Dr Jessica Meades and Dr Elliot Honeybun-Arnolda. Jess, you already know everything. We started this journey together, lived together, and travelled together, and now we are closing this chapter together. You have helped and taught me so much during this time. I am incredibly proud of you. You have been, and still are, my rock. Elliot, I want to thank you for being my escape, for always cheering me up, for getting me outside when I did not want to, and for making sure I do not go crazy in general. Thank you for becoming my big brother.

I also want to express my gratitude to my lab colleagues, always full of brilliant ideas and ready for a break to brighten up our days: Sonia Paz López, Michelle Fletcher, Kayleigh Goddard, Dr Estela Pérez Santamarina, Dr María del Carmen González Montelongo, Dr David Richards, Harry Hickey, and Sean Cullum. I extend my appreciation to my fellow work friends: Perry, Chris, Dan, Dagne, Becky, and Kasia. Special thanks to Estela, Sonia, Jess, and Michelle. I feel so lucky to have such amazing, inspiring, and strong women in my life. You are my chosen family abroad, and the best life bubble one could ask for!

Thanks to my little geniuses, Anelia and Estelle, for your limitless and beautiful energy. To my friends who covered me with wonderful food for the last four years: Martina, Gaia, Marina, Chudi, Carlos, and Héctor. And to my hometown friends: Marina, Yumi, Nacho, Ginés, Judit, Lucas, and Laura, for your unconditional friendship despite distance and time. You are always there to laugh, cry, dance, and solve the world at the dinner table.

I am eternally grateful to my family and extended family for your love and support. And from the bottom of my heart to my parents and sister. You always believed in me and also provided motivation, often by asking: when are you going to finish that thesis? I also want to thank all our cats and dogs, especially the ones who passed away during my time as a PhD student, for their (un)conditional love, keeping me company, and cuddling for many hours.

Finally, to my beloved Matt, you have been and remain to be a source of encouragement and patience through thick and thin. I thank you for being my number one supporter, for being the best life and science advisor, for never judging me, and for always making me laugh. Thank you, *rinyo*. You are my home.

*To future students, thanks for reading my thesis.
I hope it helps you find what you are looking for.*

1 Introduction

P2X ligand-gated ion channels and rationale of the project

1.1 Ion channels

Ion channels are macromolecular pores embedded in the cell membrane that allow ion exchange between the intracellular and the extracellular environment. Multiple ion channel types can coexist within the same cell, and each cell can express a different selection of ion channels, creating highly regulated networks and signalling pathways (Hille, 2001; Alberts et al., 2017).

Based on the stimulus they respond to, ion channels are divided into three superfamilies: mechano-sensitive ion channels, voltage-gated ion channels, and ligand-gated ion channels (Alberts et al., 2017). The ion channel response is called ‘gating’ as it opens or closes its pore. An open pore is permeable, a property that allows the rapid passage of small ions across the cell membrane according to their electrochemical gradient, passively diffusing from a higher ion concentration to a lower ion concentration compartment. Some of their functions include: controlling cell volume, shaping electrical signals, regulating secretion processes, and modulating the activity of other channels and other intracellular molecules by allowing the passage of ‘messenger’ calcium ions into the cell (Hille, 2001).

Ions play a central role in electric transmission across the nervous system. Thus, are predominantly expressed on membranes of excitable cells, such as neurons and muscle cells (Alberts et al., 2017). Ionic movement can be explained as an electric current across the cell membrane, affecting the resting membrane potential. Membrane potential is defined by electrical charge differences across a membrane. In resting circumstances, the membrane potential is approximately -60mV as the intracellular space contains fewer positive ions than the extracellular milieu. Passive ionic movement through ion channels makes the largest contribution to the generation of electric potential across the cell membrane (Alberts et al., 2017).

The fundamental task of a nerve cell is to receive, conduct, and transmit electrical signals. A common example used to explain this function is how the nervous system controls the contraction of a muscle fibre during an activity. Neurons are often extremely elongated and must maintain and conduct electrical signals from the neuron cell body toward its distant targets. The Central Nervous System (CNS) sends a strong wave of pulse-like electrical signals called ‘action potentials’, which can carry a message rapidly and without attenuation to the muscle motor nerves, for example. This stimulus causes an influx of positive ions in the intracellular space, shifting the membrane potential to a less negative value which causes membrane ‘depolarisation’. Voltage-gated ion channels detect these significant changes in membrane potential and open, causing further depolarisation until, within a fraction of a millisecond, the membrane potential reaches the equilibrium of sodium ions across the cell membrane, approximately +50mV. When the net sodium charge is almost zero, the cell undergoes ‘repolarisation’ through fast and automatic inactivation of sodium channels and opening voltage-gated potassium channels, causing potassium ions to move out of the cell. Thereby, the cell membrane can return to its resting membrane potential in about two milliseconds. Neighbouring regions of the axon membrane detect these changes in membrane potential and go through the same cycle. This way, the electric signal sent from the CNS to a particular nerve terminal is regenerative and self-propagating. When they

reach the nerve terminal at the neuromuscular junction, a non-electrical response is generated. This final transduction causes a membrane potential change and secretion of neurotransmitters, hormones, enzymes, and other signalling molecules, which open or close calcium-permeable ion channels expressed on the nearby muscle cells, for example. This calcium influx determines the ultimate cellular response, for example, muscle contraction (Alberts et al., 2017).

1.1.1 Mechanically-gated ion channels

Our ability to feel touch and hear sounds comes from the activation of ion channels that respond to mechanical stimuli, such as skin contact, sound waves, food texture, gravity, proprioception, muscle stretch, and blood and air flow. These stresses affect cell membranes and their associated components and activate mechanically-gated ion channels. Mechanosensitive ion channels are divided into five families: epithelial sodium channels (EnaC; touch, pH, and mechanical forces), transient receptor potential channels (TRP; light, heat, smell, pain, and mechanical forces), mechanosensitive two pore-domain potassium channels (K2P; heat, touch, and mechanical forces), Piezo ion channels (pain, touch, hearing, and mechanical forces), and mechanosensitive channels of the transmembrane protein 16/Anoctamin (TMEM16/Ano) superfamily (hearing, and mechanical forces). Mechanosensitive ion channels convert physical stimuli to electrical signals, allowing sensory neurons to generate a response within a millisecond (Ranade et al., 2015; Jin et al., 2020).

1.1.2 Voltage-gated ion channels

Voltage-gated ion channels open and close in response to membrane potential changes and include: voltage-gated potassium channels (set the resting potential, repolarise the cell membrane and allow generation of spontaneous trains of action potentials, and regulate the overall excitability of the cell), sodium channels (regulate the spike initiation of an action potential, inactivate rapidly to propagate electric signals), calcium channels (supply ‘activator’ calcium ions in fast synaptic transmissions for quick neurotransmitter release, and dominate long synaptic transmissions in secretory glands and endocrine organs, where a maintained electric signal is required), and chloride channels (contribute to membrane repolarisation and stabilise the resting membrane potential, they also play major roles in regulating intracellular pH) (Hille, 2001; Alberts et al., 2017).

Unlike voltage-gated sodium channels, voltage-gated calcium channels do not inactivate rapidly, maintaining an influx of calcium ions during long synaptic responses that are required for hormone secretion, for example. This property is due to a positive reversal potential for calcium ions, which means their extracellular concentration is much higher than their intracellular one, much larger than the reversal potential for sodium ions. As described above, calcium channels also serve as the link to transduce electrical signals into non-electrical cellular responses. Hence, calcium ions are crucial to terminate cellular excitation and supply intracellular ‘messengers’ capable of regulating many cell functions (Hille, 2001; Alberts et al., 2017).

1.1.3 Ligand-gated ion channels

Ligand-gated ion channels (LGIC) allow the passage of ions across the cell membrane in response to endogenous or exogenous ligands. Neurotransmitter-gated ion channels are LGICs specialised in mediating fast synaptic transmissions in response to a specific chemical ligand, the neurotransmitter. Acetylcholine, glutamate, γ -aminobutyric acid, glycine, serotonin, and ATP are some examples of known neurotransmitters. Each of these neurotransmitters can activate their respective receptors, allowing the passage of ions across the cell membrane, affecting the cell membrane potential, and ultimately leading to a cellular response, such as neuron synapsis or neurotransmitter release. There are three classes of ligand-gated ion channels, defined by their molecular architecture: Cys-loop receptors, ionotropic L-glutamate receptors, and P2X receptors (Alexander et al., 2011).

Pentameric receptors represent the first class of LGICs and are frequently called Cys-loop receptors. Each subunit consists of four transmembrane domains (TM), with a characteristic closed loop in the extracellular ligand binding domain and extracellular amino-terminus (N-term) and carboxy-terminus (C-term). Cys-loop receptors are further divided into two groups: cation permeable (i.e., nicotinic acetylcholine receptors (nAChR), 5-hydroxytryptamine receptors (5-HT), and zinc-activated ion channels (ZAC)), and anion permeable (i.e., γ -aminobutyric acid receptors (GABA) and glycine receptors) (Sine & Engel, 2006; Alexander et al., 2011).

The second class of LGICs are the tetrameric ionotropic glutamate receptors. Each subunit comprises an extracellular N-terminus, three transmembrane domains with a re-entrant loop between TM1 and TM3, an extracellular ligand binding domain, and an intracellular C-terminus. Ionotropic glutamate receptors are divided into three subtypes named after their selective dicarboxylic amino acid ligand: α -amino-3-hydroxy-5-methyl-4-isoxalone propionic acid (AMPA or GluA), N-methyl-D-aspartate (NMDA or GluN), and kainate (GluK) (Alexander et al., 2011).

Lastly, the third class of LGICs are the trimeric P2X receptors which respond to the neurotransmitter ATP. Seven P2X receptor subtypes have been recently cloned and named P2X1 to P2X7 (North, 2002). Each subunit has only two transmembrane domains, with intracellular C-term and N-term domains separated by a large, glycosylated, and disulphide-rich extracellular ligand binding domain (Kawate et al., 2009; section 1.2.2.2).

Nicotinic acetylcholine, 5-hydroxytryptamine, zinc-activated, ionotropic glutamate, and P2X receptors are cation-permeable ion channels and contribute to excitatory neurotransmission and synapse. In contrast, GABA and glycine receptors are anion permeable and are involved in inhibitory neurotransmission responses, repolarising a depolarised cell and stabilising its resting membrane potential (Alexander et al., 2011). While most Cys-loop and ionotropic glutamate receptors can assemble as heteromers within each class of LGIC, little is known about P2X subunit assembly (Alexander et al., 2011; Saul et al., 2013). Heteromeric receptors result from combining different pore-forming receptor subunits to form a functional ion channel. These multiple combinations result in a wide range of neurotransmitter-gated ion channels with different pharmacological and physiological

properties and expression patterns throughout the nervous system and other tissues, highlighting the importance of understanding their specific molecular structure and their therapeutic potential.

1.2 Purinergic signalling: ATP as a neurotransmitter

Adenosine 5'-triphosphate (ATP) is widely recognised for its vital role in cellular metabolism, where it acts as a ubiquitous enzyme cofactor during biosynthesis and as a cellular energy source. The idea that ATP and other extracellular nucleotides and nucleosides can act as signalling molecules was first proposed by Professor Geoffrey Burnstock under the purinergic nerve hypothesis in the early 70s (Burnstock, 1972). Despite previous evidence supporting this concept (Drury & Szent-Györgyi, 1929; Emmelin & Feldberg, 1948; Holton, 1959; Paton & Vane, 1963; Burnstock et al., 1970), it remained controversial for many years until it was established and recognised by the scientific community.

ATP is constantly produced within cells through cellular respiration and glycolysis. In neutral solutions, ATP molecules are ionised and exist primarily as free ATP anions (ATP^{4-}), but in the presence of physiological levels of magnesium ions (Mg^{2+}), the majority of ATP molecules exist as MgATP^{2-} anions in both extracellular and intracellular compartments (Li et al., 2013). Additionally, ATP molecules are large and negatively charged and cannot simply diffuse across the plasma membrane. Cell damage (e.g., damaged endothelial and smooth muscle cells following vessel wall injury) and cell death (apoptotic or necrotic cells) lead to the uncontrolled release of ATP and other large cytosolic molecules to the extracellular space (Cook & McCleskey, 2002). ATP can also be constitutively released in the extracellular space and mediate autocrine regulatory signalling (Lazarowski et al., 2000). Exocytosis following mechanical or chemical stimulation is thought to be the method by which ATP, alone or in combination with other neurotransmitters, is released to the extracellular milieu by neurons and secretory cells, such as endocrine cells and platelets (Yegutkin, 2014). But it can also be released through ATP-permeable ion channels and transporters, namely connexin (Cx) hemichannels, pannexin 1 (PANX1), calcium homeostasis modulator 1 (CALHM1), volume-regulated anion channels (VRACs), and maxi-anion channels (MACs) (Fig 1.1; Taruno, 2018). P2X7 receptors have also been proposed as possible ATP-release channels, although these studies have been hindered because P2X7 ion channels are also activated by ATP itself (Johnsen et al., 2019). There are still unknown physiologically important ATP release mechanisms to be discovered.

Ectonucleotidases, such as nucleoside triphosphate diphosphohydrolase-1 (CD39) and ecto-5'-nucleotidase (CD73), can hydrolyse these extracellular nucleotides into intermediate metabolites and nucleosides. Thus, the concentration of extracellular nucleotides and their mediated physiological functions are also highly regulated by these enzymes (Yang & Liang, 2012). Finally, nucleosides can be transported back into the cell or directly inactivated, closing the cycle (Yegutkin, 2008).

The term purinergic signalling was proposed as a form of extracellular signalling mediated by purine and pyrimidine nucleosides and nucleotides (Fig 1.2) interacting with specific cellular receptors, namely P1 and P2 receptor families (Fig 1.3; Burnstock, 1990; Ralevic & Burnstock, 1998). There is a growing

body of evidence for purinergic implications in many biological processes, including maintenance of homeostasis, modulation of vascular tone, regulation of immune responses and inflammation, pain transmission, and cancer development. (Donnelly-Roberts et al., 2007; Beamer et al., 2016; Burnstock, 2016; Di Virgilio et al., 2018).

1.2.1 P1 receptors

P1 receptors are G-protein coupled receptors (GPCR) activated by the nucleoside adenosine. Thus, they are also referred to as adenosine receptors (AR). P1 receptors are further divided into four subtypes, namely A1, A2A, A2B, and A3 (Fig 1.3). They all have seven putative transmembrane domains with an extracellular amino-terminus (N-term) and an intracellular carboxy-terminus (C-term). While the residues within the transmembrane domains are involved in ligand binding, the intracellular loops of each segment can interact with the appropriate G protein (Burnstock, 2007). A1 and A3 receptors can couple to $G\alpha_i$ proteins, causing a reduction of adenylate cyclase (AC) activity and therefore preventing the accumulation of intracellular cAMP (cyclic adenosine 5'-monophosphate). $G\alpha_s$ proteins can bind to A2A and A2B receptors leading to opposite actions (Burnstock, 2007; Abbracchio et al., 2008).

1.2.2 P2 receptors

On the other hand, P2 receptors are activated by nucleotides and are classified into two distinct subfamilies known as P2X and P2Y receptors (Burnstock & Kennedy, 1985).

1.2.2.1 P2Y receptors

P2Y receptors (P2YR) share a common feature with P1 receptors in that they are GPCRs. These receptors also have seven transmembrane domains connected by intracellular and extracellular loops, with an extracellular N-terminus and an intracellular C-terminus (Burnstock, 2007). The first P2Y receptor to be cloned was the P2Y1 subtype isolated from a chick brain in 1993 (Webb et al., 1993). Since then, eight subtypes have been cloned and characterised in mammals: P2Y1, P2Y2, P2Y4, P2Y6, and P2Y11-14 (Von KÜgelgen & Hoffmann, 2016). P2Y receptors can be separated into two groups: P2Y1-like and P2Y12-like receptors. P2Y1, P2Y2, P2Y4, P2Y6, and P2Y11 receptors couple to $G\alpha_q$ proteins and activate phospholipase C- β (PLC- β) to produce inositol triphosphate (IP_3) and diacylglycerol (DAG), ultimately increasing intracellular calcium levels. In contrast, P2Y12, P2Y13, and P2Y14 receptors are $G\alpha_i$ protein-coupled receptors which lead to a reduction of intracellular cAMP. $G\alpha_s$ proteins can also bind to P2Y11 receptors and activate AC. The ability of adenosine and uridine nucleotides to activate P2Y receptor subtypes varies. For example, P2Y11 is activated by ATP, ADP (adenosine 5'-diphosphate) is the sole agonist of P2Y1, ADP can also activate P2Y12 and P2Y13, ATP and UTP (uridine 5'-triphosphate) are equipotent agonists of P2Y2 and P2Y4, UDP (uridine 5'-diphosphate) binds to P2Y6 and P2Y14, and UDP-glucose (uridine 5'-diphosphate-glucose) can only activate P2Y14 receptors (Fig 1.3; Abbracchio et al., 2006; Von KÜgelgen & Hoffmann, 2016).

1.2.2.2 P2X receptors

P2X receptors (P2XR) are ligand-gated ion channels that open in response to the binding of extracellular ATP. Seven P2X receptor subtypes have been identified in mammals, i.e., P2X1-7 (North, 2002). The first to be cloned were the P2X1 (Valera et al., 1994) and P2X2 subtypes (Brake et al., 1994) from rat vas deferens and pheochromocytoma cells (PC12), respectively. P2X receptors share a common topology consisting of two transmembrane domains, with short intracellular amino- and carboxy-termini, separated by a large, glycosylated, and disulphide-rich extracellular domain (Fig 1.4; Kawate et al., 2009). The structure of each P2X subunit has been compared to the shape of a leaping dolphin consisting of the head, body, right and left flippers, dorsal fin, and fluke (Fig 1.4A). As described in section 1.1.3, P2X receptors have a distinctive structure amongst other ligand-gated ion channel families. P2X receptors are trimeric, formed by the association of three subunits with an overall chalice-like structure (Kawate et al., 2009; North, 2016). In summary, ATP-mediated activation of P2X receptors induces conformational changes, which result in gate opening, allowing the passage of cations (e.g., sodium (Na^+), potassium (K^+), and calcium (Ca^{2+})) across the plasma membrane (Fig 1.3; Kawate et al., 2011; Samways et al., 2011, 2012). Subsequently, this cation influx initiates different downstream signalling events, ultimately causing membrane depolarisation and increased cytoplasmic calcium levels (Samways et al., 2014).

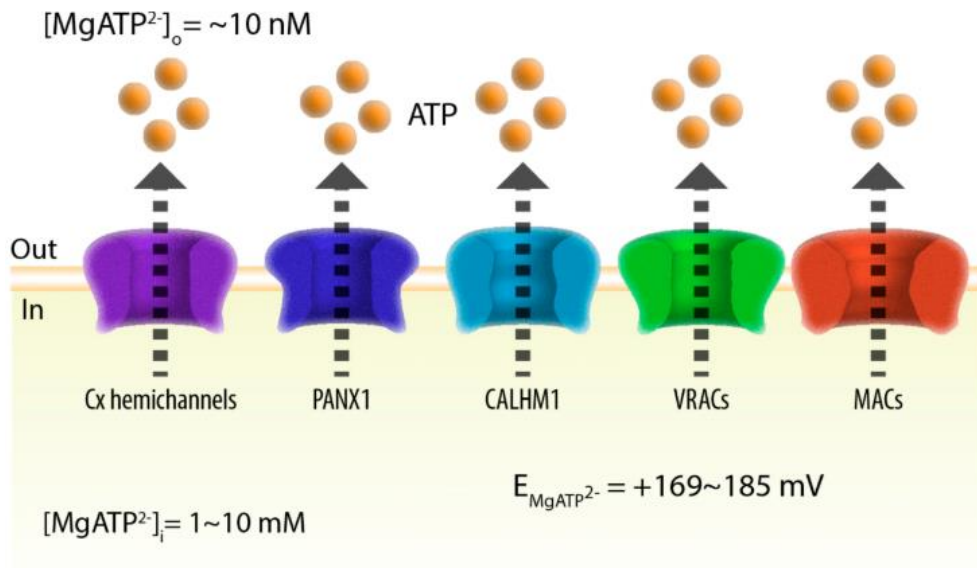


Fig 1.1. ATP-permeable ion channels and transporters. The approximate physiological $MgATP^{2-}$ concentrations are 1-10mM intracellularly $[MgATP^{2-}]_i$ and 10nM extracellularly $[MgATP^{2-}]_o$. The calculated equilibrium potential of $MgATP^{2-}$ is approximately 169-185mV. Five channel families mediate ATP release: connexin (Cx) hemichannels, pannexin 1 (PANX1), calcium homeostasis modulator 1 (CALHM1), volume-regulated anion channels (VRACs), and maxi-anion channels (MACs). ATP can also be released via exocytosis and secretion upon mechanical or chemical stimuli and as a consequence of cell damage or cell death (not shown in the figure). Adapted from Taruno, 2018.

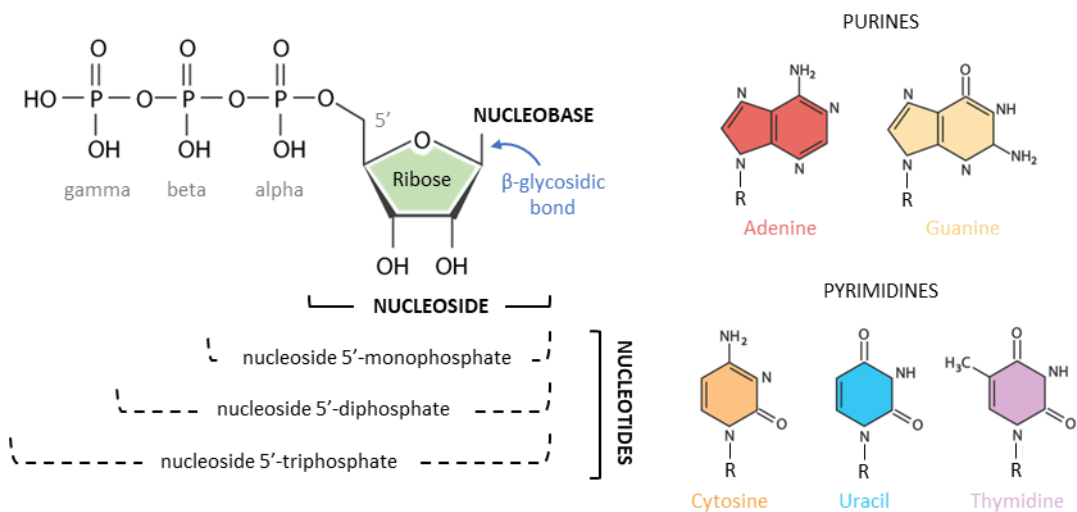


Fig 1.2. General structure of nucleosides, nucleotides, and nucleobases. Nucleosides belong to a class of organic compounds composed of a nitrogen-containing heterocyclic nucleobase, either a purine (adenine, guanine) or a pyrimidine (cytosine, uracil, thymidine), and a five-carbon sugar called ribose. The nucleobase is bound to the ribose, through a β -glycosidic bond. R represents the position where the ribose binds to in each nucleobase. Nucleotides originate from the phosphorylation of nucleosides at the 5' hydroxyl group of the sugar moiety. Three different types of nucleotides can be formed depending on how many phosphate groups are added to the phosphate tail, namely nucleoside 5'-mono, -di, or -triphosphate.

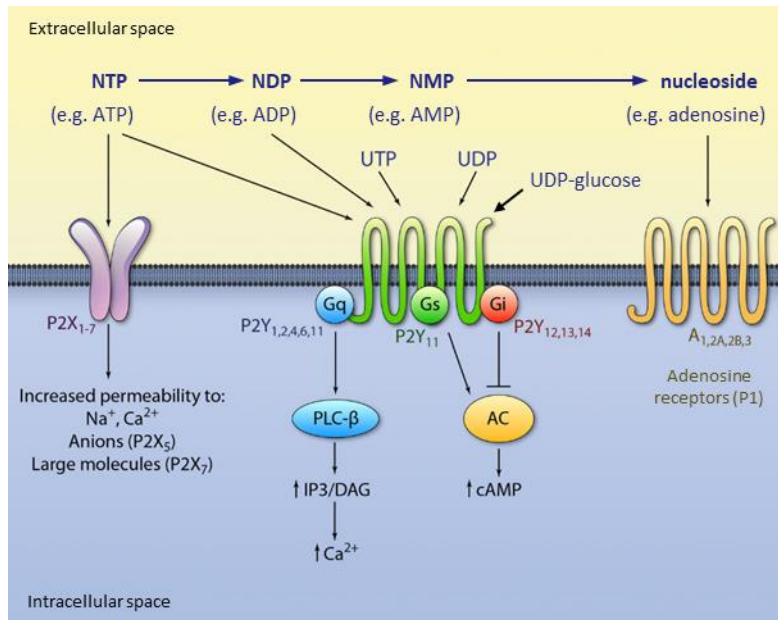


Fig 1.3. Schematic representation of P1, P2X, and P2Y receptors, and their intracellular signalling pathways. Nucleotides are released into the extracellular space and can bind to P2X and P2Y receptors, or can be broken down by ectonucleotidases (blue arrows) into intermediate metabolites and nucleosides. For example, adenosine is the degradation product of ATP, ADP, and AMP, and can bind to adenosine receptors (P1). ATP can activate ionotropic P2X receptors allowing the entry of Ca²⁺ and Na⁺ ions into the cell. In addition to endogenous ATP, metabotropic P2Y receptors can also respond to ADP, UTP, UDP, and UDP-glucose nucleotides. Both P1 and P2Y receptors are GPCRs and lead to different downstream effects depending on which G-protein binds to them. Adapted from Yang & Liang, 2012.

1.3 P2X4 receptors

The P2X4 receptor is part of the P2X ligand-gated ion channel family, introduced in sections 1.1.3 and 1.2.2. The P2X4 receptor was first cloned and characterised in 1996 from the rat brain (Soto et al., 1996) and one year later from the human brain (Garcia-Guzman et al., 1997). Since the focus of this thesis is to explore functional P2X4 subunit interactions, a comprehensive overview of P2X4 receptor structure and agonist binding site, activation and gating mechanisms, expression and trafficking patterns, pharmacological profile, and physiological roles is discussed here.

1.3.1 P2X4 receptor structure and ATP binding site

Since P2X receptors do not share homologous sequences with other known ligand-gated ion channels, functional and biochemical studies were first used to explore their molecular structure. The first biochemical evidence that P2X ion channels form a trimeric structure was reported by Nicke et al. for P2X1 and P2X3 receptors in *Xenopus laevis* oocytes (Nicke et al., 1998). This architecture was later confirmed when the crystal structures of a truncated zebrafish P2X4 receptor (zfP2X4) were published, first in the absence of ATP (Kawate et al., 2009) and successively bound to ATP molecules (Hattori & Gouaux, 2012). Their findings revealed a chalice-shaped global structure with three subunits interacting and twisting around each other, forming inter- and intra-subunit interfaces. A P2X4 subunit consists of two transmembrane domains (TM1 and TM2) with short intracellular N-term and C-term segments connected by a large, glycosylated, and disulphide-rich extracellular domain (Kawate et al., 2009). This original dolphin-like folding allowed a clear distinction between its different structural segments (Fig 1.4A). TM1 and TM2 are associated with the dolphin fluke and are structured as α -helices with the TM1 located outside the TM2. The ion pore is delineated by the association of three tilted TM2 α -helices. The large ectodomain is compared to the main body of the dolphin. It has a β -sheet structural organisation stabilised by five disulphide bonds formed by ten highly conserved cysteine residues (Fig 1.4A; Ennion & Evans, 2002a). The head, dorsal fin, and lateral flippers diverge from the dolphin's body and are structurally more flexible. The extracellular domain also contains seven putative N-glycosylation sites, although only two are strictly required for robust receptor formation, that is the formation of a functional homotrimeric receptor expressed at the cell membrane (Fig 1.4B; Rettinger et al., 2000).

Both apo state and ATP-bound crystal structures served as templates for the analysis and interpretation of previous biochemical and functional studies, in particular, the large body of mutagenesis-based structure-function data regarding the ATP binding site and the P2X channel opening mechanism (Young, 2010; Habermacher et al., 2016). The P2X receptor ATP binding pocket is located at the interface of two adjacent subunits comprising the head and left flipper of one subunit and the dorsal fin of the other (Fig 1.5). There are three potential ATP-binding pockets in a trimer, as there are three interfaces (Fig 1.4C). The early statement that three ATP molecules were required to activate the receptor (Bean, 1990) was refuted when posterior studies proposed a positive cooperation binding mechanism rather than independent binding of ATP molecules (Jiang et al., 2003). Their study showed that occupancy of only one binding site of a P2X receptor did not induce channel opening but produced a conformational

change that strongly influenced the binding of the second and third ligand molecules (Jiang et al., 2003). After the zebrafish P2X4 receptor ATP-bound structure was released, a mutagenesis-based study confirmed this cooperation principle by showing that the binding of two ATP molecules was sufficient to gate P2X receptors (Chataigneau et al., 2013).

The residues found within the ATP-binding cavity are tightly clustered and orchestrate several hydrophobic interactions, and hydrogen and salt bridge bonds with the ATP molecule. In the following lines, I summarise the residues involved in ATP molecule coordination using the zebrafish P2X4 receptor numbering and Figure 1.5B as a reference. The adenosine base is deeply inserted into the ATP-binding pocket. It interacts with lysine K70 (subunit 2 in Figure 1.5B) and threonine T189 (subunit 2) by hydrogen bonds and with leucine L191 (subunit 2) and isoleucine I232 (subunit 2) residues by hydrophobic interactions. The ribose moiety is solvent-accessible and forms hydrophobic interactions with leucine L217 (subunit 2). The long triphosphate tail of the ATP molecule folds in a U-shaped structure when bound to the receptor. Its negatively charged phosphate groups form salt bridges and hydrogen bonds with several basic and polar residues from the upper and lower domains of the two subunits, i.e., K70, K72, K316, N296, and R298 (Hattori & Gouaux, 2012). Lysine K70 (subunit 2) has a key location in the receptor and coordinates the oxygen atoms of α -, β -, and γ -phosphate groups of the ATP molecule. Lysine K316 (subunit 1) and asparagine N296 (subunit 1) mediate additional interactions with β -phosphate groups, while K72 (subunit 2), arginine R298 (subunit 1) and K316 (subunit 1) participate in the coordination of the γ -phosphate group (Fig 1.5B; Hattori & Gouaux, 2012; Chataigneau et al., 2013). Lysine residues at positions K70 (subunit 2) and K316 (subunit 1) were identified as critical residues for ATP molecule recognition and binding, and such role is highly conserved in the history of P2X receptor evolution (Jiang et al., 2000; Chataigneau et al., 2013; Fountain et al., 2007).

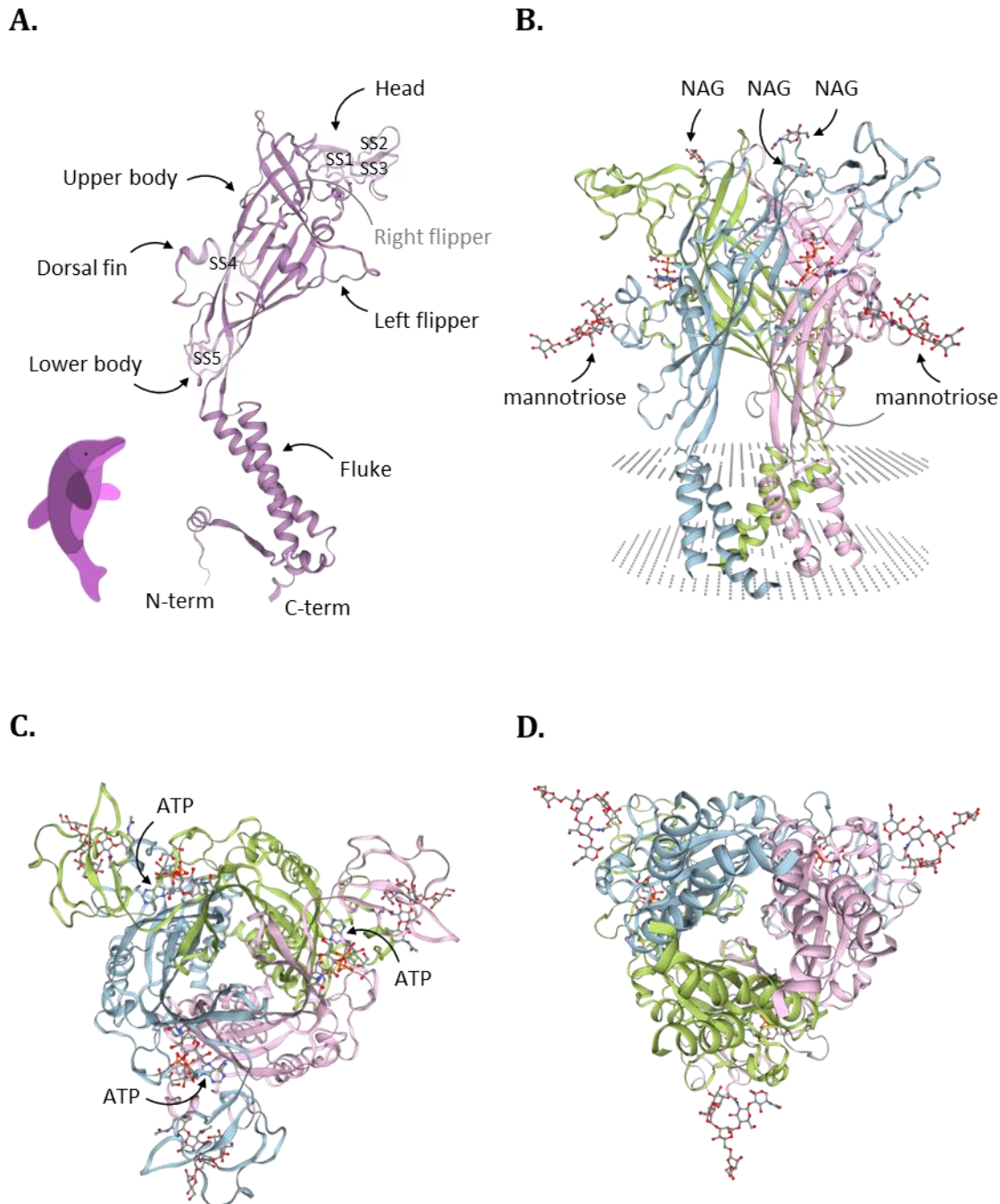


Fig 1.4. Crystal structure of the zebrafish P2X4 receptor in an ATP-bound state. (A) Cartoon representation of the dolphin-like folding of a zfP2X4 subunit comprising the body, head, dorsal fin, right and left flippers, fluke, and C- and N-termini domains. Disulphide bonds (SS1–5) are indicated, three of which are located in the head domain. This structure was obtained from the predicted AlphaFold zfP2X4 subunit model (AlphaFold repository, accession number F8W463) and shows a predicted juxtamembrane position for the intracellular N- and C-termini, not present in the published truncated zfP2X4 crystal structures (Kawate et al., 2009; Hattori & Gouaux, 2012). (B) Front view of the truncated zfP2X4 receptor crystal structure bound to ATP and embedded in a lipidic bilayer (grey dotted

area). N-glycosylation sites are indicated for the sugar ligands NAG (N-acetylglucosamine) and mannotriose (α -D-mannopyranose-(1-3)- α -D-mannopyranose-(1-3)-[α -D-mannopyranose-(1-6)] β -D-mannopyranose-(1-4)-2-acetamido-2-deoxy- β -D-glucopyranose-(1-4)-2-acetamido-2-deoxy- β -D-glucopyranose) to residues N88 and N188 of each subunit, respectively. (C, D) Top and bottom views of the truncated zfP2X4 receptor channel pore when bound to ATP, respectively. (C) Three ATP molecules bound to the intersubunit binding pockets of the zfP2X4 receptor are indicated. (B-D) These structures were obtained from the Swiss-model repository (PDB accession number 4DW1). Each subunit is shown in a cartoon representation and in a different colour (blue, green, and pink), and all ligands are shown in a ball and stick representation.

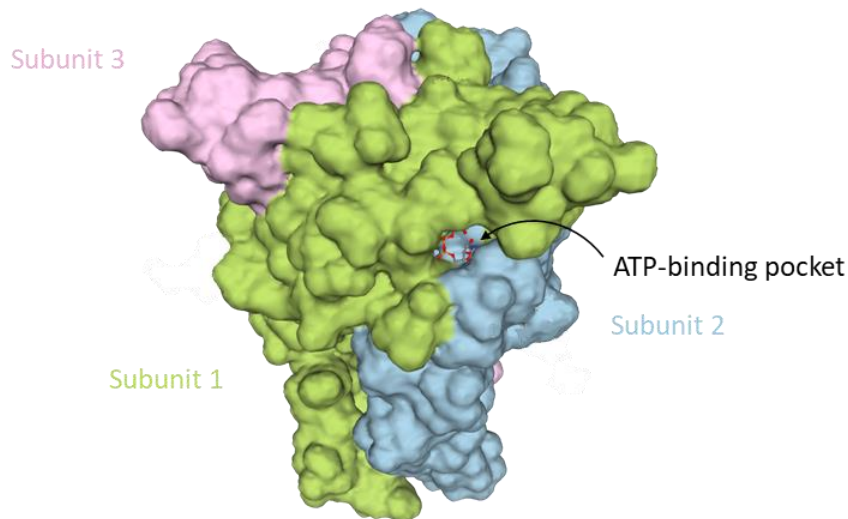
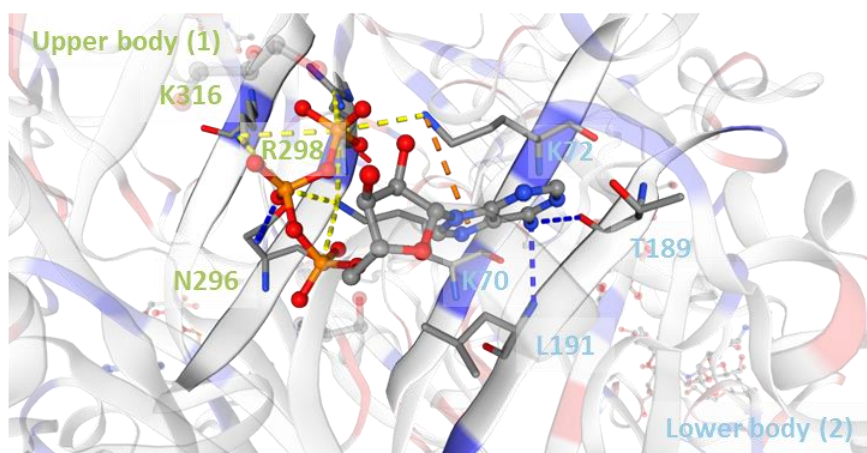
A.**B.**

Fig 1.5. The P2X4 receptor ATP-binding pocket and key residues involved in ligand recognition. (A) Surface representation of the truncated zfP2X4 receptor crystal structure highlighting the ATP-binding pocket between the subunits 1 (green) and 2 (blue). Each subunit is shown in a surface representation and in a different colour (blue, green, and pink), and the ATP molecule is shown in a ball and stick representation. (B) Close-up view of the ATP-binding pocket located in the interface between the subunits 1 (green) and 2 (blue) and key residues involved in the recognition and binding of the ATP molecule. K70 (subunit 2) coordinates interactions with the adenosine base and the triphosphate tail, while K316 (subunit 1) interacts with beta and gamma phosphate groups of the ATP molecule. T189 (subunit 2), L191 (subunit 2), and I232 (subunit 2, not shown) form interactions with the adenine base, L217 (subunit 2, not shown) with the ribose moiety, and K72 (subunit 2), N296 (subunit 1), and R298 (subunit 1) with the different phosphate groups. Hydrophobic interactions and hydrogen bonds are represented as blue dashed lines, and salt bridge bonds as yellow dashed lines. Each subunit is shown in a faded charge representation, the ATP molecule in a ball and stick representation, and the key amino acid residues in a liquorice representation. Both structures were obtained from the Swiss-model repository (PDB accession number 4DW1).

1.3.2 P2X4 receptor activation and gating mechanism

The gating of P2X4 receptors can be explained in five steps: ATP binding, jaw-like tightening of the ATP binding pocket, flexing of the lower body regions, expansion of the lateral fenestrations, and pore opening. First, the ATP-binding pocket accommodates the molecule by closing the gap between the head of one subunit and the dorsal fin of the adjacent one in a jaw-like motion, while the left flipper from the first subunit is pushed outwards. Overall, upon ATP binding, the lower body segments of each P2X4 subunit draw away from each other and rotate, causing an expansion of the extracellular vestibule, which in turn induces a shift of the outer ends of the TM2 α -helices, opening the pore in an anticlockwise iris-like motion (Hattori & Gouaux, 2012). In 2016, the X-ray crystal structure of a human P2X3 receptor in apo, ATP-bound, and desensitised states allowed visualisation of the cytoplasmic residues truncated in the previous zebrafish P2X4 structures (Mansoor et al., 2016). These structures confirmed the P2X receptor gating mechanism and showed the formation of a new domain called the ‘cytoplasmic cap’ in the ATP-bound state, consisting of two N-term and one C-term β -sheet sequential elements (Fig 1.6; Mansoor et al., 2016). This cytoplasmic cap provides structural stability to the gated receptor and is almost certainly disassembled in the closed and desensitised states of the receptor (Fig 1.6; Mansoor et al., 2016).

A common feature of most signalling membrane receptors is receptor desensitisation. In P2X receptors, channel desensitisation determines signal transduction changes over time and regulates responsiveness in the sustained presence of ATP. The desensitised state represents the transition from an agonist-bound open state to an agonist-bound closed state. It is followed by agonist unbinding and the conformational changes from the agonist-free to the resting closed state. Desensitised and open P2X receptor states are structurally different. In the desensitised state, the TM2 domain rotates and shrinks, closing the pore and causing the overall architecture of the receptor to rotate upwards and inwards. For this recoil movement to occur, Mansoor et al. proposed that the cytoplasmic cap must disassemble or become flexible to release the ‘anchor’ that fixed the TM2 in place (Mansoor et al., 2016).

P2X receptors are non-selective cation channels and are predominantly permeable to sodium, potassium, and calcium ions. The overall expansion of the extracellular vestibule creates an ample space between two adjacent subunits allowing the passage of cations through the plasma membrane via lateral fenestrations (Fig 1.6; Kawate et al., 2011; Samways et al., 2011, 2012; Hattori & Gouaux, 2012). These cations pass through the pore but do not exit the protein lumen from the bottom surface of the cytoplasmic gap because the orifice along this axis is too small. Instead, the putative pathway for ion egress is through triangular-shaped cytoplasmic fenestrations formed by the cytoplasmic cap and the TM2 segments from adjacent subunits and located within the limits of the lipidic cell membrane (Fig 1.6; Mansoor et al., 2016).

Under physiological conditions, P2X4 receptor gating causes the entry of sodium and calcium ions which ultimately cause membrane depolarisation and an elevation in cytoplasmic calcium levels (Samways et al., 2014). This membrane depolarisation is sufficient to cause the onset of action potentials in excitable

cells and initiate other calcium-dependent signalling processes in excitable and non-excitable cells (Samways et al., 2014).

Prolonged exposure to ATP and consequent sustained activation of P2X2, P2X4, and P2X7 receptors had the effect of permeating the channels to much larger ions, including the synthetic organic cation N-methyl-D-glucamine (NMDG^+) and the propidium dye YO-PRO1 (North, 2002; Peverini et al., 2018). Two main hypotheses have been considered for the formation of this large channel pore. One involves the recruitment of a supporting protein, namely pannexin-1 hemichannel (PANX1), and the other suggests the existence of an intrinsic and slow ‘pore dilation’ mechanism (Kanellopoulos et al., 2021). In 2015, the paradigm changed as research showed that gradual pore dilation was not necessary to permeate large cations. Instead, an intrinsic and immediate dye-permeable pore was formed due to a conformational and orientational change (Li et al., 2015). Evidence supporting and contrasting these mechanisms has been found. Thus, a combined mechanism might be possible (Peverini et al., 2018). The physiological role of P2X receptor permeation to larger ions has been proposed as a pathway for the release of large molecules, such as ATP itself (Johnsen et al., 2019) and spermidine, an intracellular polyamine involved in cell growth, division, and proliferation (Peverini et al., 2018), and even as a potential mechanism for drug delivery (Peverini et al., 2018).

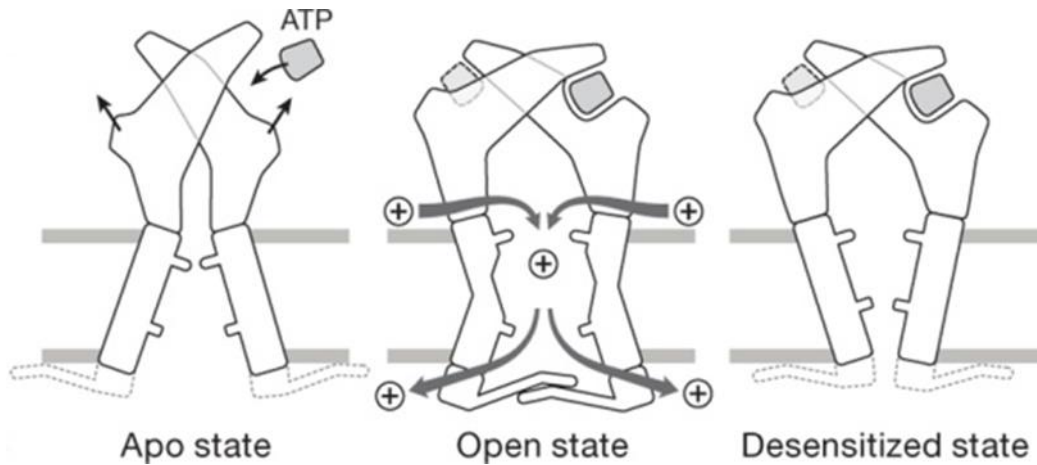


Fig 1.6. Schematic representation of the P2X receptor gating cycle. Activation of P2X receptors by ATP induces a cascade of conformational changes of the receptor which result in channel opening, thus allowing the passage of small cations through the channel pore via lateral fenestrations and exiting the protein lumen through cytoplasmic fenestrations, located within the boundaries of the cell membrane. The 'helical recoil' desensitisation mechanism switches the receptor from an ATP-bound open state to an ATP-bound closed state, which is followed by ligand unbinding and structural rearrangements to reset the receptor back to its resting state. Adapted from Mansoor et al., 2016.

1.3.2.1 Expression and trafficking of the P2X4 receptor

P2X4 receptors are one of the predominant subtypes expressed in vascular smooth muscle cells, vascular endothelial cells, neurons, microglia, and macrophages and monocytes, and their expression at the plasma membrane is critical for the responsiveness of these cells to extracellular ATP (Yamamoto et al., 2000b; Tsuda et al., 2003; Guo et al., 2004; Layhadi et al., 2018). After protein synthesis, P2X proteins undergo post-translational folding and other post-translational modifications, such as disulphide bond formation, glycosylation of the extracellular domain, and specific subunit assembly (discussed in section 1.3.4.6) to gain activity and traffic to their final destinations (Nicke et al., 1998; Kaczmarek-Hájek et al., 2012). P2X polypeptides enter the endoplasmic reticulum through a protein translocon in an unfolded state (Öjemalm et al., 2013). The folding of P2X polypeptides is dependent upon the residues located near the cytoplasmic limits of the TM1 and TM2 domains. The TM1 domain initially integrates into the endoplasmic reticulum translocon membrane (Öjemalm et al., 2013). Then, TM1 residues form orchestrated interactions with TM2 residues to integrate the TM2 domain into the endoplasmic reticulum translocon membrane and form a P2X monomer, which can subsequently assemble with other P2X monomers to form a trimer (Öjemalm et al., 2013). Thus, membrane positioning of both TM domains is crucial for an efficient P2X subunit trimerisation and the ability of P2X receptors to exit the endoplasmic reticulum translocon and be delivered to the cell membrane. Finally, P2X receptors are trafficked to the plasma membrane constitutively or through a regulated vesicle exocytosis pathway, like other functional ion channels and membrane proteins (Kaczmarek-Hájek et al., 2012).

P2X4 receptors expressed on the cell surface form non-selective cation channels, as previously explained. However, P2X4 receptors in microglia, macrophages, and vascular endothelial cells are predominantly localised intracellularly in lysosomes (Fig 1.7; Qureshi et al., 2007). Lysosomes are subcellular organelles that contain cytoplasmic material and digestive enzymes and are involved in processing unwanted substances from inside of the cell as well as foreign substances, such as bacteria, viruses, or other antigens. Therefore, for most ligand-gated ion channels, delivery to lysosomes represents an endpoint in their trafficking and function within the cell. However, this is not the case for P2X4 receptors. P2X4 receptors located at the lysosomal membrane orient their extracellular domain facing their acidic lumen and still retain their functionality (Qureshi et al., 2007; Murrell-Lagnado & Frick, 2019). P2X4 receptors can subsequently traffic to phagosomes and move out to the plasma membrane, which suggests they could have roles within these intracellular compartments as well as at the plasma membrane (Qureshi et al., 2007). It is thought that P2X4 receptors resist rapid enzymatic degradation because of their N-linked glycans, which even show partial resistance to treatment with endoglycosidase H (endo H; Qureshi et al., 2007). There are two routes for P2X4 trafficking to the lysosomes: i) direct translocation from the trans-Golgi network to lysosomes and late endosomes, and ii) endocytosis of membrane-expressed receptors. The C-term tyrosine and N-term dileucine motifs are responsible for lysosomal targeting and rapid internalisation of surface-expressed P2X4 receptors (Qureshi et al. 2007). The traffic to and from the cell membrane is highly dynamic and whether the P2X4 receptor remains within lysosomal compartments or not is dependent on the cell type and

environmental factors, such as lysosomal pH, presence of ATP, and cell damage (Qureshi et al., 2007; Murrell-Lagnado & Frick, 2019). Lysosome fusion with developing phagosomes can also deliver proteins and other molecules to the cell membrane and has been proposed as another mechanism to regulate P2X4 receptor expression and function (Murrell-Lagnado and Frick, 2019).

1.3.2.2 Polymorphisms of P2X4 receptors

Genetic polymorphisms may lead to a gene sequence variation that is neutral or promotes the gain or loss of protein function. Polymorphisms can occur in genes encoding human P2X receptors. Single nucleotide polymorphisms (SNP) are the most common type of genetic variation in humans and represent the difference of only one nucleotide in a gene sequence. For example, a guanine SNP at the 3' splice site of exon 10 of the human P2X5 gene results in the exclusion of exon 10 and causes loss of function of the P2X5 receptor (Kotnis et al., 2010). This splice variant is the most common form of P2X5 receptors in humans and will be discussed later in this thesis (Chapter 4, section 4.2.1.3; Chapter 5, section 5.2.4.4; Bo et al., 2003; King, 2022). The human P2X7 gene contains at least eight non-synonymous SNPs that can affect P2X7 receptor function, the highest number amongst the P2X ion channel family (Fuller et al., 2009; Kaczmarek-Hájek et al., 2012).

The human P2X4 gene contains four non-synonymous SNPs (Stokes et al., 2011; Kaczmarek-Hájek et al., 2012). For example, the presence of guanine instead of adenine in the human P2X4 gene caused a loss of channel function that could be associated with higher blood pressure risk (Stokes et al., 2011). This particular SNP changes the protein sequence by substituting a tyrosine for a cysteine residue at position 315 and is thought to impair channel function by forming aberrant disulphide bonding, destabilising the overall receptor structure and possibly disrupting the ATP binding pocket (Stokes et al., 2011). The other three non-synonymous SNPs found did not affect the human P2X4 channel function (Stokes et al., 2011).

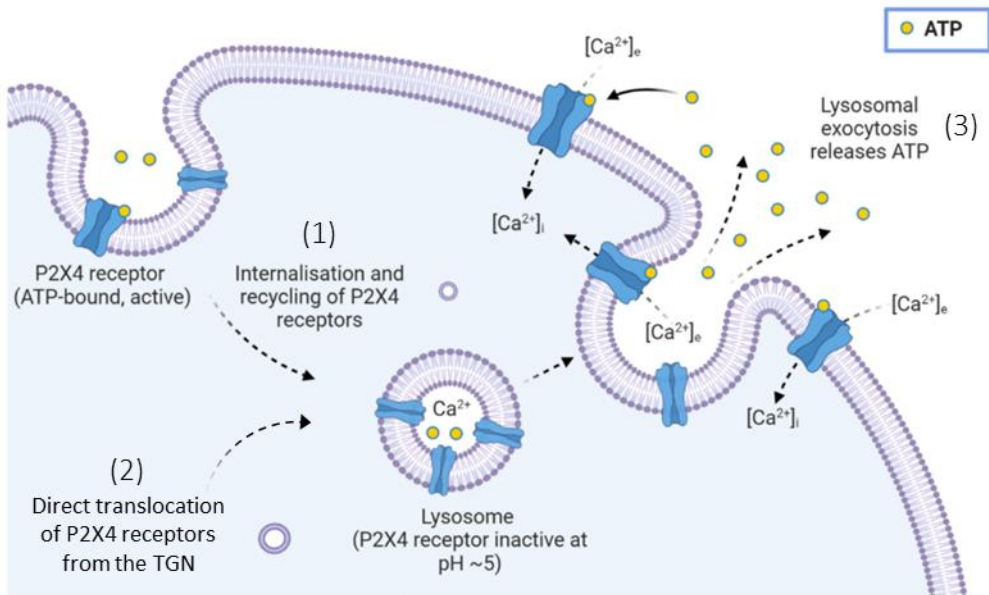


Fig 1.7. Cell surface and subcellular trafficking of P2X4 receptors. P2X4 receptors are expressed at the cell membrane, where they respond to extracellular ATP stimuli. But, P2X4 receptors are mostly expressed intracellularly at the lysosomal membrane. P2X4 receptors can translocate to the lysosomes following receptor internalisation by endocytosis (1), or direct lysosome targeting after protein formation in the trans-Golgi network (TGN; 2). Lysosomal exocytosis has been proposed as another mechanism to regulate P2X4 receptor expression and function, as well as, a mechanism to release ATP back to the extracellular space (3). P2X4 receptor trafficking to and from the cell membrane is highly dynamic and whether it remains on the lysosomal compartments or not is dependent on the cell type and environmental factors, such as lysosomal pH, presence of ATP, and cell damage. Adapted from Sophocleous et al., 2022.

1.3.3 P2X4 receptor pharmacology

Pharmacological tools are regularly used to investigate the role of ATP signalling mediated by P2X receptors. These pharmacological tools include agonists, antagonists, and allosteric modulators, which stimulate or inhibit the P2X receptor activity. The expression of P2X receptors in heterologous systems is a powerful tool to characterise the pharmacological profile of each receptor subtype (North, 2002). Furthermore, these small molecules can be used as templates for the development of high-affinity and subtype-selective compounds, which are required not only to assess their physiological function in native systems but also can be exploited as potential therapeutic agents. The human P2X4 pharmacological profile is investigated and discussed later in this thesis (Chapter 3, section 3.2.2; Chapter 5, section 5.2.2).

1.3.3.1 Agonists

The primary agonist of all homomeric and heteromeric P2X receptors is ATP. However, it acts differently depending on the sensitivity of each receptor subtype. The P2X4 receptor is one of the most sensitive subtypes as it is functional at nanomolar concentrations of ATP. Other molecules have been reported to activate P2X4 receptors, such as CTP (cytidine 5'-triphosphate), AP4A (diadenosine tetraphosphate) and other ATP analogues, namely 2-MeSATP (2-(methylthio)adenosine 5'-triphosphate), $\alpha\beta$ -MeATP (α,β -methyleneadenosine 5'-triphosphate), BzATP (2'(3')-O-(4-benzoylbenzoyl)adenosine 5'-triphosphate), γ -imidoATP (adenosine-5'-[γ -(propargyl)-imido]triphosphate), and ATP- γ -S (adenosine-5'-O-(3-thio-triphosphate)). By contrast, P2X receptors are weakly or not activated by the breakdown products of ATP, namely ADP, AMP (adenosine 5'-monophosphate), and adenosine; and UTP, UDP, and UDP-glucose, further corroborating the importance of the interaction between the three phosphate groups and the residues within the agonist-binding pocket to activate the receptor (Coddou et al., 2011; Chataigneau et al., 2013).

1.3.3.2 Positive allosteric modulators

An allosteric modulator is a molecule that can bind to a secondary binding site of a receptor. A positive allosteric modulator (PAM) enhances the binding affinity of the receptor agonist when it is present and, thus, increases receptor activity and its responses. These secondary binding sites are referred to as allosteric sites and are different to the main orthosteric sites, where the endogenous agonist binds to activate the receptor.

Ivermectin (IVM) is a natural product obtained from the fermentation processes of *Streptomyces avermitilis* bacteria and is used in human and veterinary medicine as an antiparasitic agent (Chen & Kubo, 2018). Ivermectin was discovered by Satoshi Ōmura and William C. Campbell, who were awarded the 2015 Nobel Prize in Physiology of Medicine. It was also included on the Model List of Essential Medicines of the World Health Organization (Chen & Kubo, 2018). Ivermectin is a mixture of two macrocyclic lactone derivatives known as avermectins B1a and B1b, and it is widely recognised as a positive allosteric modulator of P2X4 receptors (Priel & Silberberg, 2004). Ivermectin shows selectivity

for P2X4 receptors over other P2X receptor subtypes (Khakh et al. 1999) but also acts as a positive allosteric modulator of other ion channels, namely GABA, α 7 nicotinic acetylcholine, and glycine receptors (Chen & Kubo, 2018). There is some debate about the specific P2X4 receptor IVM binding site. Different studies showed evidence for two possible and distinct IVM binding sites, one located at the upper region of the transmembrane domains (Priel & Silberberg, 2004; Silberberg et al., 2007; Latapiat et al., 2017; Pasqualetto et al., 2018) and the other on top of the extracellular entry to the channel pore (Chen & Kubo, 2018; Weinhausen et al., 2022).

1.3.3.3 Antagonists

For a long time, research in the purinergic field has been hampered by the lack of subtype-selective antagonists. Previously, researchers relied on broad-spectrum and non-selective antagonists, such as Suramin, PPADS (pyridoxalphosphate-6-azophenyl-2',4'-disulfonic acid), and TNP-ATP (2',3'-O-(2,4,6-trinitrophenyl)-ATP). PPADS has been shown to inhibit the human P2X4 receptor fully, whilst Suramin appears to have non-specific effects at high concentrations (Garcia-Guzman et al., 1997; Jones et al., 2000; North & Surprenant, 2000).

Recent advances in the development of P2X4 receptor-selective antagonists include a benzodiazepine derivative called 5-BDBD (5-(3-bromophenyl)-1,3-dihydro-2H-benzofuro[3,2-e]-1,4-diazepin-2-one), the N-substituted phenoxazine derivatives PSB-12054 (N-(benzyloxycarbonyl)phenoxazine) and PSB-12062 (N-(p-methylphenylsulfonyl)phenoxazine), and the phenylurea derivative BX-430 (1-(2,6-dibromo-4-isopropyl-phenyl)-3-(3-pyridyl)urea) (Fischer et al., 2004; Hernandez-Olmos et al., 2012; Ase et al., 2015). The most recent ones, BAY-1797 (N-[4-(3-chlorophenoxy)-3-sulfamoylphenyl]-2-phenylacetamide) and NC-2600 (developed by Nippon Chemiphar, no information on structure or preclinical data), are orally active and display antinociceptive and anti-inflammatory effects (Werner et al., 2019; Inoue, 2021; D'Antoniogiovanni et al., 2022). Besides, the completion of phase I clinical trials for NC-2600 as a P2X4 receptor antagonist for the treatment of chronic cough and neuropathic pain seems promising (Sonnenreich, 2021; Inoue, 2021). Natural products, like Taspine, have also started to emerge from high throughput screenings as selective P2X4 antagonists. Taspine is the active molecule found in the resin of *Croton lechleri* plants, which is used by Amazonian tribes for its cicatrising and anti-inflammatory properties (Bin-Nadzirin et al., 2021).

Currently approved antidepressants, such as paroxetine and fluvoxamine, were shown to inhibit ATP-evoked rat and human P2X4 receptor-mediated responses and produced antialloodynic effects in a rat model of neuropathic pain (Nagata et al., 2009). Statins are the most common cholesterol-lowering drugs. Some, like fluvastatin, have inhibitory effects on P2X4 receptor function, possibly through their cholesterol-depleting activity, which can alter P2X4 receptor trafficking and its stability at the cell membrane (Li & Fountain, 2012; Robinson & Murrell-Lagnado, 2013).

1.3.3.4 Other P2X4 modulators

Divalent cations, including zinc (Zn^{2+}), magnesium (Mg^{2+}), copper (Cu^{2+}), cadmium (Cd^{2+}), and mercury (Hg^{2+}), were reported to modulate P2X4 receptors. For example, zinc and cadmium ions potentiated

P2X4 receptor activity, while copper and mercury ions inhibited P2X4-mediated ATP currents (Acuña-Castillo et al., 2002). Magnesium ions were reported to play a role in stabilising intersubunit interactions, favouring the active state of P2X4 receptors. Exchanging magnesium ions for potassium ions, which have higher extracellular physiological concentrations, permitted channel closing, most likely due to weaker subunit coupling (Immadisetty et al., 2022).

High concentrations of protons make the cellular environment acidic ($\text{pH} < 6.5$), which negatively modulates P2X4 receptor activity, whereas a more basic pH, above physiological pH levels, potentiates P2X4 channel activity (Qureshi et al., 2007). Since intracellular P2X4 receptors are predominantly located in acidic lysosomes, pH has been proposed as a major regulator of lysosomal P2X4 receptor activity (Frick & Murrell-Lagnado, 2019).

1.3.4 Physiological roles of the P2X4 receptor

P2X4 receptors are ubiquitously expressed throughout the body, which explains their involvement in many biological processes, including maintenance of vascular tone, regulation of inflammation, and modulation of pain transmission (Fig 1.8; Suurväli et al., 2017). It is present in neurons and neuroendocrine cells from the central and peripheral nervous systems, spinal cord microglia, vascular endothelial cells, vascular smooth muscle cells, cardiomyocytes, epithelial cells lining the airways and lungs, hepatocytes, and liver Kupffer cells (Yang & Liang, 2012; Suurväli et al., 2017). In addition, it is not only expressed at the cellular membrane but also intracellularly in lysosomes and other acidic compartments, as we have seen in section 1.3.2.1 (Fig 1.7; Qureshi et al., 2007; Xu et al., 2014).

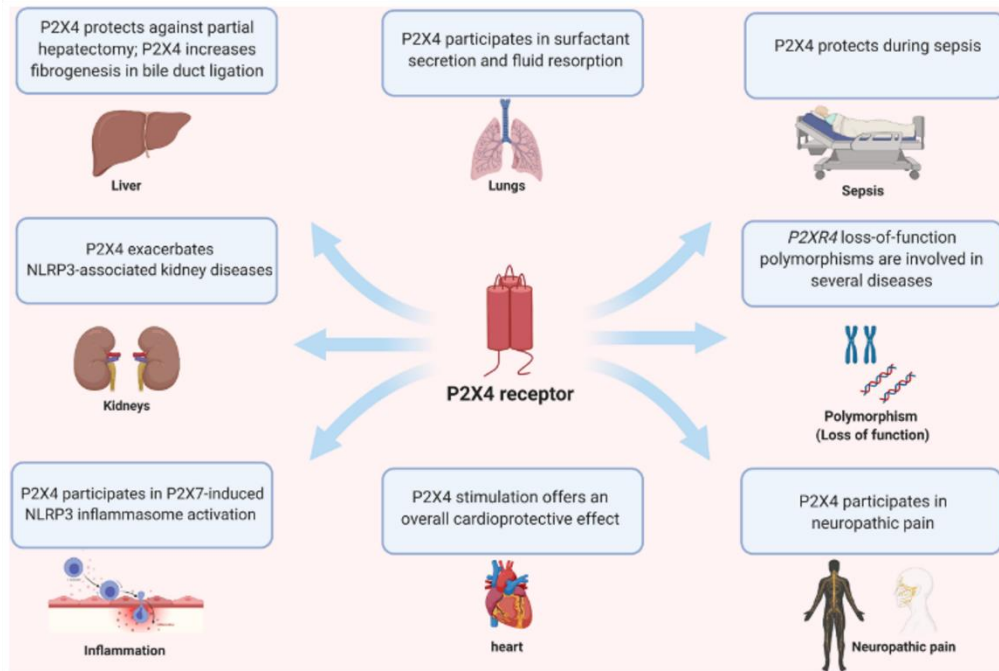


Fig 1.8. Pleiotropic effects of P2X4 receptor-mediated signalling. P2X4 receptors are ubiquitously expressed throughout the body and contribute to ATP-mediated neurotransmission in perisynaptic regions of hippocampal neurons, neuroinflammation in microglial cells, and other inflammatory responses via inflammasome activation. P2X4 receptors can also modulate normal function and disease development in various organs, including the heart, lungs, kidneys, and liver. Image obtained from Kanellopoulos et al., 2021.

1.3.4.1 Nervous system

The essence of neuronal function is to generate outputs in response to electric stimuli. Synapses are the primary site of ATP consumption. ATP mediates fast excitatory synaptic transmission in some regions of the Central Nervous System (CNS) and cell-to-cell communication in the peripheral nervous system through the activation of P2X receptors (Burnstock & Kennedy, 2011). P2X2 and P2X3 receptors are widely expressed in the CNS and account for practically all sensory nerve excitation mediated by ATP (Lewis et al., 1995; Cockayne et al., 2005). Nonetheless, there is some evidence that P2X4 receptors are widely expressed in neurons, neurosecretory cells, and microglia of the central and peripheral nervous systems, where they also play a role in ATP-mediated synapses (Rubio & Soto, 2001; Burnstock & Kennedy, 2011).

A fascinating property of the mammalian brain is its synaptic plasticity, the capacity of the brain to change and adapt to new information. Synaptic plasticity refers to the strengthening or weakening of pre-existing synapses in response to increases and decreases in their activity, respectively. P2X4 receptors expressed in microglia may be involved in synaptic plasticity by releasing substances that can directly act on presynaptic terminals to regulate neurotransmitter release, namely ATP. In this way, P2X4 receptor knockout (KO) mice produced significantly lower calcium responses upon repeated stimulation with ATP in mice hippocampal neurons, which was further confirmed when ivermectin increased ATP-evoked calcium responses in wild-type mice (George et al., 2016). Also in mice hippocampal neurons, P2X4 receptors were found to be concentrated at the perisynaptic region of presynaptic and postsynaptic membranes (Rubio & Soto, 2001). Furthermore, bacterial lipopolysaccharides (LPS)-stimulated microglia induced release of ATP and brain-derived neurotrophic factor (BDNF), which triggered presynaptic P2X4 receptors and modulated synaptic plasticity in mice hippocampal neurons (George et al., 2016).

Neuropathic pain is a common consequence of damage to the nervous system, and its causes are divided into four categories: disease, injury, infection, and loss of limb. It is described as persistent pain arising from a modification of pain processing pathways in the spinal cord. It is also known as allodynia, hypersensitivity, or chronic pain. ATP can act on the P2X4 receptors expressed in neurons during pain signalling, highlighting its potential as a therapeutic target to alleviate neuropathic pain (Tsuda et al., 2013; Stokes et al., 2017). After peripheral nerve injury, damaged sensory neurons cause the activation of microglia in the spinal cord, which change their morphology and gene expression and increase in cell number. These activated microglia upregulate gene expression of P2X4 receptors. Subsequent activation of P2X4 receptors by extracellular ATP contributes to the production and release of cytokines and other inflammatory mediators, such as brain-derived neurotrophic factor (BDNF). The release of BDNF causes an altered transmembrane anion gradient in sensory neurons through the downregulation of the neuronal potassium-chloride co-transporter 2 (KCC2). The increase of intracellular chloride anions induces membrane depolarisation of these sensory neurons and shifts the GABA-mediated responses from inhibition to excitation, ultimately resulting in hyperexcitability of these neurons and, thus, triggering neuropathic pain. These results were also proven in P2X4 receptor KO mice, which

showed reduced or no pain-related behaviours after peripheral nerve injury compared to wild-type mice (Tsuda et al., 2013; Stokes et al., 2017). Thus, P2X4 receptors play a central role in neuropathic pain caused by injury to peripheral nerves.

Recent studies propose that P2X4 receptors are involved in the development of neuroinflammatory and neurodegenerative diseases, like multiple sclerosis, Parkinson's disease, and Alzheimer's disease. All of them are demyelinating diseases in which myelin, the protective covering surrounding nerve fibres, breaks down, nerves and nerve fibres become frayed, and ultimately neurons die. Potentiation of P2X4 receptors by ivermectin improved oligodendrocyte-mediated remyelination of neurons in a mouse model of multiple sclerosis (Zabala et al., 2018). Similarly, in a dopamine-depletion mouse model of Parkinson's disease, the potentiation of P2X4 receptors by ivermectin enhanced motor behaviour in the presence of levodopa, a therapeutic agent used for the treatment of Parkinson's disease, whereas P2X4 receptor KO mice exhibited an attenuated levodopa-induced motor behaviour (Khoja et al., 2016). Future advances in the selective stimulation of P2X4 receptors to modulate neuroinflammatory responses and promote the repair of myelin damage seem promising routes to develop drugs for the treatment of neurodegenerative diseases.

Excessive alcohol use can cause neurological disorders, which can be mild, moderate, or severe. Lasting changes in the brain caused by alcohol misuse perpetuate alcohol use disorder and make individuals vulnerable to relapse. Some studies demonstrated that P2X4 is involved in alcohol use disorder (Gofman et al., 2014; Lowe et al., 2020). Excessive alcohol use was linked to enhanced neuroinflammation, upregulating P2X4 receptors and promoting microglial activation, which induced the release of pro-inflammatory mediators and peripheral macrophage recruitment into the CNS in a mouse model of chronic alcohol consumption (Gofman et al., 2014; Lowe et al., 2020). Hence, P2X4 receptors represent a possible target for the prevention of alcohol use disorder (Franklin et al., 2014).

1.3.4.2 Cardiovascular system

Cardiovascular disease (CVD) is the leading cause of death globally (about 30%). CVD refers to all illnesses that affect the heart and blood vessels. P2X4 receptors are involved in endothelium-dependent changes in vascular tone and blood flow, emphasising its potential as a therapeutic target for the treatment of hypertension, atherosclerosis, and other CVD-related symptoms.

Shear stress regulates P2X4 receptor expression in vascular endothelial cells, which might play a central role in modulating cellular responses to changes in blood flow (Yamamoto et al., 2000a). In vascular endothelial cells, ATP-mediated activation of P2X4 receptors ultimately causes an increase in intracellular calcium levels, which stimulates the activity of the endothelial nitric oxide synthase (eNOS), leading to nitric oxide (NO) production and its release to the extracellular space. Nitric oxide can act at membrane receptors expressed on neighbouring smooth muscle cells resulting in a reduction of intracellular calcium levels. In consequence, the vascular smooth muscle cells relax, causing vasodilation. This mechanism was confirmed in P2X4 receptor KO mice, which not only displayed reduced quantities of NO and higher blood pressure phenotypes but also showed markedly impaired

flow-dependent vascular remodelling compared to wild-type mice (Yamamoto et al., 2006). Additionally, as mentioned in section 1.3.2.2, a P2X4 receptor loss of function SNP led to decreased ATP binding and was associated with high blood pressure in humans (Stokes et al., 2011). The role of P2X4 receptors in maintaining flow-induced vasodilatation is vital in physiological vascular homeostasis.

Other studies reported that extracellular ATP could cause a modest increase in contractility and cytosolic calcium levels in cardiomyocytes. In transgenic mice overexpressing cardiac P2X4 receptors, this contractility was enhanced without causing cardiac hypertrophy or failure. The proposed mechanism was that P2X4-mediated intracellular calcium increase might activate calcium-dependent proteins in close vicinity of the receptor, possibly eNOS, which would increase NO production and disperse the amount of calcium surrounding the sarcoplasmic reticulum, enhancing its loading and, thus, cardiac function in these mice (Yang & Liang, 2012). Later studies by the same group determined that P2X4-mediated intracellular calcium increase induced eNOS activity and confirmed a cardioprotective role for P2X4 receptors during heart failure in conditional cardiac-specific P2X4 receptor KO mice models (Yang et al., 2014).

1.3.4.3 Respiratory system

P2X4 receptors are expressed in epithelial cells lining the airways and lungs. In particular, P2X4 receptors are expressed in alveoli which are found at the end of bronchioles and are responsible for gas exchange (Miklavc et al., 2013). There are two main alveolar cell types: alveolar type I and alveolar type II cells. Alveolar type I cells cover the majority of the alveolar surface and are responsible for efficient gas exchange between the alveolus and the pulmonary capillaries (Wirsching et al., 2020). Whereas alveolar type II cells synthesise, store, and release pulmonary surfactant into the alveolar lumen, reducing surface tension and optimising the conditions for gas exchange (Wirsching et al., 2020). P2X4 receptors are expressed at the cell membrane of alveolar type II cells and intracellularly in their lamellar bodies (Miklavc et al., 2013). Lamellar bodies are large acidic organelles that store pulmonary surfactants. P2X4 receptors expressed on these lamellar bodies promote exocytosis, facilitating surfactant and ATP release in alveolar type II cells. The released ATP can then act in an autocrine manner and activate P2X4 receptors increasing intracellular calcium levels (Fois et al., 2018a). Fusion-activated calcium entry can promote exocytosis of other lamellar bodies and fluid reabsorption, which helps maintain an optimal environment for efficient gas exchange and lung function (Fois et al., 2018b; Kanellopoulos et al., 2021).

P2X4 receptor expression is elevated in asthmatic patients and in the asthmatic disease mouse model. Asthma is a chronic lung condition that occasionally causes breathing problems. Asthma is caused by airway inflammation upon exposure to allergens or smoke. Selective blocking of P2X4 receptors alleviated many asthmatic symptoms (e.g., eosinophilia, inflammation, and mucus production; Chen et al., 2016; Zech et al., 2016). In contrast, P2X4 receptor stimulation enhanced the allergic reaction in an allergen-induced airway inflammation mice model (Chen et al., 2016; Zech et al., 2016). Consequently, P2X4 receptors can be therapeutic drug targets against asthma and other airway diseases.

1.3.4.4 Immune system

Inflammation is a protective immune response to harmful stimuli, such as pathogens or cell death, and is tightly regulated. Insufficient inflammation can lead to persistent infection of pathogens, while excessive inflammation can cause chronic or systemic inflammatory diseases (e.g., rheumatoid arthritis (RA) and multiple sclerosis (MS)). Pathogen-associated molecular patterns (PAMPs), derived from invading pathogens, and danger-associated molecular patterns (DAMPs), induced as a result of endogenous stress, are recognised by pattern-recognition receptors (PRRs). Activation of PRRs by PAMPs or DAMPs triggers downstream signalling cascades and initiates an immune response. Inflammasomes are clusters of cytoplasmic proteins that assemble in the cytosol after detecting stress or infection threats. P2X4 and P2X7 receptors activate NLRP3 (NLR family pyrin domain containing 3) inflammasomes (Dunton et al., 2018; Han et al., 2020). NLRP3 inflammasomes require a PAMP signal, like bacterial lipopolysaccharides (LPS) and a DAMP signal, such as extracellular ATP, for activation. NLRP3 activation leads to transcription of NF- κ B (nuclear factor κ -light-chain-enhancer of activated B cells) and upregulation of genes encoding pro-inflammatory molecules and other proteins for inflammasome assembly. Maturation and secretion of these pro-inflammatory cytokines and chemokines (i.e., IL-1 β and IL-18) result in pyroptosis, an inflammatory form of cell death (Kanellopoulos et al., 2021).

Some implications of NLRP3 activation are exacerbated ischemic acute kidney injury (AKI) and the development of rheumatoid arthritis (RA). Acute kidney injury is a major healthcare challenge as there are no effective preventive or curative measures for its treatment. AKI is frequently developed after renal ischemia and reperfusion injury in patients undergoing a cardiac, vascular, or liver transplant (Han et al., 2020). In this study, P2X4-deficient mice showed significantly attenuated NLRP3 inflammasome signalling after renal ischemia and reperfusion injury compared to wild-type controls (Han et al., 2020). Similarly, rheumatoid arthritis is another chronic inflammatory response caused by severe joint damage. In both human patients and in the RA mouse model, downregulation of P2X4 receptors by antisense RNA suppressed the production of pro-inflammatory cytokines, improving joint inflammation and reducing joint destruction (Li et al., 2014). Therefore, limiting the inflammatory response by selectively blocking P2X4 receptors could be a potential therapy in clinical ischemic AKI and RA.

The most extreme response of the immune system to an infection is sepsis. Sepsis is a life-threatening medical emergency and occurs when an existing infection triggers an inflammatory chain reaction throughout the body. The extracellular levels of ATP increase during sepsis, acting on P2X4 receptors and initiating an immune response against bacterial antigens. In chronic inflammation and autoimmune disease, increased P2X4 receptor activity aggravates tissue damage, as described above. However, the potentiation of P2X4 receptor activity protected against organ damage and improved survival rates in a mouse model of sepsis (Csóka et al., 2018).

1.3.4.5 Digestive system

The liver has a unique capacity among other organs to regenerate itself after damage. A liver can regrow to its average size even after removing up to 90% of it. Hepatectomy is a surgical procedure performed to treat various liver diseases, such as the removal of benign and malignant hepatic tumours, intrahepatic stones, liver infection, and cirrhosis. This operation is incredibly challenging because of the liver's unique anatomic architecture and causes several postoperative complications, including fever, infections, haemorrhage, bile leakage, and even liver failure (Jin et al., 2013). Extracellular ATP levels rise in blood and bile and contribute to liver regeneration after partial hepatectomy in rats and mice (Gonzales et al., 2010; Besnard et al., 2016). P2X4 receptors are expressed in hepatocytes and Kupffer cells, the resident macrophages of the liver. These P2X4 receptors are fundamental for the maintenance of liver functions and may be the target of released ATP upon hepatectomy procedures to induce liver regeneration (Gonzales et al., 2010; Besnard et al., 2016). P2X4 receptor KO mice displayed slow liver regeneration, hepatocyte necrosis, and impaired biliary system function after hepatectomy (Besnard et al., 2016). P2X4 receptor KO mice also showed reduced release of ATP and other lysosomal enzymes (Besnard et al., 2016). So, P2X4 receptors contribute to liver regeneration and biliary homeostasis during postsurgical liver regeneration.

As mentioned in section 1.3.4.1, P2X4 receptors are associated with alcohol use disorder. Excessive alcohol drinking not only causes damage to the brain but also affects the liver and can lead to alcohol-related liver disease and, ultimately, cirrhosis. Selective inhibition of P2X4 receptors alleviated alcohol-induced inflammation in mice bone marrow-derived macrophage (BMDM) cells and in the livers of fatty liver disease mice models (Xia et al., 2022). In other words, P2X4 receptors may induce the activation of NLRP3 inflammasomes, exacerbating inflammatory responses, while inhibiting P2X4 expression could effectively block alcohol-related liver disease.

1.4 Aim and objectives

Over the past fifteen years, there has been a growing interest in how P2X subunits arrange to form functional channels. Like other ligand-gated channels, P2X receptors can form by homo- or hetero-oligomeric subunit assembly (North, 2002). To date, six P2X purinergic homotrimeric receptors have been described in humans. The human P2X6 homotrimer is considered a silent receptor, as ATP evoked no currents in *Xenopus laevis* oocytes and HEK293 cells (North, 2002). Yet little is known about the possible existence of functional human P2X heteromers. In 1999, a biochemical study predicted eleven possible P2X heteromers using co-immunoprecipitation assays (Torres et al., 1999). However, only seven have been functionally tested, and just the P2X2/3 heteromer has been fully established and confirmed in human cell models (Saul et al., 2013; Burnstock, 2018). An in-depth discussion about P2X receptor heteromerisation and their association with other ion channels and proteins is provided in Chapter 4 (section 4.1) of this thesis.

Different approaches have been taken to probe the existence of P2X heteromers, but the majority of evidence was gained through electrophysiological studies using recombinant and native rodent models. Thus, there is a significant research gap regarding which human P2X receptor subtypes can form functional heteromers and if so, what are their subunit stoichiometries and physiological relevance. As with other ligand-gated ion channels, the subunit composition of P2X receptors defines not only their pharmacological properties but also their functional roles in physiological and pathophysiological processes, which can ultimately lead to the development of more selective therapeutics.

As mentioned above, the research community exclusively recognises the P2X2/3 heteromeric receptor because of its distinct pharmacological profile, resulting from the combination of P2X2 and P2X3 homomeric channel properties (Lewis et al., 1995). In 2006, Wilkinson et al. proposed and used the ‘dead receptor’ hypothesis to find out the subunit stoichiometry of the rat P2X2/3 heterotrimeric receptor (Wilkinson et al., 2006). Their hypothesis was based on the concept that at least two agonist binding sites are required for P2X channel activation (Jiang et al., 2003), so the occupancy of only one binding site would not induce channel opening. This theory was later confirmed when the X-ray crystal structures of the zebrafish P2X4 receptor (zfP2X4) in the closed and ATP-bound states were released (Kawate et al., 2009; Hattori & Gouaux, 2012), and the ATP binding site was scrutinised by site-directed mutagenesis and electrophysiological analysis (Chataigneau et al., 2013). Lysines at positions K72 and K316 (zebrafish P2X4 numbering) were identified as critical residues for ATP molecule recognition and binding, and such role appeared to be highly conserved in the P2X receptor evolution (Jiang et al., 2000; Chataigneau et al., 2013; Fountain et al., 2007). Thus, we sought to use double lysine-to-alanine non-functional P2X mutants as ‘dead receptor’ tools to probe for human P2X4 heteromeric assembly. More details on the dead receptor hypothesis are described in section 3.1 of Chapter 3.

As described in section 1.3 of this chapter, the human P2X4 receptor is expressed primarily in cells and tissues of the vascular, immune, and central nervous systems. It is involved in physiological and pathophysiological processes (e.g., maintenance of blood pressure, modulation of pain signalling, and regulation of inflammation). Hence, the human P2X4 receptor is a promising drug target for treating neuropathic pain and cardiovascular disease. Understanding its stoichiometry and protein assembly is key for the development of more selective therapeutics.

Thus, the major aim of this thesis is to gain biochemical and functional evidence of which human P2X subunits can interact with human P2X4 subunits. The following objectives were set:

1. To provide a reliable and reproducible method for the study of human P2X4 subunit assembly. Human astrocytoma cells were used as a cell line model and human P2X double mutant subunits as ‘dead receptor’ tools to investigate P2X4 receptor function by intracellular calcium mobilisation measurements and to assess protein expression levels and physical protein-protein interactions by Western blotting and co-immunoprecipitation assays.
2. To systematically examine functional interactions of the human P2X4 wild-type subunit with other human P2X subunits following the proposed approach, contrasting potential candidates with current literature views.

2 Materials and methods

2.1 Materials and reagents

All reagents used throughout this study were purchased from ThermoFisher Scientific (Loughborough, UK), also the distributors for Applied Biosystems, Corning, Fisher Scientific, Gibco, and Invitrogen. Reagents purchased from other suppliers will be detailed throughout this chapter. Lists of commonly used drugs are provided in the following Tables 2.1, 2.2, and 2.3.

Table 2.1. List of exogenous nucleotides and ligands.

Compound	Supplier	Concentration (μ M)	Vehicle	Reference
ATP	Abcam	0.01–300	Water	Burnstock, 2007
$\alpha\beta$ -MeATP	Sigma	0.01–100	Water	Jones et al., 2000
2-MeSATP	Tocris	0.01–100	Water	Garcia-Guzman et al., 1997
BzATP	Sigma	0.01–100	Water	Abdelrahman et al., 2017
AP4A	Sigma	0.01–300	Water	Abdelrahman et al., 2017
ATP- γ -S	Tocris	0.01–300	Water	Michel et al., 1997
γ -imidoATP	Sigma	0.01–100	Water	Abdelrahman et al., 2017
CTP	Sigma	0.01–100	Water	Garcia-Guzman et al., 1997
Carbachol	Sigma	100	Water	Burnett et al. 2011

Water, deionised water.

Table 2.2. List of broad-spectrum purinergic receptor antagonists.

Compound	Supplier	Concentration (μ M)	Vehicle	Reference
PPADS	Sigma	0.1–100	Water	Jones et al., 2000
Suramin	Sigma	0.01–100	Water	Jones et al., 2000
TNP-ATP	Tocris	0.1–100	Water	Abdelrahman et al., 2017

Water, deionised water.

Table 2.3. List of human P2X4 selective antagonists.

Compound	Supplier	Concentration (μ M)	Vehicle	Reference
BAY-1797	Cambridge Biosciences	0.03–10	DMSO	Werner et al., 2019
5-BDBD	Tocris	0.01–30	DMSO	Bidula et al., 2021
BX-430	Tocris	0.03–30	DMSO	Ase et al., 2015
PSB-12062	Sigma	0.01–20	DMSO	Hernandez-Olmos et al., 2012
Taspine	Santa Cruz Biotechnology	0.01–30	DMSO	Bin-Nadzirin et al., 2021

DMSO, dimethyl sulfoxide.

2.2 Cell culture

All cell culture techniques were performed under strict sterile conditions in a Class II Microbiology Safety Cabinet.

2.2.1 Human 1321N1 astrocytoma cells

1321N1 is a human astrocytoma cell line isolated in 1972 as a sub-clone of the 1181N1 cell line, which in turn was isolated from the parent line U-118 MG, a cell line derived from a human glioma (Macintyre et al., 1972). 1321N1 cells are a suitable model for studies of neurological diseases. 1321N1 cells have an astral-like morphology, grow in adhesion, and form interconnections as the cell density increases. This cell line was available in-house and will be referred to as the 1321N1 parental astrocytoma cell line throughout this study.

Another human 1321N1 astrocytoma cell line stably expressing the human P2X4 receptor was also available in the laboratory. This cell line was generated from stable transfection of the human P2X4 receptor gene into the 1321N1 parental astrocytoma cell line. This cell line will be denoted as the human P2X4 stable astrocytoma cell line throughout this study.

2.2.1.1 General maintenance and cell passage

The 1321N1 parental and human P2X4 stable astrocytoma cell lines were cultured in Dulbecco's Modified Eagle Media containing high glucose (4.5g/L) and L-Glutamine (DMEM; Lonza, UK), supplemented with 10% foetal bovine serum (FBS; HyCloneTM, UK) and 1% penicillin/streptomycin antibiotic solution containing 50U/mL of Penicillin and 50µg/mL of Streptomycin (Pen/Strep). This combination will be referred to as DMEM complete growth media.

All cells were cultured under rigorous sterile conditions and maintained in 75cm² uncoated tissue culture flasks (T75) or multi-well plates in a humidified environment at 37°C in the presence of 5% carbon dioxide (CO₂). These conditions will be stated as cell culture conditions throughout this report. Cells were sub-cultured when approximately 70-80% confluence was reached. Before splitting the cells, cells were briefly rinsed twice with sterile phosphate-buffered saline (PBS; Lonza, UK) to remove non-adherent cells, debris, and serum traces. Then, cells were dispersed from the bottom of the flask using Trypsin-EDTA (Lonza, UK) and collected at approximately 260x g for 5 minutes. The cell pellet was resuspended in DMEM complete growth media and counted using a Neubauer haemocytometer. Cells were then diluted into new T75 culture vessels at a density of approximately 2x10⁴ cells/mL for cell line maintenance or seeded for experimental use.

2.2.1.2 Cryopreservation and thawing

First or early passage 1321N1 parental and human P2X4 stable astrocytoma cells that were not required for immediate experiments were stored in liquid nitrogen for future use. This was attained by detaching cells from their culture flasks using Trypsin-EDTA and pelleting them at 260x g for 5 minutes. Human 1321N1 astrocytoma cells were then resuspended in cryopreservation media, which consisted of 63%

[v/v] DMEM, 27% [v/v] FBS, and 10% [v/v] DMSO (dimethyl sulfoxide; Sigma-Aldrich, UK). Cells were immediately transferred to cryovials (Nunc, Sigma-Aldrich, UK) at an approximate density of 1×10^6 cells/mL. The cryovials were then placed in a Mr Frosty™ freezing container containing isopropanol to achieve a cooling rate of 1°C/min while stored at -80°C overnight (O/N). Finally, the cryovials were transferred to a liquid nitrogen tank at -196°C for long-term storage.

When required for experimental use, cryovials were taken from the liquid nitrogen tank and kept in dry ice before rapid thawing in a 37°C water bath. The cryovials were decontaminated by spraying with 70% ethanol, and from this point, all operations were carried out under strict aseptic conditions. The defrosted cells were immediately diluted in DMEM complete growth media and centrifuged at 260x g for 5 minutes to remove the freezing media. The pellet was resuspended in fresh culture media and placed in a T75 culture flask. Cells were grown in cell culture conditions until 70-80% confluence was reached, at which point, cell passage was performed as aforementioned.

2.3 DNA constructs

Human P2X receptor pcDNA 3.1 (+) constructs were purchased from Biomatik (Ontario, Canada) containing epitope tags in the carboxy-terminus (C-term) immediately upstream of the stop codon 'TGA' or 'TAA'. The oligopeptide sequences used were 'EYMPME' for EE, 'DYKDDDDK' for FLAG, and 'YPYDVPDYA' for HA epitopes. All sequences were optimised for high expression in mammalian cells according to the human codon usage bias and included the Kozak consensus sequence 'GCCACC' right before the start codon 'ATG' to encourage the translation and increase the expression of the protein of interest. The cloning of each gene was done at the 5' EcoRI and 3' Xhol restriction sites 'GAATT' and 'CTCGAG', respectively, which were located within the Multiple Cloning Site (MCS) of the pcDNA 3.1 (+) backbone vector. The human P2X1-7 receptor nucleotide and peptide sequences can be found in Annex 1.A and the oligonucleotide and oligopeptide sequences of each epitope tag used can be found in Annex 1.B. We also purchased a pcDNA 3.1 (+) plasmid containing the $\alpha 7$ nicotinic acetylcholine receptor ($\alpha 7$ nAChR) gene insert from Addgene (Teddington, UK). The manufacturer did not provide cloning information. A list of all DNA constructs used can be found in Table 2.4.

The structure of a pcDNA 3.1 (+) vector is shown in Figure 2.1. Some common features include: i) human cytomegalovirus (CMV) immediate early promoter for high recombinant protein expression in mammalian cells, ii) T7 bacteriophage promoter for mRNA synthesis in bacterial cells, iii) the Multiple Cloning Site (MCS) which contains the gene of interest, iv) bovine growth hormone (bGH) polyadenylation signal, v) simian virus 40 (SV40) mammalian promoter with its origin of replication (ori) and polyadenylation signal, vi) aminoglycoside phosphotransferase mammalian selection gene which confers resistance to neomycin (NeoR), kanamycin (KanR), and G418 (Geneticin), vii) β -lactamase bacterial selection gene (bla) and promoter which confer resistance to ampicillin and other related antibiotics, and viii) a pcDNA 3.1 bacterial origin of replication (ori).

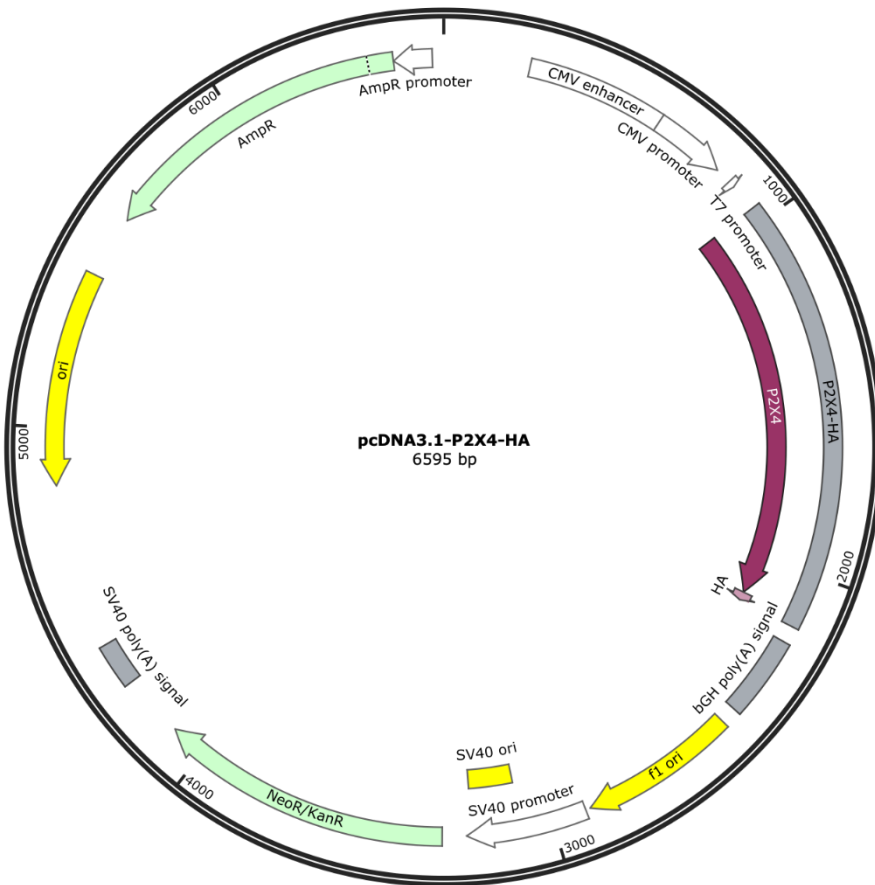


Fig 2.1. Map of a pcDNA 3.1 (+) vector encoding the human P2X4 gene with a C-terminus HA epitope. This pcDNA 3.1 vector contains a bacterial origin of replication (ori) and a simian virus 40 (SV40) mammalian origin of replication. The Human cytomegalovirus (CMV) immediate early promoter and the T7 bacteriophage promoter allow high expression of the gene of interest (human P2X4 HA-tagged) in mammalian and bacterial cells, respectively. The bovine growth hormone polyadenylation signal (bGH poly(A)) and the SV40 polyadenylation signal terminate gene transcription and ensure mRNA stability. The aminoglycoside phosphotransferase gene confers resistance to neomycin (NeoR), kanamycin (KanR), and G418 (Geneticin) and can be used for mammalian selection. The β -lactamase bacterial selection gene (bla) confers resistance to ampicillin (AmpR) and other related antibiotics. The bla promoter is encoded upstream of the AmpR gene. The f1 bacteriophage ori is a benign remnant of the original plasmid. The total length of the pcDNA 3.1 (+) plasmid encoding the human P2X4 HA-tagged gene is 6595 base pairs (bp). Image produced using the SnapGene software.

Table 2.4. List of gene constructs purchased.

Gene insert name	Gene insert size (bp)	C-term epitope	Bacterial resistance	Mammalian selection	Manufacturer
Empty vector	–	–	Ampicillin	G418	Addgene
CHRNA7	1511	–	Ampicillin	G418	Biomatik
hP2X1 WT	1218	EE	Ampicillin	G418	Biomatik
hP2X2 WT	1434	EE	Ampicillin	G418	Biomatik
hP2X3 WT	1212	EE	Ampicillin	G418	Biomatik
hP2X4 WT	1185	EE	Ampicillin	G418	Biomatik
hP2X5 WT	1353	EE	Ampicillin	G418	Biomatik
hP2X6 WT	1344	EE	Ampicillin	G418	Biomatik
hP2X7 WT	1806	EE	Ampicillin	G418	Biomatik
hP2X1 WT	1224	FLAG	Ampicillin	G418	Biomatik
hP2X2 WT	1440	FLAG	Ampicillin	G418	Biomatik
hP2X3 WT	1218	FLAG	Ampicillin	G418	Biomatik
hP2X4 WT	1191	FLAG	Ampicillin	G418	Biomatik
hP2X5 WT	1359	FLAG	Ampicillin	G418	Biomatik
hP2X6 WT	1350	FLAG	Ampicillin	G418	Biomatik
hP2X7 WT	1812	FLAG	Ampicillin	G418	Biomatik
hP2X1 WT	1227	HA	Ampicillin	G418	Biomatik
hP2X2 WT	1443	HA	Ampicillin	G418	Biomatik
hP2X3 WT	1221	HA	Ampicillin	G418	Biomatik
hP2X4 WT	1194	HA	Ampicillin	G418	Biomatik
hP2X5 WT	1362	HA	Ampicillin	G418	Biomatik
hP2X6 WT	1353	HA	Ampicillin	G418	Biomatik
hP2X7 WT	1815	HA	Ampicillin	G418	Biomatik

bp, base pair.

2.3.1 Generation of P2X double mutant receptors

Wild-type (WT) human P2X1-7 constructs containing a C-term FLAG tag were used as DNA templates to generate the required double lysine-to-alanine non-functional mutants. Lysine (K) to alanine (A) substitutions were introduced by mutagenic Polymerase Chain Reaction (PCR) using the Q5 site-directed mutagenesis kit (New England BioLabs, UK) for rapid and site-specific DNA mutagenesis.

2.3.1.1 Primer design

Lysine (K) to alanine (A) substitutions were introduced in corresponding positions K67 and K313 (numbering referred to the human P2X4 WT protein sequence) in all human P2X1-7 WT constructs. These substitutions were created by incorporating an ‘AAG’ (coding for K) to ‘GCC’ (coding for A) mismatch in the centre of the mutagenic forward primer, including at least ten complementary nucleotides on the 3’ end of the mutation. The reverse primer was designed so that the 5’ ends of the two primers annealed back-to-back and its sequence was 100% complementary to the complementary strand. Mutagenic primer sequences were constructed using the New England BioLabs online design software, NEBaseChanger™ (NEBaseChanger.neb.com). All primers were acquired in a lyophilised form and were reconstituted at 100µM in molecular biology-grade water (HyClone™, UK). For experimental use, primers were further diluted to 10µM. 100µM primer stocks and 10µM working solutions were stored at -20°C until required. The primer sequences used and the specific amino acid and codon positions for each receptor subtype can be found in Table 2.5.

2.3.1.2 Polymerase Chain Reaction (PCR)

Mutagenic PCRs were carried out to obtain the human P2X1-7 double mutant receptors. Firstly, C-term FLAG-tagged WT DNA sequences were used as an initial template to produce a single K67A mutant DNA for each human P2X receptor subtype (numbering referred to the human P2X4 WT peptide sequence). Then, the K67A single mutant DNA was used as a template to introduce the second K313A mutation (also corresponding to the human P2X4 WT protein sequence enumeration), thus generating all human P2X1-7 double mutant constructs. Each reaction was performed in a thin-walled PCR tube containing: 1X Q5 Hot Start High-Fidelity 2X Master Mix, 0.5µM of corresponding forward and reverse primers, 20ng of template DNA, and molecular biology grade water to get a total volume of 25µL. The Q5 Hot Start High-Fidelity 2X Master Mix contained the polymerase buffer (not detailed by the manufacturer), deoxynucleoside triphosphates (dNTPs), magnesium ions (Mg^{2+}), and the Q5 Hot Start High-Fidelity DNA Polymerase. PCR reactions were performed in a thermocycler (Veriti, Applied Biosystems, UK) with the following thermal profile: Initial denaturation at 98°C for 30 seconds, followed by 25 cycles of denaturation at 98°C for 10 seconds, annealing at different temperature conditions according to each human P2X subtype for 30 seconds, and extension at 72°C for 5 minutes to allow robust amplification of the DNA, and finalised with 2 minutes at 72°C for the final extension. The annealing temperatures for each set of primers are specified in Table 2.5. The extension time was calculated according to the DNA polymerase reading speed of 30 seconds/Kb and approximately 7Kb of total plasmid length. All PCR products obtained were used immediately or stored at 4°C until required.

Table 2.5. Numbering of human P2X1-7 lysine (K) to alanine (A) substitutions and their respective AAG codon positions (bp). Detailed sequences for each mutagenic primer set and the annealing temperatures used for PCR.

Mutant	AAG (bp)	Primer sequence (5' – 3')	T _a (°C)
hP2X1 [K68A]	214 – 216	F CGTGTCTGTGgccCTCAAGGGACTCG R CTGCTAACGAGGCCGCTA	50
hP2X1 [K309A]	937 – 939	F CCACCTCTTCgccGTGTTCGGCATTAG R CGGTAGTTGTTCCGTT	60
hP2X2 [K81A]	253 – 255	F TATTATCACAgccGTGAAGGGATTACAACATCTGAGCAC R GAAGACTCAGGCCGGTC	60
hP2X2 [K319A]	967 – 969	F CACACTGATCgccGCTTACGGCATTAGAATTG R CGTGTGGTGGTTCCGTTA	60
hP2X3 [K63A]	199 – 201	F TGTGGTGACAgccGTGAAGGGCAG R GAGGACTCAATAGCGGTG	50
hP2X3 [K299A]	907 – 909	F CACACTGCTGgccGCTTCGGAATTAGATTGACG R CGGTACTCGCTGCCGTTC	60
hP2X4 [K67A]	211 – 213	F CGTGACCACAgccGTGAAGGGAGTGG R CTAGACACCACGGAGTCG	50
hP2X4 [K313A]	949 – 951	F CACACTGATTgccGCTTACGGATTAGATTGACATTATTGTG R CGCTGCTCGTTCCAGCG	60
hP2X5 [K69A]	217 – 219	F CGTGATCACAgccGTGAAGGGCGTG R GCGGACTGGAGAGATGTG	60
hP2X5 [K314A]	952 – 954	F CACACTCATGgccGCTTACGGATTAGATTGACG R CGGAACCTCCACTCCAGCG	60
hP2X6 [K78A]	244 – 246	F TATTATTACAgccCTGAAGGGGGTGTCCG R GAGAACTGTGGCTCCAGG	50
hP2X6 [K315A]	955 – 957	F AACACTCCTGgccCTGTACGGCATTAGATTG R CTAGCCTCCACTCCTGGC	60
hP2X7 [K64A]	202 – 204	F CGTGCACACAgccGTGAAGGGATC R CTAGAAATCACTGGCTCC	50
hP2X7 [K311A]	943 – 945	F CACACTGATTgccGTGTTCGGAATTAGGTT R CGCTTCTCCACGTTGTT	60

bp, base pair.

2.3.1.3 Kinase, Ligase, DpnI treatment and enrichment

The amplified product was then treated with a unique enzyme mix containing kinase, ligase, and DpnI (KLD) enzymes. This combination allowed efficient phosphorylation of linear DNA, rapid circularisation of the PCR product, and removal of the plasmid template DNA by DpnI digestion of adenine-methylated 'GATC' sites. 1µL of PCR product was mixed with 1X of 2X KLD Reaction Buffer, 1X of 10X KLD Enzyme Mix, and molecular grade water to achieve a total volume of 10µL. The mixture was incubated for 30 minutes at room temperature (RT) to obtain the mutated plasmid.

2.4 High-efficiency transformation of plasmid

Following KLD treatment, the enriched product was transformed into competent *Escherichia coli* (*E. coli*) cells for DNA extraction and sequence verification and long-term plasmid storage. 50µL of high-efficiency competent *E. coli* cells (strain number C2987H; New England BioLabs, UK) were thawed on ice for 10 minutes. Then, 5µL of the KLD mixture were added to the cells, gently mixed with a pipette tip, and incubated for 30 minutes on ice. Afterwards, cells were heat-shocked at 42°C for 30 seconds and immediately incubated for five more minutes on ice. Finally, the transformed cells were further incubated for 1 hour at 37°C in 450µL of Super Optimal broth with Catabolite repression outgrowth media (SOC; New England BioLabs, UK), thus allowing recovery and initial expression of the antibiotic resistance enzyme β-lactamase.

After incubation and under sterile conditions, 50µL and 200µL of the *E. coli* culture were spread onto two pre-warmed Luria Bertani (LB) agar plates supplemented with 100µg/mL of ampicillin and incubated facing down O/N at 37°C. A single colony from each plate was selected and inoculated in 10mL of LB broth supplemented with 100µg/mL ampicillin. These cultures were left gently shaking at 200 revolutions per minute (rpm) O/N at 37°C for DNA isolation.

2.4.1 Generation of *Escherichia coli* competent cells

High-efficiency competent *E. coli* cells were purchased from New England BioLabs (strain number C2987H; UK). C2987H cells were streaked on an LB agar plate and incubated O/N at 37°C. Single colonies of *E. coli* were inoculated into 10mL of LB broth and expanded O/N at 37°C and 200rpm. Then 1mL of cell culture was added onto 4mL of LB broth and left to grow for two more hours at 37°C and 200rpm. To make *E. coli* C2987H glycerol stocks for long-term storage, 600µL of cells were mixed with 400µL of 50% sterile glycerol and flash-frozen in dry ice before storing the cryovials at -80°C. The remaining *E. coli* cells grown were collected by centrifugation at 805x g for 10 minutes at 4°C. Pelleted cells were gently resuspended in a cold 0.1M CaCl₂ (calcium chloride) solution. Finally, 50µL of *E. coli* C2987H competent cells were aliquoted and kept at -80°C ready to use when required.

2.4.2 LB broth and agar preparation

To make Luria Bertani (LB) broth media, 10g of LB broth powder were dissolved in 500mL of distilled water according to the manufacturer's recommendation in a Duran bottle and sterilised by autoclaving. The sterile LB broth solution was stored at room temperature for future use.

To prepare the LB agar plates, 10g of LB agar powder were dissolved in 250mL of distilled water as per the manufacturer's instructions in a Duran bottle and sterilised by autoclaving. 100µg/mL of ampicillin were added aseptically into lukewarm LB agar and mixed to ensure a homogeneous solution. Immediately after, approximately 20mL of agar were carefully pipetted in sterile Petri dishes. The plates were left to solidify in the Class II Microbiology Safety Cabinet at room temperature and then stored at 4°C for up to two weeks.

2.5 Preparation of glycerol stocks, DNA extraction, and sequencing

Prior to DNA extraction from the transformed *E.coli* cultures, 1.2mL from each culture tube and 400µL of 50% sterile glycerol were added into cryotubes in a sterile setting for long-term storage. These glycerol stocks were clearly labelled and kept at -80°C for future experimental use. Glycerol stock preparation was done twice for each purchased or mutated plasmid.

Following the growth of bacteria, the transformed *E.coli* cultures were centrifuged at 805x g for 20 minutes at RT, and the clear supernatant was discarded. Gentle lysis of the cells, solubilisation of DNA, and removal of contaminants (proteins, RNA, and other macromolecules) were performed using E.Z.N.A Plasmid Mini Kit I (Omega Bio-Tek, UK) according to the manufacturer's protocol. The extracted DNA plasmids were then quantified using Nanodrop spectrophotometry (NanoDrop® ND-1000 UV-Vis Spectrophotometer, Agilent, UK) and NanoDrop 1000c software. For nucleic acid quantification, the software used a modified Beer-Lambert equation:

$$c = \frac{A \times 50}{b}$$

Where c is the nucleic acid concentration in ng/µL, A is the absorbance in absorbance units, 50 is the extinction coefficient for double-stranded DNA in ng-cm/µL, and b is the path length in cm. For the NanoDrop 1000 Spectrophotometer, path lengths of 1.0 and 0.2mm were used as detailed in the user manual. The absorbance was read at 260 and 280nm, with the ratio 260/280 used to assess the purity of nucleic acids. A 260/280 ratio value of 1.8 was considered pure for DNA samples. A secondary measure for DNA purity was the absorbance ratio at 260 and 230nm, which controls for unwanted organic compound contamination, namely salt, peptides, or phenol remains. The 260/230 ratio values were often higher than the respective 260/280 values and fell in the 2-2.2 range.

Finally, 5µL at 100ng/µL of each purified plasmid were sent for sequencing for plasmid verification (Source Bioscience Sequencing, Cambridge, UK). Samples were sequenced from both strands using

CMV or bGH primers for sense and antisense DNA chain readings, respectively. All DNA samples were kept at -20°C.

2.6 Transient transfection of parental 1321N1 astrocytoma cells

Human 1321N1 cells are known to be devoid of P2X receptors (Communi et al., 1996). Cell transfection is a standard methodology used to introduce foreign DNA into cells. It enables the study of gene function and regulation and recombinant protein production in mammalian cells. The previously mentioned 1321N1 astrocytoma cell line that stably expresses the human P2X4 receptor was created by stable transfection of the human P2X4 gene in 1321N1 parental cells. For stable transfection, introduced DNA is integrated into the host genome and sustains transgene expression over time, even after host cells replicate and divide. In contrast, transiently transfected genes are only expressed for a limited time and are not integrated into the host genome. Therefore, they are not passed down through cell division.

1321N1 parental cells were regularly tested for biological contamination to guarantee a healthy and viable culture before transfection and were used between passages P4 and P12 for optimal cell transfection. 1321N1 cells were always kept at 70-80% confluence and were seeded in 96-well plates at 12,500 cells/well and kept for 24 hours in cell culture conditions before transfection. Cells were allowed to adhere to the bottom of the wells and to expand until a 70-80% monolayer was formed. Cells that were too confluent squeezed together, visually changed morphology, reducing their original size, and underwent contact inhibition resulting in poor uptake of DNA and decreased expression of the transfected gene. However, too few cells in the culture resulted in poor growth without cell-to-cell contact. The key to ensuring optimal confluence was reliably achieved at the time of transfection was to maintain a standard splitting and seeding protocol from experiment to experiment. It is important to note that some cell death was inevitable regardless of the transfection method used.

There are three main types of transfection methods: biological (i.e., virus-mediated transfection, also known as transduction), chemical (i.e., cationic polymer, lipid, amino acid), and physical (i.e., direct microinjection, biolistic particle delivery, electroporation). My selections were three different chemical reagents described in the following passages 2.6.1, 2.6.2, and 2.6.3. Human P2X4 plasmid DNA was prepared, as explained in section 2.5. DNA yields of approximately 30µg with a 260/280 ratio of 1.8 were obtained routinely from 10mL bacterial cultures. Opti-MEM™ I Reduced-Serum Medium (Opti-MEM; Gibco™, Life Technologies, UK) is an improved Minimal Essential Media (MEM) widely recommended for cationic lipid transfection reagents and was used as transfection media for all three methodologies. All transfection procedures, including DNA and chemical reagent preparations, were done under strict sterile conditions.

The ideal approach was determined empirically and was selected for: high transfection efficiency, low cell toxicity, accessibility and convenience, and reproducibility. To assess human P2X4 WT transfection, intracellular calcium mobilisation assays were carried out as outlined in the methods section 2.8. The

optimisation process is detailed later in Chapter 3 (Tables 3.1 and 3.2) of this thesis, showing the specific transfection conditions used and their graded efficiencies.

2.6.1 TurboFect

TurboFect Transfection Reagent (TurboFect) is a cationic polymer that interacts with DNA to form small, stable, and highly diffusible complexes which are readily endocytosed and ruptured in the cytosol, releasing the DNA and allowing it to translocate to the nucleus. TurboFect was provided as a sterile aqueous solution and stored at 4°C.

TurboFect and DNA dilutions were immediately prepared before cell transfection. Firstly, human P2X4 WT DNA was diluted to the desired final amounts per well in sterile 1.5mL Eppendorf tubes with 100µL Opti-MEM. Secondly, TurboFect was vortexed and added into each diluted DNA tube. The TurboFect/DNA complexes were incubated for 15' at RT. Meanwhile, DMEM complete growth media was replaced with 180µL/well of fresh DMEM complete growth media. After incubation, 20µL of TurboFect/DNA complex were added carefully into each well following the desired layout. The 96-well plate was gently rocked and incubated for 48 hours in cell culture conditions before assessing human P2X4 WT transfection.

2.6.2 X-tremeGENE

X-tremeGENE™ HP DNA Transfection Reagent (X-tremeGENE; Roche, UK) is a multi-component reagent that forms a complex with DNA and then transports the complex into the cells. X-tremeGENE was supplied in a sterile 80% ethanol solution and stored at -20°C.

Before starting the transfection protocol, X-tremeGENE was warmed to RT and vortexed. DNA was diluted in 100µL of Opti-MEM in a sterile 1.5mL Eppendorf tube and gently pipetted up and down to mix. X-tremeGENE was added to the diluted DNA, and each condition was incubated for 15 or 30' at RT. In the meantime, the DMEM complete growth media was replaced with 100µL/well of fresh DMEM complete growth media. Afterwards, 5 or 10µL of each X-tremeGENE:DNA ratio were added dropwise into each well, according to the desired layout, and the plates were gently swirled to ensure even distribution. Six hours post-transfection, each well was topped-up with 100µL of fresh DMEM complete growth media. Finally, cells were incubated for 48 hours before measuring human P2X4 WT receptor activity.

2.6.3 Lipofectamine 2000

Lipofectamine™ 2000 Transfection Reagent (Lipofectamine 2000) is a cationic lipid that forms liposomes containing the DNA of interest. These vesicles can easily fuse with the cell membrane due to their lipidic nature and release genetic material into the cell. This process is also known as lipofection, and it is extensively referenced in the literature as a reliable cell transfection method. Lipofectamine 2000 was provided as a sterile aqueous solution and stored at 4°C.

In this case, two separate Eppendorf tubes were used for DNA and Lipofectamine 2000 preparations. The human P2X4 WT plasmid was diluted in Opti-MEM and mixed by pipetting up and down. Likewise, Lipofectamine 2000 was vortexed before use and diluted into desired concentration in Opti-MEM. Calculations for final amounts of plasmid DNA and Lipofectamine 2000 were always done with a 10% surplus, accounting for pipetting errors. This process was done slowly and avoided touching any plastic tube walls. Both tubes were incubated for five minutes at RT. From here, three different approaches were taken as the protocol was perfected with time:

- a. Initially, equal volumes were mixed and further incubated for 5 minutes at RT. Meanwhile, old DMEM complete growth media was replaced with 190µL/well of fresh DMEM complete growth media. Then, slowly and dropwise, 10µL of transfection complex were added into each well.
- b. Secondly, equal volumes of plasmid and Lipofectamine 2000 were mixed by gentle pipetting up and down and incubated for 20 minutes at RT. Again, old media was replaced with 190µL/well of fresh DMEM complete growth media and 10µL of transfection complex were added into each well.
- c. Finally, equal volumes were mixed by gentle pipetting cautiously, not touching the plastic walls of any tube, and left at RT for 20 minutes to form the transfection complexes. This time, cells were deliberately washed twice with DMEM media without antibiotics supplemented only with 10% FBS (DMEM transfection media) and 150µL of DMEM transfection media were added into the wells. After incubation, 50µL of the transfection complex were ejected into the wells dropwise, aiming not to touch any plastic walls. Plates were lightly rocked side to side.

As detailed later in Table 3.1, sometimes the transfection media was replaced with DMEM complete growth media 6 hours post-transfection. All plates were left in cell culture conditions for 48 hours until assessment. The optimised transient transfection protocol used is summarised in Table 2.6.

2.7 Transient co-transfection of 1321N1 parental astrocytoma cells

Transient co-transfection of 1321N1 parental cells was done using the Lipofectamine 2000 transfection reagent. For calcium mobilisation experiments, cells were seeded at 1.25×10^4 cells per well in a 96-well plate and left in cell culture conditions for approximately 24 hours when cells reached 70-80% confluence. Different sterile Eppendorf tubes were used for plasmid combinations and Lipofectamine 2000 preparations. Calculations for final amounts of plasmid DNA and Lipofectamine 2000 were also done with a 10% surplus, accounting for pipetting errors. 200ng of each plasmid of interest per well were diluted in Opti-MEM and combined by pipetting. 0.5µL of Lipofectamine 2000 per well were diluted in Opti-MEM prudently mixed without touching the walls. Both tubes were incubated for 5-10 minutes at RT. Equal volumes of Lipofectamine 2000 dilution and each plasmid combination were mixed and further incubated for 25-30 minutes at RT to allow the formation of the co-transfection complexes. Then, cells were washed twice in DMEM transfection media, and 150µL/well of DMEM transfection media were added. After incubation, 50µL of the transfection complex mixture were added into each well in a dropwise manner and plates were carefully rocked side to side. Transfection media was

replaced with DMEM complete growth media approximately six hours after transfection. Plates were left in cell culture conditions for 48 hours before experimentation. The optimised transient co-transfection protocol used is summarised in Table 2.6.

2.7.1 Scaled-up transient co-transfection of 1321N1 parental astrocytoma cells

The transient co-transfection of 1321N1 parental cells protocol was scaled up to a 6-well plate format for protein expression and protein interaction studies (Table 2.6). First, approximately 1.25×10^5 cells/well were seeded in a 6-well plate. Cells were grown in cell culture conditions for 36 hours until 80% confluence was reached. Then 4000ng of each plasmid per well were diluted in Opti-MEM and mixed in a 15mL sterile Falcon tube. Similarly, 10 μ L of Lipofectamine 2000 per well were carefully combined with Opti-MEM in another 15mL sterile Falcon tube. Again, final amounts of plasmid DNA and Lipofectamine 2000 were calculated for a 10% surplus to account for pipetting errors. Both tubes were incubated separately for five minutes at RT. Equal volumes of Lipofectamine 2000 and DNA preparations were gently combined by pipetting up and down, aiming not to touch any plastic surfaces, and further incubated for 25-30 minutes at RT. DMEM complete growth media was removed, and cells were washed twice in DMEM transfection media. Cells were left in 1700 μ L/well of transfection media, and 300 μ L of desired transfection complex solution were added smoothly and dropwise into each well. Plates were gently rocked side to side. Finally, the transfection media was replaced with DMEM complete growth media approximately six hours post-transfection. Cells were left in cell culture conditions for 48 hours before experimentation.

Table 2.6. Optimised protocol outline for transient transfection and co-transfection of human 1321N1 parental astrocytoma cells. All amounts are given on a per well basis.

Component	One plasmid		Two plasmids
	96-well	96-well	6-well
Number of cells	12,500	12,500	12,500
Final Lipofectamine 2000	0.5 μ L	0.5 μ L	10 μ L
Final DNA	200ng	200ng + 200ng	4000ng + 4000ng
Opti-MEM for each dilution	25 μ L	25 μ L	150 μ L
Final DNA/reagent complex	50 μ L	50 μ L	300 μ L
DNA/reagent complex formation	25-30'	25-30'	25-30'
Final volume	200 μ L	200 μ L	2mL
Pen/Strep present?	No	No	No
Media change	6h	6h	6h

2.8 Calcium mobilisation assay

Calcium mobilisation assays were performed to detect intracellular calcium changes upon activation of purinergic and muscarinic receptors present in 1321N1 astrocytoma cells. Fura-2 is a ratiometric fluorescent dye which binds to free intracellular calcium. Its membrane-permeable derivative called Fura-2 acetoxyethyl (AM) ester (Abcam, Cambridge, UK) was used to load the 1321N1 astrocytoma cells (Grynkiewicz et al., 1985). The acetoxyethyl (AM) moiety allows Fura-2 to cross the cell membrane. Once in the cytosol, the AM group is cleaved by cellular esterases, resulting in a negatively charged fluorescent dye that remains inside the cell. This allows the formation of Fura-2 and calcium intracellular complexes. Fura-2 has a constant emission peak at 510nM and changes its excitation peak from 380nm to 340nm in response to calcium binding. Consequently, the fluorescence measurement at 510nm with two excitation wavelengths (340nm for calcium-bound states and 380nm for calcium-free states) allowed us to quantify and represent the change in intracellular calcium levels as a fluorescence ratio, *F ratio* (340/380). Using the *F ratio* increases the accuracy and reproducibility of results because it limits photobleaching effects and counteracts variables, including cell thickness and differing local Fura-2 concentrations (Grynkiewicz et al., 1985).

2.8.1 Calcium mobilisation buffers

Salt-buffered saline (SBS) physiological solution was prepared in deionised water. It contained (mM): 130 sodium chloride (NaCl), 5 potassium chloride (KCl), 1.2 magnesium chloride ($MgCl_2$), 1.5 calcium chloride ($CaCl_2$), 8 D-(+)-glucose, and 10 HEPES (4-(2-hydroxyethyl)-1-piperazineethanesulfonic acid). SBS was titrated to physiological pH 7.3-7.4 with sodium hydroxide (NaOH) and made up to a volume of 1L. The solution was thoroughly mixed by magnetic stirring before measuring its osmolality. Osmolality was measured using a K-7400S Semi-Micro Osmometer (Knauer, Germany) and measured the number of solute particles dissolved in 1Kg of water. It can also be called osmolarity when calculated for 1L of water. This value is important because it affects the electrolyte-water balance of the cells. Osmotic equilibrium is reached when the number of solutes is equal between the intracellular and the extracellular environment. This equilibrium is maintained through osmosis, the diffusion of water molecules from a low solute concentration area to a higher concentration area. In an isotonic solution, the flow of water in and out of the cell happens at the same rate. Once the solution was homogenous, 150 μ L of SBS were pipetted into a 1.5mL Osmometer Eppendorf tube (Knauer, Germany). This tube was carefully attached to the measuring head, which in turn was balanced on the osmometer device. The osmometer uses a freezing point approach which is proportional to the osmotic pressure of a solution. The osmolality can be directly read from the display screen given in mOsm. The physiological serum osmolality is approximately 300mOsm. The SBS solution usually gave hypoosmotic values of 260-280mOsm. Incubating the 1321N1 astrocytoma cells with a hypotonic solution would cause them to swell due to an influx of water molecules into the cells, potentially bursting. D-mannitol was used to adjust the SBS osmolality following this calculation:

$$1L \times \frac{1Kg}{1L} \times \frac{a\text{ mOsmol}}{1Kg} \times \frac{1mmol\text{ D-mannitol}}{1mOsmol} \times \frac{1mol}{1000mmol} \times \frac{182.17g}{1mol} = b\text{ g}$$

Where a are the mOsmol left to achieve a 300mOsm molality, and b the amount of D-mannitol required, calculated in grams. The D-mannitol was then weighed, added to the SBS solution, and thoroughly mixed before measuring the osmolality again for further adjustments until the value displayed was about 300mOsm.

Finally, the Fura-2 loading buffer (Fura-2 AM LB) solution was made of SBS supplemented with 0.01% [w/v] of pluronic acid F-127 and 2µg/mL of Fura-2 AM (Abcam, Cambridge, UK). A 1mg/mL Fura-2 AM stock was prepared in DMSO, aliquoted, and kept at -20°C in an opaque box until required. Fura-2 AM was always freshly added at the time of experimentation.

2.8.2 Intracellular calcium measurements

Human P2X4 stable 1321N1 astrocytoma cells were seeded at an initial cell density of 2.5×10^4 cells/well in a 96-well plate. Cells were maintained in cell culture conditions O/N, allowing cells to adhere to the bottom of the wells and form a confluent monolayer. When cells were ready for experimentation, DMEM complete growth media was removed, and cells were carefully washed with SBS and loaded with Fura-2 AM LB for 1 hour at 37°C while protected from the light. After incubation, cells were washed twice with SBS. All buffers were pre-warmed to 37°C. When applicable, cells were incubated with antagonists or vehicle control for 30 minutes at 37°C before starting the assay. Finally, cells were placed in a FlexStation 3 microplate reader (Molecular Devices, UK), which recorded the dual-excitation (340nm and 380nm) single-emission (510nm) fluorescence ratio for the Fura-2 dye as detailed above. Readings were taken every 3 seconds over 250 seconds. After 20 seconds, cells were challenged with 50µL of receptor agonists (nucleotides or carbamylcholine (Carbachol)), administered automatically by the FlexStation 3 device. The same procedure was followed for transiently transfected 1321N1 parental astrocytoma cells 48 hours post-transfection. One-second sampling was used to detect human P2X3 activity. All experiments were performed at 37°C.

F ratio (340/380) values were used to quantify the change in intracellular calcium levels at every time point and were exported from the SoftMax Pro FlexStation 3 software (version 5.4.5; Molecular Devices, UK) as trace data. Peak and area under the curve values were also exported. For details regarding the data analysis, see section 2.13.1.

2.9 Western blotting

Western blotting is a widely used molecular biology technique to separate and identify different proteins present in a sample. This technique involves gel electrophoresis to separate proteins by molecular weight. These are then transferred to a membrane, where the proteins of interest can be recognised by specific antibodies and detected by chemiluminescence.

2.9.1 Protein extraction and sample preparation

When ready for experimentation, cells were washed twice with ice-cold PBS pH 8.0. Cell scrapers were used to harvest the cells of each well and were transferred into 1.5mL Eppendorf tubes. Cells were pelleted by centrifugation at 4,000x *g* for 20 minutes at 4°C and the supernatant was discarded. The cell pellet was resuspended in 20µL of ice-cold solubilisation buffer (150mM NaCl, 1mM MgCl₂, 1mM CaCl₂, 2% [v/v] Triton X-100, 20mM Tris-HCl pH 7.6) supplemented with 1X EDTA-free protease inhibitor cocktail (Complete™ tablets, Roche, UK) and homogenised for two hours in a rotating wheel at 4°C. Homogenates were cleared to remove cell debris at 12,000x *g* for 20 minutes at 4°C. Finally, the resulting supernatant was collected, and the total protein concentration of each sample was assessed using the colourimetric Pierce™ BCA protein assay (Sigma-Aldrich, UK), according to the manufacturer's instructions. Protein yields of 100µg per well were routinely obtained.

Whole-cell protein samples were prepared by mixing 25µg of total protein extract with 4µL of 5X sample buffer (240mM Tris-HCl pH 6.8, 12% [w/v] Sodium Dodecyl Sulphate (SDS), 30% [v/v] glycerol, 0.05% [w/v] bromophenol blue) containing 50mM dithiothreitol (DTT) in a final volume of 20µL, and boiled for 10 minutes at 96°C.

2.9.2 SDS polyacrylamide gel electrophoresis and membrane transference

The SDS polyacrylamide gel was composed of a 5% stacking gel (125mM Tris pH 6.8, 5% [v/v] acrylamide 30% 37.5:1, 0.1% [w/v] SDS, 0.05% [v/v] ammonium persulphate (APS), 0.1% [v/v] tetramethylethylenediamine (TEMED)) and a 10% resolving gel (375mM Tris pH 8.8, 10% [v/v] acrylamide 30% 37.5:1, 0.1% [v/v] SDS, 0.05% [v/v] APS, 0.05% [v/v] TEMED). Samples were loaded along with the Precision Plus Dual Colour Bio-Rad protein ladder (Bio-Rad Laboratories, UK) and ran in 1X electrophoresis buffer (25mM Tris, 192mM glycine, 0.1% [w/v] SDS) at 90V until the dye front surpassed the bottom of the stacking phase, and then at 120V until the dye front reached the lower end of the resolving phase.

Once the SDS polyacrylamide gel electrophoresis (SDS-PAGE) finished, proteins were transferred to an Immobilon-P polyvinylidene difluoride (PVDF) membrane (0.45µm pore size; Millipore, UK) using the mini trans blot module (Bio-Rad Laboratories, UK) containing ice-cold transfer buffer (25mM Tris, 192mM glycine, 20% [v/v] methanol) at 90V for 90 minutes in the cold room at 4°C.

2.9.3 Membrane blocking, protein detection, and visualisation

When proteins were completely transferred, PVDF membranes were incubated with a blocking solution containing PBST (1X PBS, 0.1% [v/v] Tween-20 (Sigma-Aldrich, UK)) and 5% [w/v] semi-skimmed milk for a minimum of 1 hour at RT on a rocking platform. Then, membranes were incubated with the relevant primary antibodies diluted in PBST and 5% [w/v] semi-skimmed milk O/N on a tube rolling platform in the cold room at 4°C.

The following day, membranes were washed thrice with PBST for 10 minutes at RT on a rocking platform and incubated with the pertinent horseradish peroxidase (HRP) conjugated secondary antibodies,

diluted in blocking solution, for two hours at RT. Afterwards, membranes were washed three more times with PBST for 10 minutes at RT on a rocking platform before visualisation. Finally, membranes were incubated in Pierce™ ECL Western blotting solution for two minutes and developed using the ChemiDoc™ Imaging System (Bio-Rad Laboratories, UK) which used the ImageLab software (version 6.1; Bio-Rad Laboratories, UK). Tables 2.7 and 2.8 contain the complete list of primary and secondary antibodies used, respectively. Further details about Western blot image data analysis are provided in section 2.13.2.

If re-probing was required, the PVDF membranes were incubated in stripping buffer (0.2M NaOH) for 40 minutes at RT with gentle rocking, washed thrice in PBST for 10 minutes, and re-blocked before applying other primary antibodies.

2.10 Biotinylation assay

Biotinylation refers to the covalent labelling of proteins with biotin, and it is used to capture and analyse membrane proteins with streptavidin-coated beads. The protocol proposed by Young (2020) was followed and adapted for 1321N1 human astrocytoma cells and the experimental system used.

At the time of experimentation, cells were washed twice with ice-cold PBS pH 8.0 and treated with 0.5mg/mL of biotin solution (EZ-Link™ Sulfo-NHS-LC-Biotin dissolved in 1X PBS pH 8.0) for one hour at 4°C. After, cells were washed twice with ice-cold PBS-TG (1X PBS pH 8.0, 25mM Tris, 192mM glycine) to quench the crosslinking reaction. These procedures were always done in the cold room to prevent protein degradation. Then, protein extraction and quantification were performed as explained above (section 2.9.1). To capture the biotin-labelled proteins, 80µg of protein extract were mixed with 25µL of streptavidin agarose resin (pre-washed and purged twice in ice-cold solubilisation buffer) in a final volume of 500µL of ice-cold solubilisation buffer supplemented with 1X EDTA-free protease inhibitor cocktail. The samples were incubated O/N on a rotator disk at 4°C. The following day, the streptavidin-biotin-protein complexes were washed and purged three times in the cold solubilisation buffer. Finally, the biotinylated proteins were eluted in 25µL of sample buffer containing 50mM DTT and boiled for 10 minutes at 96°C. Western blotting was performed as formerly described in sections 2.9.2 and 2.9.3. The antibodies used can be found in Tables 2.7 and 2.8.

2.11 Co-immunoprecipitation assay

Co-immunoprecipitation (Co-IP) is commonly used for the detection of intact protein complexes by using an antibody that binds to a target protein, which is believed to be a part of a larger complex of proteins or ligands. Thus, it is utilised to study physical protein-to-protein interactions.

Whole-cell protein extracts were obtained and quantified as described in section 2.9.1. 4µL of appropriate primary antibodies were added to 80µg of total protein samples in a 500µL final volume of solubilisation buffer supplemented with 1X EDTA-free protease inhibitor cocktail (1:125 dilution). To precipitate target proteins, samples were incubated O/N on a rotator disk at 4°C. Protein G

DynabeadsTM (2.8µm superparamagnetic beads) were vortexed and sensibly washed twice with solubilisation buffer using a magnetic separation rack (Dynal^R MPCTM-S Magnetic Particle Concentrator). The antigen-antibody immunocomplexes from the day before were added to 25µL of pre-cleared protein G DynabeadsTM and incubated for 2 hours on a rotator disk at RT. Subsequently, immunoprecipitates were methodically washed three times in the solubilisation buffer for one minute on ice using the magnetic separation rack. Immunoprecipitates were firstly eluted using 25µL of elution buffer (0.2mM glycine pH 2.8) and secondly using 25µL of sample buffer containing 50mM DTT. All samples were boiled at 96°C for 10 minutes. Finally, Western blotting was performed as detailed above (sections 2.9.2 and 2.9.3). The antibodies used can also be found in Tables 2.7 and 2.8.

2.12 Immunocytochemistry

Immunocytochemistry is another technique used to assess the presence of specific proteins in cultured cells and was used to determine cell transfection efficiency under a fluorescent microscope. Human 1321N1 parental cells were transiently transfected in a 96-well plate, as aforementioned. Twenty-four hours later, cells were carefully peeled off by gentle resuspension in 100µL/well of PBS. Pre-autoclaved sterile 10mm glass coverslips were each placed in the wells of a 24-well plate. Then, 30µL of cell suspension were placed on top of each coverslip and left in cell culture conditions for 4 hours to attach to the surface of the coverslip. Subsequently, each well was topped up with DMEM complete growth media to prevent the cells from drying out.

The following day, 48 hours post-transfection, cells were washed twice in PBS and fixed with 4% [w/v] paraformaldehyde pH 7.4 (PFA) for 15 minutes at RT. The PFA was washed off twice with PBS for 5 minutes at RT. Cells were permeabilised with 0.25% [v/v] Triton X-100 for 10 minutes at RT. Cells were washed three times in PBS for 5 minutes at RT. Non-specific binding was blocked with 1% [w/v] of bovine serum albumin (BSA) for a minimum of 45 minutes on a rocking platform at RT. Next, cells were incubated with rabbit anti-P2X4 C-terminus epitope (Alomone Labs, Israel), mouse anti-FLAG (Sigma-Aldrich, UK), or rabbit anti-α7 nAChR (Alomone Labs, Israel) primary antibodies (1:1000 in 1% [w/v] BSA; Table 2.7) O/N on a rocking platform at 4°C. Cells incubated without primary antibodies were used as controls for non-specific secondary antibody staining.

The excess primary antibody was removed by washing thrice in PBS for 10 minutes. Cells were incubated with appropriate goat anti-mouse Alexa Fluor 488 or donkey anti-rabbit Alexa Fluor 488 conjugated secondary antibodies (Abcam, UK; 1:1000 in 1% [w/v] BSA; Table 2.8) for 2 hours on a rocking platform at RT while protected from the light. After incubation, cells were washed three more times in PBS for 10 minutes. Finally, cells were mounted onto glass microscope slides using FluoroshieldTM mounting media with DAPI (4',6-diamidino-2-phenylindole; Abcam, UK) and sealed with clear nail varnish. Cell visualisation was done under the Zeiss Apotome Imager M2 microscope (Axiovert 200M; Zeiss, Cambridge, UK) equipped with a Zeiss AxioCam HRm, and fluorescent images were acquired using the Axiovision 4.8 software. Exposure settings for the green (Alexa Fluor 488) and blue (DAPI) channels remained constant throughout imaging.

Table 2.7. List of primary antibodies used for immunocytochemistry and Western blotting.

Name	Host	Conjugated	Manufacturer	Commercial reference	Application	Dilution
α - α 7 nAChR	Rb	–	Alomone Labs	ANC-007	WB, ICC	1/1000
α -EE tag	Rb	–	Millipore	AB3788	WB	1/10-1000
α -EE tag	Rb	–	Bethyl Labs	A190-111A	WB	1/10-1000
α -EE tag	Rb	–	Cell Signalling	2448S	WB	1/10-1000
α -FLAG tag	Ms	–	Sigma-Aldrich	F1804	WB, ICC	1/1000
α -FLAG tag	Ms	HRP	ThermoFisher	MA1-91878	WB	1/1000
α -HA tag	Rb	–	ThermoFisher	SG77	WB	1/1000
α -His tag	Ms	–	ThermoFisher	11533923	WB	1/1000
α -P2X4 CT	Rb	–	Alomone Labs	APR-002	WB, ICC	1/1000
α -P2X4 EC	Rb	–	Alomone Labs	APR-024	WB	1/1000
α - β actin	Ms	HRP	Sigma-Aldrich	A3854	WB	1/4000

CT (C-terminus), EC (extracellular), HRP (horseradish peroxidase), ICC (immunocytochemistry), Ms (mouse), Rb (rabbit), WB (Western Blot)

Table 2.8. List of secondary antibodies used for immunocytochemistry and Western blotting.

Host	Target	Conjugated	Manufacturer	Commercial reference	Application	Dilution
Gt	α -Ms	AF488	Abcam	ab150113	ICC	1/1000
Dy	α -Rb	AF488	Abcam	ab150073	ICC	1/1000
Gt	α -Ms	HRP	ThermoFisher	15271378	WB	1/1000
Gt	α -Rb	HRP	ThermoFisher	15217664	WB	1/1000
Gt	α -Ms F(ab') ₂	HRP	Abcam	ab5887	WB	1/2000
Gt	α -Rb F(ab') ₂	HRP	Abcam	ab6112	WB	1/2000
Gt	α -Ms Light chain	HRP	Jackson ImmunoResearch	115-035-174	WB	1/1000

AF488 (Alexa Fluor 488), Dy (donkey), Gt (goat), HRP (Horseradish peroxidase), ICC (immunocytochemistry), Ms (mouse), Rb (rabbit), WB (Western Blot)

2.13 Data and statistical analysis

All data and statistical analysis were performed using Excel (Microsoft Corporation) and OriginPro software (Origin Lab version 9.95, UK). Data distribution was tested using a Shapiro-Wilk test for normality of the mean and Levene's test for equality of variances. Data that followed a parametric distribution were analysed with 2-tailed student's t-tests. Non-parametric datasets were assessed using Mann-Whitney tests. The threshold for statistical significance was considered for P values lower than 0.05 throughout (* $P < 0.05$, ** $P < 0.01$, *** $P < 0.001$).

In this thesis, all data are expressed as mean \pm SEM (Standard Error of the Mean). All experiments were performed in triplicates or quintuplets (technical repeats within one experiment) and repeated three to five times, as indicated by the 'N' number of biological repeats in every figure legend.

2.13.1 Calcium mobilisation assay data analysis

As mentioned in section 2.8.2, the changes in intracellular calcium levels upon cell stimulation with exogenous nucleotides and Carbachol were quantified as *F ratio* (340/380) values for every time point over 250s and were exported from the SoftMax Pro FlexStation 3 software (version 5.4.5; Molecular Devices, UK) as trace data. Peak and area under the curve (AUC) values were also exported from the same software for data and statistical analysis.

It is important to note that data normalisation to stated values was applied to control for inter-experimental variation and thus, obtain more representative datasets. For the pharmacological characterisation of the human P2X4 receptor, all agonist concentration-response and time-response data were normalised to the maximal response to 30 μ M ATP, and all antagonist concentration-response and time-response data were normalised to respective 1.5 μ M ATP submaximal responses in the presence of vehicle control (SBS or 0.5% [v/v] DMSO). For calcium mobilisation assays performed on transiently transfected 1321N1 parental astrocytoma cells, there often was plate-to-plate variation due to differences in cell transfection efficiency. To minimise the effects of this variation, data were normalised to respective maximal 100 μ M Carbachol responses as an internal control for cell viability and transfection efficiency within each plate.

Trace data values were quantified as the difference between the highest and the lowest calcium response (max-min) at each time point. Any negative values recorded before the 20s time point, when the automatic addition of exogenous nucleotides or Carbachol occurred, were considered blank responses and were replaced by zeroes before normalisation. Trace data points were then normalised as described above and plotted against time.

Peak values represented the maximal response magnitude over the 250s. Although the SoftMax Pro FlexStation 3 software was used to export the peak data values, all trace data were manually checked to avoid plotting outlier or artefact peak values. Any exported peak value obtained past the 70s time point was considered a fluorescence outlier or artefact and was manually changed for the peak value obtained between the 20s and 70s time frame. These were considered more accurate peak calcium

responses for the human P2X4 receptor and were thereby used for peak data and statistical analysis. All peak data were represented as concentration-response curves, where the peak calcium responses were plotted against the common logarithm (Log_{10}) of each concentration tested and were individually fitted using a modified Hill equation (Hill1 function on the OriginPro software) as outlined below:

$$Y = \text{START} + (\text{END} - \text{START}) \frac{x^n}{k^n + x^n}$$

Where k represents the Michaelis constant and n is the number of cooperative sites. The EC_{50} (half maximal effective concentration) and IC_{50} (half maximal inhibitory concentration) values were obtained according to the fitted curve and were equal to the k value in the Hill1 equation.

The area under the curve (AUC) is another value provided by the SoftMax Pro FlexStation 3 software. AUC values are defined as the integral of the intracellular calcium response as a function of time. Thus, AUC data encompasses both the initial response and the sustained calcium response phase over the recorded 250s, representing the net calcium movement upon application of exogenous compounds. The AUC data analysis was carried out as the peak data analysis but was only performed in specific cases where effects on the sustained calcium response phase could have been missed by solely analysing peak data.

All calcium mobilisation statistical analysis was performed as described at the beginning of section 2.13.

2.13.2 Western blot image data analysis

Western blot image analysis was used to semi-quantify the relative amount of each protein of interest and compare the different protein expression levels between experimental conditions. A Western blot image is composed of pixels which contain signal intensity information. The signal emitted by the protein of interest in an image can be measured as the total signal intensity information for all the pixels contained within that band. Therefore, this signal is directly proportional to the amount of protein present in that band. Images obtained from the ImageLab software (version 6.1; Bio-Rad Laboratories, UK) were saved as JPG files and analysed with the Fiji image processing software (Fiji Is Just ImageJ version 1.53; SciJava, UK).

The rectangular tool was used to draw a box around the protein of interest band, including all of the band intensity signal with the minimal amount of surrounding background. The total pixel intensity for that band was then measured using the command Ctrl+M in Fiji. The same box size was used for all the lanes in each Western blot image therefore, the size of the box was set for the largest protein of interest band and moved across the blot to obtain all the required measurements. Background measurements for each lane were also taken using the same size box but positioned just above the protein of interest band. Thus, each protein band had its unique level of background. All measurements were copied into Excel and data was transformed as detailed below.

A white pixel has an intensity value of zero and a black pixel has an intensity value of 255. The total pixel intensity values for each protein of interest and background bands were inverted by subtracting each

measurement from 255. Then, the net amount of protein was quantified by subtracting the inverted background from the inverted protein values, giving a more accurate measure of the amount of signal intensity that came from the protein of interest in each lane. To minimise protein expression variability between experiments, all net protein values were suitably normalised to β -actin loading controls as detailed below.

For the normalisation of whole-cell Western blots, the net amount of protein of interest was divided by the net amount of net whole-cell β -actin loading controls in each lane. To obtain the relative cell surface protein of interest expression levels in biotinylation experiments, the net cell surface protein values were normalised to the respective net whole-cell β -actin loading controls. Similarly, for co-immunoprecipitation assays, the relative immunoprecipitated protein expression levels were obtained by normalising each net immunoprecipitated protein against its respective net whole-cell β -actin loading control. Thus, the expression levels of each protein of interest were expressed as ratio values relative to the corresponding whole-cell β -actin loading controls, reducing variability caused by protein loading errors and potential differences in transient protein expression levels between experiments.

Finally, all Western blot image data were plotted as column graphs using the OriginPro software and statistical analysis was carried out as detailed in the beginning of section 2.13.

3 The hypothesis of the dead receptor and validation of the experimental system

3.1 Introduction

Over the past fifteen years, there has been a growing interest in how P2X subunits arrange to form functional channels. Different approaches have been taken to probe the existence of P2X heteromers. These included: i) biophysical methods looking at the channel structure, dynamics, or permeation properties with spectroscopy, electrophysiology, and calcium imaging assays; ii) biochemical methods such as Western blotting and immunoprecipitation, and iii) molecular biology techniques like genetic engineering to form P2X concatemers. However, the answers to which human P2X receptors can form functional heteromers remain controversial.

So far, only the P2X2/3 heteromeric receptor has been established and accepted by the purinergic signalling community. The P2X2/3 receptor is slowly desensitising and $\alpha\beta$ -MeATP-sensitive, resulting from the combination of P2X2 and P2X3 homomeric channel properties, respectively. This pharmacologically distinct profile has been observed in both human and rodent heterologous and native systems (Lewis et al., 1995; Saul et al., 2013; Burnstock, 2018). However, further investigations were required to elucidate the P2X2/3 receptor subunit stoichiometry. Does it contain one P2X2 subunit and two P2X3 subunits or two P2X2 subunits and one P2X3 subunit? Does the explicit subunit composition affect channel function? Does it impact its pharmacological properties?

Wilkinson et al. published an electrophysiological approach to answer some of these questions and provide information about the subunit assembly of the P2X2/3 heteromeric receptor (Wilkinson et al., 2006). They used HEK293 cells transiently transfected with rat P2X2 and rat P2X3 DNA constructs and proposed what they called the ‘dead receptor’ hypothesis (Wilkinson et al., 2006). The dead receptor hypothesis was based on two concepts proposed earlier by the same research group. Firstly, they identified that lysines at positions K70 and K316 (zebrafish P2X4 numbering) were critical for ATP molecule recognition and binding, and therefore channel function (Jiang et al., 2000). In addition, the occupancy of at least two agonist binding sites was required for P2X channel activation (Jiang et al., 2003). This second study suggested that the occupancy of only one binding site would not induce channel opening and was the foundation of the proposed dead receptor hypothesis. Both concepts were confirmed when the X-ray crystal structures of the zebrafish P2X4 receptor in apo and ATP-bound states were released (Kawate et al., 2009; Hattori & Gouaux, 2012), and the ATP binding site was scrutinised by mutagenesis and electrophysiological analysis (Chataigneau et al., 2013). These two lysines are highly conserved among P2X receptor subtypes and through P2X receptor evolution (Fountain et al., 2007). K70 and K316 (zebrafish P2X4 numbering) mediate the coordination of the adenosine base and the triphosphate tail of the ATP molecule (Fig 1.5B) and are located in the agonist binding pocket at the interface between two subunits. In this way, the K70 (zebrafish P2X4 numbering) of one subunit and the K316 (zebrafish P2X4 numbering) of another are involved in the same agonist binding interface (Fig 1.5B). In 2006, their idea was to block the agonist binding sites by mutating the corresponding key lysines K69 and K308 in the rat P2X2 receptor and K63 and K299 in the rat P2X3 receptor to alanine residues and generating what they called ‘dead receptors’. The function of the

heteromeric P2X2/3 receptor, when lysine-to-alanine mutations were introduced, depended greatly on whether they were in the P2X2 or the P2X3 subunit, as described below (Wilkinson et al., 2006).

When HEK293 cells were co-transfected with P2X3 wild-type subunits and P2X2 single mutant subunits, the P2X2/3 receptor function was rescued (Fig 3.1A). However, when HEK293 cells were co-transfected with P2X2 wild-type subunits and single mutant P2X3 subunits, this rescue did not occur (Fig 3.1A). These results suggested that a wild-type P2X3 subunit could rescue the function of a P2X2 receptor with a single lysine-to-alanine mutation, but not vice versa (Wilkinson et al., 2006). Furthermore, the P2X2/3 receptor function was completely abolished when both ectodomain lysines were mutated in the same P2X2 subunit (Fig 3.1A). Thus, a wild-type P2X3 subunit could rescue the activity of a single P2X2 mutant but not of a double P2X2 mutant subunit (Wilkinson et al., 2006). But, what did these data mean in terms of the stoichiometry of rat P2X2/3 receptors?

The failure to rescue receptor function in the P2X2 subunit with both lysines mutated by wild-type P2X3 subunits demonstrated that only one dead P2X2 subunit was enough to block receptor function. Thus, they proposed a 1:2 subunit organisation in favour of the P2X3 subunit. Following this proposed subunit stoichiometry, the presence of a single dead P2X2 subunit would still provide for two functional agonist binding sites able to recognise the agonist molecule and activate the receptor (Fig. 3.1B, left and middle panels; Wilkinson et al., 2006). However, a double-dead P2X2 subunit would prevent agonist binding at two sites and therefore, the binding of just one agonist molecule would not be enough to overcome the energy barrier to change the receptor conformation and consequently, gate the channel (Fig. 3.1B, right panel; Wilkinson et al., 2006).

The research community gained new information on the agonist binding mechanism and the roles of these key ectodomain lysine residues in P2X receptor gating thanks to the work carried out by Wilkinson et al. and confirmed in later investigations. It is crucial to investigate the subunit organisation of all P2X receptors because it will build on our understanding of ATP signalling in physiologically relevant systems, give us insights on novel P2X receptor subtypes which may have different pharmacological properties, and open new routes for the development of more selective therapeutics.

In addition, Wilkinson et al. provided a method to functionally differentiate between subunit assemblies in rat P2X2/3 receptors. Thereby, their dead receptor hypothesis could be expanded into the seven P2X receptor subtypes to find novel functional heteromeric interactions and their subunit arrangements, unveiling potential differences in receptor pharmacology and ion channel properties. Thus, we sought of using the dead receptor hypothesis to investigate functional interactions of the human P2X4 receptor by intracellular calcium assays and complement these data with physical protein-protein interaction studies. Figure 3.1C shows a visual representation of the dead receptor hypothesis using human P2X4 receptors. There is evidence that human P2X4 receptors can form functional homotrimers (North, 2002; Coddou et al., 2011; Illes et al, 2021). According to the hypothesis of the dead receptor, a homomeric human P2X4 wild-type receptor would have three available agonist-binding sites and could produce a calcium response when the agonist is applied (Fig 3.1C, left panel). Potential interactions between human P2X4 wild-type and P2X4 dead subunits would limit the functional agonist-binding sites

to one, which would not be sufficient to gate the receptor (Fig 3.1C, middle panel). So, when P2X4 wild-type subunits are co-expressed with other human P2X dead receptor subunits, the effects observed in the agonist-evoked intracellular calcium responses could help us detect potential human P2X4 subunit interactions (Fig 3.1C, right panel). If interactions occurred, the functional agonist-binding sites would be limited, thus a reduction in agonist-evoked calcium responses would be observed compared to human P2X4 wild-type homotrimeric receptors. If no interactions occurred, the agonist-evoked calcium responses would not be altered compared to human P2X4 wild-type homotrimeric receptors. Figure 3.2 illustrates the sequence alignment between the rat P2X2 (rP2X2) and the human P2X1-7 receptors (hP2X1-7) and highlights the corresponding conserved residues that participate in the binding of ATP. Equivalent lysine residues in positions K69 and K308 of the rat P2X2 were mutated to alanine residues to produce the human P2X1-7 dead receptors as advised in the dead receptor hypothesis (Annex 2 contains the complete sequence alignments).

Wilkinson et al. used HEK293 cells as their model system for the co-transfection of rat P2X2 and P2X3 receptor constructs and patch-clamp electrophysiology studies. HEK293 cells are efficient transfection hosts, but they express endogenous ATP-sensitive receptors such as P2Y1, P2Y2, and P2Y4 (Fischer et al., 2003, 2005). For studies of P2X receptor activity using patch-clamp electrophysiology, these endogenous receptors do not represent a problem as they are GPCRs and do not contribute to cation influx so, any changes in current measurements upon ATP stimulation would be due to the activation of the transfected P2X receptors. However, these GPCRs cause a large increase in intracellular calcium levels when activated by ATP and thus, the contribution of transfected P2X receptors to these responses is difficult to isolate when performing intracellular calcium mobilisation experiments (Fischer et al., 2003). Consequently, we thought of using human 1321N1 astrocytoma cells which are void of endogenous ATP-activated receptors (Communi et al., 1996). This unique feature meant that applying ATP and other analogues would not give endogenous calcium responses that could mask the specific P2X receptor-mediated intracellular calcium responses. To use the dead receptor hypothesis, P2X receptors would have to be transfected and expressed in these cells in the same way they were in HEK293 cells by Wilkinson et al.

This chapter entails the secrets of how to successfully transfect P2X4 receptors in human 1321N1 astrocytoma cells and provides proof-of-concept data for the use of dead receptors as tools to explore functional human P2X4 subunit interactions.

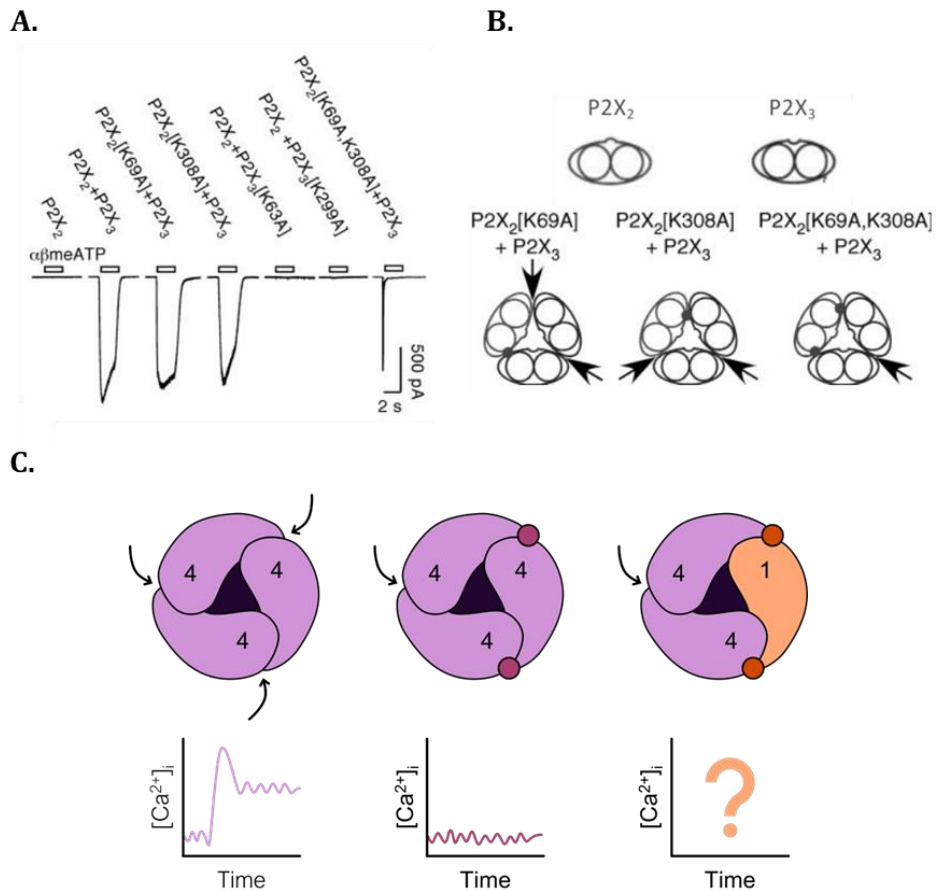


Fig 3.1. Visual representation of the dead receptor hypothesis. (A-B) Co-expression of rat P2X2 and P2X3 subunits in HEK293 cells by Wilkinson et al. (2006). (A) Currents evoked by the application of $\alpha\beta$ -MeATP. P2X3 WT subunits completely rescued channel function when co-expressed with P2X2 [K69A] and P2X2 [K308A] single mutants, but not with the P2X2 [K69A, K308A] double mutant. In contrast, P2X2 WT subunits did not rescue channel function when co-expressed with either P2X3 [K63A] or P2X3 [K299] single mutants. (B) Schematic illustration of the proposed P2X2/3 heteromer subunit stoichiometry and the available ligand-binding sites. Each subunit is represented as an ellipse with two circles inside (corresponding to each TM domain). The solid circles indicate the substitution of lysine for alanine residues and the arrows indicate the $\alpha\beta$ -MeATP-binding pockets. A single P2X2 mutant provided two $\alpha\beta$ -MeATP-binding sites and P2X2/3 receptor function was rescued (left and middle panels), whilst a P2X2 double-dead mutant only had one $\alpha\beta$ -MeATP-binding site which was not enough to gate the P2X2/3 receptor (right panel). (C) Visual representation of how dead receptor tools can affect intracellular calcium responses. A homomeric human P2X4 receptor with three available ATP-binding sites (arrows) produces a calcium response when the agonist is applied (left panel). The presence of a P2X4 [K67A, K313A] dead subunit, limits the functional ATP-binding sites to one, which is not sufficient to gate the receptor (middle panel). The effects we observe in intracellular calcium measurements can help us detect potential human P2X4 subunit interactions when co-expressed with other human P2X dead receptor subunits (right panel). If interactions occur, the functional agonist-binding sites will be limited, thus a reduction in ATP-evoked calcium responses will be observed. If no interactions occur, the ATP-evoked calcium responses will not be altered.

hP2X1WT	FLYEKGYQTSSG- L ISSVSV K LKG L AVTQ-----LPGLGPQVWDVADYVFPAQGDNSF	100
hP2X2WT	FIVQKSYQESETGPES I TK V KGITTSE-----HKVWDVEEYVKPPEGGSVF	108
rP2X2WT	FIVQKSYQDSETGPES I TK V KGITMSE-----DKVWDVEEYVKPPEGGSVV	96
hP2X3WT	FLHEKAYQVRDTAIES S VVT K VKGSGLYA-----NRVMDVSDYVTPPQGTSVF	90
hP2X4WT	FVWEKGYQETDSV-VSSVTT K VKGAVTN-----TSKLGFRIWDVADYVIPAQEENSL	99
hP2X5WT	FLIKKGYQDVDTSLQS A VIT K VKGVAFTN-----TSDLGQRIWDVADYVIPAQGENVF	101
hP2X6WT	LLAKKGYQERDLEPQFS I IT K LKGVS T Q-----IKE L GNRLWDVADFVKPPQGENVF	110
hP2X7WT	LVSDKLYQRKEP- V ISSVHT K VKGIAEVKEEIVENGVKLHVSVFDTADYTFPLQG-NSF	102
	: : . * * * . . : : . * : * * : * . : * . : : . * : . .	
hP2X1WT	GLYE---EKNLSPGFNFRFARHFVE-NGTNYRHLF K VFGIRFDILVDGKAGKF <small>DII</small> PTMT	333
hP2X2WT	RLDPKH--VPASSGYNFRFAKYYKINGTT-TRTLI K AYGIRIDVIVHGQAGKF <small>SLI</small> PTII	343
rP2X2WT	RLDPKY--DPASSGYNFRFAKYYKINGTTTTRTLI K AYGIRIDVIVHGQAGKF <small>SLI</small> PTII	332
hP2X3WT	RLDSVSEKSSVSPGYNFRFAKYYKMENGSEYRTLL K AFGIRFDVLVYGNAGKF <small>N</small> IIPTII	323
hP2X4WT	RLDTRDVEHNVSPGYNFRFAKYYRDLAGNEQRTLI K AYGIRFDIIVFGKAGKF <small>DII</small> PTMI	337
hP2X5WT	RLDNK-LSKS V SSGGYNFRFARYRDAAGVEFRTLM K AYGIRFDVMVNGKAGKF <small>SI</small> PTII	338
hP2X6WT	LQE-----KSYNFRTATHWWEQPGVEARTLL K LYGIRFDILVTGQAGKFGLIPTAV	339
hP2X7WT	RLDDKTTNVSLYPGYNFRYAKYYKE-NNVEKRTLI K VFGIRFDILVFGTGGKF <small>DII</small> QLVV	335
	. : * * * . : : * * : * : * : * : * . * * * . : *	

Fig 3.2. Clustal-Omega Multiple Sequence Alignment of rat P2X2 and human P2X1-7 receptors. Residues in bold are the key lysines in positions K69 and K308 (rat P2X2 numbering) that were mutated to generate the human P2X1-7 dead receptor tools. Residues highlighted in grey are conserved charged and polar amino acids K69, K71, N288, R290, R304, and K308 (rat P2X2 numbering), and underlined residues correspond to strongly conserved amino acid properties S65 (rat P2X2 numbering). These residues were chosen based on the ATP-binding scrutiny performed by site-directed mutagenesis and electrophysiology techniques (Jiang et al., 2000).

3.1.1 Aim and objectives

This thesis chapter aims to provide a reliable and reproducible method for studying human P2X4 subunit assembly. This new approach combined the techniques mentioned above and pharmacological tools with the firm intention to provide clarity on the P2X multimerisation matter. The specific objectives to fulfil were:

1. To optimise the transfection procedure for 1321N1 parental astrocytoma cells with human P2X4 receptors.
2. To confirm that the model system accurately represented human P2X4 receptor activity and its pharmacological properties.
3. To demonstrate that human P2X4 subunits interact to form a functional homomeric channel using dead receptor tools.
4. To validate the experimental system as a well-rounded approach for evidencing human P2X heteromeric interactions.

3.2 Results

3.2.1 Transient transfection and expression of the human P2X4 receptor in a heterologous system

Using human 1321N1 astrocytoma cells as the model to assess homo- and heteromeric assembly of human P2X4 subunits had beneficial and adverse aspects. Human 1321N1 cells are void of endogenous purinergic receptors (Communi et al., 1996). Therefore, the application of extracellular nucleotides would not trigger any intracellular calcium responses. To explore human P2X4 receptor interactions using the dead receptor hypothesis, the human P2X4 receptor must be successfully transfected and expressed in these cells in a similar way as P2X2 and P2X3 receptors were transfected in HEK293 cells by Wilkinson et al. Ironically, these cells are poor transfection hosts (Fig 3.3).

Several factors can influence the outcome of transfection experiments: i) the transfection method chosen and the amount of reagent used, ii) the DNA quality and quantity, iii) the health and viability of the cell line, iv) passage number, v) cell confluence, and vi) the presence or absence of serum and antibiotics in the media. A thorough optimisation process of 1321N1 astrocytoma cell transfection was required to find the perfect balance between cell viability and high transfection efficiency.

1321N1 parental cells were regularly tested for biological contamination to guarantee a healthy and viable culture before transfection and were used between passages P4 and P12 for optimal transient cell transfection (Fig 3.4). 1321N1 cells were always kept at 70-80% confluence at the time of transfection. Cells that were too confluent squeezed together, visually changed morphology, reducing their original size, and underwent contact inhibition resulting in poor uptake of DNA and decreased expression of the transfected gene. However, too few cells in the culture resulted in poor growth without cell-to-cell contact. The key to ensuring optimal confluence was reliably achieved at the time of transfection was to maintain a standard splitting and seeding protocol from experiment to experiment. It is important to note that some cell death was inevitable regardless of the transfection method used.

There are three main types of transfection methods: biological (i.e., virus-mediated transfection, also known as transduction), chemical (i.e., cationic polymer, lipid, amino acid), and physical (i.e., direct microinjection, biolistic particle delivery, electroporation). Three chemical transfection reagents were tested, including TurboFect, X-tremeGENE and Lipofectamine 2000 (described earlier in sections 2.6.1, 2.6.2, and 2.6.3 of Chapter 2).

Firstly, TurboFect was not a suitable transfection reagent, as shown in Figure 3.5. Carbachol-evoked control responses through endogenous muscarinic receptors expressed in 1321N1 human astrocytoma cells showed that the presence of TurboFect at 0.2, 0.4 and 0.6 μ L combined with either 100ng, 200ng or 300ng of human P2X4 WT FLAG-tagged plasmid DNA did not affect cell viability (Fig 3.5B). However, the application of 30 μ M ATP did not evoke any intracellular calcium influx responses (11.9 \pm 1.29% for 200ng and 0.4 μ L; Fig 3.5A and B). Moreover, transfection using higher amounts of TurboFect (1 μ L,

1.2 μ L and 2 μ L) combined with either 100ng, 200ng or 300ng of human P2X4 WT FLAG-tagged plasmid had major cytotoxicity effects in 1321N1 human astrocytoma cells as represented by no ATP-evoked responses or Carbachol-evoked control responses (Fig 3.5C and D). These data inferred low and unsuccessful cell transfection rates using TurboFect as a transfection reagent.

Secondly, small ATP-evoked responses were observed 48 hours post-transfection using 1000ng of human P2X4 WT FLAG-tagged plasmid combined with 6 μ L of X-tremeGENE transfection reagent ($30.0\pm5.86\%$; Fig 3.6A and B). Similar results were obtained when 1321N1 human astrocytoma cells were transiently transfected using 2000ng of plasmid and 5 μ L of X-tremeGENE reagent ($34.5\pm1.64\%$, $p>0.05$; Fig 3.6A and B). Different initial cell densities and transfection complex incubation times were tested to determine their effect on ATP-evoked calcium responses in transiently transfected 1321N1 human astrocytoma cells. A significant reduction of ATP-evoked calcium responses was evidenced when seeding 1.25×10^4 cells per well 24 hours before transfection. Thus, a lower cell number could not counteract the cytotoxicity effects caused by the presence of 1000ng of plasmid DNA and 6 μ L of X-tremeGENE ($46.5\pm3.21\%$ vs $11.6\pm2.20\%$, $p<0.001$; Fig 3.6A and B). An equivalent outcome was obtained using 2000ng of plasmid DNA and 5 μ L of X-tremeGENE ($44.3\pm3.99\%$ vs $6.83\pm2.18\%$, $p<0.001$; Fig 3.6A and B). Each transfection reagent requires different incubation times to form the DNA-reagent complexes before cell transfection. According to the manufacturer, once desired amounts of X-tremeGENE and plasmid DNA are mixed, a 15-minute incubation period is necessary. Increasing this time to 30 minutes did not improve cell transfection efficiency, as shown in Figures 3.6C and 3.6D ($42.1\pm2.61\%$ vs $22.4\pm1.52\%$ for 1000ng and 6 μ L, $p<0.001$).

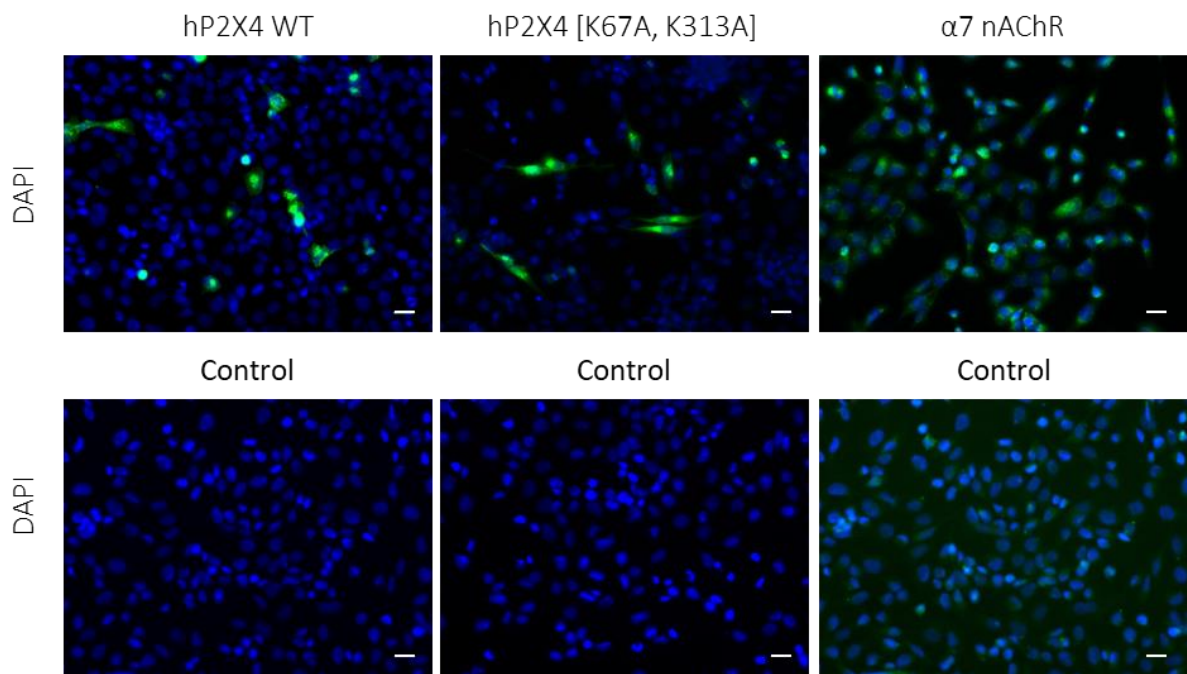
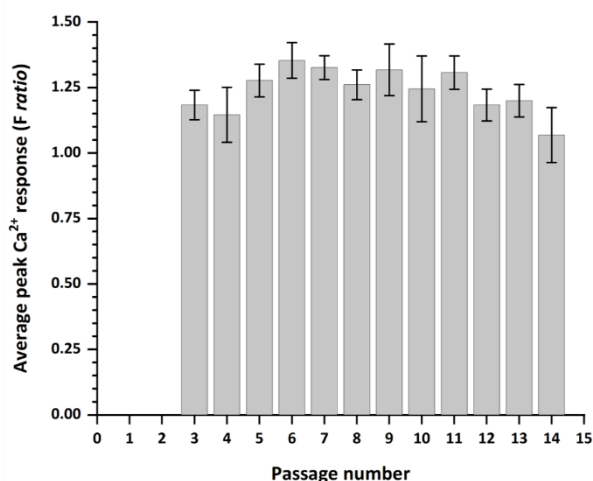


Fig 3.3. Human 1321N1 parental astrocytoma cells are poor transfection hosts. Immunocytochemical staining for human 1321N1 astrocytoma cells transiently transfected with either hP2X4 WT, hP2X4 [K67A, K313A], or α 7 nAChR receptors. Images were taken at 20X augmentation and scale bars represent 25 μ m. Details on staining can be found in Chapter 2 (section 2.12). Images were representative of three independent experiments ($N=3$).

A.



B.

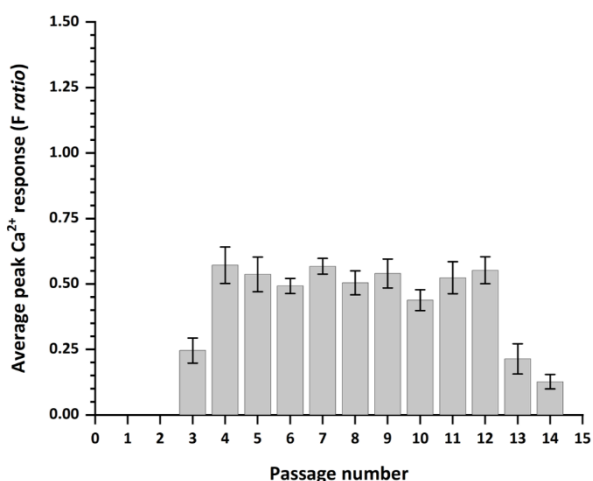


Fig 3.4. The effect of passage on the magnitude of 30 μM ATP-evoked calcium responses in human P2X4 stably and transiently transfected 1321N1 astrocytoma cells. Averaged 30 μM ATP-evoked intracellular calcium responses in human P2X4 stably (A) and transiently transfected (B) 1321N1 astrocytoma cells. Data were represented as mean \pm SEM ($N=3$).

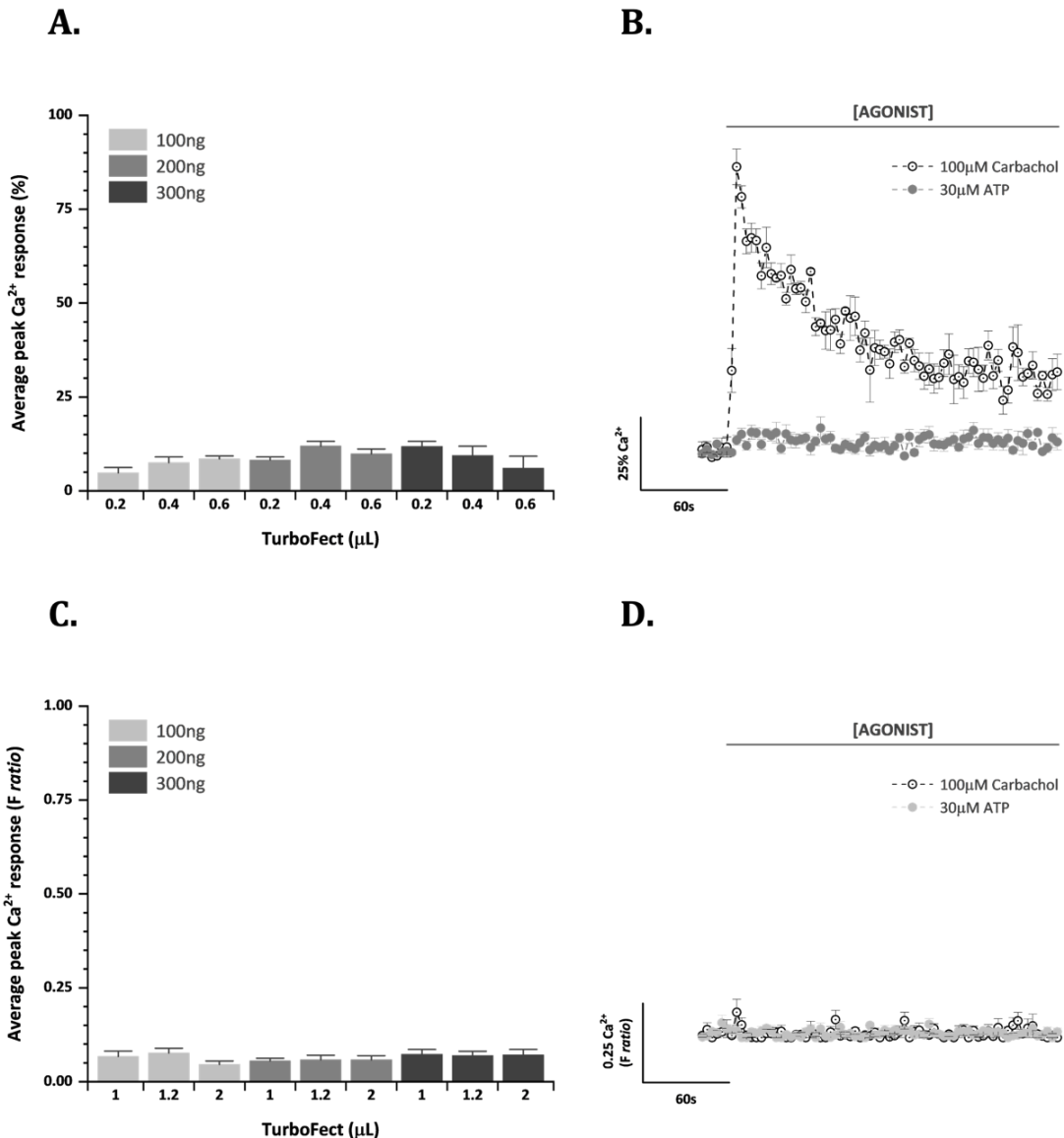


Fig 3.5. TurboFect was not a suitable reagent for transient transfection of human P2X4 WT in 1321N1 parental astrocytoma cells. (A, C) Comparison of average peak Ca^{2+} responses upon stimulation with 30 μM ATP using various transfection conditions. Final hP2X4 WT plasmid DNA amounts were expressed in ng per well and final TurboFect transfection reagent amounts were expressed in μL per well. (B, D) Example of averaged time-resolved intracellular Ca^{2+} responses elicited by 30 μM ATP (closed circles) compared to Ca^{2+} influx caused by 100 μM Carbachol application as a cell viability control (open circle with dot) in 1321N1 astrocytoma cells transiently transfected with either 200ng of plasmid and 0.4 μL of TurboFect (B) or 100ng of plasmid and 1.2 μL of TurboFect (D). (A, B) Data were normalised to the maximal response to 100 μM Carbachol. (C, D) Raw data were obtained from SoftMax Pro Flex Station 3 software. All data were represented as mean \pm SEM ($N=3$).

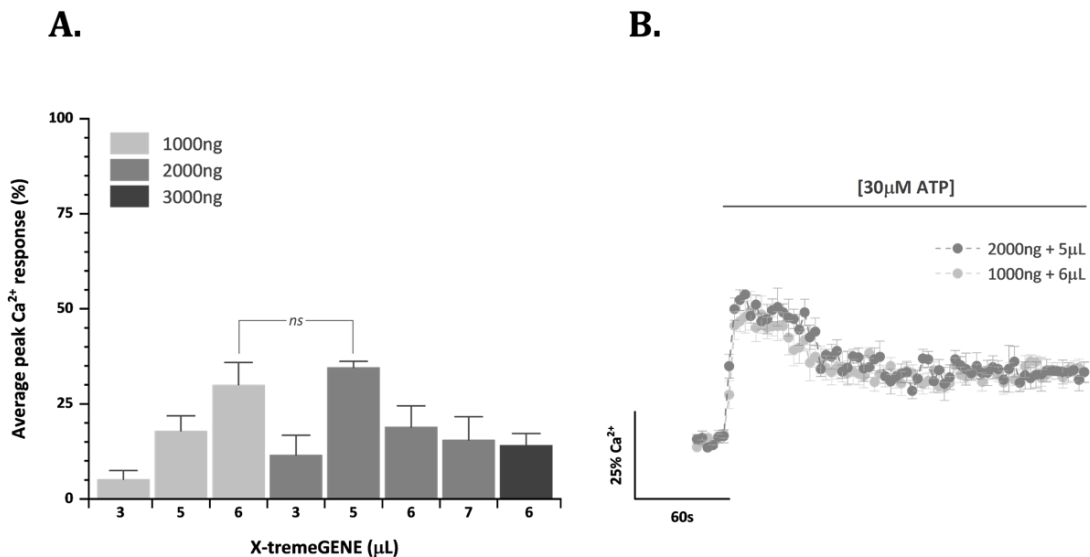


Fig 3.6. X-tremeGENE reagent had low success rates for transient transfection of human P2X4 WT in 1321N1 parental astrocytoma cells. (A) Comparison of average peak Ca^{2+} responses upon stimulation with 30 μM ATP using various transfection conditions. Final hP2X4 WT plasmid DNA amounts were expressed in ng per well and final X-tremeGENE transfection reagent amounts were expressed in μL per well. (B) Example of averaged time-resolved intracellular Ca^{2+} responses elicited by 30 μM ATP in 1321N1 astrocytoma cells transiently transfected with either 1000ng of plasmid and 6 μL of X-tremeGENE (light grey circles) or 2000ng of plasmid and 5 μL of X-tremeGENE (middle grey circles). All data were normalised to the maximal response to 100 μM Carbachol. Data were represented as mean \pm SEM ($N=5$).

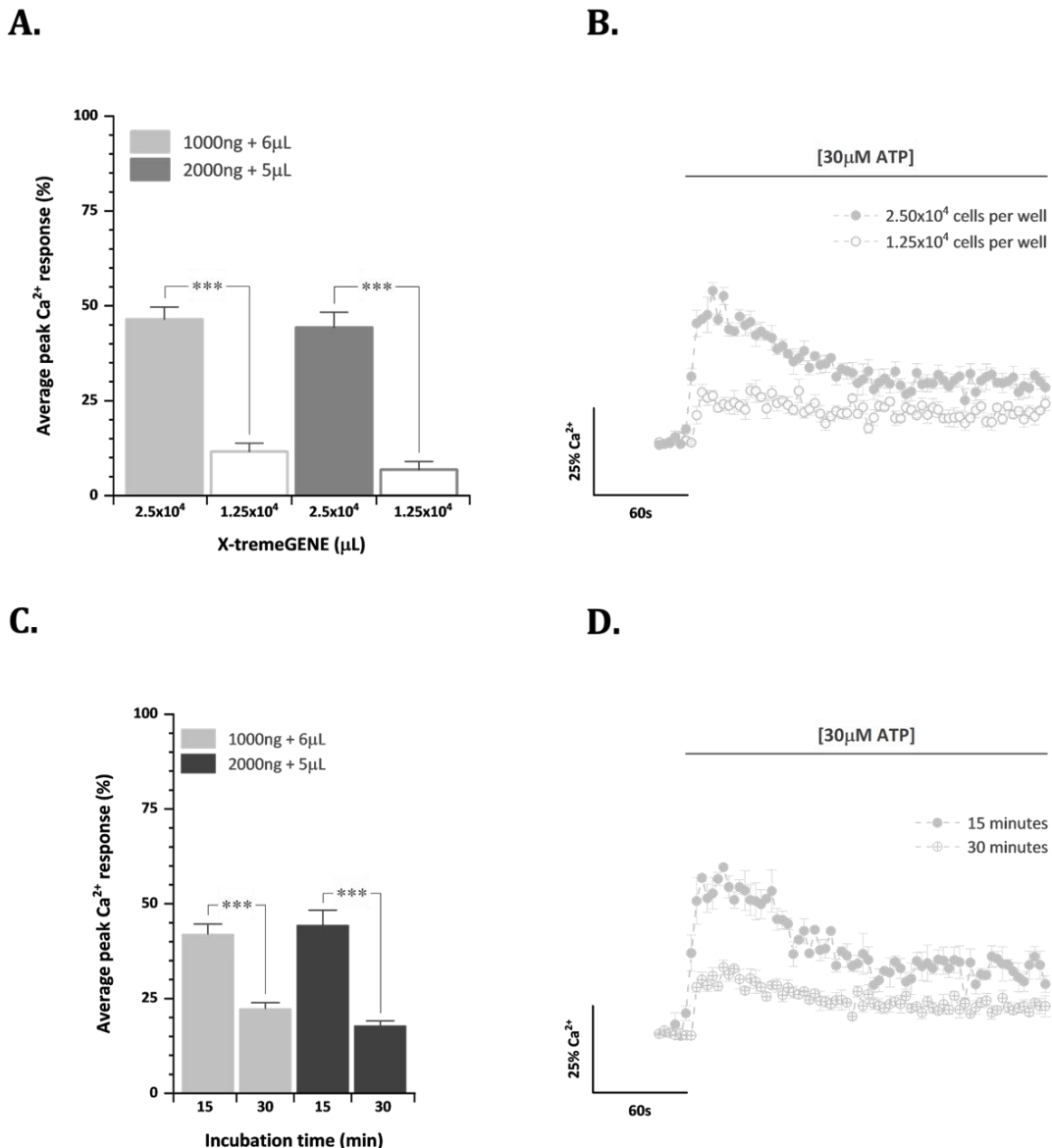


Fig 3.7. Changes in initial cell density and transfection complex incubation times did not improve the transfection efficiency and success rates of X-tremeGENE. (A, C) Comparison of different initial cell seeding densities effects (A) and transfection complex incubation times (C) on average peak Ca^{2+} responses upon stimulation with 30 μ M ATP. Final hP2X4 WT plasmid DNA and X-tremeGENE transfection reagent amounts were expressed on a per-well basis. (B) Averaged time-resolved intracellular Ca^{2+} responses elicited by 30 μ M ATP in 1321N1 astrocytoma cells transiently transfected with 1000ng of plasmid and 6 μ L of X-tremeGENE at either 2.50x10⁴ (closed light grey circles) or 1.25x10⁴ (open light grey circles) initial seeding densities. (D) Averaged time-resolved intracellular Ca^{2+} responses elicited by 30 μ M ATP in 1321N1 astrocytoma cells transiently transfected with 1000ng of plasmid and 6 μ L of X-tremeGENE with a prior 15-minute (closed light grey circles) or a 30-minute (light grey circles with a cross) incubation period. All data were normalised to the maximal response to 100 μ M Carbachol. Data were represented as mean \pm SEM ($N=3$).

Finally, Lipofectamine showed medium transfection efficiency rates that were highly improved by optimisation processes (Fig 3.8 and 3.9). Following the manufacturer's recommendations, various amounts of Lipofectamine 2000 and human P2X4 WT FLAG-tagged plasmid DNA were tested. The biggest ATP-evoked intracellular calcium responses were obtained using 200ng or 300ng of plasmid mixed with 0.5µL of Lipofectamine 2000 ($72.8\pm6.28\%$ and $56.7\pm4.80\%$, respectively, $p>0.05$; Fig 3.8A and B). The same conditions were tested in parallel using either 1.25×10^4 or 2.5×10^4 cells per well as initial cell densities. Data showed that increasing initial cell numbers did not correlate with more noticeable ATP-evoked calcium responses or more efficient cell transfection. The ATP-evoked maximal calcium responses were significantly reduced by roughly 35% and 15% when cells were seeded at 2.5×10^4 cells per well and transiently transfected using 200ng or 300ng of plasmid DNA with 0.5µL of Lipofectamine 2000, respectively ($p<0.001$ and $p<0.05$, correspondingly; Fig 3.9A and B). Furthermore, data showed that 200ng of human P2X4 WT FLAG-tagged DNA and 0.5µL of Lipofectamine 2000 transfection conditions were consistently giving the biggest ATP-evoked calcium responses compared to 300ng of DNA and 0.5µL of Lipofectamine 2000 ($76.1\pm5.76\%$ vs $62.5\pm2.13\%$, $p<0.05$; Fig 3.9A). According to the manufacturer, antibiotics in the cell culture media and Lipofectamine 2000 transfection reagent could cause cytotoxicity effects and lower transfection efficiencies. As mentioned before, transfection complex incubation times vary depending on the reagent used. Lipofectamine 2000 and DNA mixtures are typically incubated only for 5 minutes at room temperature. Even though ATP and Carbachol-induced calcium responses obtained were already highly efficient and suggestive of healthy cells, removing the antibiotics from the DMEM complete growth media, as well as increasing the transfection complex incubation time to 20 minutes, significantly improved cell transfection efficiency, increasing the ATP-evoked calcium responses by approximately 30% ($61.56\pm3.00\%$ vs $89.1\pm3.98\%$, $p<0.05$; Fig 3.9C and D).

Whole-cell and cell membrane expression levels for human P2X4 WT FLAG-tagged subunits were assessed by biotinylation and Western blotting to ensure transient cell transfection produced high amounts of the protein of interest. Protein detection revealed two bands at 60KDa and 120KDa. The former corresponded to the human P2X4 monomeric molecular weight and showed higher expression levels at whole-cell levels than at cell surface (1.43 ± 0.24 au vs 0.48 ± 0.15 au, respectively, $p<0.05$; Fig 3.10A and B). There are various possibilities to explain the 120KDa bands: i) most likely corresponded to folding and assembly artefacts of the overexpressed protein, ii) to highly glycosylated protein, or iii) to protein oligomerisation. Interestingly, the expression levels of these higher bands were significantly higher at the cell surface rather than at whole-cell levels (0.43 ± 0.18 au vs 1.16 ± 0.17 au, respectively, $p<0.05$; Fig 3.10A and B). In addition, the 120KDa form predominated over the 60KDa at cell surface levels ($p<0.05$; Fig 3.10B).

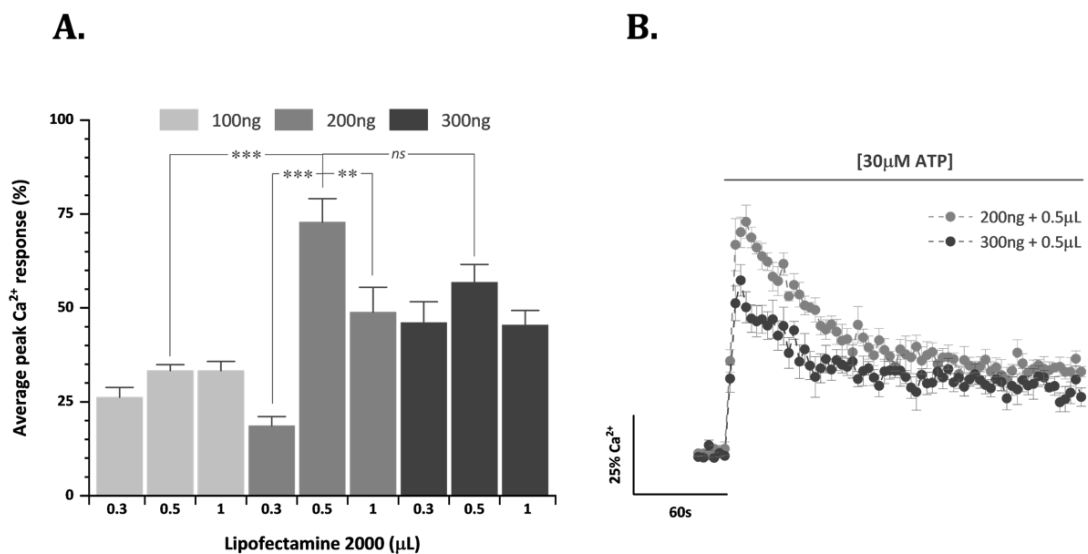


Fig 3.8. Successful transient transfection of human P2X4 WT in 1321N1 parental astrocytoma cells using Lipofectamine 2000 reagent. (A) Comparison of average peak Ca^{2+} responses upon stimulation with 30 μ M ATP using various transfection conditions. Final hP2X4 WT plasmid DNA amounts were expressed in ng per well and final Lipofectamine 2000 transfection reagent amounts were expressed in μ L per well. (B) Averaged time-resolved intracellular Ca^{2+} response elicited by 30 μ M ATP in 1321N1 astrocytoma cells transiently transfected with either 200ng or 300ng of plasmid and 0.5 μ L of Lipofectamine 2000. All data were normalised to the maximal response to 100 μ M Carbachol. Data were represented as mean \pm SEM ($N=5$).

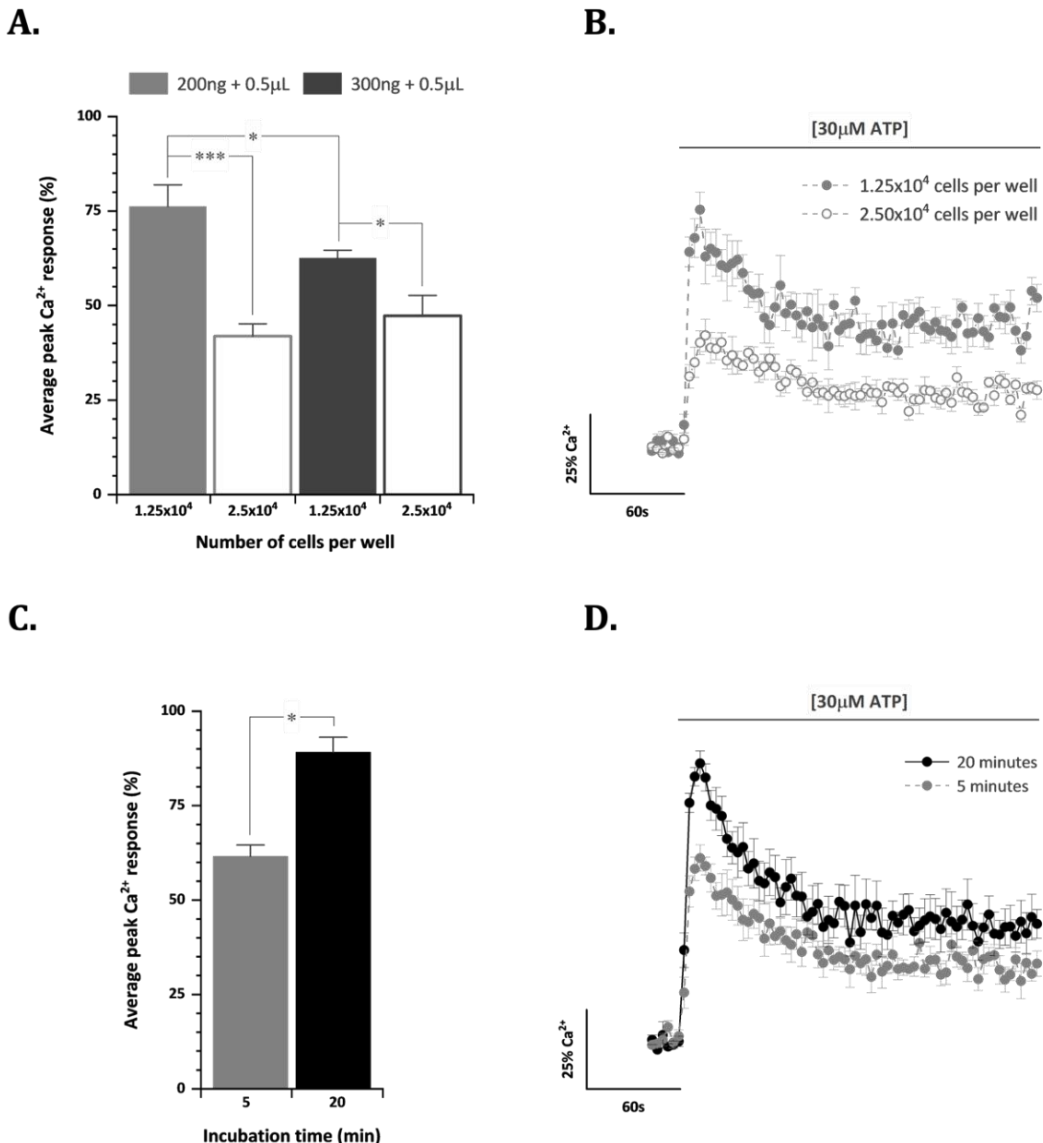


Fig 3.9. Optimisation of human P2X4 WT transient transfection protocol in 1321N1 parental astrocytoma cells using Lipofectamine 2000 reagent. (A) Comparison of different initial cell seeding densities effects on average peak Ca²⁺ responses upon stimulation with 30µM ATP. Final hP2X4 WT plasmid DNA and Lipofectamine 2000 transfection reagent amounts were expressed on a per-well basis. (B) Averaged time-resolved intracellular Ca²⁺ responses elicited by 30µM ATP in 1321N1 astrocytoma cells transiently transfected with 200ng of plasmid and 0.5µL of Lipofectamine 2000 at either 1.25x10⁴ (closed grey circles) or 2.50x10⁴ (open grey circles) initial seeding densities. (C) Comparison of different transfection complex incubation times on average peak Ca²⁺ responses upon stimulation with 30µM ATP. Final hP2X4 WT plasmid DNA and Lipofectamine 2000 transfection reagent amounts were expressed on a per-well basis. (D) Averaged time-resolved intracellular Ca²⁺ responses elicited by 30µM ATP in 1321N1 astrocytoma cells transiently transfected with 200ng of plasmid and 0.5µL of Lipofectamine 2000 with a prior 5-minute (closed grey circles) or a 20-minute (closed black circles) incubation period. All data were normalised to the maximal response to 100µM Carbachol. Data were represented as mean ± SEM ($N=5$).

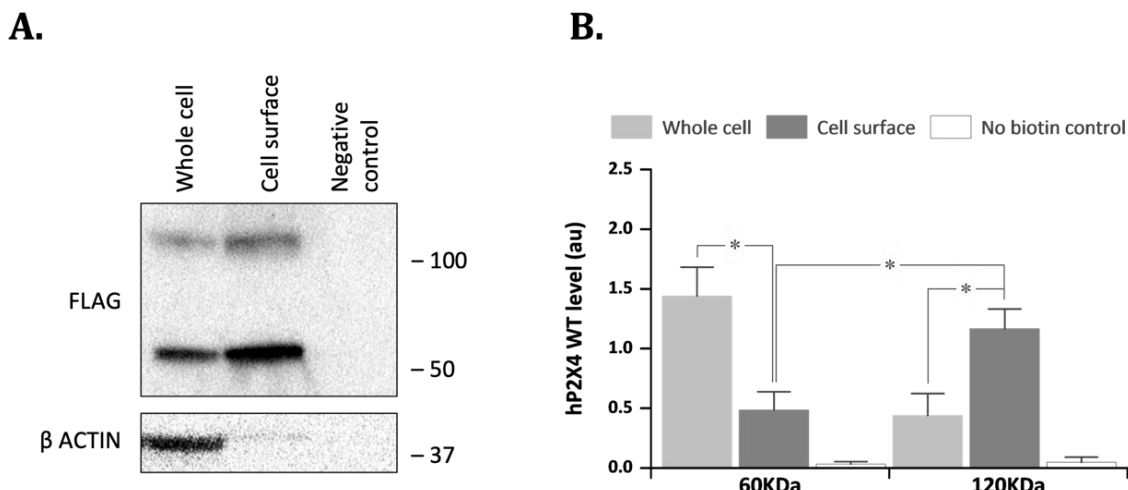


Fig 3.10. Whole-cell and cell surface expression levels of human P2X4 WT FLAG-tagged subunits in transiently transfected 1321N1 parental astrocytoma cells. (A) Representative immunoblot for hP2X4 WT FLAG-tagged protein (top) and β -actin loading control (bottom). Molecular weight size standards were indicated in KDa. Lane 1 corresponded to a whole-cell sample, lane 2 to cell surface protein lysate, and lane 3 was a negative control for biotin labelling. (B) Comparison of densitometric analysis of hP2X4 WT FLAG-tagged protein levels relative to loading control for whole-cell and cell surface lysates. Data were represented as mean \pm SEM ($N=3$).

The complete cell transfection optimisation process for human 1321N1 parental astrocytoma cells was summarised in Tables 3.1 and 3.2. All reagents and specific transfection conditions used were detailed and graded depending on cell viability effects and ATP-evoked maximal calcium responses obtained. The ideal approach was determined empirically and was selected for: high transfection efficiency, low cell toxicity, accessibility and convenience, and reproducibility. Table 2.6 (Chapter 2) summarises the optimised procedure and conditions for transient transfection of 1321N1 parental astrocytoma cells.

Table 3.1. Summary of the conditions used to transiently transfet human 1321N1 parental astrocytoma cells using Turbofect and X-tremeGENE reagents.

Reagent	Number of cells	Final DNA (ng)	Final reagent (μ L)	Incubation time	Complex (μ L)	Media change (h)	Cell viability [◊]	Ca^{2+} assay (h)	Success [◊]
TurboFect	12500	100	0.2, 0.4, 0.6	15'	20	—	2	48	Fail
TurboFect	12500	100	1, 1.2, 2	15'	20	—	0	48	Fail
TurboFect	12500	200	0.2, 0.4, 0.6	15'	20	—	2	48	Fail
TurboFect	12500	200	1, 1.2, 2	15'	20	—	0	48	Fail
TurboFect	12500	300	0.2, 0.4, 0.6	15'	20	—	2	48	Fail
TurboFect	12500	300	1, 1.2, 2	15'	20	—	0	48	Fail
X-tremeGENE	25000	1000	3	15'	5	6 (top-up)	3	48	Fail
X-tremeGENE	25000	1000	5	15'	5	6 (top-up)	3	48	Low
X-tremeGENE	25000	1000	6	15'	5	6 (top-up)	2	48	Medium
X-tremeGENE	12500	1000	6	15'	5	6 (top-up)	1	48	Fail
X-tremeGENE	25000	1000	6	30'	5	6 (top-up)	2	48	Low
X-tremeGENE	25000	2000	3	15'	5	6 (top-up)	3	48	Low
X-tremeGENE	25000	2000	5	15'	5	6 (top-up)	3	48	Medium
X-tremeGENE	12500	2000	5	15'	5	6 (top-up)	1	48	Fail
X-tremeGENE	25000	2000	5	30'	5	6 (top-up)	2	48	Low
X-tremeGENE	25000	2000	6	15'	5	6 (top-up)	2	48	Low
X-tremeGENE	25000	2000	7	15'	5	6 (top-up)	2	48	Low
X-tremeGENE	12500	2000	7	15'	5	6 (top-up)	1	48	Fail
X-tremeGENE	25000	3000	6	15'	5	6 (top-up)	2	48	Low
X-tremeGENE	12500	3000	6	15'	5	6 (top-up)	2	48	Fail
X-tremeGENE	25000	1000	3, 5, 6	15'	10	6 (top-up)	0	48	Fail
X-tremeGENE	25000	2000	3, 5, 6	15'	10	6 (top-up)	0	48	Fail

Number of cells, final DNA, and final reagent amounts are given in a per-well basis. [◊] Cell viability ranking: 0 (cell death), 1 (40% confluence), 2 (70% confluence), 3 (confluent monolayer); [◊] Success ranking: fail (no responses), low (0.2 F ratio), medium (0.4 F ratio or inconsistencies), high (0.6 F ratio and consistency throughout).

Table 3.2. Summary of the conditions used to transiently transfet human 1321N1 parental astrocytoma cells using the Lipofectamine 2000 reagent.

Number of cells	Final DNA (ng)	Final reagent (μ L)	Incubation time	Complex (μ L)	Pen/Strep present?	Media change (h)	Cell viability ϕ	Ca^{2+} assay (h)	Success w
12500	100	0.3	5'	10	Yes	—	2	48	Low
12500	100	0.5	5'	10	Yes	—	2	48	Low
12500	100	1	5'	10	Yes	—	1	48	Low
12500	200	0.3	5'	10	Yes	—	2	48	Low
12500	200	0.5	5'	10	Yes	—	2	48	Medium-High
12500	200	0.5	20'	10	Yes	—	2	48	Medium-High
12500	200	0.5	20'	50	No	6	2	48	High
12500	200	0.8	5'	10	Yes	6	2	48	Low
25000	200	0.8	5'	10	Yes	6	2	48	Low
12500	200	1	5'	10	Yes	—	2	48	Medium
12500	200	1	5'	10	Yes	6	2	48	Medium
25000	200	1	5'	10	Yes	—	1	48	Medium
25000	200	1	5'	10	Yes	6	2	48	Medium
12500	300	0.3	5'	10	Yes	—	2	48	Low
12500	300	0.5	5'	10	Yes	—	2	48	Medium
12500	300	0.8	5'	10	Yes	6	2	48	Low
25000	300	0.8	5'	10	Yes	6	2	48	Low
12500	300	1	5'	10	Yes	—	2	48	Medium
12500	300	1	5'	10	Yes	6	2	48	Medium
25000	300	1	5'	10	Yes	—	1	48	Medium
25000	300	1	5'	10	Yes	6	2	48	Medium
12500	400	0.5	20'	50	No	6	2	48	High

Number of cells, final DNA, and final reagent amounts are given in a per-well basis. The optimised conditions are highlighted in bold. ϕ Cell viability ranking: 0 (cell death), 1 (40% confluence), 2 (70% confluence), 3 (confluent monolayer); w Success ranking: fail (no responses), low (0.2 F ratio), medium (0.4 F ratio or inconsistencies), high (0.6 F ratio and consistency throughout).

3.2.2 Pharmacological characterisation of the human P2X4 receptor in a heterologous system

3.2.2.1 ATP-evoked calcium responses in 1321N1 astrocytoma cells stably expressing the human P2X4 receptor

Activation of P2X4 ionotropic receptors leads to a temporary elevation of intracellular calcium levels due to small cation ion entry from the extracellular space. To ascertain whether the human P2X4 receptors stably expressed in 1321N1 astrocytoma cells were functionally active, exogenous ATP was applied and real-time changes in intracellular calcium levels were monitored.

ATP evoked a concentration-dependent increase in intracellular calcium levels, reaching the maximal response amplitude at a concentration of 30 μ M (Table 3.3; Fig 3.11). ATP had a half maximal effective concentration (EC_{50}) of $0.74\pm0.18\mu$ M. Figure 3.7B depicts time-resolved intracellular calcium responses upon human P2X4 receptor activation with 30 μ M ATP. ATP induced an initial rapid calcium response that slowly decayed to a sustained elevated phase (approximately 60% above baseline). P2X4 receptors have been reported to have a slow desensitisation phase, as well as P2X2 receptors (North & Surprenant, 2000). Furthermore, ATP did not evoke endogenous calcium responses in untransfected 1321N1 parental cells (Fig 3.12), confirming that ATP-evoked calcium responses recorded were due to the presence of human P2X4 receptors. Carbachol was used as a control for cell viability since 1321N1 astrocytes express M3 and M5 muscarinic acetylcholine receptors (Bayon et al., 2007; Burnett et al., 2011). Accordingly, Carbachol evoked an intracellular calcium increase which decayed to approximately 30% above baseline over the recorded time period (Fig 3.12).

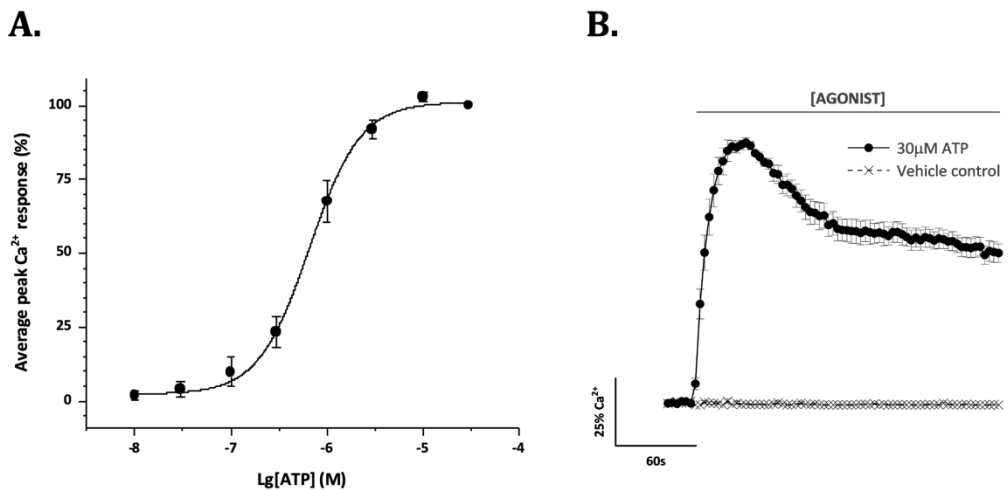


Fig 3.11. ATP mediated a Ca^{2+} response in human P2X4 1321N1 stable astrocytoma cells in a concentration-dependent manner. (A) ATP concentration-response curves for the peak magnitude of intracellular Ca^{2+} influx. (B) Averaged time-resolved intracellular Ca^{2+} influx elicited by 30 μM ATP. All data were normalised to the maximal response observed in the majority of replicates, which was the response to 30 μM ATP. Data were represented as mean \pm SEM ($N=7$).

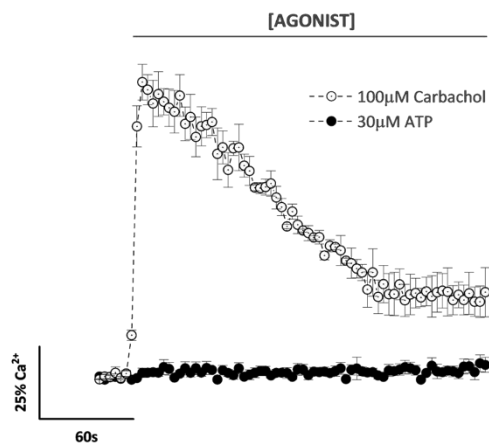


Fig 3.12. ATP did not cause an endogenous Ca²⁺ response in 1321N1 parental astrocytoma cells. Averaged time-resolved intracellular Ca²⁺ response elicited by 30μM ATP (closed circles) compared to Ca²⁺ influx caused by 100μM Carbachol application as a cell viability control (open circles). All data were normalised to the maximal response to 100μM Carbachol. Data were represented as mean ± SEM ($N=3$).

3.2.2.2 Agonist-evoked calcium responses in 1321N1 astrocytoma cells stably expressing the human P2X4 receptor

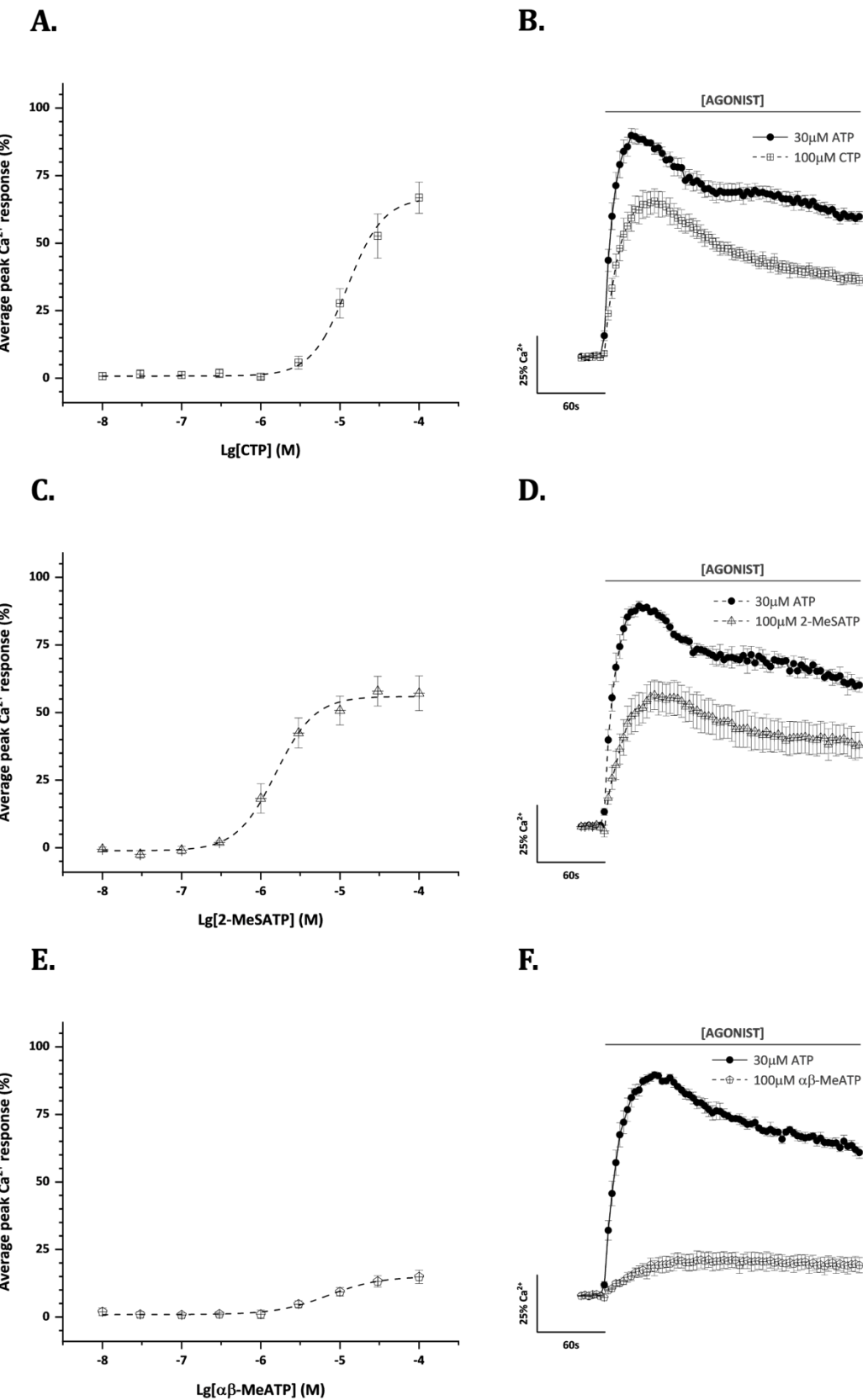
The effects of exogenous CTP and different ATP analogues were measured to characterise the pharmacological profile of the human P2X4 receptor heterologously expressed in 1321N1 astrocytoma cells.

Application of CTP, 2-MeSATP, α,β -MeATP, BzATP and γ -imidoATP evoked a calcium response in human P2X4 receptor stable 1321N1 astrocytoma cells (Table 3.3; Fig 3.13). It is important to note a significant rightward shift in the agonist concentration-response curves compared to ATP stimulation control. ATP and all compounds tested were then ranked in order of potency (EC_{50}): ATP ($0.74\pm0.18\mu M$) > 2-MeSATP ($1.66\pm0.24\mu M$) >> α,β -MeATP ($6.52\pm0.69\mu M$) = BzATP ($10.7\pm2.44\mu M$) > CTP ($20.0\pm4.22\mu M$) = γ -imidoATP ($20.3\pm1.59\mu M$). Furthermore, all five triggered the maximal calcium influx response at a concentration of $100\mu M$ whilst ATP produced its maximal effects at $30\mu M$. Analysis was also performed to rank them in order of efficacy: ATP (100%) >> γ -imidoATP ($84.0\pm5.01\%$) > CTP ($66.8\pm5.76\%$) = 2-MeSATP ($57.9\pm5.51\%$) > BzATP ($35.0\pm3.82\%$) >> α,β -MeATP ($14.8\pm2.43\%$). γ -imidoATP evoked the largest increase in intracellular calcium levels after ATP. However, its effects were only evident at $30\mu M$ and $100\mu M$ concentrations making it also the less potent compound for human P2X4 receptor activation, together with CTP. The human P2X4 receptor desensitisation phase after the application of $100\mu M$ γ -imidoATP was typically sustained over time at approximately 40% above baseline (Fig 3.13J). CTP and 2-MeSATP had similar efficacy values for human P2X4 receptor activation, and both caused this receptor to slowly desensitise over time (approximately 30% above baseline; Fig 3.13B and D). The latter was also ranked the most potent ATP analogue. BzATP and α,β -MeATP induced the smallest intracellular calcium responses in human P2X4 stable 1321N1 astrocytoma cells but placed third in the human P2X4 potency rank. BzATP caused the human P2X4 receptor to slowly desensitise at approximately 20% above baseline (Fig 3.13H). Besides, α,β -MeATP maintained the human P2X4 receptor activated throughout the recorded time period at approximately 15% above baseline levels, suggesting this compound affected the desensitisation of the human P2X4 receptor (Fig 3.13F). In addition, intracellular calcium responses were not reported after applying either ATP- γ -S or AP4A at any of the concentrations tested (Fig 3.14).

Table 3.3. Summary of agonist-evoked responses via human P2X4 receptors stably expressed in 1321N1 astrocytoma cells.

Agonist	EC ₅₀ (μM)	P value	E _{max} (μM)	Efficacy (%)	P value
ATP	0.74±0.18		30	100±0.00	<0.01
CTP	20.0±4.22	<0.01	100	66.8±5.76	<0.01
2-MeSATP	1.66±0.24	<0.05	100	57.9±5.51	<0.01
α,β-MeATP	6.52±0.69	<0.01	100	14.8±2.43	<0.01
BzATP	10.7±2.44	<0.05	100	35.0±3.82	<0.01
γ-imidoATP	20.3±1.59	<0.001	100	84.0±5.01	<0.01
ATP-γ-S	/	/	/	/	/
AP4A	/	/	/	/	/

Statistical analysis was performed against 30μM ATP-evoked calcium responses in SBS.



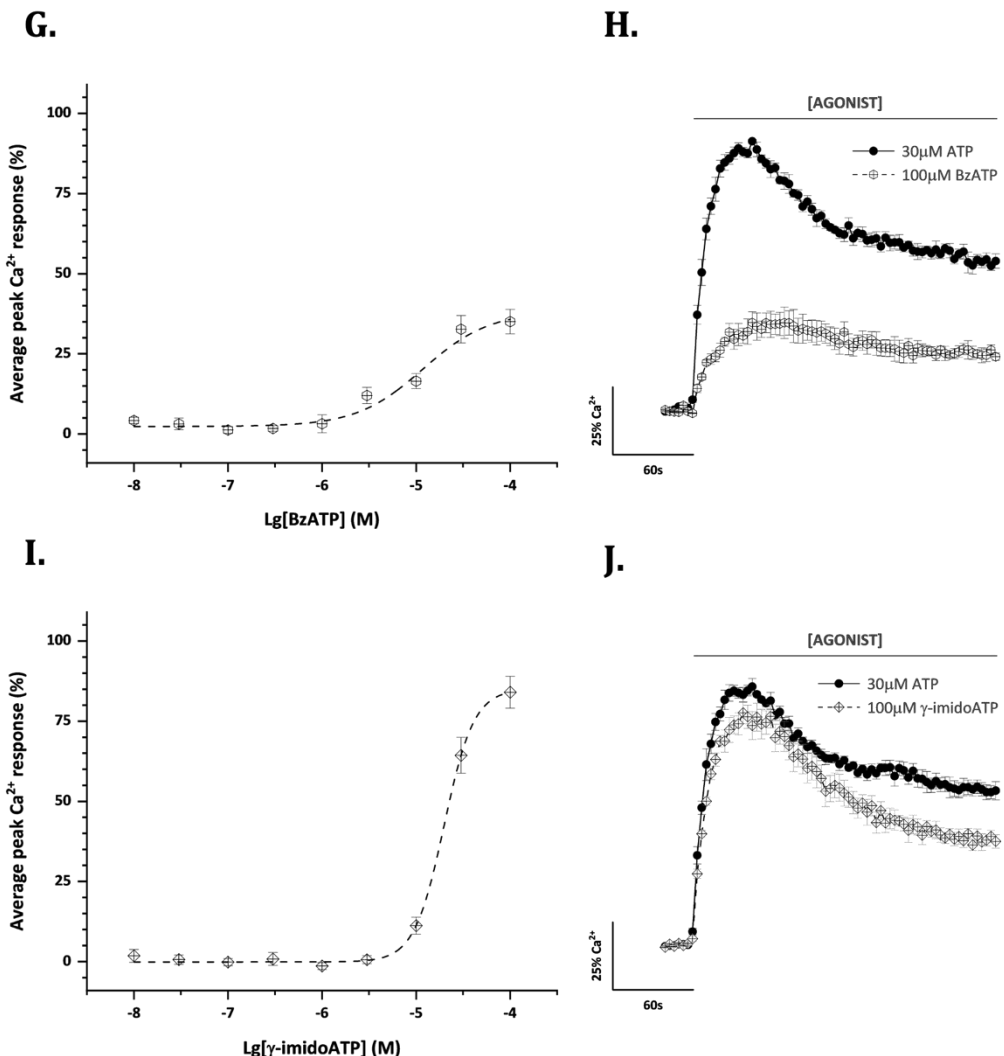


Fig 3.13. Pharmacological characterisation of the human P2X4 receptor in 1321N1 stable astrocytoma cells. Concentration-response curves for the peak magnitude of intracellular Ca^{2+} entry evoked by (A) CTP ($N=7$), (C) 2-MeSATP ($N=5$), (E) $\alpha\beta\text{-MeATP}$ ($N=7$), (G) BzATP ($N=5$), (I) $\gamma\text{-imidoATP}$ ($N=5$). Averaged time-resolved intracellular Ca^{2+} responses elicited by (B) $100\mu\text{M}$ CTP ($N=7$), (D) $100\mu\text{M}$ 2MeSATP ($N=5$), (F) $100\mu\text{M}$ $\alpha\beta\text{-MeATP}$ ($N=7$), (H) $100\mu\text{M}$ BzATP ($N=5$), (J) $100\mu\text{M}$ $\gamma\text{-imidoATP}$ ($N=5$). Agonists were also tested at $300\mu\text{M}$ concentrations for all calcium mobilisation assays but showed smaller responses compared to the calcium responses mediated by $100\mu\text{M}$ concentrations of agonist (these data points were not shown as the Hill1 function would not fit the sigmoidal curve). All data were normalised to the maximal response to $30\mu\text{M}$ ATP. Data were represented as mean \pm SEM.

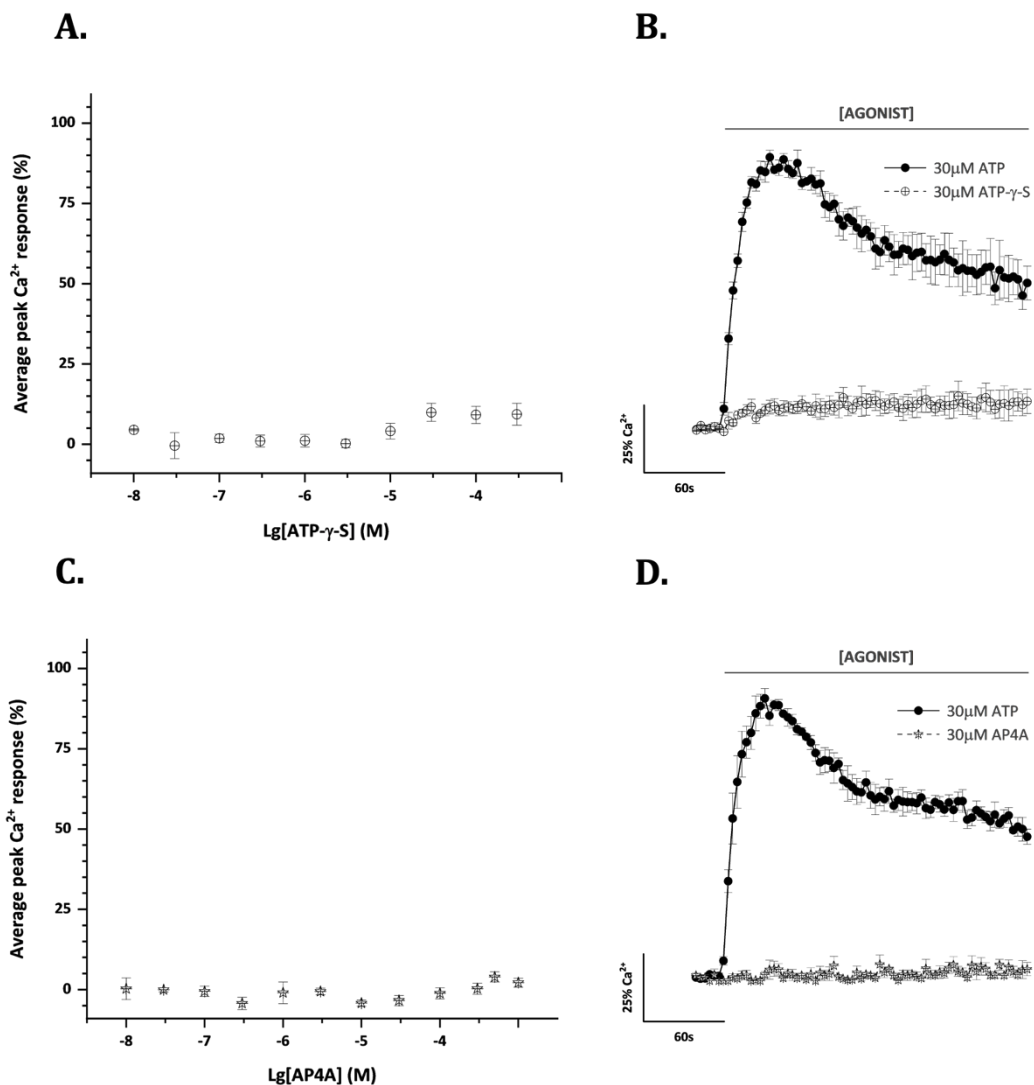


Fig 3.14. Application of ATP- γ -S and AP4A did not induce Ca^{2+} responses in 1321N1 astrocytoma cells stably expressing human P2X4 receptors. Lack of intracellular Ca^{2+} influx evoked by (A) ATP- γ -S and (C) AP4A at various concentrations. Averaged time-resolved intracellular Ca^{2+} responses elicited by 30 μM ATP compared to (B) 30 μM ATP- γ -S and (D) 30 μM AP4A. All data were normalised to the maximal response to 30 μM ATP. Data were represented as mean \pm SEM ($N=3$).

3.2.2.3 Investigating the inhibitory effects of broad-spectrum P2X receptor antagonists in human P2X4 receptor stable 1321N1 astrocytoma cells

Broad-spectrum P2 antagonists proved to be and still are useful pharmacological tools for understanding the P2X4 ion channel function and its physiological roles. These molecules were tested to corroborate the pharmacological profile of heterologously expressed human P2X4 receptors in 1321N1 astrocytoma cells. To investigate the inhibitory effects of broad-spectrum P2 receptor antagonists on human P2X4 receptor activity, 1321N1 stable astrocytoma cells were incubated for 30 minutes with varying drug concentrations and stimulated with 1.5 μ M ATP. This sub-maximal ATP concentration was determined by extrapolating the EC₈₀ value from the ATP-evoked concentration-response curve for the human P2X4 receptor (1.51 \pm 0.28 μ M; Fig 3.11A).

Human P2X4 receptors displayed sensitivity to the broad-spectrum antagonists TNP-ATP and PPADS but not Suramin (Table 3.4; Fig 3.15 and 3.16). The presence of Suramin did not cause any significant inhibitory effects on the ATP-evoked calcium response even at high concentrations ranging from 10 μ M to 100 μ M (Fig 3.16A). The average maximal response to ATP, even in the presence of 100 μ M Suramin, was about 102.1 \pm 2.38% compared to vehicle control responses ($p>0.05$; Fig 3.16). As Suramin is commonly used as a general P2 receptor antagonist, these results suggest that the human P2X4 receptor is relatively insensitive to blockade by the conventional antagonist. TNP-ATP and PPADS are known non-selective P2X antagonists. In contrast to Suramin, both TNP-ATP and PPADS inhibited the human P2X4-evoked intracellular calcium response to ATP in a concentration-dependent manner (Fig 3.15A and C). The half maximal inhibitory concentration (IC₅₀) values obtained were 16.6 \pm 4.71 μ M and 33.8 \pm 16.6 μ M, respectively ($p>0.05$). The two compounds attained a complete blockage of the calcium response at a concentration of 100 μ M (Fig 3.15). To fully characterise their mode of action, the effects of 100 μ M TNP-ATP and 100 μ M PPADS on an ATP concentration-response curve were analysed. ATP provoked a concentration-dependent calcium influx in the presence of 100 μ M TNP-ATP (Fig 3.17A and B). Its presence did not affect the ATP-evoked maximal response at 30 μ M compared to the control (96.8 \pm 4.08%, $p>0.05$; Fig 3.17B) but caused a substantial rightward shift of the curve, significantly increasing the ATP EC₅₀ value to 10.1 \pm 2.18 μ M ($p<0.05$; Fig 3.17A). Thus, TNP-ATP demonstrated competitive inhibition of human P2X4 receptors stably expressed 1321N1 astrocytoma cells. On the other hand, 100 μ M PPADS caused a significant reduction of ATP-evoked calcium responses at concentrations ranging from 1 μ M to 30 μ M, reaching only a 43.1 \pm 7.53% maximal response amplitude at 30 μ M ($p<0.01$; Fig 3.17C and D), whilst ATP potency remained unchanged (0.81 \pm 0.27 μ M, $p>0.05$; Fig 3.17C). These data suggested that PPADS inhibited human P2X4 receptors stably expressed in 1321N1 astrocytoma cells in a non-competitive fashion.

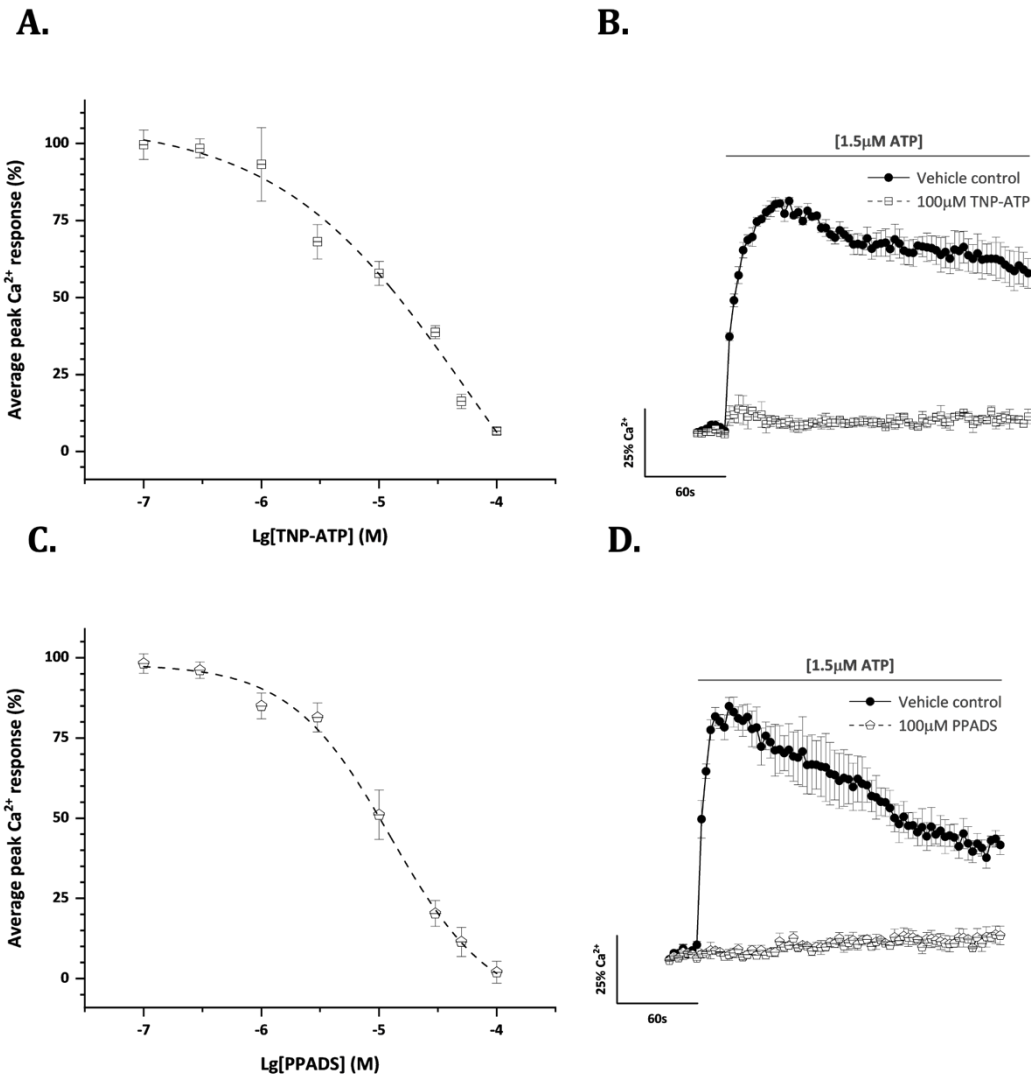


Fig 3.15. Broad-spectrum P2X receptor antagonists inhibited the Ca^{2+} response to ATP in 1321N1 astrocytoma cells stably expressing human P2X4 receptors. Inhibition concentration-response curves for the peak magnitude of intracellular Ca^{2+} entry evoked by $1.5\mu\text{M ATP}$ in the presence of (A) TNP-ATP ($N=5$) and (C) PPADS ($N=5$). Averaged time-resolved intracellular Ca^{2+} responses to ATP in the presence (open shapes) and absence (closed circles) of (B) $100\mu\text{M TNP-ATP}$ ($N=5$) and (D) $100\mu\text{M PPADS}$ ($N=5$). All data were normalised to respective $1.5\mu\text{M ATP}$ responses in the presence of vehicle control. Data were represented as mean \pm SEM.

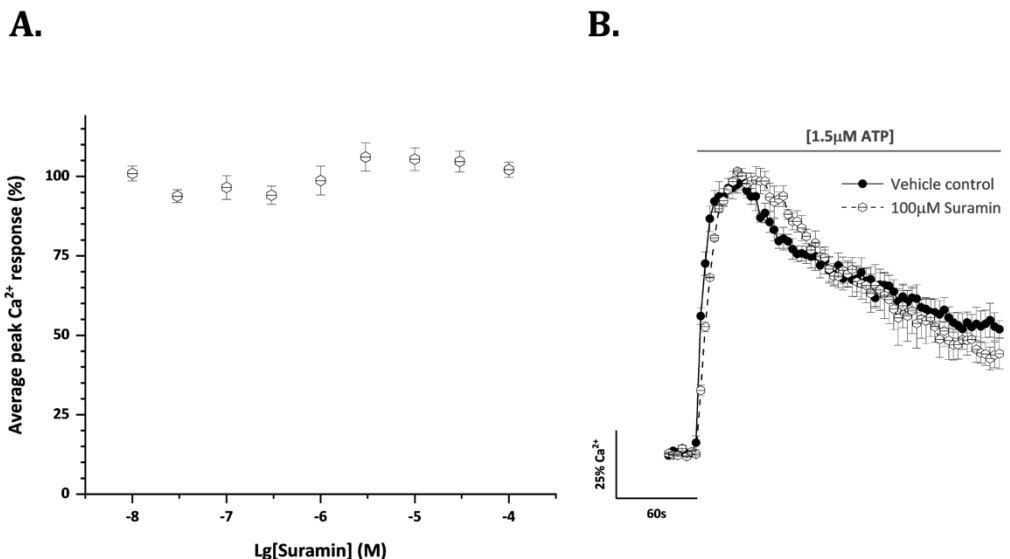
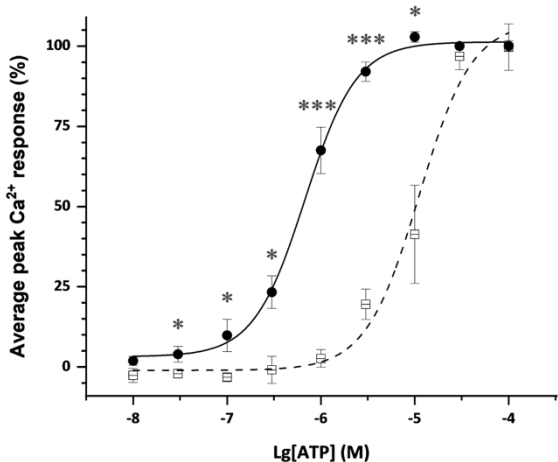
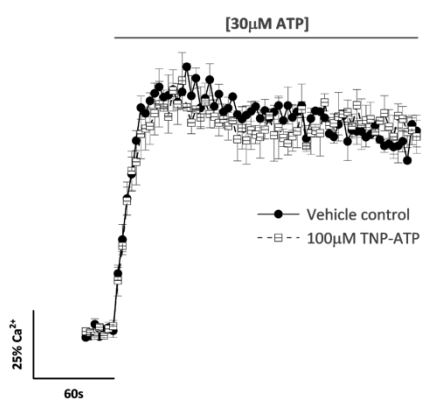


Fig 3.16. Broad-spectrum P2X receptor antagonist Suramin did not affect the ATP-mediated Ca^{2+} response in 1321N1 cells stably expressing human P2X4 receptors. (A) Peak magnitude of intracellular Ca^{2+} influx evoked by $1.5\mu\text{M ATP}$ in the presence of Suramin at various concentrations. (B) Averaged time-resolved intracellular Ca^{2+} responses to ATP in the presence (open shapes) and absence (closed circles) of $100\mu\text{M}$ Suramin. Data were normalised to $1.5\mu\text{M ATP}$ responses in the presence of vehicle control. Data were represented as mean \pm SEM ($N=5$).

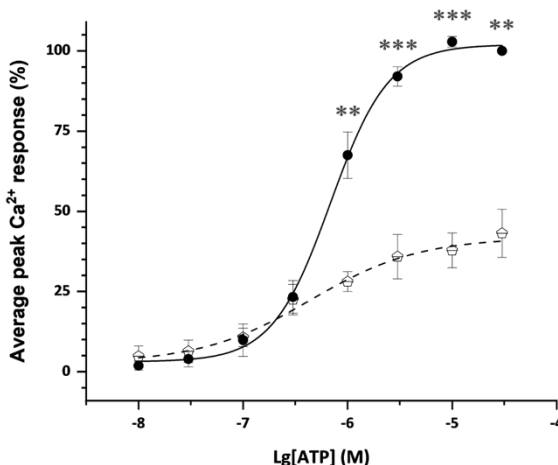
A.



B.



C.



D.

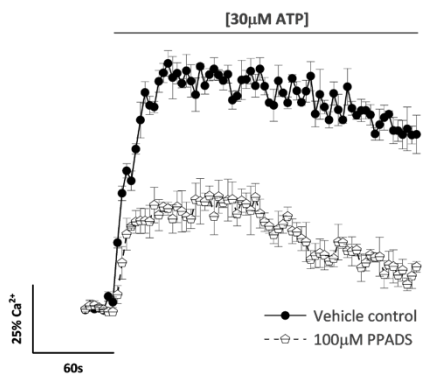


Fig 3.17. Inhibitory effects on ATP-induced Ca²⁺ responses after treatment with TNP-ATP and PPADS in 131N1 astrocytoma cells stably expressing human P2X4 receptors. Comparison of concentration-response curves for the peak magnitude of intracellular Ca²⁺ entry upon stimulation with ATP in the presence of (A) 100 μM TNP-ATP ($N=3$) and (C) 100 μM PPADS ($N=3$) versus ATP alone ($N=7$). Averaged time-resolved intracellular Ca²⁺ responses to 30 μM ATP in the presence (open shapes) and absence (closed circles) of (B) 100 μM TNP-ATP ($N=3$) and (D) 100 μM PPADS ($N=3$). All data were normalised to respective maximal responses to 30 μM ATP. Data were represented as mean \pm SEM.

3.2.2.4 Investigating the inhibitory effects of selective P2X4 receptor antagonists in 1321N1 astrocytoma cells stably expressing the human P2X4 receptor

A lack of selective antagonists has hampered research into P2X4 receptors. Recent advances in small molecule development revealed more potent and selective P2X4 receptor antagonists. These new commercially available drugs were tested to complete the pharmacological profile of heterologously expressed human P2X4 receptors in 1321N1 astrocytoma cells. All five antagonists were not soluble in deionised water or SBS but in DMSO instead (Table 2.3). DMSO is a polar aprotic solvent that dissolves both polar and nonpolar compounds, and it is the most widely used organosulfur solvent in research. Rigorous control of human P2X4 receptor activation by ATP in the presence of DMSO as the vehicle control was performed before proceeding with the pharmacological study. The presence of DMSO at 0.5% (v/v) did not alter the human P2X4 receptor response to exogenous ATP, preserving its potency ($0.81 \pm 0.05 \mu\text{M}$; $p > 0.05$) and efficacy values ($102.1 \pm 4.28\%$ at $30 \mu\text{M}$ ATP, $p > 0.05$) compared to control (Fig 3.18). The ATP EC₅₀ concentration also remained unchanged ($1.73 \pm 0.13 \mu\text{M}$ vs $1.51 \pm 0.28 \mu\text{M}$, $p > 0.05$; Fig 3.18).

All five selective antagonists tested BAY-1797, BX-430, PSB-12062, 5-BDBD, and Taspine significantly reduced the ATP-evoked calcium response in a concentration-dependent manner (Table 3.5; Fig 3.19). The IC₅₀ values were then extrapolated from inhibition concentration-response curves (Fig 3.19A, C, E, G, and I) and statistically compared between them to obtain a potency rank of selective and broad-spectrum antagonists for the human P2X4 receptor: BAY-1797 ($0.21 \pm 0.07 \mu\text{M}$) = PSB-12062 ($0.24 \pm 0.04 \mu\text{M}$) = BX-430 ($0.42 \pm 0.16 \mu\text{M}$) > 5-BDBD ($1.31 \pm 0.28 \mu\text{M}$) = Taspine ($1.54 \pm 0.33 \mu\text{M}$) > TNP-ATP ($16.6 \pm 4.71 \mu\text{M}$) = PPADS ($33.8 \pm 16.6 \mu\text{M}$). The human P2X4 receptor displayed similar sensitivity to blockage by BAY-1797, PSB-12062 and BX-430 with sub-micromolar potency values and causing complete inhibition of ATP-evoked calcium responses at concentrations of $10 \mu\text{M}$, $10 \mu\text{M}$, and $20 \mu\text{M}$, respectively (Fig 3.19A-F). The effects of maximal inhibitory concentrations (I_{max}) on ATP-evoked concentration-response curves were also measured to understand their mode of action. The presence of $10 \mu\text{M}$ BAY-1797 and $20 \mu\text{M}$ PSB-12062 significantly reduced the ATP-evoked maximal calcium responses by approximately 76% ($p < 0.001$; Fig 3.20A and B) and 36% ($p < 0.001$; Fig 3.20E and F) upon application of $30 \mu\text{M}$ ATP, respectively. PSB-12062 also caused a rightward shift of the concentration-response curve, significantly increasing the ATP potency value to $2.64 \pm 0.94 \mu\text{M}$ ($p < 0.05$; Fig 3.20E) whereas BAY-1797 significantly reduced the ATP potency value to $0.16 \pm 0.03 \mu\text{M}$ ($p < 0.001$; Fig 3.20A). These results suggested that both PSB-12062 and BAY-1797 act as negative allosteric modulators of the human P2X4 receptor. Surprisingly, the presence of $10 \mu\text{M}$ BX-430 entirely stopped ATP from elucidating a calcium response at any concentration tested ($2.76 \pm 4.22\%$ at $30 \mu\text{M}$ ATP, $p < 0.001$; Fig 3.20C and D), suggesting a non-competitive and irreversible mode of inhibition. 5-BDBD and Taspine were second best on the human P2X4 inhibition potency rank and caused their maximal inhibitory effects at $30 \mu\text{M}$ concentrations (Fig 3.19G-J). Amongst all compounds tried, Taspine was the only molecule derived from a natural product. It acted as a non-competitive antagonist for the human P2X4 receptor and inhibited the $30 \mu\text{M}$ ATP-evoked maximal calcium responses by approximately 67% ($p < 0.001$; Fig 3.20I and J) without affecting its affinity for ATP ($\text{EC}_{50} 1.10 \pm 0.67 \mu\text{M}$, $p > 0.05$; Fig 3.20I).

Finally, 5-BDBD caused a significant rightward shift of the ATP-evoked calcium response, significantly reducing its affinity for ATP ($EC_{50} 5.83 \pm 0.32 \mu M$, $p < 0.01$; Fig 3.20G), but did not change the ATP efficacy reaching the maximal response at $30 \mu M$ ($90.1 \pm 8.22\%$ vs vehicle control, $p > 0.05$; Fig 3.20G and H). These data revealed a competitive mode of action for 5-BDBD at human P2X4 receptors heterologously expressed in 1321N1 astrocytoma cells.

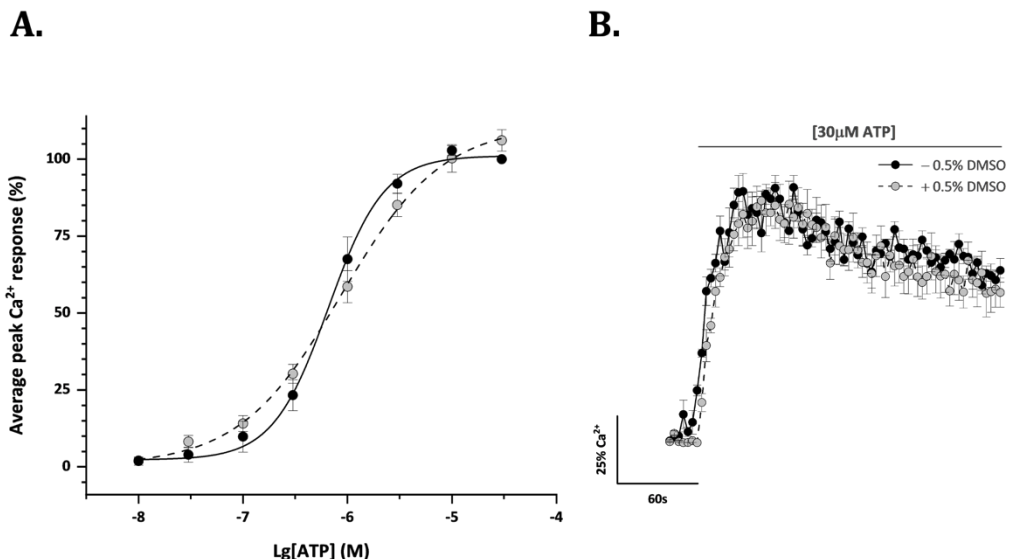
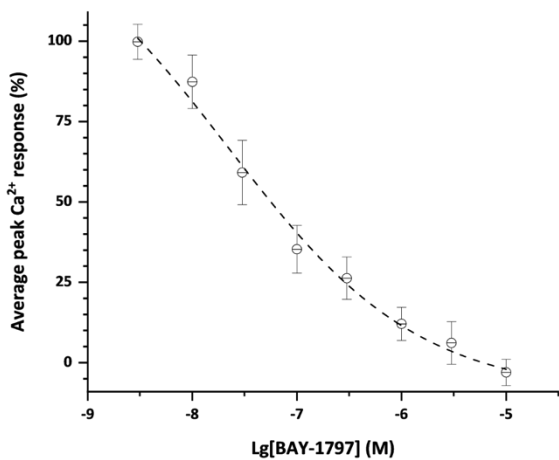
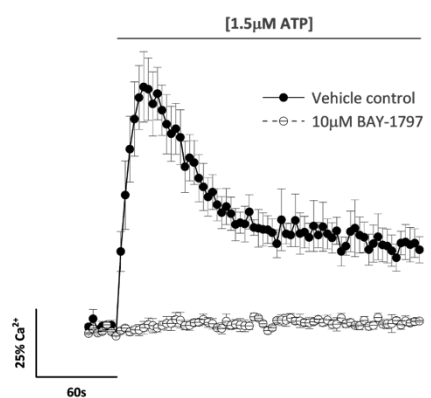


Fig 3.18. 30-minute incubation with the organic solvent DMSO did not affect human P2X4 receptor sensitivity to ATP in stable 1321N1 astrocytoma cells. (A) Concentration-response curves for the peak magnitude of intracellular Ca^{2+} influx evoked by ATP in the presence (grey circles) and absence (closed circles) of 0.5% (v/v) DMSO. (B) Averaged time-resolved intracellular Ca^{2+} responses to 30 μM ATP in the presence (grey circles) and absence (closed circles) of 0.5% (v/v) DMSO. All data were normalised to the maximal response to 30 μM ATP without DMSO. Data were represented as mean \pm SEM ($N=6$).

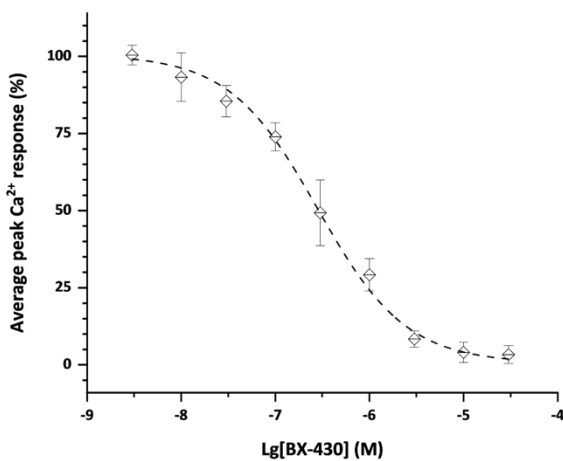
A.



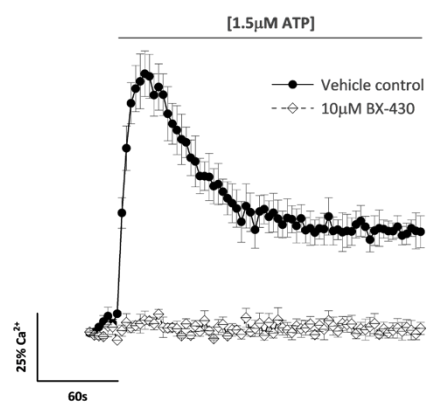
B.



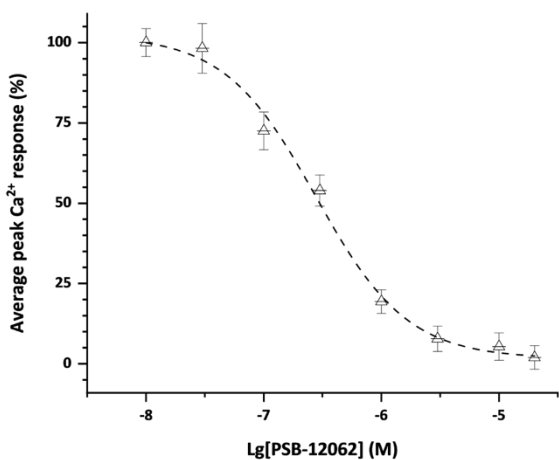
C.



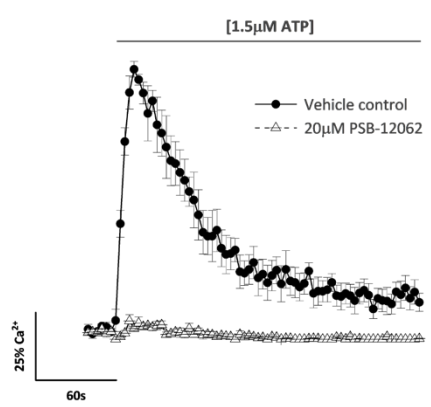
D.



E.



F.



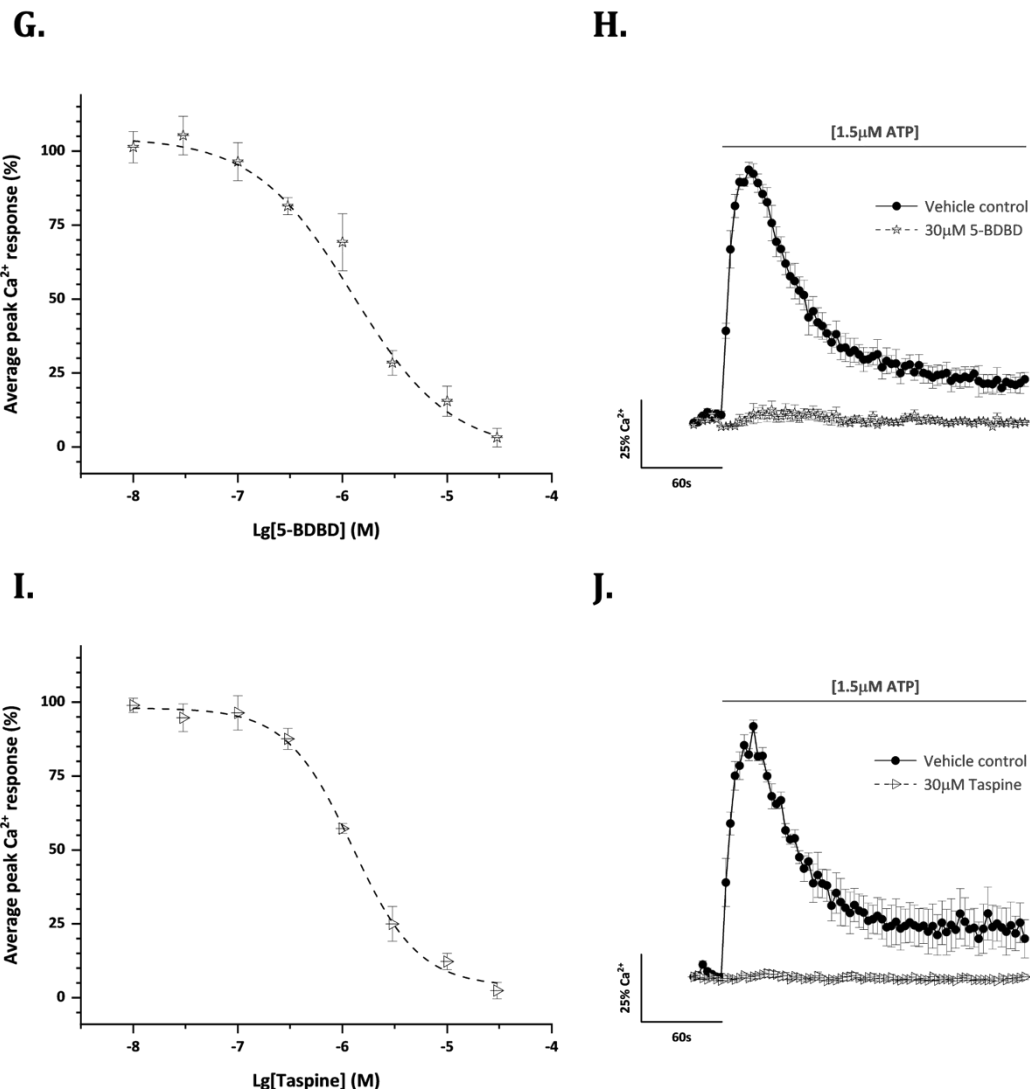
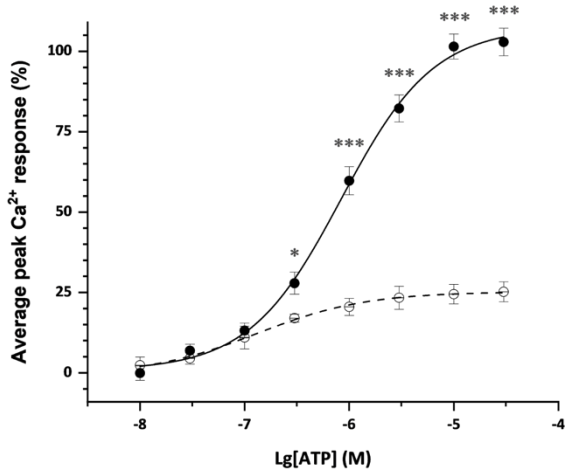
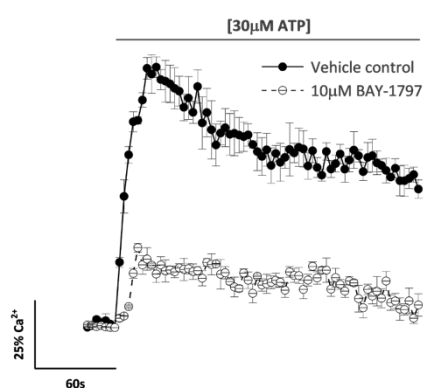


Fig 3.19. Selective antagonism of the human P2X4 receptor inhibited the Ca^{2+} response to ATP in 1321N1 stable astrocytoma cells. Inhibition concentration-response curves for the peak magnitude of intracellular Ca^{2+} entry evoked by $1.5\mu\text{M ATP}$ in the presence of (A) BAY-1797 ($N=5$), (C) BX430 ($N=5$), (E) PSB-12062 ($N=5$), (G) 5-BDBD ($N=5$), (I) Taspine ($N=5$). Averaged time-resolved intracellular Ca^{2+} responses to ATP in the presence (open shapes) and absence (closed circles) of (B) $10\mu\text{M}$ BAY-1797 ($N=5$), (D) $10\mu\text{M}$ BX430 ($N=5$), (F) $20\mu\text{M}$ PSB-12062 ($N=5$), (H) $30\mu\text{M}$ 5-BDBD ($N=5$), (J) $30\mu\text{M}$ Taspine ($N=5$). All data were normalised to respective $1.5\mu\text{M ATP}$ responses in the presence of vehicle control. Data were represented as mean \pm SEM.

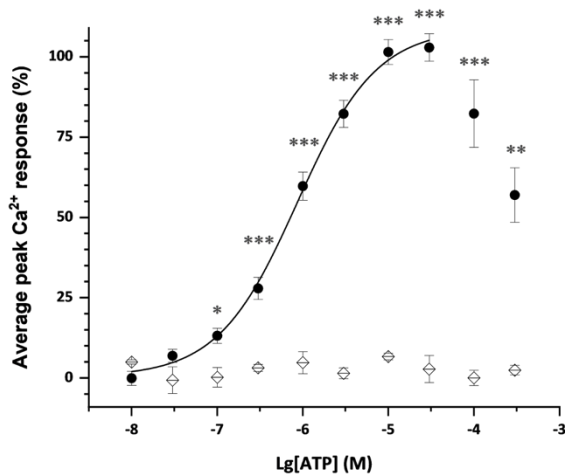
A.



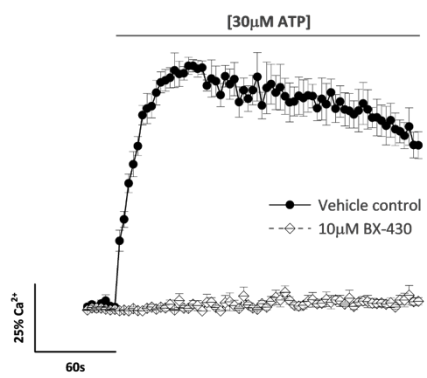
B.



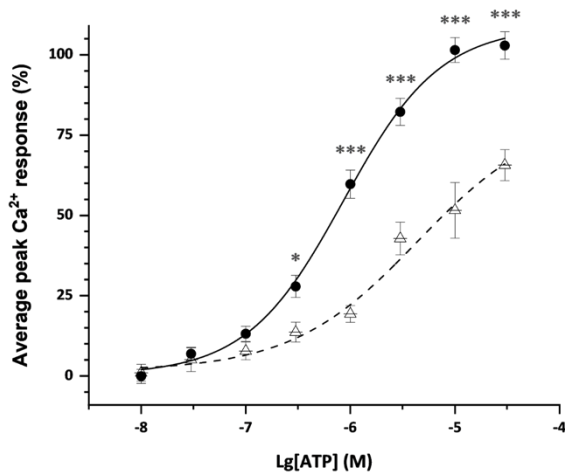
C.



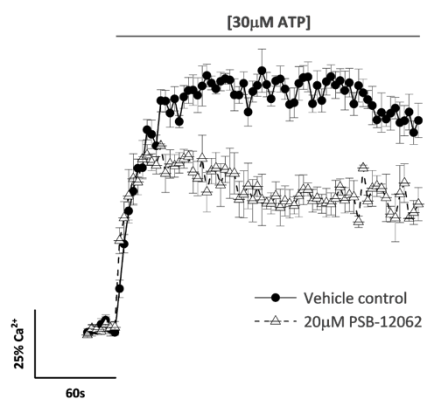
D.



E.



F.



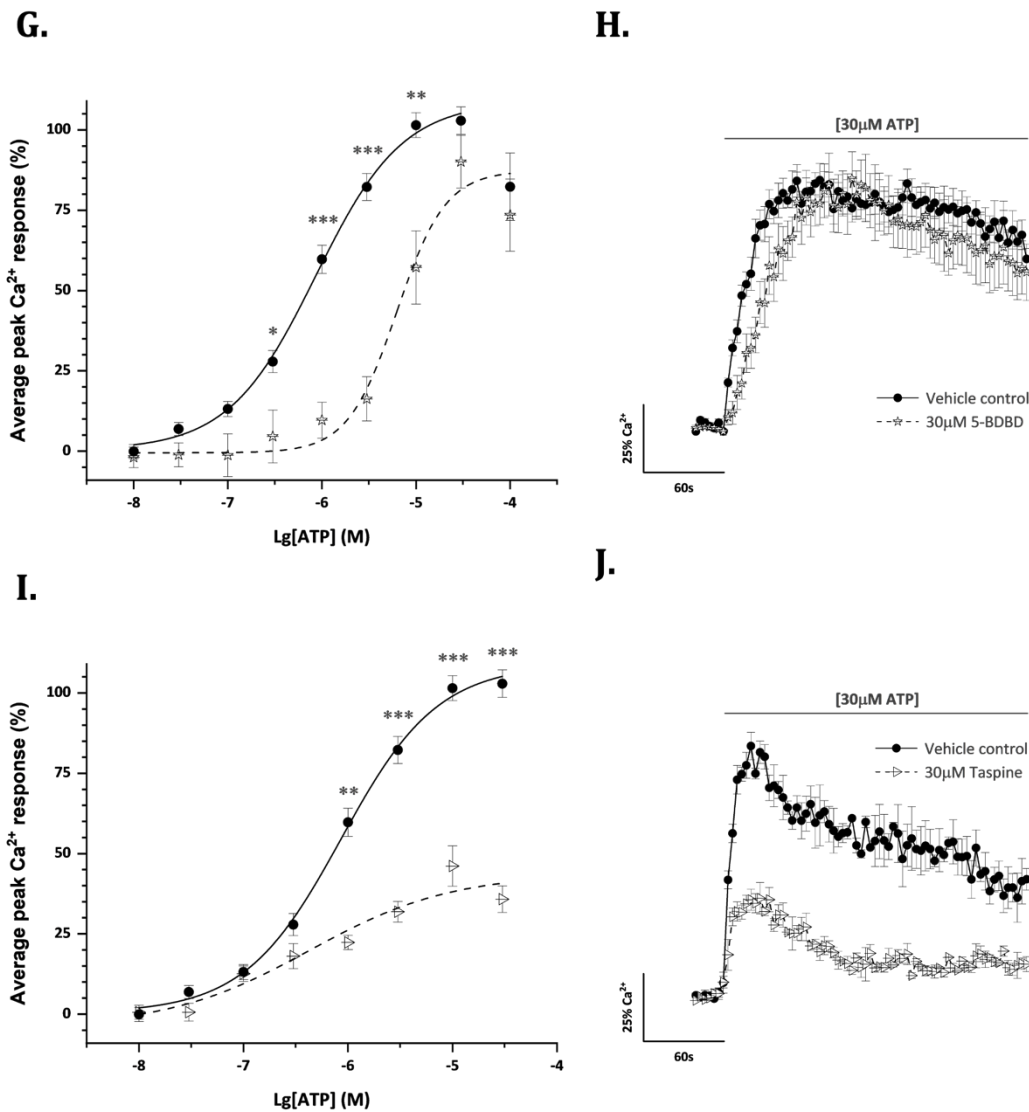


Fig 3.20. Inhibitory effects on ATP-evoked Ca^{2+} responses after treatment with various selective human P2X4 receptor antagonists in 1321N1 stable astrocytoma cells. Comparison of concentration-response relationship for the peak magnitude of intracellular Ca^{2+} responses in the presence of (A) $10\mu\text{M}$ BAY-1797 ($N=3$), (C) $10\mu\text{M}$ BX430 ($N=3$), (E) $20\mu\text{M}$ PSB-12062 ($N=3$), (G) $30\mu\text{M}$ 5-BDBD ($N=3$), and (I) $30\mu\text{M}$ Taspine ($N=3$) versus vehicle control ($N=6$). Averaged time-resolved intracellular Ca^{2+} responses to $30\mu\text{M ATP}$ in the presence (open shapes) and absence (closed circles) of (B) $10\mu\text{M}$ BAY-1797 ($N=3$), (D) $10\mu\text{M}$ BX430 ($N=3$), (F) $20\mu\text{M}$ PSB-12062 ($N=3$), (H) $30\mu\text{M}$ 5-BDBD ($N=3$), and (J) $30\mu\text{M}$ Taspine ($N=3$). All data were normalised to respective maximal responses to $30\mu\text{M ATP}$ in the presence of vehicle control. Data were represented as mean \pm SEM.

Table 3.4. Effects of broad-spectrum antagonists on the ATP-evoked responses via human P2X4 receptors stably expressed in 1321N1 astrocytoma cells.

Antagonists	IC ₅₀ (μM)	I _{max} (μM)	EC ₅₀ (μM)	P value	Efficacy (%)	P value	Mode of action
TNP-ATP	16.6±4.71	100	10.1±2.18	<0.05	96.8±4.08	ns	C
PPADS	33.8±16.6	100	0.81±0.27	ns	43.1±7.53	<0.01	NC
Suramin	/	/	/		/		/

C, competitive; NC, non-competitive; ns, non-significant. Statistical analysis was performed against 1.5 μM ATP-evoked calcium responses in SBS.

Table 3.5. Effects of human P2X4 selective antagonists on the ATP-evoked responses in stable 1321N1 astrocytoma cells.

Antagonists	IC ₅₀ (μM)	I _{max} (μM)	EC ₅₀ (μM)	P value	Efficacy (%)	P value	Mode of action
BAY-1797	0.21±0.07	10	0.16±0.03	<0.001	25.2±3.11	<0.001	NC
BX-430	0.42±0.16	10	/	/	2.76±4.22	<0.001	NC
PSB-12062	0.24±0.04	20	2.64±0.94	<0.05	65.7±4.79	<0.001	NC
5-BDBD	1.31±0.28	30	5.83±0.32	<0.01	90.1±8.22	ns	C
Taspine	1.54±0.33	30	1.10±0.67	ns	35.8±10.1	<0.001	NC

C, competitive; NC, non-competitive; ns, non-significant. Statistical analysis was performed against 1.5 μM ATP-evoked calcium responses in SBS containing 0.5% [v/v] of DMSO.

3.2.3 The hypothesis of the dead receptor and validation of the experimental system

3.2.3.1 Mutations of conserved ectodomain lysine residues caused a significant loss of function at human P2X4 receptors

The human P2X4 receptor is formed by the association of three pore-forming subunits. Thus, three P2X4 monomers must combine to form a functional homotrimeric channel. Following the dead receptor hypothesis, if an interaction occurred between human P2X4 WT and human P2X4 [K67A, K313A] double mutant subunits, a significant reduction in channel function would become evident (Fig 3.1). Originally, we sought to use the human P2X4 WT stable 1321N1 astrocytoma cell line to analyse the effects of conserved lysine residue mutations on channel function because these cells were poor transfection hosts, and the methodology was adjusted for transfection of only one plasmid DNA. Thereby, 1321N1 astrocytoma cells stably expressing the human P2X4 receptor were transiently transfected with human P2X4 [K67A, K313A] dead subunits. To do so, I followed the optimised transient transfection method outlined in section 3.2.1.

Biotinylation and Western blotting showed high protein expression levels of the human P2X4 [K67A, K313A] FLAG-tagged dead subunits in whole-cell (1.04 ± 0.23 au) and cell membrane (0.90 ± 0.25 au) lysates ($p>0.05$; Fig 3.21A and B). Furthermore, FlexStation 3 data showed a small but significant reduction of the intracellular calcium response evoked by $30\mu M$ ATP when human P2X4 [K67A, K313A] dead subunits were transiently transfected in human P2X4 WT stable 1321N1 astrocytoma cells ($66.7\pm5.33\%$ vs pcDNA 3.1 plasmid control, $p<0.01$; Fig 3.22A and D). Transient transfection of human P2X4 [K67A] and human P2X4 [K313A] single lysine-to-alanine mutants also significantly reduced the intracellular calcium responses to $30\mu M$ ATP by approximately 35% and 42%, respectively ($p<0.01$ for both vs pcDNA 3.1 plasmid control; Fig 3.22B and D). The observed reduction of the ATP-evoked calcium response could be a consequence of a restricted expression of human P2X4 wild-type proteins, compromised by the additional gene and protein expression of the human P2X4 dead subunits. To ensure that double lysine-to-alanine mutations represented a true loss of function of the human P2X4 receptor activity and were not due to a reduction of wild-type channel expression, a control for protein expression was carried out. Transient transfection of a different ligand-gated ion channel, i.e., human $\alpha 7$ nicotinic acetylcholine receptor ($\alpha 7$ nAChR), did not affect the ATP-evoked intracellular calcium response in 1321N1 astrocytoma cells stably expressing human P2X4 WT receptors ($88.9\pm5.35\%$, $p>0.05$ vs pcDNA 3.1 plasmid control; Fig 3.22C and D).

However, by using stable 1321N1 cells, the identification of functional human P2X4 receptor variants may have been precluded, particularly if the dead receptor tools exhibited lower protein expression levels at the cell membrane compared to an overexpressed human P2X4 WT receptor, thus covering their real effects in channel function. Therefore, the results obtained could have been over- or under-estimated, and the failure rate may have been higher than expected. Consequently, I wanted to use the human 1321N1 parental astrocytoma cells as the experimental model organism to explore human P2X4 heteromerisation, ensuring fair protein expression competition between wild-type and double

mutants, thereby reducing the pre-screening bias and improving the standard of the research. Further transient transfection of human 1321N1 parental astrocytoma cells tests were timely to determine the most efficient conditions to co-transfect two different plasmids into these cells. To control for gene and protein expression bias towards either wild-type or dead subunits, i) all genes were purchased in the same backbone vector pcDNA 3.1 (+) and contained a strong human cytomegalovirus (CMV) immediate early promoter for high recombinant protein expression in mammalian cells, and ii) equal amounts of both wild-type and double mutant plasmids were introduced into the cells. To determine the maximal amount of plasmid DNA for successful cell co-transfection whilst maintaining cell viability, I used the protocol determined in section 3.2.1.

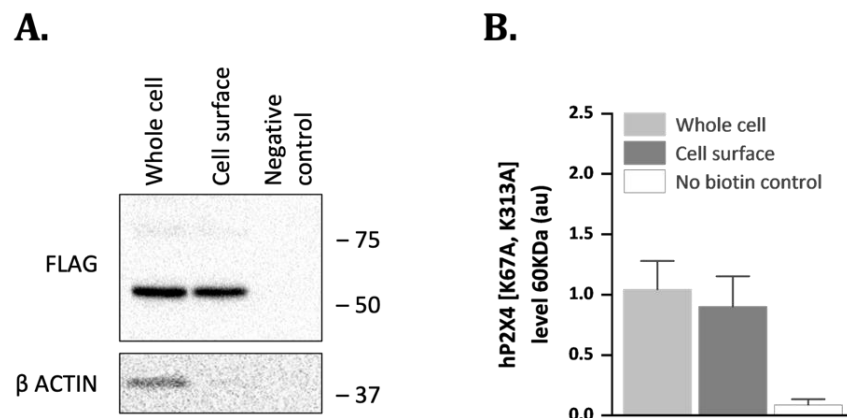


Fig 3.21. Whole-cell and cell surface expression levels of human P2X4 [K67A, K313A] transiently transfected in human P2X4 WT stable 1321N1 astrocytoma cells. (A) Representative immunoblot for hP2X4 [K67A, K313A] FLAG-tagged protein, with corresponding β -actin loading controls. Molecular weight size standards were indicated in kDa. Lane 1 corresponded to the whole-cell sample, lane 2 to cell surface protein lysate, and lane 3 was a negative control for biotin labelling. (B) Comparison of densitometric analysis of hP2X4 [K67A, K313A] FLAG protein levels relative to loading control for whole-cell and cell surface lysates. Data were represented as mean \pm SEM ($N=3$).

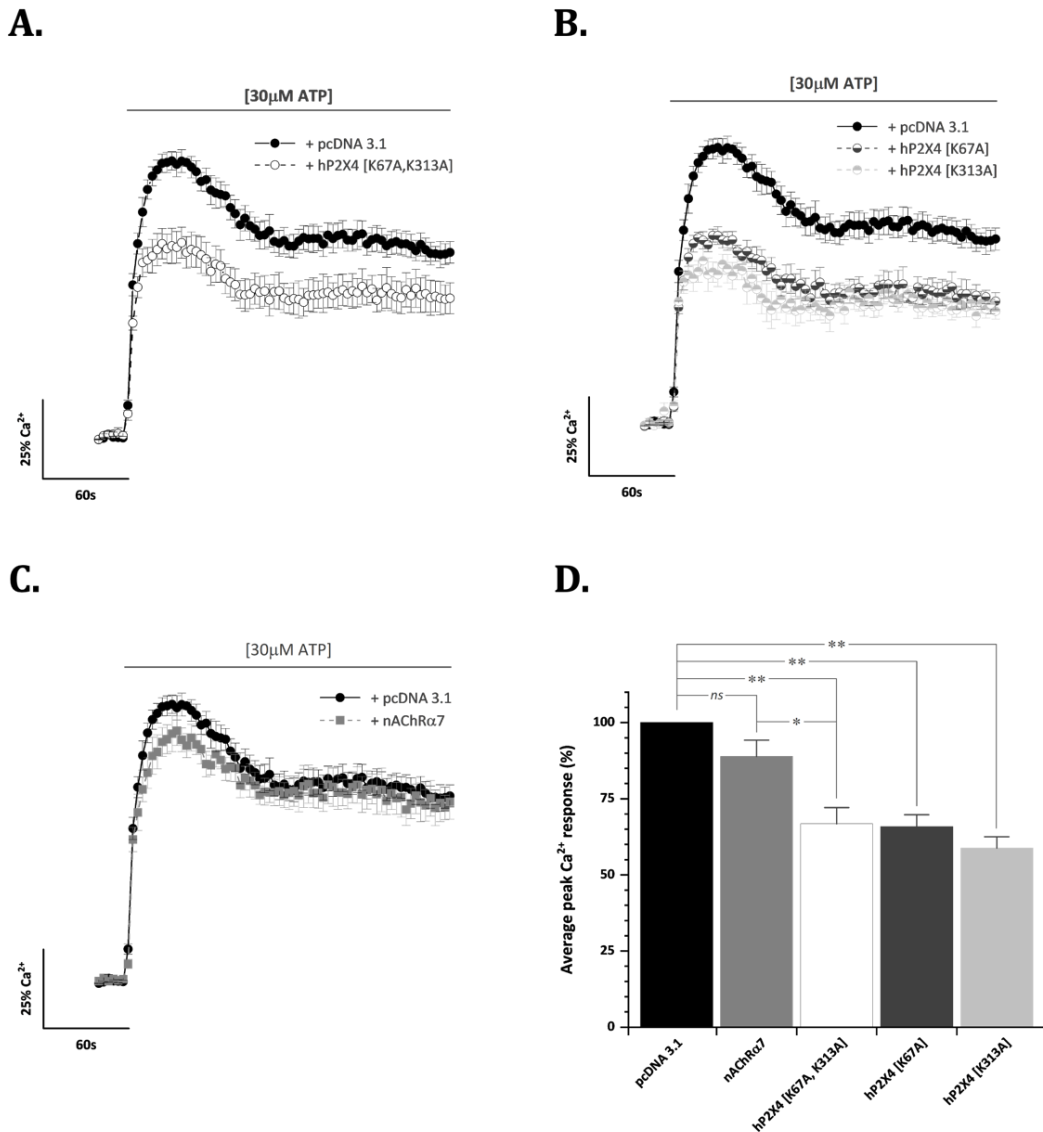


Fig 3.22. Mutations of conserved ectodomain lysine residues caused a minor loss of function at human P2X4 receptors. (A – C) Pairs of averaged time-resolved intracellular Ca^{2+} influx elicited by 30 μM ATP in hP2X4 WT stable 1321N1 astrocytoma cells transiently transfected with (A) hP2X4 [K67A, K313A] double dead mutant (open circles), (B) hP2X4 [K67A] (dark grey circles) and hP2X4 [K313A] (light grey circles) single mutants, and (C) human α 7 nicotinic acetylcholine receptor (nAChR α 7, grey squares) compared to pcDNA 3.1 plasmid control responses (closed circles). (D) Comparison of peak magnitude of intracellular Ca^{2+} responses induced by 30 μM ATP at hP2X4 WT, hP2X4 lysine mutant receptors, and human α 7 nicotinic acetylcholine receptor (nAChR α 7). All data were normalised to respective maximal 30 μM ATP responses in the presence of pcDNA 3.1 as a plasmid control. Data were represented as mean \pm SEM ($N=7$).

Human 1321N1 parental astrocytoma cells transiently transfected with either 200ng or 400ng of human P2X4 WT DNA per well had identical ATP-evoked intracellular calcium responses ($81.3\pm7.65\%$ vs $88.9\pm4.90\%$, respectively, $p>0.05$; Fig 3.23A and C), suggesting doubling the amount of plasmid DNA did not alter transfection efficiency or cell viability. According to the hypothesis of the dead receptor, 200ng would correspond to the human P2X4 WT plasmid and the other 200ng to the double mutant plasmid, thereby totalling 400ng per well. Final amounts of 150ng and 300ng of human P2X4 WT plasmid were also tested using the improved transfection methodology, but the ATP-evoked calcium responses obtained were significantly different between them ($58.7\pm3.95\%$ vs $81.8\pm2.90\%$, respectively, $p<0.01$; Fig 3.23B and C). It is important to note a significant improvement in transfection efficiency following the new optimised transfection protocol even when using 300ng of plasmid and $0.5\mu\text{L}$ of Lipofectamine 2000 compared to initial transfection conditions ($81.8\pm2.90\%$ vs $62.5\pm2.13\%$, $p<0.001$; Fig 3.23C and 3.5A, respectively). Nonetheless, these results meant that using 150ng of each wild-type and double mutant plasmids totalling 300ng per well of plasmid DNA would probably increase data variability and contribute to protein expression differences, affecting the strength of the study.

Consequently, 1321N1 parental astrocytoma cells were successfully co-transfected with 200ng of human P2X4 WT EE-tagged and 200ng of human P2X4 [K67A, K313A] FLAG-tagged subunits. The $30\mu\text{M}$ ATP-evoked calcium response was significantly reduced by about 50% in the presence of human P2X4 dead subunits compared to human P2X4 WT co-transfected with pcDNA 3.1 as a plasmid control ($54.3\pm4.27\%$, $p<0.01$; Fig 3.24A and C). Cells transiently co-transfected with human P2X4 WT EE-tagged subunits, and either human P2X4 WT FLAG-tagged subunits or human $\alpha 7$ nicotinic acetylcholine receptors (nAChR $\alpha 7$) responded to $30\mu\text{M}$ ATP comparably to plasmid control ($106.0\pm7.15\%$ and $109.2\pm7.04\%$, respectively, $p>0.05$ between them and vs plasmid control; Fig 3.24). To conclude, the human P2X4 loss of function was more evident using the co-transfection approach and was the gateway to validate the hypothesis of the dead receptor in this heterologous system. Despite all recommendations taken, the system was still biased towards one concentration of one particular agonist, namely $30\mu\text{M}$ ATP. To rule this pre-screening bias out and ensure a more robust yet practical data collection, we analysed the effects of dead receptor tools on human P2X4 WT channel function using ATP concentration-responses instead.

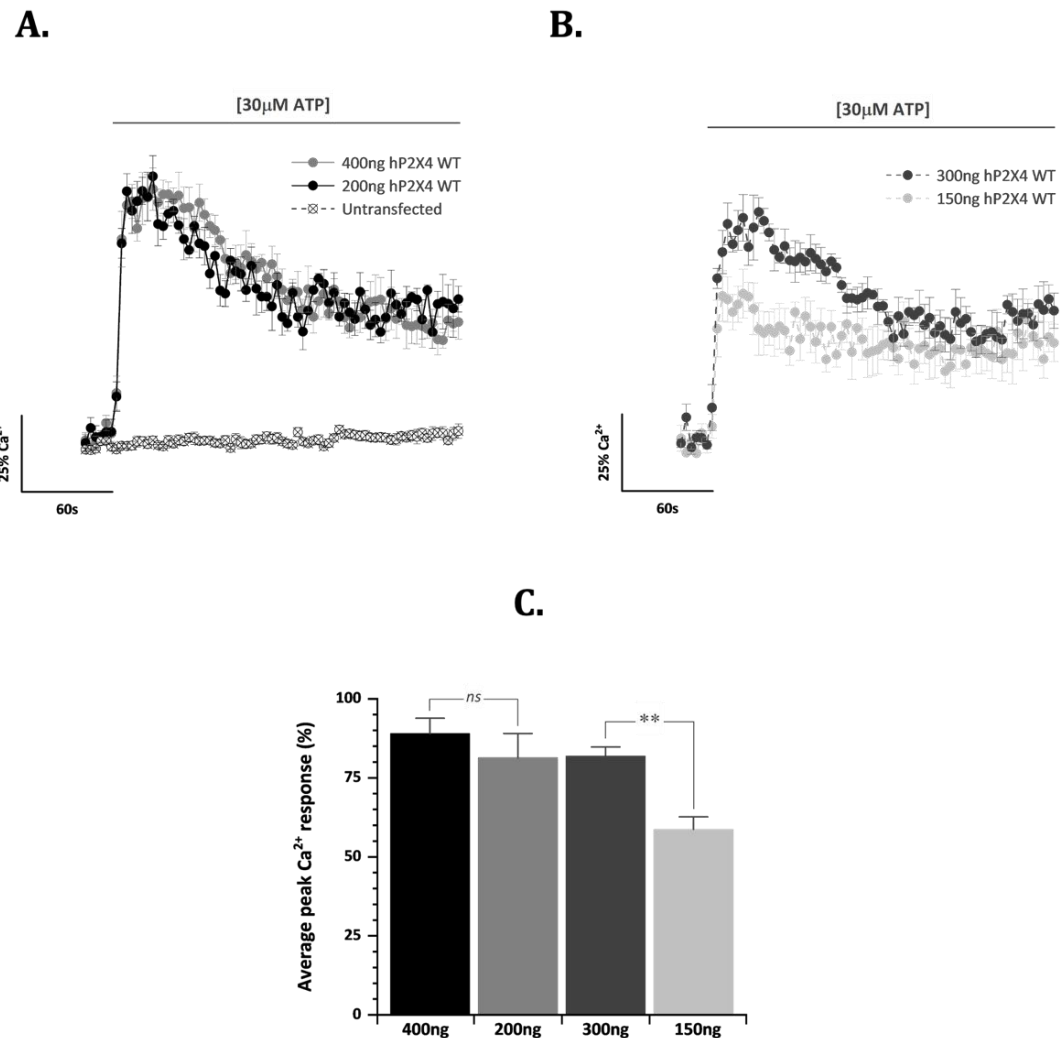


Fig 3.23. Determination of the maximal amount of plasmid DNA for successful transient co-transfection of 1321N1 parental astrocytoma cells using Lipofectamine 2000. (A, B) Pairs of averaged time-resolved intracellular Ca²⁺ response elicited by 30μM ATP in 1321N1 astrocytoma cells transiently transfected with (A) 200ng and 400ng of hP2X4 WT plasmid, and (B) 150ng and 300ng of hP2X4 WT plasmid. (C) Comparison of average peak Ca²⁺ responses upon stimulation with 30μM ATP using different amounts of plasmid DNA. Final hP2X4 WT plasmid DNA amounts were expressed in ng per well. All data were normalised to the maximal response to 100μM Carbachol. Data were represented as mean ± SEM ($N=5$).

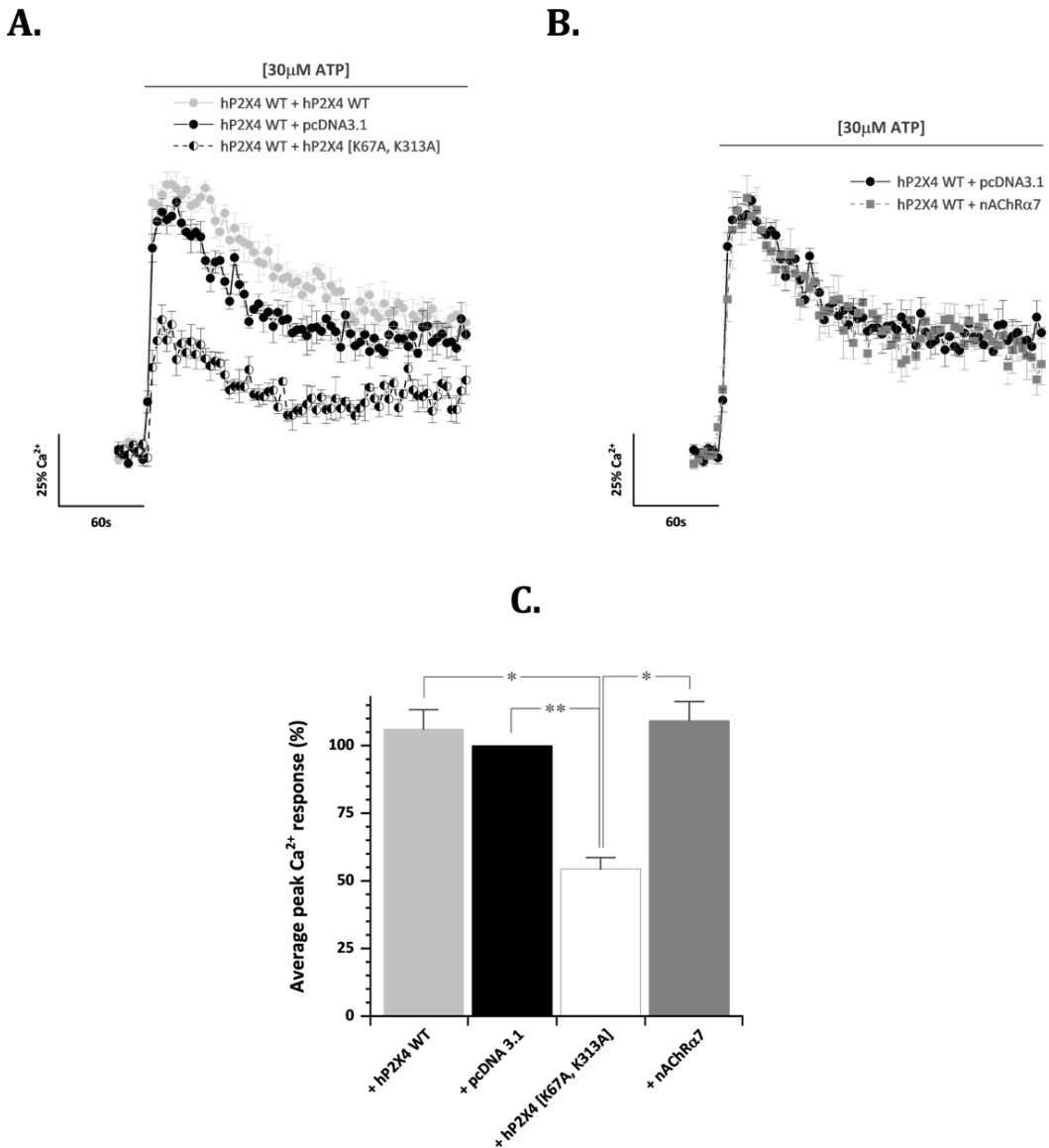


Fig 3.24. Mutations of conserved ectodomain lysine residues caused a significant loss of function at human P2X4 receptors. (A – C) Pairs of averaged time-resolved intracellular Ca^{2+} influx elicited by 30 μ M ATP in 1321N1 parental astrocytoma cells transiently co-transfected with hP2X4 WT EE in combination with (A) hP2X4 WT FLAG (light grey circles) or hP2X4 [K67A, K313A] double dead mutant (half moon circles), and with (B) human α 7 nicotinic acetylcholine receptor (nAChRa7, grey squares) compared to co-transfection with pcDNA 3.1 plasmid control responses (closed circles). (C) Comparison of peak magnitude of intracellular Ca^{2+} responses induced by 30 μ M ATP at hP2X4 WT, hP2X4 lysine mutant receptors, and human α 7 nicotinic acetylcholine receptor (nAChRa7). All data were normalised to respective maximal 30 μ M ATP responses in the presence of pcDNA 3.1 as a plasmid control. Data were represented as mean \pm SEM ($N=5$).

3.2.3.2 Human P2X4 WT subunits interacted and formed functional homotrimeric receptors

As a first step into exploring the heteromeric assembly of human P2X4 receptors, we wanted to determine whether human P2X4 subunits could indeed form homotrimers. To test this, I used co-immunoprecipitation assays where human P2X4 WT constructs were tagged with two different epitope tags, namely HA and FLAG, and co-transfected into 1321N1 parental astrocytoma cells. One human P2X4 subunit was immuno-precipitated using the appropriate anti-tag antibody (for example, anti-FLAG), and the precipitate was analysed by Western blot using the other anti-tag antibody (anti-HA). If interaction occurred between human P2X4 WT HA and FLAG-tagged subunits, a P2X4-specific band would be present in the co-immunoprecipitate lane.

Initially, we purchased all human P2X1-7 WT plasmids with a FLAG tag and an EE tag, so co-immunoprecipitation assays would be assessed using anti-FLAG and anti-EE antibodies. Firstly, antibodies targeting both C-terminal epitopes were assessed by Western blot to determine human P2X4 specificity and best working conditions. Human P2X4 WT FLAG-tagged proteins transiently expressed in 1321N1 astrocytoma cells were specifically detected at 60KDa by the anti-FLAG unconjugated antibody but not by the anti-FLAG HRP conjugated antibody (Fig 3.25A). The latter detected unspecific bands at approximately 75KDa, even in untransfected 1321N1 cell controls (Fig 3.25A). Figure 3.25B-D showed unspecific binding of anti-EE tag antibodies from various manufacturers (i.e., Cell Signalling, Merck, and Bethyl Labs) in both 1321N1 astrocytoma cells stably and transiently expressing human P2X4 WT EE-tagged receptors.

Before changing all EE-tagged plasmids, we considered using the commercially available anti-P2X4 antibodies. However, both anti-P2X4 intracellular and extracellular epitope antibodies lacked specificity in human P2X4 WT transiently transfected 1321N1 astrocytoma cells. The former detected a P2X4-specific band at 60KDa but also detected unspecific bands at lower molecular weights, even in untransfected 1321N1 cell controls (Fig 3.26). The latter did not detect any bands, probably because of the denaturation of the extracellular epitope under the conditions used (Fig 3.26).

Lastly, I tried an anti-HA tag antibody which presented specificity for human P2X4 WT HA-tagged proteins transiently expressed in 1321N1 astrocytoma cells and detected it at approximately 60KDa, too (Fig 3.27). Thus, we purchased the remaining human P2X subtypes containing an HA C-terminal tag. These data not only provided information about which antibodies to use but also ensured that the presence of C-terminal epitope tags did not alter human P2X4 WT expression patterns. To summarise, I used human P2X4 WT HA-tagged constructs combined with other P2X FLAG-tagged subunits for interaction studies.

To ensure that human P2X4 WT HA-tagged subunits also retained their functional integrity, intracellular calcium responses evoked by various concentrations of ATP were measured in 1321N1 parental astrocytoma cells transiently co-transfected with human P2X4 WT HA and pcDNA 3.1 plasmid control (Fig 3.28). The ATP concentration-response curve gave a half maximal effective concentration (EC_{50}) of $2.40 \pm 0.79 \mu M$ which was higher compared to the value obtained in human P2X4 WT stable cells

($0.74 \pm 0.18 \mu\text{M}$, $p < 0.05$; Fig 3.28A and 3.11A). Transiently transfected human P2X4 WT HA-tagged conserved its kinetic properties over time with a sustained desensitisation phase at approximately 60% of the maximal response (Fig 3.28B).

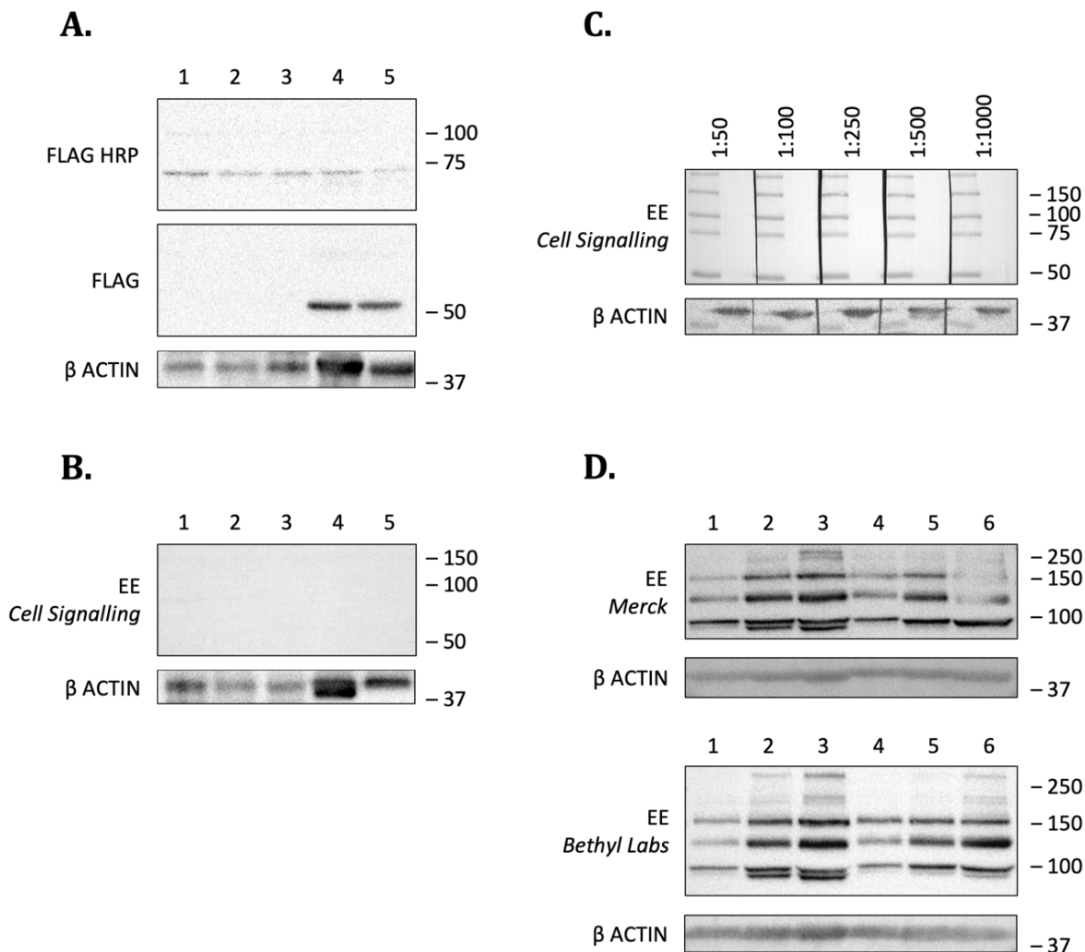


Fig 3.25. Determination of antibody specificity and protein titration in 1321N1 astrocytoma cells stably expressing human P2X4 WT receptors. (A) Representative immunoblot for hP2X4 [K67A, K313A] FLAG-tagged protein transiently transfected in 1321N1 hP2X4 stable astrocytoma cells using 1:1000 Ms α -FLAG HRP-conjugated (top) and 1:1000 Ms α -FLAG unconjugated primary antibody (middle) primary antibodies, and for β -actin loading control (bottom). (B) Representative immunoblot for hP2X4 WT EE-tagged protein stably expressed in 1321N1 cells using 1:1000 Rb α -EE primary antibody (top, *Cell Signalling*) and for β -actin loading control (bottom). Lanes for A and B blots corresponded to: untransfected 1321N1 parental cells (1, 50 μ g protein lysate), hP2X4 WT EE-tagged 1321N1 stable 1321N1 astrocytoma cells transiently transfected with either pcDNA 3.1 plasmid control (2, 50 μ g protein lysate), nAChR α 7 (3, 50 μ g protein lysate), or hP2X4 [K67A, K313A] FLAG-tagged (4, 100 μ g protein; and 5, 50 μ g protein lysate) ($N=3$). (C) Rb α -EE antibody (*Cell Signalling*) titration using 50 μ g of protein lysate from hP2X4 WT EE-tagged stable 1321N1 astrocytoma cells (top) with respective β -actin loading control (bottom). Miniblotts corresponded to 1:50, 1:100, 1:250, 1:500, and 1:1000 Rb α -EE antibody dilutions ($N=1$). Lanes corresponded to: ladder (1) and 50 μ g of whole-cell lysates. (D) Other Rb α -EE antibodies from *Merck* (top) and *Bethyl Labs* (bottom) were unspecific in 1321N1 parental astrocytoma cells transiently transfected with hP2X4 WT EE. Lanes corresponded to: 25 μ g (1), 50 μ g (2) and 80 μ g (3) of hP2X4 WT EE transients; and 25 μ g (4), 50 μ g (5) and 80 μ g (6) of 1321N1 untransfected parental protein lysates ($N=2$). Molecular weight size standards were indicated in kDa.

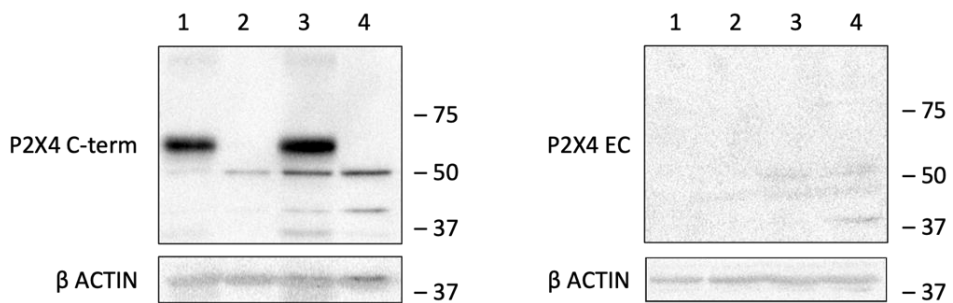


Fig 3.26. Lack of specificity for Ms α -P2X4 C-terminus (C-term) and Ms α -P2X4 extracellular (EC) antibodies in 1321N1 astrocytoma cells transiently transfected with human P2X4 WT EE tagged receptors. Representative immunoblots for hP2X4 WT EE-tagged protein transiently transfected in 1321N1 cells using 1:500 Ms α -P2X4 C-term (left panel) and 1:500 Ms α -P2X4 EC epitope (right panel) with respective β -actin loading controls. Lanes corresponded to: hP2X4 WT EE transients (1, 25 μ g protein lysate; 3, 50 μ g protein lysate) and 1321N1 untransfected parental cells (2, 25 μ g protein lysate; 4, 50 μ g protein lysate). Molecular weight size standards were indicated in KDa ($N=2$).

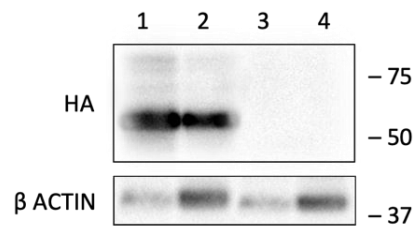


Fig 3.27. Determination of antibody specificity and protein titration in 1321N1 astrocytoma cells transiently expressing human P2X4 WT HA-tagged receptors. (A) Representative immunoblot for hP2X4 WT HA-tagged protein transiently transfected in 1321N1 parental cells using 1:1000 Ms α -HA (top) and for β -actin loading controls (bottom). Lanes corresponded to: hP2X4 WT HA transients (1, 25 μ g protein lysate; 2, 50 μ g protein lysate) and 1321N1 untransfected parental cells (3, 25 μ g protein lysate; 4, 50 μ g protein lysate). Molecular weight size standards were indicated in KDa ($N=2$).

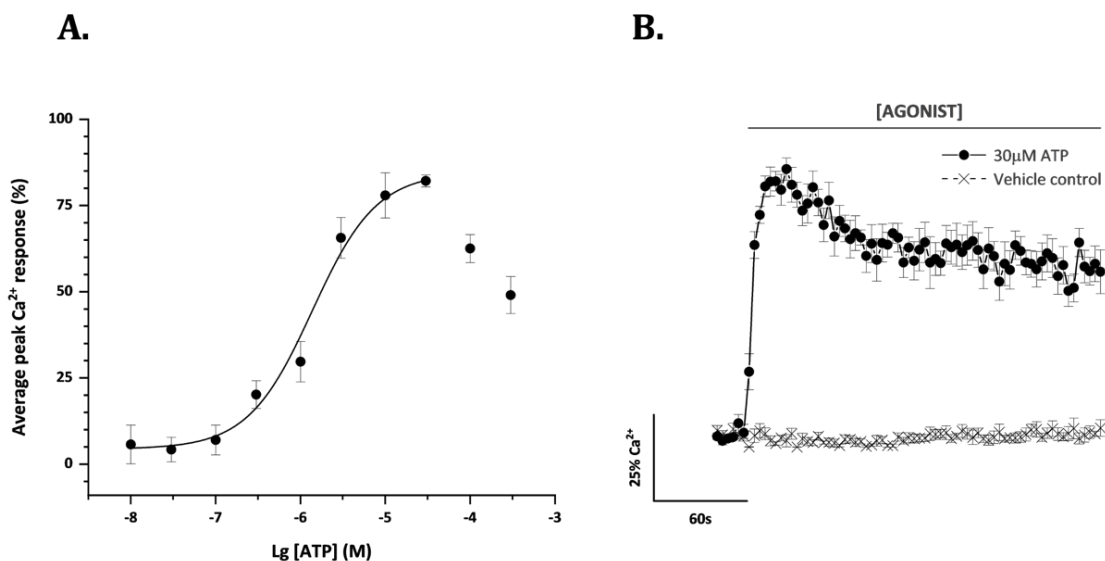


Fig 3.28. ATP evoked a Ca^{2+} response via human P2X4 WT receptors transiently transfected in 1321N1 parental astrocytoma cells in a concentration-dependent manner. (A) ATP concentration-response curves for the peak magnitude of intracellular Ca^{2+} influx in 1321N1 parental astrocytoma cells transiently co-transfected with hP2X4 WT HA-tagged receptors and pcDNA 3.1 plasmid control. (B) Averaged time-resolved intracellular Ca^{2+} influx elicited by 30 μM ATP. All data were normalised to respective maximal 100 μM Carbachol responses. Data were represented as mean \pm SEM ($N=5$).

Subunit interaction is essential to form a functional P2X4 ion pore. Co-immunoprecipitation studies were performed to assess human P2X4 WT homo-oligomeric assembly using human P2X4 WT HA and FLAG-tagged constructs transiently co-transfected in 1321N1 astrocytoma cells. Input lanes corresponded to whole-cell lysate controls before immunoprecipitation and ensured that the detection of protein complexes was due to specific interaction with the precipitated protein and not because they were already present at high levels in the original lysate. The human P2X4 WT HA-tagged protein was immunoprecipitated using an anti-HA antibody and analysed with an anti-FLAG antibody for interaction blots. Data showed a positive interaction between human P2X4 WT HA and FLAG-tagged subunits, detecting a major P2X4-specific 60KDa band, corresponding to its monomeric protein weight, and a heavier band at approximately 120KDa (Fig 3.29A). Similar results were obtained when human P2X4 WT FLAG subunits were pulled down using anti-FLAG antibodies. A positive immunocomplex with human P2X4 WT HA subunits was detected using the anti-HA antibody (Fig 3.29B). To ensure the immunoprecipitation process worked, I also analysed the precipitates with the antibody used for protein pull-down. For example, if anti-FLAG antibodies were used for human P2X4 WT FLAG-tagged immunoprecipitation, then anti-FLAG antibodies would be used to blot for precipitated human P2X4 WT FLAG-tagged proteins, and vice versa. Distinct 50KDa bands and fainter 25KDa bands were detected in all precipitation lanes and even for interaction blots when immunoprecipitation was done using the anti-FLAG antibody (Fig 3.29A and B). Following the immunoprecipitation protocol, before SDS-PAGE and Western blotting, all precipitates were eluted and boiled. This elution and denaturation process causes all proteins and antibodies present in the precipitated complex to detach and lose their tertiary and secondary structures. Therefore, the antibodies break down into their structural constituents, namely heavy and light chains, with molecular weights of 50KDa and 25KDa, respectively. To verify that those background bands corresponded to antibody denaturation and not to unspecific protein detection, I used untransfected 1321N1 parental cell lysates and performed immunoprecipitations using both anti-HA and anti-FLAG antibodies. Figures 3.29C and D confirmed denaturation of antibodies was occurring by the detection of 50KDa and 25KDa bands using anti-rabbit and anti-mouse HRP conjugated secondary antibodies, respectively. These secondary antibodies are routinely used in Western blotting and detect both heavy and light chains of the primary antibody used for blotting and denatured antibody parts in immunoprecipitation studies. The human P2X4 monomeric molecular weight, as well as the other P2X subunits, is close to that of heavy antibody chains. Consequently, using those secondary antibodies could cause misinterpretation of immunoprecipitation data.

To surpass this problem, I tested other HRP-conjugated secondary antibodies to reduce non-specific signals while detecting interaction complexes. The first option was to use secondary antibodies that only detect the IgG light chain because their molecular weight is far apart. Detection of 25KDa bands would not affect the interpretation of P2X immunoprecipitation data. Anti-rabbit light chain antibody detected high molecular weight bands of approximately 250KDa and 150KDa and did not reduce background signals at 50KDa, masking the human P2X4 WT HA-tagged specific band (Fig 3.30A). In the same way, the anti-mouse light chain antibody failed to detect human P2X4 WT FLAG-tagged proteins specifically, yet it detected higher bands at 250KDa and 150KDa and a fainter 50KDa band too (Fig

3.30B). Next, I sought to use an IP detection reagent called VeriBlot which should only detect native IgG proteins allowing the detection of (co-)immunoprecipitated proteins without masking them with heavy and light antibody chain bands. However, it did not detect any human P2X4 WT FLAG-specific bands and still showed faint background signals at 50KDa and 25KDa (Fig 3.30C). Finally, another option was to use F(ab')₂ fragment HRP conjugated secondary antibodies. F(ab')₂ antibody fragments are generated by pepsin enzyme digestion of full-size antibodies, removing most of the Fc region (crystallisable fragment) while leaving the two antigen-binding (ab') parts intact and linked by disulphide bonds. These antibodies only recognise the F(ab')₂ fragments of either rabbit or mouse immunoglobulin G, thus avoiding recognition of denatured antibody parts in the immunoprecipitated samples, namely Fc regions or heavy and light antibody chains. Both anti-mouse and anti-rabbit F(ab')₂ HRP conjugated secondary antibodies specifically detected human P2X4 WT FLAG and HA-tagged proteins at 60KDa respectively, and completely removed the 50KDa background signal (Fig 3.30D and E). Higher molecular weight bands were detected at 110KDa and 150KDa, most likely corresponding to residual F(ab')₂ fragments and full-sized IgG proteins in immunoprecipitated samples, respectively. Nevertheless, these higher background signals would not affect the interpretation of P2X co-immunoprecipitation data. To conclude, all co-immunoprecipitates were then analysed using 1:1000 anti-FLAG and anti-HA primary antibodies and detected with 1:2000 anti-mouse F(ab')₂ and anti-rabbit F(ab')₂ HRP conjugated secondary antibodies, respectively.

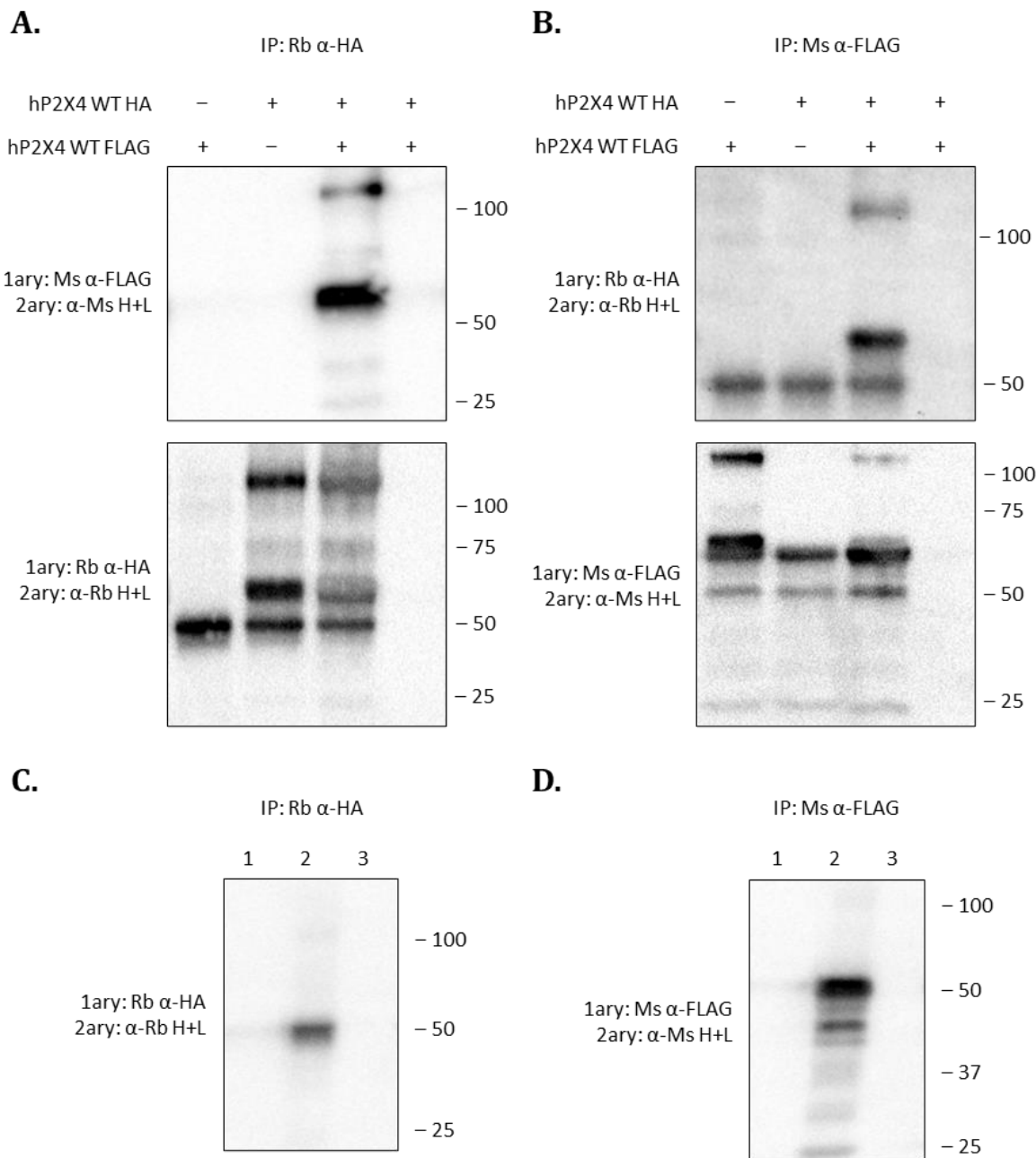


Fig 3.29. Common HRP-conjugated secondary antibodies detecting heavy and light antibody chains were not a good choice for co-immunoprecipitation studies in transiently co-transfected 1321N1 parental astrocytoma cells. (A) Representative immunoblots for transient hP2X4 WT HA- and FLAG-tagged proteins after immunoprecipitation using Rb α -HA, and developed using 1:1000 Gt α -Ms (H+L) HRP for interaction blot (top) or 1:1000 Gt α -Rb (H+L) for pull-down control (bottom). Lanes 1-3 corresponded to immunoprecipitated protein complexes and lane 4 was an IgG negative control for immunoprecipitation without antibody. (B) Representative immunoblots for transient hP2X4 WT HA- and FLAG-tagged proteins after immunoprecipitation using Ms α -FLAG, and developed using 1:1000 Gt α -Rb (H+L) HRP-conjugated antibodies for interaction blot (top) or 1:1000 Gt α -Ms (H+L) HRP-conjugated antibodies for pull-down control (bottom). Lanes 1-3 corresponded to immunoprecipitated protein complexes and lane 4 was an IgG negative control for immunoprecipitation without antibody.

Note background bands detected at 50KDa and 25KDa in immunoblots A and B. (C, D) Representative pull-down control minoblots in 1321N1 untransfected parental astrocytoma cells for α -HA and α -FLAG antibodies after immunoprecipitation using α -HA or α -FLAG antibodies, and developed using 1:1000 Gt α -Rb (H+L) or Gt α -Ms (H+L) HRP-conjugated secondary antibodies, respectively. Miniblot lanes corresponded to: 50 μ g 1321N1 untransfected whole protein lysate (1), 1321N1 untransfected immunoprecipitated complex (2), and IgG negative control for immunoprecipitation without antibody (3). Note background bands were still detected at 50KDa and 25KDa. Molecular weight size standards were indicated in KDa (N=3).

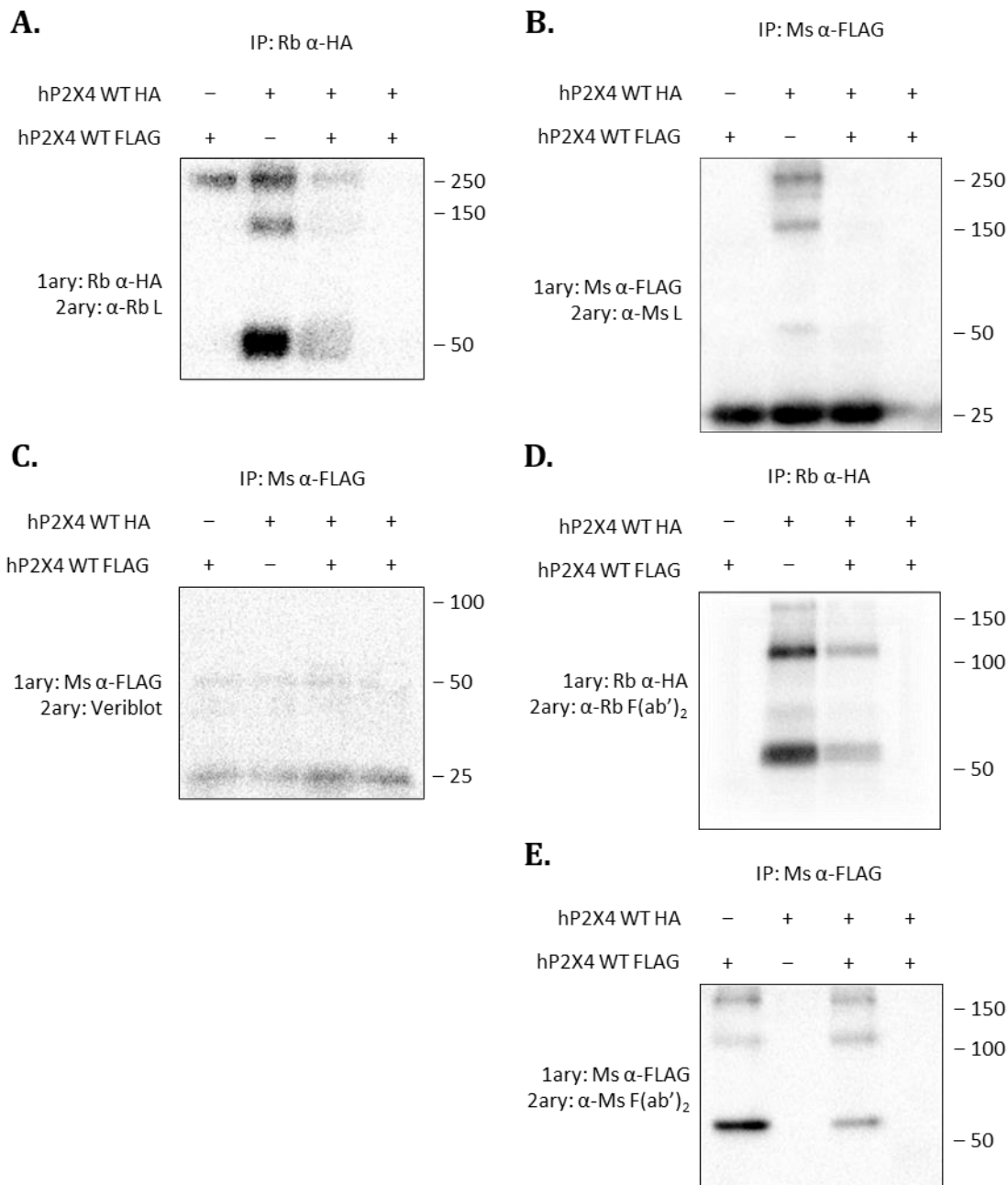


Fig 3.30. Determination of which secondary antibodies to use for co-immunoprecipitation studies in transiently co-transfected 1321N1 parental astrocytoma cells. (A, B) Representative pull-down control immunoblots for transient hP2X4 WT HA- and FLAG-tagged proteins after immunoprecipitation using α -HA or α -FLAG antibodies, and developed using 1:2000 Gt α -Rb Light (L) chain or Gt α -Ms L chain HRP-conjugated secondary antibodies, respectively. Lanes 1-3 corresponded to immunoprecipitated protein complexes and lane 4 was an IgG negative control for immunoprecipitation without antibody. Note background bands detected at 250kDa, 150kDa, and 25kDa in immunoblots A and B; and no P2X4 specific bands detected in B. (C) Representative pull-down control immunoblot for transient hP2X4 WT HA- and FLAG-tagged proteins after immunoprecipitation using α -FLAG antibody, and developed using 1:2000 Veriblot reagent. Note background bands were detected at 50kDa and 25kDa and no P2X4-specific bands were detected. (D, E) Representative pull-down control immunoblots for transient hP2X4

WT HA- and FLAG-tagged proteins after immunoprecipitation using α -HA or α -FLAG antibodies, and developed using 1:2000 Gt α -Rb F(ab')₂ or Gt α -Ms F(ab')₂ HRP-conjugated secondary antibodies, respectively. Lanes 1-3 corresponded to immunoprecipitated protein complexes and lane 4 was an IgG negative control for immunoprecipitation without antibody. Note no background bands were detected at 50KDa or 25KDa. Molecular weight size standards were indicated in KDa (N=3).

Following this new protocol, co-immunoprecipitation studies were repeated to accurately assess human P2X4 WT homo-oligomeric assembly using human P2X4 WT HA and FLAG-tagged constructs transiently co-transfected in 1321N1 parental astrocytoma cells. The human P2X4 WT FLAG-tagged protein was immunoprecipitated using an anti-FLAG antibody and analysed with an anti-HA antibody for interaction blots. Data showed a positive interaction between human P2X4 WT FLAG and HA-tagged subunits (Fig 3.31A and B). A major P2X4-specific 60KDa band corresponding to its monomeric protein weight and a heavier band at approximately 120KDa were detected (Fig 3.31A). Densiometric analysis showed no significant differences between whole-cell (1.81 ± 0.53 au) and co-immunoprecipitated (1.74 ± 0.47 au) expression levels of human P2X4 WT HA-tagged subunits ($p>0.05$; Fig 3.31B). Reciprocate human P2X4 WT HA-tagged pull-down using an anti-HA antibody, and analysis of protein interaction with an anti-FLAG antibody were assessed for completeness. Results also showed a positive interaction between human P2X4 WT HA and FLAG-tagged subunits (Fig 3.31C and D). Bands at 60KDa and 120KDa were detected, and another heavier band at approximately 180KDa (Fig 3.31C). Similarly, the densiometric analysis showed no significant differences between whole-cell (0.41 ± 0.10 au) and co-immunoprecipitated (1.16 ± 0.40 au) expression levels of human P2X4 WT FLAG-tagged subunits ($p>0.05$; Fig 3.31D). Note a smaller but not significantly different amount of human P2X4 FLAG-tagged protein at whole-cell input levels compared to human P2X4 HA-tagged protein levels when co-expressed together ($p>0.05$; Fig 3.31). The most probable explanation for this would be different antigen-antibody affinity rather than protein expression competition in this heterologous system. Nevertheless, the amount of human P2X4 WT FLAG and HA-tagged protein interaction complex was equivalent using either combination of pull-down and immunoblotting antibodies ($p>0.05$; Fig 3.31).

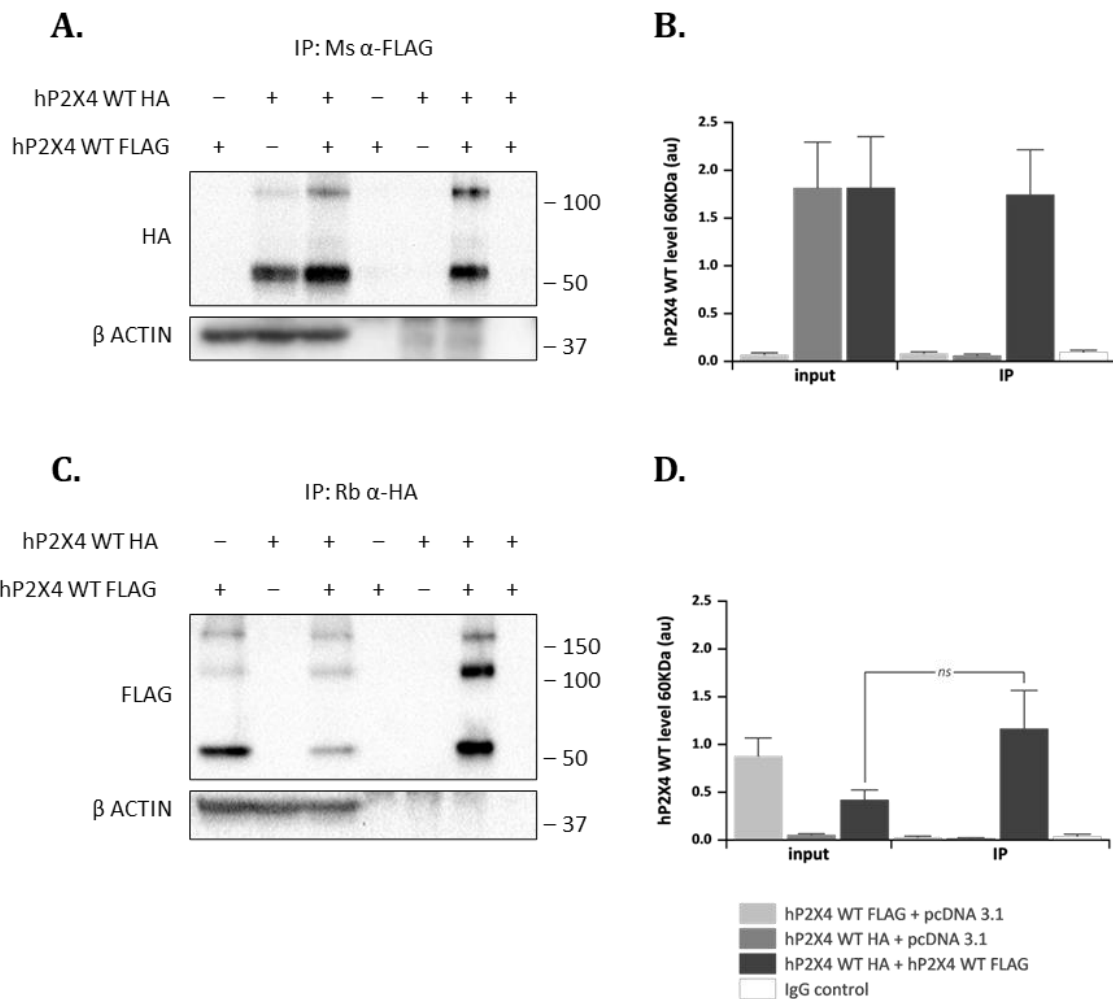


Fig 3.31. Homomeric interaction of human P2X4 WT subunits in transiently co-transfected 1321N1 parental astrocytoma cells. (A) Representative immunoblot for hP2X4 WT HA-tagged protein after immunoprecipitation using anti-FLAG antibody, and for the β -actin loading control. (B) Comparison of densitometric analysis of hP2X4 WT HA-tagged protein level relative to loading control for input and co-immunoprecipitated complexes. (C) Representative immunoblot for hP2X4 WT FLAG-tagged protein after immunoprecipitation using anti-HA antibody, and for the β -actin loading control. (D) Comparison of densitometric analysis of hP2X4 WT FLAG-tagged protein level relative to loading control for input and co-immunoprecipitated complexes. Molecular weight size standards were indicated in KDa. Lanes 1-3 corresponded to whole-cell protein lysates and lanes 4-7 to immunoprecipitated protein complexes. Lane 7 was an IgG negative control for immunoprecipitation without antibody. Data were represented as mean \pm SEM ($N=3$).

3.2.3.3 Proof of concept demonstrated human P2X4 WT subunits interact with human P2X4 [K67A, K313A] dead subunits

Original evidence that human P2X4 [K67A, K313A] dead subunits caused a significant loss of human P2X4 wild-type channel function, as well as proof that human P2X4 subunits underwent homo-oligomeric assembly, were used as starting points to further validate the dead receptor hypothesis in this heterologous system. Hence, the proof of concept consisted in demonstrating i) a reduction of human P2X4 WT activity in the presence of human P2X4 [K67A, K313A] dead subunits upon application of various concentrations of ATP and ii) a physical interaction between human P2X4 WT and human P2X4 [K67A, K313A] proteins.

Whole-cell and cell membrane expression levels for human P2X4 WT HA-tagged and human P2X4 [K67A, K313A] FLAG-tagged subunits were assessed by biotinylation and Western blotting so that the proof of concept could be interpreted with confidence. Figure 3.32A showed high expression of human P2X4 WT HA-tagged protein at 60KDa for both whole-cell (1.48 ± 0.39 au) and cell surface lysates (0.92 ± 0.27 au, $p>0.05$; Fig 3.32B). Moreover, there were no significant differences in the whole-cell (1.34 ± 0.36 au) and cell-surface lysates (0.77 ± 0.26 au) when human P2X4 WT HA was co-transfected with human P2X4 [K67A, K313A] FLAG-tagged subunits ($p>0.05$; Fig 3.32B). It is critical to note that human P2X4 [K67A, K313A] FLAG-tagged dead subunits were also highly expressed at both whole-cell (0.93 ± 0.11 au) and cell surface levels (0.99 ± 0.17 au, $p>0.05$; Fig 3.32A). However, co-expression with human P2X4 WT HA-tagged subunits significantly reduced its expression at the cell membrane (0.59 ± 0.05 au vs 1.27 ± 0.26 whole-cell control, $p<0.05$; Fig 3.32B). Higher molecular weight species were also detected at 120KDa and 180KDa for both human P2X4 WT HA-tagged and P2X4 [K67A, K313A] FLAG-tagged, which seemed to be the preferred states for the human P2X4 WT protein at the cell membrane (Fig 3.32).

Furthermore, calcium mobilisation assays were performed in 1321N1 cells transiently co-transfected cells to evaluate the dead receptor theory and complement previous data (section 3.2.3.1). Results showed that transient co-transfection of human P2X4 WT HA-tagged and human P2X4 [K67A, K313A] FLAG-tagged dead subunits significantly reduced the ATP-evoked calcium response compared to human P2X4 WT HA-tagged transiently transfected with plasmid control in 1321N1 parental astrocytoma cells (Fig 3.33). This reduction occurred in a concentration-dependent manner from 300nM to 300 μ M ATP concentrations ($p<0.01$ and $p<0.001$, respectively; Fig 3.33A). Maximal inhibitory effects were reached at a 30 μ M ATP concentration with a nearly 60% reduction of the calcium response ($24.2\pm1.58\%$ vs $82.1\pm1.77\%$ plasmid control, $p<0.001$; Fig 3.33) whilst still maintaining a sustained desensitisation phase over time (approximately 20% above baseline; Fig 3.33B). Nevertheless, the human P2X4 WT ATP potency was not affected when co-transfected with human P2X4 [K67A, K313A] dead subunits ($1.11\pm0.30\mu$ M, $p>0.05$; Fig 3.33A).

Finally, interactions between human P2X4 WT and human P2X4 [K67A, K313A] dead subunits occurred in co-immunoprecipitation assays (Fig 3.34). Both anti-FLAG and anti-HA immunoprecipitates showed human P2X4-specific protein bands at 60KDa, plus a higher band at 120KDa. Anti-FLAG pull-down and

anti-HA analysis also detected a 180KDa band. It is key to note that expression levels of human P2X4 WT HA-tagged proteins were significantly reduced in the precipitate complex lane (0.69 ± 0.18 au) compared to input control (1.58 ± 0.22 au) when human P2X4 [K67A, K313A] FLAG-tagged was used for protein pull-down ($p<0.05$; Fig 3.34B). However, when human P2X4 WT HA-tagged was used for immunoprecipitation, human P2X4 [K67A, K313A] FLAG-tagged protein levels remained unchanged compared to input control (1.62 ± 0.42 au vs 0.78 ± 0.45 au, respectively, $p>0.05$; Fig 3.34D). These data supported the different antigen-antibody affinity explanations, like in the co-expression of human P2X4 WT HA and WT FLAG-tagged proteins (Fig 3.31).

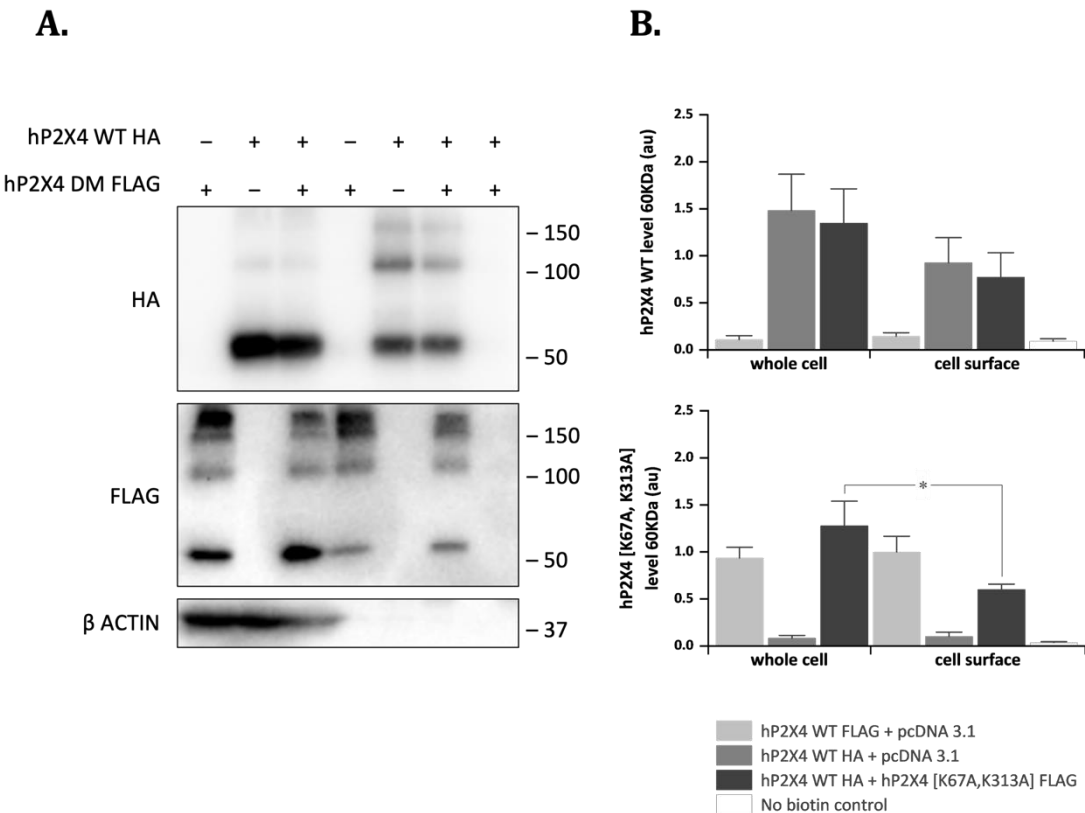


Fig 3.32. Whole-cell and cell surface expression levels of human P2X4 WT and human P2X4 [K67A, K313A] subunits in transiently co-transfected 1321N1 parental astrocytoma cells. (A) Representative immunoblot for hP2X4 WT HA-tagged protein (top), hP2X4 [K67A, K313A] FLAG-tagged protein (middle), and β -actin loading control (bottom). Molecular weight size standards were indicated in kDa. Lanes 1-3 corresponded to whole-cell samples and lanes 4-7 to cell surface protein lysates. Lane 7 was a negative control for biotin labelling. (B) Comparison of densitometric analysis of hP2X4 WT HA-tagged (top) and hP2X4 [K67A, K313A] FLAG-tagged (bottom) protein levels relative to loading control for whole-cell and cell surface lysates. Data were represented as mean \pm SEM ($N=3$).

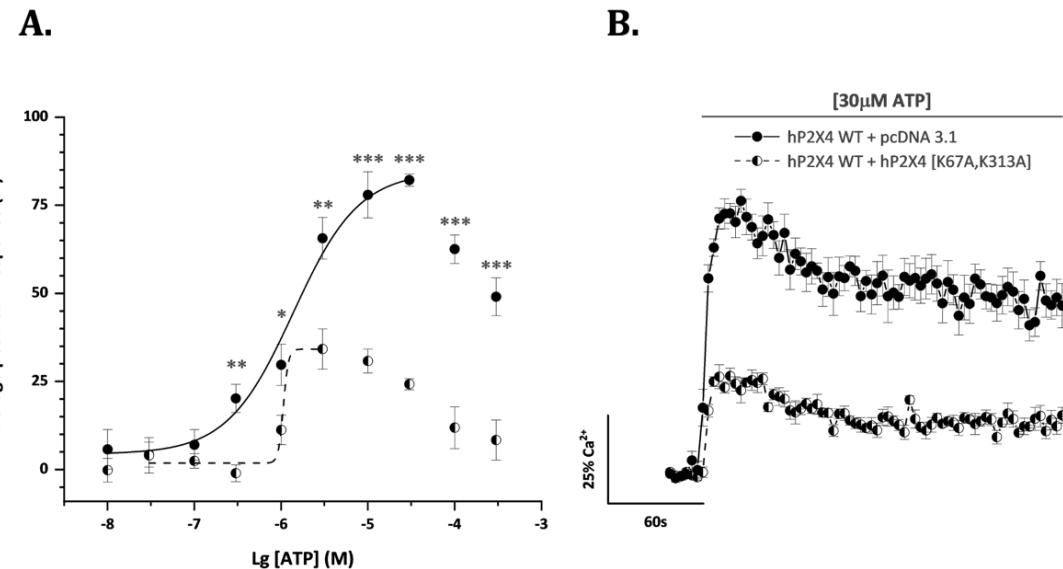


Fig 3.33. The human P2X4 [K67A, K313A] dead subunit had a dominant negative effect on human P2X4 WT ATP-induced Ca^{2+} responses in transiently co-transfected 1321N1 parental astrocytoma cells. (A) ATP concentration-response curves for the peak magnitude of intracellular Ca^{2+} influx in the presence (half moon circles) and absence (closed circles) of hP2X4 [K67A, K313A]. (B) Averaged time-resolved intracellular Ca^{2+} influx elicited by 30 μM ATP in the presence (half moon circles) and absence (closed circles) of hP2X4 [K67A, K313A]. All data were normalised to respective maximal 100 μM Carbachol responses. Data were represented as mean \pm SEM ($N=5$).

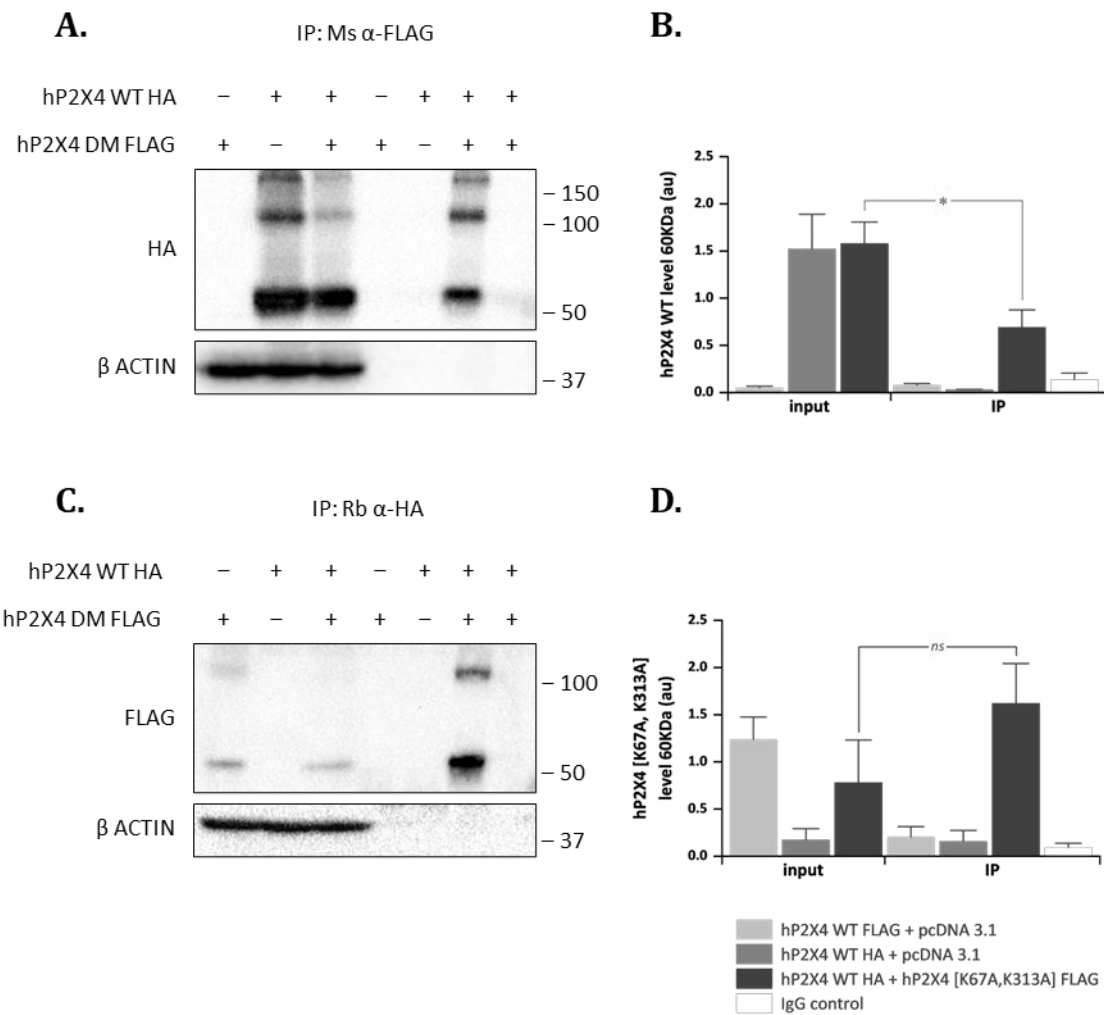


Fig 3.34. Human P2X4 WT subunits interacted with human P2X4 [K67A, K313A] dead subunits in transiently co-transfected 1321N1 parental cells. (A) Representative immunoblot for hP2X4 WT HA-tagged protein after immunoprecipitation using anti-FLAG antibody, and for the β -actin loading control. (B) Comparison of densitometric analysis of hP2X4 WT HA-tagged protein level relative to loading control for input and co-immunoprecipitated complexes. (C) Representative immunoblot for hP2X4 [K67A, K313A] FLAG-tagged protein after immunoprecipitation using anti-HA antibody, and for the β -actin loading control. (D) Comparison of densitometric analysis of hP2X4 [K67A, K313A] FLAG-tagged protein level relative to loading control for input and co-immunoprecipitated complexes. Molecular weight size standards were indicated in kDa. Lanes 1-3 corresponded to whole-cell protein lysates and lanes 4-7 to immunoprecipitated protein complexes. Lane 7 was an IgG negative control for immunoprecipitation without antibody. Data were represented as mean \pm SEM ($N=3$).

3.2.3.4 Dead receptor tools demonstrated functional interactions between human P2X2 and human P2X3 subunits

The dead receptor hypothesis proved to be a good model to detect and validate human P2X4 homomeric interactions in transiently co-transfected 1321N1 parental astrocytoma cells. Before exploring possible functional human P2X4 heteromeric interactions, I wanted to demonstrate if the experimental system could also accurately identify the existence of the well-established P2X2/3 heteromer. As mentioned in the introduction, each P2X receptor subtype has a different pharmacological profile. ATP activates P2X2 and P2X3, but its analogue $\alpha\beta$ -MeATP activates only the P2X3 subtype. P2X3 is also known for its fastest desensitisation amongst the P2X family of receptors, whilst P2X2 has a slow desensitisation phase. Thereby, P2X2/3 heterotrimers distinctly respond to $\alpha\beta$ -MeATP and present a gradual desensitisation phase over time. The hypothesis is based on the concept that only one dead subunit is necessary to block or reduce channel activation completely. Literature previously suggested a 1:2 subunit stoichiometry for the rat P2X2/3 heteromer in favour of the P2X3 subtype (Wilkinson et al., 2006). Thus, I co-transfected 1321N1 parental astrocytoma cells with human P2X2 [K81A, K319A] FLAG-tagged dead subunits and human P2X3 WT HA-tagged subunits.

Similarly, protein expression levels for both human P2X2 and human P2X3 subtypes were assessed to confirm that the presence of C-terminal epitope tags did not alter their protein expression patterns and to confidently interpret the intracellular calcium mobilisation data and the protein interaction studies. Results showed high expression levels for human P2X3 WT HA-tagged at both whole-cell and cell-surface levels (1.34 ± 0.30 au and 1.81 ± 0.16 au, respectively, $p > 0.05$; Fig 3.35A and B). Human P2X2 WT FLAG-tagged subunits were also substantially expressed at a whole-cell level (1.78 ± 0.47 au) and to a lesser but not significant extent at the cell membrane (1.13 ± 0.13 au, $p > 0.05$; Fig 3.35C and D). Moreover, human P2X2 [K81A, K319A] FLAG-tagged dead subunits were equally expressed at whole-cell (1.74 ± 0.23 au) and cell membrane levels (1.45 ± 0.17 au, $p > 0.05$; Fig 3.35E and F). Cell surface expression levels of human P2X2 wild-type and double mutant subunits were also akin ($p > 0.05$).

To determine the effects of human P2X2 [K81A, K319A] dead subunits on the human P2X3 WT agonist-induced calcium responses, I initially performed calcium mobilisation assays on 1321N1 parental astrocytoma cells transiently co-transfected with human P2X2 WT FLAG-tagged and human P2X3 WT HA-tagged subunits. Data showed a concentration-dependent calcium response to α,β -MeATP with a potency of 36.2 ± 12.0 μ M (Fig 3.36A). Additionally, the receptor activation profile was characteristic of that previously reported for rat and human P2X2/3 heteromeric receptors: a maximal calcium response reaching $44.4 \pm 5.23\%$ of peak magnitude upon application of 100μ M α,β -MeATP and a slow desensitisation phase over time at about 35% above baseline (Fig 3.36C; Wilkinson et al., 2006; Kowalski et al., 2015)). A β -MeATP did not activate human P2X2 WT receptors transiently transfected in 1321N1 parental astrocytoma cells (Fig 3.36E and F). As expected, 100μ M ATP also evoked a calcium response in 1321N1 parental astrocytoma cells transiently co-transfected with human P2X2 WT FLAG-tagged and human P2X3 WT HA-tagged subunits reaching $104 \pm 2.18\%$ of peak magnitude upon agonist application with a high sustained desensitisation phase over time (Fig 3.36D). Besides, maximal agonist-evoked

calcium responses were significantly different when using either 100 μ M ATP or 100 μ M $\alpha\beta$ -MeATP ($p<0.001$; Fig 3.36B), making ATP a more efficacious agonist in activating human P2X2/3 receptors.

In agreement with the hypothesis of the dead receptor (Fig 3.1), the presence of human P2X2 [K81A, K319A] dead subunits completely blocked the human P2X3 WT $\alpha\beta$ -MeATP-evoked calcium influx in a concentration-independent manner in transiently co-transfected 1321N1 parental cells as shown in Figures 3.36A – C. Maximal effects were observed at 100 μ M $\alpha\beta$ -MeATP concentrations with a complete calcium response reduction compared to the human P2X2 WT and human P2X3 WT control combination ($2.42\pm3.08\%$, $p<0.001$; Fig 3.36B and C). Similarly, the calcium response evoked by 100 μ M ATP was also completely abolished when human P2X2 [K81A, K319A] dead subunits were present ($4.35\pm2.29\%$, $p<0.001$; Fig 3.36B and D).

The human P2X2 WT FLAG-tagged protein was immunoprecipitated using an anti-FLAG antibody and analysed with an anti-HA antibody for interaction with human P2X3 WT HA-tagged subunits. Immunoblots showed major human P2X3-specific 60KDa bands in input and immunoprecipitated lanes corresponding to its monomeric protein weight and suggestive of a positive interaction with human P2X2 WT subunits (Fig 3.37A and B). Densiometric analysis showed a significant reduction in human P2X3 WT HA protein expression levels before (1.53 ± 0.16 au) and after co-immunoprecipitation (0.68 ± 0.17 au, $p<0.05$; Fig 3.37B) possibly due to reduced antibody affinity during anti-FLAG pull-down. Reciprocal human P2X3 WT HA-tagged pull-down with anti-HA antibody and analysis of protein interaction with anti-FLAG antibody were also performed. Results also showed a positive interaction between human P2X2 WT FLAG-tagged and human P2X3 WT HA-tagged subunits (Fig 3.37C and D). Bands at approximately 70KDa were detected corresponding to the human P2X2 monomeric molecular weight (Fig 3.37C). In contrast, the densiometric analysis showed no significant differences between whole-cell (0.70 ± 0.18 au) and co-immunoprecipitated (0.96 ± 0.13 au) expression levels of human P2X2 WT FLAG-tagged subunits ($p>0.05$; Fig 3.37D). Moreover, there were no significant differences between co-immunoprecipitated levels of human P2X2 WT FLAG-tagged and P2X3 WT HA-tagged monomeric proteins (0.96 ± 0.13 au and 0.68 ± 0.17 au, respectively, $p>0.05$; Fig 3.37).

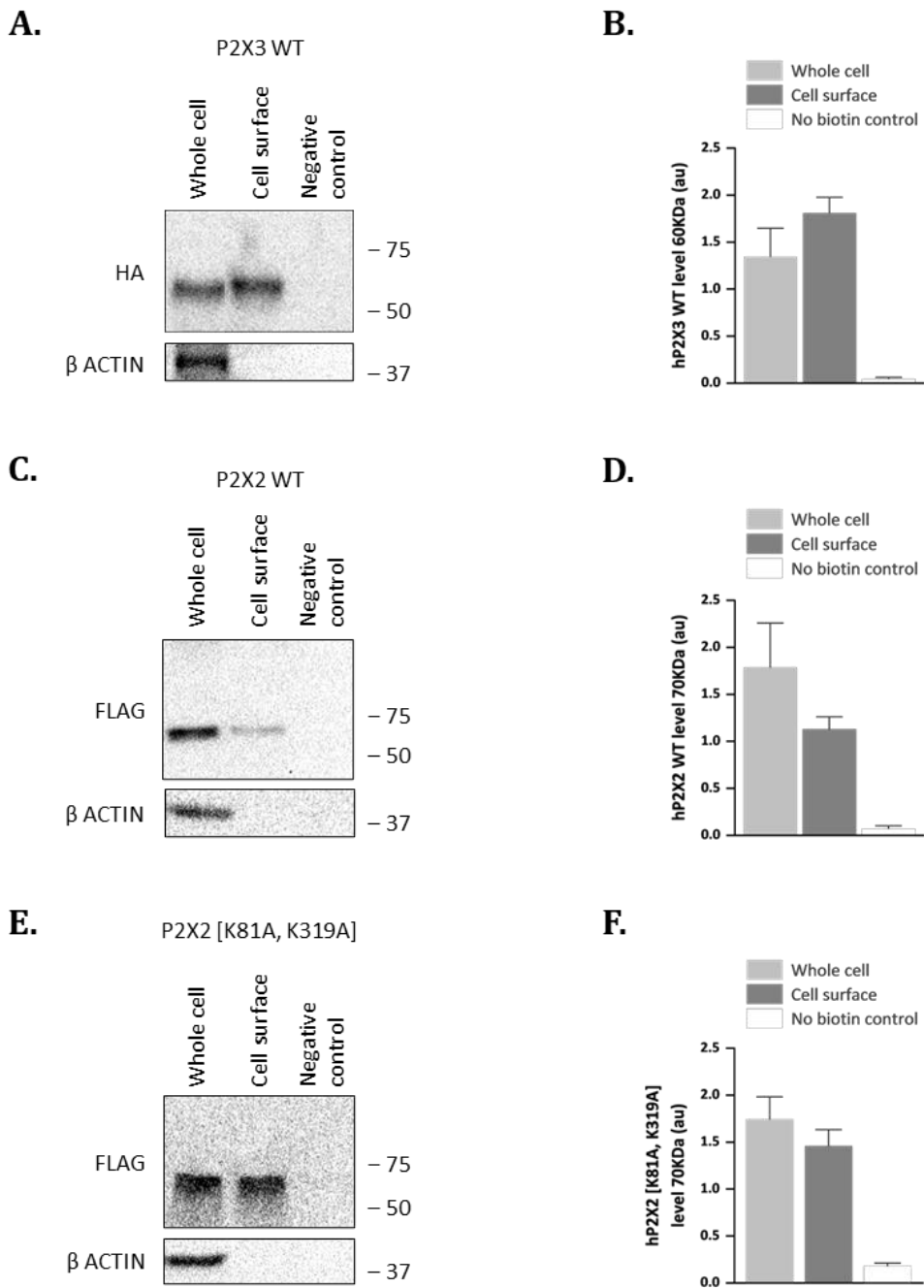
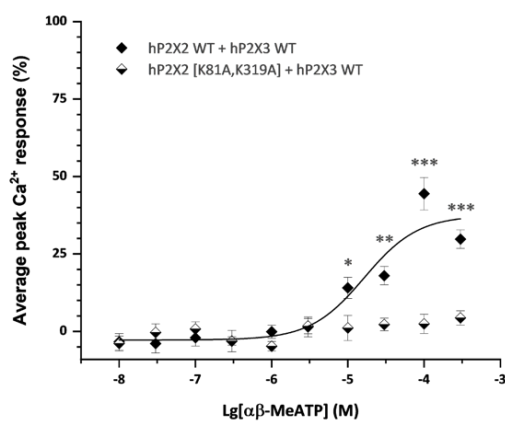
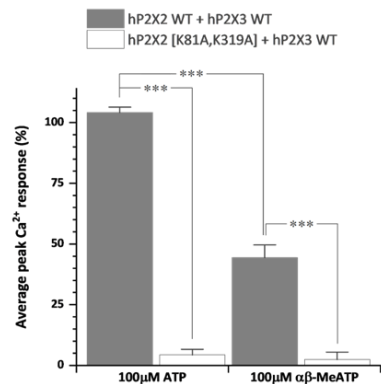


Fig 3.35. Whole-cell and cell surface expression levels of human P2X3 WT, human P2X2 WT, and human P2X2 [K81A, K319A] subunits in transiently co-transfected 1321N1 parental astrocytoma cells. (A, C, E) Representative immunoblot for (A) hP2X3 WT HA-tagged protein, (C) hP2X2 WT FLAG-tagged protein, and (E) hP2X2 [K81A, K319A] FLAG-tagged protein, with corresponding β-actin loading controls. Molecular weight size standards were indicated in KDa. Lane 1 corresponded to whole-cell samples, lane 2 to cell surface protein lysates, and lane 3 was a negative control for biotin labelling. (B, D, F) Comparison of densitometric analysis of (B) hP2X3 WT HA, (D) hP2X2 WT FLAG, and (F) hP2X2 [K81A, K319A] FLAG protein levels relative to loading control for whole-cell and cell surface lysates. Data were represented as mean ± SEM ($N=3$).

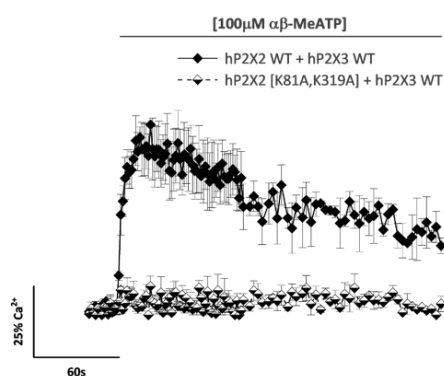
A.



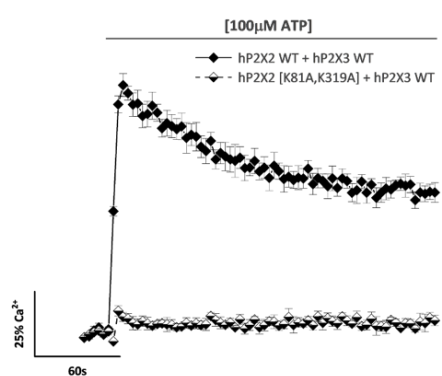
B.



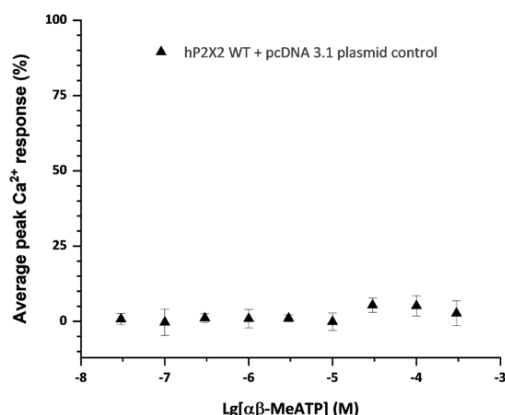
C.



D.



E.



F.

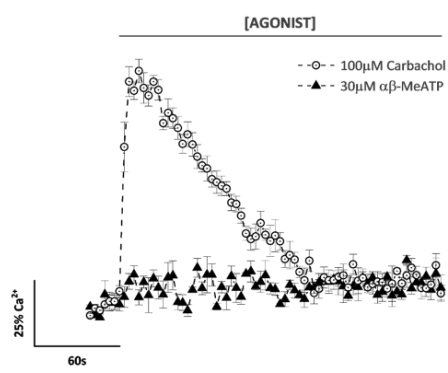


Fig 3.36. Validation of the hypothesis of the dead receptor as a good tool to probe for functional human P2X heteromers. (A – D) The hP2X2 [K81A, K319A] dead subunit had a dominant negative effect on hP2X3 WT ATP and αβ-MeATP-induced Ca²⁺ responses in transiently transfected 1321N1 parental cells. (A) αβ-MeATP concentration-response curve for the peak magnitude of intracellular Ca²⁺ influx in the presence (half diamonds) and absence (closed diamonds) of hP2X2 [K81A, K319A]. (B) Comparison of average peak Ca²⁺ responses mediated by 100 μM ATP and 100 μM αβ-MeATP in the presence and absence of hP2X2 [K81A, K319A]. (C, D) Averaged time-resolved intracellular Ca²⁺ influx elicited by

100 μ M $\alpha\beta$ -MeATP (C) and 100 μ M ATP (D) in the presence (half diamonds) and absence (closed diamonds) of hP2X2 [K81A, K319A]. (E, F) $\alpha\beta$ -MeATP did not induce a Ca^{2+} response via hP2X2 WT transiently transfected 1321N1 parental cells. (E) $\alpha\beta$ -MeATP concentration-response curve for the peak magnitude of intracellular Ca^{2+} influx. (F) Averaged time-resolved intracellular Ca^{2+} influx elicited by 30 μ M $\alpha\beta$ -MeATP (closed triangles) compared to Ca^{2+} influx caused by 100 μ M Carbachol as a cell viability control (open circles). All data were normalised to respective maximal 100 μ M Carbachol responses. Data were represented as mean \pm SEM ($N=5$).

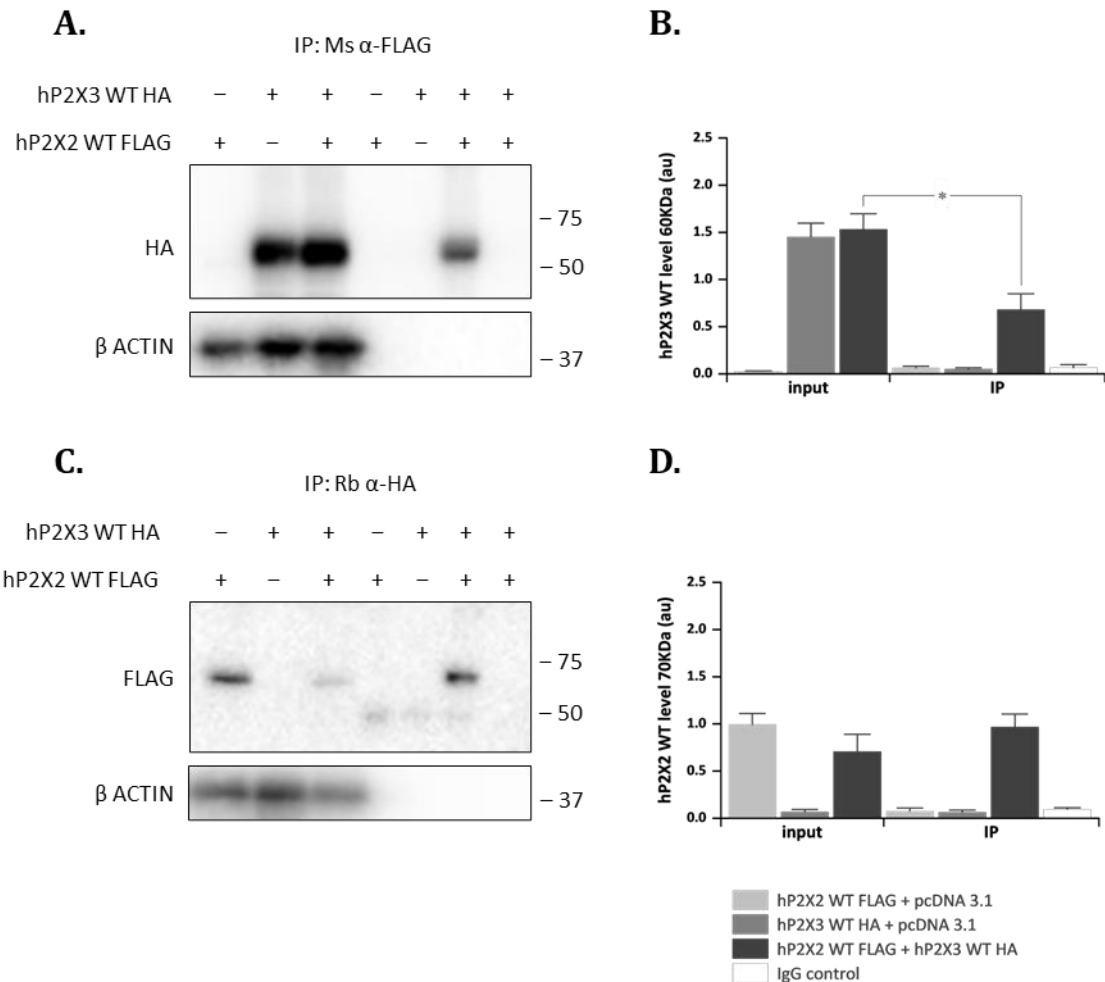


Fig 3.37. Heteromeric interaction of human P2X2 WT and human P2X3 WT subunits in transiently co-transfected 1321N1 parental astrocytoma cells. (A) Representative immunoblot for hP2X3 WT HA-tagged protein after immunoprecipitation using anti-FLAG antibody, and for the β -actin loading control. (B) Comparison of densitometric analysis of hP2X3 WT HA-tagged protein level relative to loading control for input and co-immunoprecipitated complexes. (C) Representative immunoblot for hP2X2 WT FLAG-tagged protein after immunoprecipitation using anti-HA antibody, and for the β -actin loading control. (D) Comparison of densitometric analysis of hP2X2 WT FLAG-tagged protein level relative to loading control for input and co-immunoprecipitated complexes. Molecular weight size standards were indicated in KDa. Lanes 1-3 corresponded to whole-cell protein lysates and lanes 4-7 to immunoprecipitated protein complexes. Lane 7 was an IgG negative control for immunoprecipitation without antibody. Data were represented as mean \pm SEM ($N=3$).

3.3 Discussion

3.3.1 Successful transient transfection of 1321N1 parental astrocytoma cells with the human P2X4 receptor

To explore functional interactions of the human P2X4 receptor expressed in 1321N1 parental astrocytoma cells, it is necessary to carry out cell transfection efficiently. Unfortunately, these cells show a particular resistance to transfection (Fig 2.2). A thorough optimisation process of cell transfection was performed to successfully transfet and express the human P2X4 receptor in human 1321N1 parental astrocytoma cells. An optimised gene sequence for the human P2X4 wild-type receptor containing a C-terminal FLAG tag and cloned into a pcDNA 3.1 backbone vector was used for transfection into 1321N1 parental astrocytoma cells. Human 1321N1 astrocytoma cells are void of endogenous purinergic receptors (Communi et al., 1996). Thus, the application of extracellular ATP did not trigger any endogenous intracellular calcium responses (Fig 3.12). Thereby, any ATP-evoked intracellular calcium response was treated as an indirect measure of human P2X4 receptor activity and transfection efficiency.

A 2011 study compared and optimised five different nonviral transfection methods in human 1321N1 astrocytoma cells and found that microporation was the most efficient technique for transgene delivery into these cells (Marucci et al., 2011). However, this physical transfection method had advantages and limitations. For example, high transfection efficiency (95%) and low cell mortality were achieved by microporation (Marucci et al., 2011). But this laborious procedure requires a commercial buffer and a specific electroporator machine (Microporator) by which only a few cells can be transfected, making it a low throughput and expensive technique, so not as accessible and convenient as other chemical methods. This group also tested other chemical methods for human 1321N1 astrocytoma cell transfection. These were: calcium phosphate, Arrest-In, FuGENE and Lipofectamine, which gave 40%, 78%, 70% and 50% transfection efficiencies, respectively (Marucci et al., 2011). There are many commercially available products to chemically transfet cells which are easier to use and can also get high transfection efficiencies, although it is variable depending on cell type and conditions. To date, there is no ideal method for plasmid transfection into human 1321N1 parental astrocytoma cells.

In this thesis, we proposed a reliable and consistent transient transfection protocol using the cationic lipid Lipofectamine 2000 reagent (Fig 3.8 and 3.9; Table 3.2). Several factors influence the outcome of transfection experiments: i) the transfection method chosen and the amount of reagent used, ii) the DNA quality and quantity, iii) the health and viability of the cell line, iv) passage number, v) cell confluency, and vi) the presence or absence of serum and antibiotics in the media. Some of these factors were controlled for as detailed in Chapter 2, section 2.6, such as providing a healthy and viable cell culture and keeping working cell passages from P4 to P12 for optimal cell transfection (Fig 2.3). Specifically, three different chemical transfection reagents (namely, TurboFect, X-tremeGENE and Lipofectamine 2000) were tested to transfet the human P2X4 wild-type gene into human 1321N1 parental astrocytoma cells. The optimisation process is detailed in Tables 3.1 and 3.2, showing the

specific transfection conditions used and their graded efficiencies. The graded system was useful to empirically determine the ideal approach selected for high transfection efficiency, low cell toxicity, reagent accessibility and convenience, and experiment reproducibility.

TurboFect transfection reagent showed high toxicity effects in human astrocytoma cells (Fig 3.5C and D; Table 3.1) and poor transfection efficiency ($11.9 \pm 1.29\%$ for 200ng of plasmid and $0.4\mu\text{L}$ of reagent; (Fig 3.5A and B; Table 3.1). The X-tremeGENE transfection technique had low success rates and was inconsistent among experiments with ATP-evoked calcium responses ranging from $30.0 \pm 5.86\%$ to $46.5 \pm 3.21\%$ using the same transfection conditions (Fig 3.6 and 3.7; Table 3.1). Results suggested that the best condition was the combination of 200ng of plasmid DNA and $0.5\mu\text{L}$ of Lipofectamine 2000, changing the medium after six hours of transfection, which showed $72.8 \pm 6.28\%$ ATP-evoked intracellular calcium responses (Fig 3.8) whilst maintaining cell viability (Table 3.2). After lowering the initial seeding density to 1.25×10^4 cells per well, increasing the Lipofectamine 2000-DNA complex incubation time to 20 minutes, and removing the antibiotics from the cell culture media, higher transfection efficiency rates were consistently achieved ($89.1 \pm 3.98\%$; Fig 3.9; Table 3.2). In general, antibiotics can be present in the media for transient transfection, but because cationic lipid reagents such as Lipofectamine 2000 increase cell permeability, they might also increase the amount of antibiotics delivered into the cells, resulting in cytotoxicity effects and lower transfection efficiencies (according to the manufacturer ThermoFisher Scientific, UK). The study mentioned above did not mention details regarding cell culture media used nor transfection complex incubation times for any transient transfection technique investigated (Marucci et al., 2011).

Human P2X4 subunit-specific protein bands were identified at 60KDa molecular weight by anti-FLAG immunoblotting at both whole-cell and cell surface levels, further verifying a successful human P2X4 receptor transfection in human astrocytoma cells (Fig 3.10). The human P2X4 receptor subunit has a theoretical molecular weight of 44KDa and contains seven putative N-glycosylation sites, although only two are strictly required for robust receptor formation (Rettinger et al., 2000). The band detected at approximately 60KDa is therefore considered a glycosylated P2X4 subunit (Hu et al., 2002). The lower human P2X4-specific 44KDa band was not detected under the sample conditions we used: i) the solubilisation buffer contained 2% Triton X-100 which is a non-ionic detergent used for milder protein extraction, and ii) the final concentration of SDS detergent in the sample buffer was 2.4%. The results obtained using these conditions agree with previously published data and support glycosylation as a necessary modification in maintaining detergent solubility properties of P2X receptors (Hu et al., 2002). A Western blotting sample buffer containing 0.5-1.3% SDS may provide mild enough conditions to conserve the non-glycosylated P2X4 receptors. Higher molecular weight species of 120KDa were also shown at both whole-cell and cell surface levels (Fig 3.10). Other recombinant and native human P2X4 protein expression studies reported greater molecular weight species of 120KDa and 180KDa under denaturing and reducing conditions and were suggested to be multimeric receptors (Bergmann et al., 2019; Glass et al., 2002). Accordingly, the higher 120KDa band is interpreted to be a human P2X4 dimer formed by subunit multimerisation (Nicke et al., 2005). A Western blotting lysis buffer containing 1%

Triton X-100 might provide mild enough conditions for detecting the 180kDa band, thought to be the trimeric human P2X4 receptor form.

These results evidenced that successful and reproducible transient transfection of human astrocytoma cells is possible, overcoming a major problem related to the investigation of P2X receptor properties. HEK293 cells have been the most frequent cell model used to assess the role of recombinant P2X receptors in inducing changes in intracellular calcium levels because they are good transfection hosts. Nevertheless, HEK293 cells endogenously express other P2 receptor subtypes, namely P2Y1, P2Y2 and P2Y4, which also respond to ATP and other extracellular nucleotides (Fischer et al., 2003, 2005), causing large intracellular calcium changes and potentially interfering with P2X receptor-mediated calcium signals (He et al., 2003). Excitable mouse gonadotropin-releasing hormone-secreting cells (GT1) are void of endogenous P1 and P2 receptors and can be used as another alternative cell line to study the activity of purinergic P2X receptors (Koshimizu et al., 1998; He et al., 2003). However, the majority of the research in P2X heteromerisation has been done using rodent model systems (Table 4.1). Therefore, the human 1321N1 astrocytoma cell model was a more suitable system to provide new insights into the human P2X heteromerisation matter.

3.3.2 Heterologously expressed human P2X4 receptor accurately reflected its specific pharmacological properties

The focus of this section was to study the pharmacology of human P2X4 receptors to define the accuracy of using human P2X4 receptors heterologously expressed in human 1321N1 astrocytoma cells as our model system. The reader should be aware that many recognised properties of P2X4 and other P2X receptors are based on data from recombinant channels, and variables such as EC₅₀ and IC₅₀ estimates depend on the experimental conditions employed (e.g., cell type, receptor orthologue, stable electrophysiological or calcium influx conditions), as well as in establishing data analysis fundamentals. With these limitations in mind, the data discussed here will be put in context with current knowledge of P2X4 pharmacology.

As previously discussed, the human 1321N1 astrocytoma cell line is a suitable cell line model for studying the pharmacology of recombinant human P2X4 receptors. In Figure 3.8, we demonstrated that ATP did not evoke any intracellular calcium responses in these cells. Previous literature revealed that human 1321N1 astrocytoma cells endogenously express other receptors, such as M3 and M5 muscarinic acetylcholine receptors (Bayon et al., 1997; Burnett et al., 2011). These receptors are G-protein coupled receptors activated by the neurotransmitter acetylcholine. Like P2X receptors, their activation ultimately causes an increase in intracellular calcium levels. There are non-selective muscarinic receptor agonists commercially available, such as carbamylcholine (Carbachol). Carbachol was used as a positive control for cell viability, ensuring the correct interpretation of calcium data in human 1321N1 parental astrocytoma cells (Fig 3.12). Cells transiently and stably expressing human P2X4 receptors presented concentration-dependent intracellular calcium responses upon ATP stimulation (Fig 3.28 and 3.11, respectively). Comparable results were obtained from transient and stable human astrocytoma cells: i) the maximal amplitude of intracellular calcium influx was evoked by

30 μ M ATP concentrations, ii) the ATP potency values were 2.40 \pm 0.79 μ M and 0.74 \pm 0.18 μ M, respectively ($p<0.05$), and iii) ATP induced an initial rapid calcium response that slowly decayed to a sustained elevated phase over time (approximately 60% above baseline; Fig 3.28 and 3.11). These data agree with previous studies on recombinant human P2X4 receptor ATP-evoked intracellular calcium responses, which stated ATP half maximal effective concentrations (EC_{50}) in the low micromolar range, e.g., 6.32 μ M and 0.73 μ M in human 1321N1 astrocytoma cells (Bianchi et al., 1999; Abdelrahman et al., 2017), 7.4 μ M in *Xenopus laevis* oocytes (Garcia-Guzman et al., 1997), and 1.4 μ M in HEK293 cells (Jones et al., 2000). Moreover, the human P2X4 receptor subtype was reported to have a slow desensitisation phase, as well as human P2X2 receptors (Bianchi et al., 1999; North & Surprenant, 2000; North, 2002). These results confirmed that the calcium responses caused by ATP application were due to the expression of human P2X4 receptors and not to the presence of other endogenous receptors in human 1321N1 astrocytoma cells and added value to our transient transfection technique.

Homomeric human P2X4 receptors are activated most efficiently by ATP but can also be partially activated by CTP and other ATP analogues. All compounds tested were ranked in order of potency (EC_{50}) as follows: ATP (0.74 \pm 0.18 μ M) > 2-MeSATP (1.66 \pm 0.24 μ M) >> $\alpha\beta$ -MeATP (6.52 \pm 0.69 μ M) = BzATP (10.7 \pm 2.44 μ M) > CTP (20.0 \pm 4.22 μ M) = γ -imidoATP (20.3 \pm 1.59 μ M) (Fig 3.11 and 3.13; Table 3.3). These agonist-evoked intracellular calcium responses showed a similar potency profile to that reported for human and rat P2X4 receptors transiently expressed in *Xenopus laevis* oocytes: ATP >> 2-MeSATP > CTP > $\alpha\beta$ -MeATP (Garcia-Guzman et al., 1997; Soto et al., 1996). Furthermore, all five compounds evoked the maximal calcium influx responses at a concentration of 100 μ M whilst ATP produced its maximal effects at 30 μ M. Data analysis allowed us to rank them in order of efficacy (maximal response): ATP (100%) >> γ -imidoATP (84.0 \pm 5.01%) > CTP (66.8 \pm 5.76%) = 2-MeSATP (57.9 \pm 5.51%) > BzATP (35.0 \pm 3.82%) >> $\alpha\beta$ -MeATP (14.8 \pm 2.43). Partial agonism was reported for CTP and 2-MeSATP, but no significant responses were detected for $\alpha\beta$ -MeATP at human P2X4 receptors transiently transfected in *Xenopus laevis* oocytes (Garcia-Guzman et al., 1997). By definition, a partial agonist has lower efficacy than a full agonist and induces a sub-maximal activation when occupying the total receptor population. Thus, it cannot produce the maximal response regardless of the concentration required. Our data also shared similarities with two original studies using human 1321N1 astrocytoma cells stably expressing human P2X4 receptors. The first study used intracellular calcium influx and electrophysiology assays to determine the human P2X4 pharmacological profile in stable human astrocytoma cells and found that 2-MeSATP and BzATP were equally as potent as ATP (5.66 μ M and 6.31 μ M vs 6.32 μ M, respectively) but did not completely activate the human P2X4 channel (80% of ATP response for both), and $\alpha\beta$ -MeATP functioned as a weak partial agonist (EC_{50} value of 5.08 μ M and 50% of ATP response; Bianchi et al., 1999). The second study used intracellular calcium influx and radioligand binding assays and showed sub-micromolar potencies for ATP (0.73 μ M), 2-MeSATP (0.28 μ M), BzATP (0.51 μ M) and $\alpha\beta$ -MeATP (0.81 μ M) while γ -imidoATP had an EC_{50} value of 6.56 μ M at activating human P2X4 receptors (Abdelrahman et al., 2017). In contrast, this second report found all compounds to be full agonists compared to ATP (Abdelrahman et al., 2017). In addition, no significant responses (<5-10% of ATP evoked response) were detected at any concentration tested (from 0.01 μ M to 300 μ M) of AP4A and

ATP- γ -S (Fig 3.14). These data were in contrast with the two previous reports. The first showed partial agonism of both APA4 and ATP- γ -S at human P2X4 receptors stably expressed in human astrocytoma cells with EC₅₀ values of 6.2 μ M and 4.96 μ M, mediating sub-maximal calcium responses of 59% and 61% compared to the ATP-evoked responses, respectively (Bianchi et al., 1999). The second reported full agonism of AP4A with an EC₅₀ value of 0.14 μ M but did not test ATP- γ -S (Abdelrahman et al., 2017). ATP- γ -S is widely used as a non-hydrolyzed ATP analogue and later experiments I performed using mouse P2X4 receptors stably expressed in 1321N1 astrocytoma cells showed that ATP- γ -S did cause a concentration-dependent influx of calcium acting as a partial agonist with micromolar potency (data not shown). These experiments worked as a positive control to show that ATP- γ -S worked in the conditions tested and also emphasised the importance of characterising the P2X4 receptor activity and pharmacological profiles in different species. Diadenosine polyphosphates are naturally found in the central nervous system and act as neurotransmitters activating P2X2 and P2Y1 receptors and other non-ATP sensitive receptors, ultimately causing an increase in intracellular calcium levels (Pintor et al., 1996, 1997). AP4A was later tested in 1321N1 astrocytoma cells stably expressing the mouse P2X4 receptor but did not evoke any intracellular calcium responses either (data not shown). Although these data do not rule out the possibility that AP4A could activate human P2X4 receptors, are suggestive of other mechanisms by which these signalling molecules may mediate their physiological effects.

We also examined the effects of broad-spectrum P2 antagonists and P2X4 selective antagonists to characterise the human P2X4 pharmacological profile further. Recombinant human P2X4 receptors displayed sensitivity to the broad-spectrum antagonists TNP-ATP and PPADS but not to Suramin (Fig 3.15 and 3.16; Table 3.4). A previous report found that Suramin had poor inhibitory effects at human P2X4 receptors when expressed in *Xenopus laevis* oocytes, with a half maximal inhibitory concentration (IC₅₀) value of 178.1 μ M (Garcia-Guzman et al., 1997), while others also failed to show human P2X4 receptor inhibition by Suramin when expressed in human astrocytoma and HEK293 cells (Bianchi et al., 1999; Jones et al., 2000). In agreement, these data suggest that human P2X4 receptors are relatively insensitive to blockade by the conventional antagonist Suramin. TNP-ATP and PPADS are known non-selective P2X antagonists. In contrast to Suramin, both TNP-ATP and PPADS inhibited the human P2X4-mediated intracellular calcium response to ATP in a dose-dependent manner with potency (IC₅₀) values of 16.6 \pm 4.71 μ M and 33.8 \pm 16.6 μ M, respectively (Fig 3.15; Table 3.4). TNP-ATP demonstrated a competitive inhibition mode of action, shifting the human P2X4 receptor ATP potency value to 10.1 \pm 2.18 μ M ($p<0.05$ vs 0.74 \pm 0.18 μ M) without affecting its effectivity (96.8 \pm 4.08%, $p>0.05$; Fig 3.17A and B; Table 3.4). Others found that human P2X4 receptors were blocked more effectively with TNP-ATP (IC₅₀ values of 1.4 μ M and 1.5 μ M) also in a competitive manner when expressed in human astrocytoma and HEK293 cells, respectively (Abdelrahman et al., 2017; Balazs et al., 2013). On the other hand, PPADS did not affect the ATP potency value (0.81 \pm 0.27 μ M, $p>0.05$), but it caused a significant reduction in ATP-evoked maximal calcium responses (43.1 \pm 7.53%, $p<0.01$), indicating that PPADS acted as a non-competitive inhibitor of the recombinant human P2X4 receptor (Fig 3.17C and D; Table 3.4). PPADS also proved to be an effective inhibitor of human P2X4 receptors with IC₅₀ values of 27.5 μ M and 9.6 μ M when expressed in *Xenopus laevis* oocytes and HEK293 cells, respectively (Garcia-Guzman et al.,

1997; Jones et al., 2000). Contrarily, another study reported no inhibitory effects of PPADS at human P2X4 receptors when expressed in human astrocytoma cells (Bianchi et al., 1999).

Indeed, sensitivity to broad-spectrum antagonists has been used to define P2X4-mediated responses, but it is not the most effective way to discern between P2X receptor subtypes in native systems. Recent advances in the development of new small molecules that selectively target the P2X4 receptor subtype are more powerful tools for investigating the role of P2X4 receptors in heterologous and native systems. All five selective antagonists tested BAY-1797, BX-430, PSB-12062, 5-BDBD, and Taspine significantly reduced the ATP-mediated calcium response in a concentration-dependent manner (Table 3.5; Fig 3.19). The complete potency rank of selective and broad-spectrum antagonists for the human P2X4 receptor obtained was BAY-1797 ($0.21\pm0.07\mu M$) = PSB-12062 ($0.24\pm0.04\mu M$) = BX-430 ($0.42\pm0.16\mu M$) > 5-BDBD ($1.31\pm0.28\mu M$) = Taspine ($1.54\pm0.33\mu M$) > TNP-ATP ($16.6\pm4.71\mu M$) = PPADS ($33.8\pm16.6\mu M$), confirming broad-spectrum antagonists to be the worst to effectively and selectively inhibit human P2X4 receptors.

The first P2X4 inhibitor 5-BDBD was described by Bayer in 2004 (Fischer et al., 2004) but had modest effects on other P2X receptors (Coddou et al., 2019). The potency results for 5-BDBD obtained in the present study at the human P2X4 receptor (IC_{50} of $1.31\pm0.28\mu M$; Fig 3.19G-H; Table 3.5) are well in agreement with the literature potency values of $0.35\mu M$ and $0.78\mu M$ obtained in transfected human astrocytoma cells (Abdelrahman et al., 2017; Bidula et al., 2022) and of $1.5\mu M$ when expressed in HEK293 cells (Balazs et al., 2013). Our data suggested that 5-BDBD may competitively inhibit the human P2X4 receptors since ATP affinity was compromised (EC_{50} $5.83\pm0.32\mu M$, $p<0.01$), but no significant reduction of the ATP response maxima was observed ($90.1\pm8.22\%$, $p>0.05$; Fig 3.20G-H; Table 3.5). Previously, 5-BDBD also showed a significant rightward shift of the ATP-evoked calcium responses at human and rat P2X4 receptors with EC_{50} values of $11.2\mu M$ and $15.9\mu M$, respectively, whilst the magnitude of response was unaffected when expressed in HEK293 cells (Balazs et al., 2013; Coddou et al., 2019). However, in 2017 an allosteric mode of action was proposed after radioligand binding assays showed weak displacement of [^{35}S]ATP- γ -S upon 5-BDBD in human astrocytoma cells (Abdelrahman et al., 2017). Therefore, we cannot exclude the possibility that 5-BDBD decreases the ligand-binding affinity of the human P2X4 channels by allosteric modulation. These results were verified in human P2X4 receptor stable astrocytoma cells where the presence of $30\mu M$ 5-BDBD caused a 68% reduction of ATP response maxima, as well as a significant increase in ATP potency ($10\mu M$; Bidula et al., 2022). Their study proposed a negative allosteric action of 5-BDBD by intersubunit interactions in the body region of the human P2X4 receptor (Bidula et al., 2022). This is not totally unexpected, and there is evidence that compounds that are apparently competitive antagonists are, in fact, negative allosteric modulators (Zhang et al., 2015; Gao & Jacobson, 2017). It is important to mention that our data analysis showed significant reductions of ATP response maxima at all other concentrations tested ($0.3\mu M$ to $10\mu M$; Fig 3.20G), so increasing the 'N' number would probably bring down the $30\mu M$ ATP-evoked calcium responses, agreeing with the growing evidence to support an allosteric mode of action of 5-BDBD.

5-BDBD provided a starting point to develop more potent and selective antagonists for this receptor. Indeed, recently discovered BAY-1797, PSB-12062, and BX-430 were the most potent selective antagonists for human P2X4 receptors with sub-micromolar IC₅₀ potency values (Fig 3.19A-F; Table 3.5). BAY-1797 and PSB-12062 significantly reduced the ATP-mediated maximal calcium responses by 76% and 36%, respectively ($p<0.001$ for both), but only PSB-12062 caused a rightward shift of the dose-response curve significantly increasing the ATP potency value to $2.64\pm0.94\mu\text{M}$ ($p<0.05$; Fig 3.20A-B and E-F; Table 3.5). These results suggested that PSB-12062 acted as a negative allosteric modulator and BAY-1797 acted as a non-competitive inhibitor of the human P2X4 receptor agreeing with current observations (Hernandez-Olmos et al., 2012; Ase et al., 2015; Sophocleous et al., 2020). PSB-12062 was first described in 2012 and showed effective allosteric inhibition of human P2X4 receptors with a potency of $1.38\mu\text{M}$ in stable human astrocytoma cells (Hernandez-Olmos et al., 2012). BAY-1797 showed highly effective non-competitive inhibition of human P2X4 receptors and little to no inhibitory effects on other P2X receptor subtypes, with IC₅₀ values of $0.21\mu\text{M}$ and $0.10\mu\text{M}$ when expressed in HEK293 and human astrocytoma cells and reducing the ATP-evoked responses by approximately 25% and 55% in HEK293 and human astrocytoma cells, respectively (Werner et al., 2019). In addition, the presence of $10\mu\text{M}$ BX-430 entirely stopped ATP from evoking a calcium response at any concentration tested ($2.76\pm4.22\%$ at $30\mu\text{M}$ ATP, $p<0.001$; Fig 3.20C-D), also suggesting a non-competitive allosteric mode of action. In 2015, high-throughput screening of a compound library identified BX-430 as a selective non-competitive human P2X4 antagonist (IC₅₀ of $0.54\mu\text{M}$) with no effect on rat and mouse P2X4 orthologs expressed in HEK293 cells (Ase et al., 2015). Later, the same group proposed an allosteric binding site for BX-430 in the pre-TM2 upper body region of the human P2X4 receptor (Ase et al., 2019).

Natural products have also been a valuable source of P2X4 modulators, such as Ivermectin. Taspine, an alkaloid extract of the plant *Croton lechleri*, is used in traditional medicine by Amazonian tribes for wound healing and was recently identified as an inhibitor of the human P2X4 receptors with anti-inflammatory properties (Bin Nadzirin et al., 2021). Characterisation studies demonstrated Taspine selectivity for inhibiting human P2X4 activity in a non-competitive manner (IC₅₀ of $1.54\pm0.33\mu\text{M}$; Fig 3.19I-J and 3.16I-J; Table 3.5) over P2X2, P2X3, P2X2/3 or P2X7 receptor subtypes (Bin Nadzirin et al., 2021). In this study, Taspine and 5-BDBD showed similar half-maximal inhibitory concentrations ($p>0.05$; Table 3.5). We proposed that Taspine indirectly suppressed the human P2X4 receptor by inhibition of the PI3-kinase and depletion of phosphoinositides (PI) rather than through direct antagonism of the receptor (Bin Nadzirin et al., 2021).

However, all these selective human P2X4 antagonists are poorly water-soluble. While dilution in the organosulfur solvent DMSO, had no effects on the ATP-evoked intracellular calcium responses (Fig 3.18), analogues of these inhibitors or new small molecules with greater water solubility would make better and easier-to-use pharmacological tools for both *in vitro* and *in vivo* use.

In summary, recombinant human P2X4 receptors were distinguished for their partial activation with nucleotide analogues other than ATP and their complete inhibition by the competitive inhibitor TNP-

ATP and the negative allosteric modulators PPADS, BAY-1797, PSB-12062, BX-430, 5-BDBD, and Taspine.

To conclude, our results showed that intracellular calcium signals accurately reflected the human P2X4 receptor-specific pharmacology. Thereby, any ATP-evoked intracellular calcium response will be treated as an indirect measure of human P2X4 receptor activity in the following discussed arguments.

3.3.3 The use of dead receptor tools as a reliable experimental system to evidence functional homo- and hetero-oligomeric human P2X subunit interactions

The publication of the X-ray crystal structures of the closed and ATP-bound zebrafish P2X4 receptor (Kawate et al., 2009; Hattori & Gouaux, 2012) served as templates for the analysis and interpretation of previous work. In particular, for the large body of mutagenesis-based structure-function data regarding the ATP binding site and P2X channel opening mechanism (For reviews see Young, 2010 and Habermacher et al., 2016). Lysine residues at positions K70 and K316 (zebrafish P2X4 receptor numbering) were identified as key residues for ATP molecule recognition and binding, and such role was highly conserved in the P2X receptor evolution (Jiang et al., 2000; Chataigneau et al., 2013; Fountain et al., 2007). It was confirmed that the P2X receptor ATP binding pocket is located at the interface of two adjacent subunits comprising the head and left flipper of one subunit and the dorsal fin of another (Fig 1.5). So, there are three potential ATP-binding pockets in a functional P2X trimer. Initially, it was believed that three ATP molecules were required to activate the receptor (Bean, 1990). Later studies revealed that occupancy of only one binding site of the P2X receptor did not induce channel opening but produced a conformational change that strongly influenced the binding of the second and third ligand molecules, suggestive of positive cooperation rather than independent binding (Jiang et al., 2003). This principle was confirmed by a mutagenesis-based study of the ATP binding site after the zebrafish P2X4 receptor ATP-bound structure was released, which showed that the binding of two ATP molecules was sufficient to gate the receptors (Chataigneau et al., 2013).

As previously mentioned, the P2X2/3 heteromeric receptor is exclusively recognised by the research community because of its distinct pharmacological profile resulting from the combination of P2X2 and P2X3 homomeric channel properties (Lewis et al., 1995). In 2006, Wilkinson et al. proposed and used the dead receptor hypothesis to find out the subunit stoichiometry of the rat P2X2/3 heterotrimer (Fig 3.1; Wilkinson et al., 2006). Their hypothesis was based on three concepts mentioned above: i) lysines in positions K70 and K316 (zebrafish P2X4 receptor numbering) are crucial for the recognition and binding of ATP molecules, ii) at least two agonist binding sites are required for P2X channel activation and iii) occupancy of only one agonist binding site does not induce channel opening (Fig 3.1). Single lysine-to-alanine mutations in K63 and K299 residues for the rat P2X3 prevented P2X2/3 channel function in HEK293 cells. Wild-type rat P2X3 rescued the P2X2/3 receptor function when co-expressed with rat P2X2 [K69A] and [K308A] single lysine-to-alanine mutants, but not when both residues were mutated (Fig 3.1; Wilkinson et al., 2006). These data suggested a 1:2 subunit stoichiometry favouring the P2X3 subunit (Wilkinson et al., 2006). Their results agreed with a preceding analysis of P2X subunit arrangements that used engineered cysteine substitutions at the outer ends of the transmembrane

domain to join P2X2 and P2X3 subunits by disulphide bonds (Jiang et al., 2003). Considering these experiments were carried out during the pre-structure time, we can firmly say these data greatly contributed to the current knowledge that K70 and K316 residues (equivalent zebrafish P2X4 receptor numbering) from two different subunits interact with the ATP molecule and coordinate agonist binding.

Before exploring possible functional human P2X4 heteromeric interactions, I first wanted to demonstrate if the proposed dead receptor hypothesis could accurately identify the human orthologue of the well-established P2X2/3 heteromer. This study showed that $\alpha\beta$ -MeATP evoked slow-desensitising intracellular calcium responses in a concentration-dependent manner in human 1321N1 astrocytoma cells transiently co-transfected with human P2X2 wild-type and human P2X3 wild-type subunits, but no responses were observed when only the human P2X2 wild-type subunit was present (Fig 3.36). Experiments to exemplify an $\alpha\beta$ -MeATP-evoked intracellular calcium influx in human astrocytoma cells transiently transfected with human P2X3 wild-type subunits were also carried out. Although the FlexStation 3 device's quickest 1-second sampling settings were set, they were not fast enough to detect any human P2X3 receptor-mediated calcium responses. The human P2X3 receptor subtype is characterised for having the fastest desensitisation among the human P2X family of receptors within the millisecond range (Garcia-Guzman et al., 1997; Bianchi et al., 1999). This probably justifies why we could not detect its activity in the FlexStation 3 device, but we could see it in whole-cell patch-clamp electrophysiology experiments (Richards et al., 2019). Our lab previously reported intracellular calcium responses upon application of $\alpha\beta$ -MeATP in human P2X3 stable astrocytoma cells using 1-second sampling (Bin Nadzirin et al., 2021). In this study, we could only detect human P2X3 wild-type channel activity when transiently co-expressed with human P2X2 wild-type subunits. These arguments suggested that despite achieving high protein expression amounts of human P2X3 wild-type subunits at both whole-cell and cell membrane levels (Fig 3.35A-B), our transient transfection protocol highly optimised for human P2X4-mediated calcium responses required further improvement to obtain $\alpha\beta$ -MeATP-evoked calcium signals for the human P2X3 wild-type receptor. Nevertheless, our results align with the characteristic P2X2/3 heterotrimer pharmacological profile, previously identified as a sustained response to $\alpha\beta$ -MeATP (Lewis et al., 1995). ATP evoked an intracellular calcium response twice as big as the one evoked by $\alpha\beta$ -MeATP in human 1321N1 parental astrocytoma cells transiently co-transfected with human P2X2 and human P2X3 wild-type subunits ($p<0.001$; Fig 3.36B). Altogether, these results indicated that ATP fully activates both human P2X2 and P2X3 wild-type receptors, but its analogue $\alpha\beta$ -MeATP activates only the human P2X3 subtype acting as a partial agonist of the human P2X3 subtype. Whole-cell and cell surface expression levels of human P2X2 wild-type and P2X2 [K81A, K319A] dead subunits were comparable between them and to human P2X3 wild-type subunit expression levels (Fig 3.35). Substitutions of K81 and K319 of the human P2X2 receptor (equivalent to the K69 and K308 positions in rat P2X2 receptors) by alanine residues caused a significant loss of channel function, resulting in a 100-fold reduction in channel sensitivity to both $\alpha\beta$ -MeATP and ATP (Fig 3.36A-D). These results inferred that a wild-type P2X3 subunit did not rescue channel function when co-expressed with a human P2X2 [K81A, K319A] dead subunit, suggesting that the human P2X2 double mutant subunit had a dominant negative effect in channel function. Our data aligned with the findings

of Wilkinson et al. in the rat orthologue (Wilkinson et al., 2006). Moreover, physical subunit interactions were observed for human P2X3 wild-type with human P2X2 wild-type proteins (Fig 3.37A-B). In agreement with this, no human P2X3 wild-type proteins were detected when the extracts of cells separately transfected with human P2X2 FLAG-tagged wild-type or P2X3 HA-tagged wild-type subunits were subjected to the anti-FLAG purification procedure. Reciprocate co-immunoprecipitation data also showed positive interaction bands for human P2X2 wild-type subunits when co-expressed with human P2X3 wild-type subunits but not when individually transfected after anti-HA purification (Fig 3.37C-D). Both functional and biochemical data results insinuated that the formation of heteromeric complexes between human P2X2 and P2X3 wild-type subunits possibly occurred. Experiments to confirm physical interaction between human P2X2 [K81A, K319A] dead subunits and human P2X3 wild-type subunits should be pursued for completion.

The two main limitations of this study are: i) the FlexStation 3 device provides an averaged intracellular calcium influx measurement from a confluent cell culture and ii) the gene expression of transient co-transfection methods has an unpredictable nature. The recorded responses potentially came from cell populations with different receptor expression profiles, including: human P2X2 homomers, human P2X3 homomers, mixed human P2X2 and P2X3 homomers, human P2X2/3 heteromers, mixed human P2X2 and P2X2/3 receptors, and mixed human P2X3 and P2X2/3 receptors, and inevitably some untransfected cells. Considering these limitations, we cannot make any assumptions about subunit arrangements in this experimental system. Initially and as detailed in the hypothesis of the dead receptor, it was assumed that P2X2/3 receptors consisted of two P2X3 subunits and one P2X2 subunit (Jiang et al., 2003; Wilkinson et al., 2006), but the inverse subunit combination was later shown to be functional in heterologous expression systems, opening the possibility of flexible P2X2/3 subunit assembly determined by the relative subunit availability (Kowalski et al., 2015). Further work to elucidate human P2X2/3 heteromeric subunit stoichiometry is required.

In conclusion, these data verified the use of dead receptors as reliable tools to prove the existence of functional and physical human P2X2 and P2X3 subunit interactions and confirmed that both ectodomain lysines K70 and K316 (equivalent zebrafish P2X4 receptor numbering) were crucial for agonist recognition and receptor activation, agreeing with previous publications (Jiang et al., 2000, 2003; Wilkinson et al., 2006; Chataigneau et al., 2013).

Before exploring possible functional human P2X4 heteromeric interactions, the next goal was to demonstrate that human P2X4 subunits functionally and physically interacted to form a functional homomeric channel using dead receptor tools. We have seen that ATP evoked intracellular calcium responses in a concentration-dependent manner through stably expressed human P2X4 wild-type receptors (Fig 3.11), as well as through transiently transfected human P2X4 wild-type receptors (Fig 3.28). Moreover, we claimed that our heterologous system accurately reflected the human P2X4 pharmacological properties in section 5.2.2.

The corresponding lysines in positions 67 and 313 of the human P2X4 subunit (equivalent to the K69 and K308 positions in rat P2X2 receptors) were substituted by alanine residues as per the hypothesis of

the dead receptor (Fig 3.1). Initial experiments reported a small but significant reduction of the human P2X4 ATP-evoked calcium responses when the dead subunit was transiently expressed in the stable cell line (35% reduction vs plasmid control, $p<0.01$; Fig 3.22A and D). Similar results were observed when human P2X4 [K67A] and human P2X4 [K313A] single alanine mutants were transiently transfected into human P2X4 wild-type stable astrocytoma cells (35% and 42% reduction, respectively, $p<0.01$ for both vs plasmid control; Fig 3.22B and D). Although these data seemed promising, we faced two big concerns using human 1321N1 astrocytoma cells stably expressing human P2X4 receptors as our model.

Firstly, the observed reductions of the ATP-evoked calcium responses could be a consequence of a restricted expression of human P2X4 wild-type proteins due to additional gene and protein expression of transiently transfected human P2X4 dead subunits. Besides, human P2X4 [K67A, K313A] FLAG-tagged dead subunits were highly expressed at whole-cell and cell surface levels when transiently transfected in human P2X4 stable astrocytoma cells (1.04 ± 0.23 au and 0.90 ± 0.25 au, respectively, $p>0.05$; Fig 3.21). Precisely, gene expression is controlled on two levels. First, transcription is controlled by limiting the amount of mRNA produced from a particular gene. The second level of control is through post-transcriptional events that regulate the translation of mRNA into proteins. To ensure that single and double lysine-to-alanine mutations represented a true loss of human P2X4 receptor function and were not due to a reduction of wild-type channel expression at the cell membrane, a control for protein expression was carried out. Transient transfection of a different ligand-gated ion channel, i.e., human $\alpha 7$ nicotinic acetylcholine receptor ($\alpha 7$ nAChR), did not affect the ATP-induced intracellular calcium response in 1321N1 astrocytoma cells stably expressing human P2X4 WT receptors ($88.9\pm5.35\%$, $p>0.05$ vs plasmid control; Fig 3.22C-D). Whole-cell Western blots to detect the protein expression of human $\alpha 7$ nicotinic acetylcholine receptors were unsuccessful. We used a rabbit anti-nAChR $\alpha 7$ (1:1000, ANC-007 from Alomone Labs) targeting an extracellular epitope which could have been denatured under the conditions used. Other studies reported low expression levels of human $\alpha 7$ nicotinic acetylcholine receptor when transfected in HEK293 cells, even when co-expressed with RIC-3, an associated protein required for efficient receptor folding, assembly, and functional expression of homomeric human $\alpha 7$ nAChR receptors (Gong et al., 2016). This group used a different antibody from Santa-Cruz Biotechnology (SC-5544) which was discontinued and we could not try. Intracellular calcium measurements could not detect signals generated by the opening of $\alpha 7$ nAChR receptors in response to $100\mu M$ acetylcholine. Using high concentrations of another agonist (i.e., nicotine at $100\mu M$, $300\mu M$ and $1mM$) could prove the functional activity of $\alpha 7$ nAChR receptors as it was previously reported in HEK293 cells (Gong et al., 2016). Co-transfection of human $\alpha 7$ nAChR receptors with RIC-3 would perhaps improve our functional data. Nevertheless, we were able to show expression of human $\alpha 7$ nAChR receptors in immunocytochemistry assays which aligned with expression patterns shown by other studies (Gong et al., 2016) and supported that native protein structure was necessary for recognition of the extracellular epitope by the antibody we used (Fig 2.2). These results were fundamental to correctly interpret the role of ectodomain lysine residues in human P2X4 subunits and receptor function.

And secondly, important antibody specificity issues were encountered when we wanted to detect human P2X4 wild-type subunit expression, as detailed in Chapter 3, section 3.2.3.2. The stably expressed human P2X4 wild-type receptor had a small EE tag at the C-terminal end, which would be used for co-immunoprecipitation studies. Immunoblotting with rabbit anti-EE (Cell Signalling) antibodies did not detect any human P2X4 EE-tagged protein bands at various concentrations (Fig 3.25B and D). We thought the issue might have been that the stable receptor contained a different tag. However, sequencing analysis confirmed the presence of the nucleotide sequence “GAATATATGCCGATGGAA” (5’–3’), which corresponds to the EYMPME peptide sequence, also called EE tag. Two rabbit anti-EE antibodies (Merck and Bethyl Labs) also failed to detect human P2X4 specific protein bands (Fig 3.25D). As claimed previously, the heterologously expressed human P2X4 wild-type receptor accurately represented its receptor-specific pharmacological profile, so the issue had to be the antibody itself. We then considered using the commercially available anti-P2X4 antibodies to demonstrate the presence of human P2X4 wild-type proteins and for co-immunoprecipitation assays. However, both anti-P2X4 intracellular and extracellular epitope antibodies lacked specificity for human P2X4 wild-type receptors in transiently transfected 1321N1 astrocytoma cells (Fig 3.26). The former detected high expression of 60KDa bands corresponding to the human P2X4-specific glycosylated molecular weight (Hu et al., 2002) but also detected lower molecular weight unspecific bands of approximately 50KDa, 45KDa and 37KDa, in transiently transfected and untransfected parental astrocytoma cell lysates (Fig 3.26). The latter did not detect any human P2X4 specific bands, most likely because of the denaturation of the extracellular epitope under the conditions used (Fig 3.26). These options were discarded because all failed to detect clear human P2X4-specific protein bands in human 1321N1 astrocytoma cells. Reducing the amount of antibody used could have removed these unspecific bands. However, I used 1:125 antibody dilutions for protein pull-down in co-immunoprecipitation assays and thus, this antibody would not have been an option to get a clean immunoprecipitated band. Furthermore, it would have been more difficult to prove a functional interaction between human P2X4 subunits for the hypothesis of the dead receptor proof-of-concept. Finally, we purchased a human P2X4 plasmid containing a HA C-terminus tag instead. The mouse anti-HA tagged antibody specifically detected the 60KDa band for glycosylated human P2X4 receptors transiently expressed in human 1321N1 parental cells while no background signals were observed (Fig 3.27). These data not only provided information about which antibodies to use but also ensured that the presence of a HA C-terminal epitope tag did not alter human P2X4 wild-type protein expression.

Considering these limitations, the identification of functional human P2X4 receptor variants may have been hampered by using stable 1321N1 cells, particularly if the dead receptor tools exhibited lower protein expression levels at the cell membrane compared to an overexpressed human P2X4 wild-type receptor or vice versa, thus covering their real effects in channel function. Therefore, the results obtained could have been misestimated. Moreover, there was no suitable antibody to purify stably expressed human P2X4 wild-type receptors specifically, compromising the critical biochemical study of this thesis. Consequently, I optimised transient co-transfection of human 1321N1 parental astrocytoma cells as the new experimental system and used human P2X4 WT HA-tagged constructs combined with

other P2X FLAG-tagged subunits for functional protein interaction studies. Doubling the amount of plasmid DNA did not alter transfection efficiency or cell viability as human 1321N1 parental astrocytoma cells transiently transfected with either 200ng or 400ng of human P2X4 wild-type plasmid DNA showed identical ATP-evoked intracellular calcium responses ($81.3\pm7.65\%$ vs $88.9\pm4.90\%$, respectively, $p>0.05$; Fig 3.23).

Furthermore, transient co-transfection of human P2X4 wild-type and P2X4 [K67A, K313A] dead subunits into human 1321N1 parental astrocytoma cells showed an approximately 50% reduction of the $30\mu\text{M}$ ATP-evoked calcium responses, which was much greater compared to previous observations in stable astrocytoma cells (Fig 3.24). Co-transfection with human $\alpha 7$ nicotinic acetylcholine receptors did not affect the intracellular calcium responses mediated by human P2X4 wild-type receptors ($109.2\pm7.04\%$, $p>0.05$ vs plasmid control; Fig 3.24). Despite all recommendations taken, the system was still biased towards one concentration of one agonist, namely $30\mu\text{M}$ ATP. To rule this pre-screening bias out and ensure a more robust yet practical data collection, we analysed the effects of dead receptor tools on human P2X4 channel function using ATP concentration-response curves instead. Analysing ATP concentration-response data not only improved the strength of the study but also provided us with more information regarding potential effects on the human P2X4 wild-type ATP efficacy and potency values. Significant human P2X4 wild-type loss of function when human P2X4 [K67A, K313A] subunits were transiently co-transfected in parental astrocytoma cells became evident at various concentrations of ATP extending from 300nM to $300\mu\text{M}$ ($p<0.01$ and $p<0.001$, respectively; Fig 3.33). Maximal inhibitory effects were also reached at a $30\mu\text{M}$ ATP concentration with a nearly 60% reduction of the calcium response ($p<0.001$ vs plasmid control; Fig 3.33). Co-transfection of human P2X4 [K67A, K313A] did not affect the human P2X4 wild-type ATP EC_{50} ($1.11\pm0.30\mu\text{M}$ vs $2.40\pm0.79\mu\text{M}$ for plasmid control, $p>0.05$; Fig 3.33A). This information suggested that the number of functional human P2X4 receptors at the cell membrane was not affected by co-transfection with human P2X4 dead subunits, as the affinity for ATP remained unchanged. These aligned with our dead receptor hypothesis, where dead subunits would analogously act like non-competitive inhibitors of the human P2X4 wild-type receptor, suppressing its activity by restricting the number of available ATP binding sites (Fig 3.1). In addition, both human P2X4 HA-tagged wildtype subunits and P2X4 [K67A, K313A] FLAG-tagged dead subunits were highly expressed at whole-cell and cell surface levels in parental astrocytoma cells (Fig 3.32). Expression levels of human P2X4 dead subunits were comparable to previous data obtained in stable human P2X4 astrocytoma cells (Fig 3.21). While human P2X4 wild-type expression levels remained constant when co-expressed with human P2X4 dead subunits, confirming our previous statement, a smaller amount of monomeric human P2X4 [K67A, K313A] dead receptors was detected at the cell membrane when co-expressed with human P2X4 wild-type subunits (Fig 3.32). These data allowed us to demonstrate the suspected different protein expression patterns, which were a primary concern of this study. This apparent reduction is possibly explained by an increment in the expression of human P2X4 [K67A, K313A] higher molecular weight species at the cell membrane that were not observed previously in stable cells. As discussed in section 5.2.1, these greater molecular weight species of 120KDa and 180KDa were considered human P2X4 dimeric and trimeric receptors formed by subunit

multimerisation, respectively (Bergmann et al., 2019; Glass et al., 2002). Cells regulate the number of receptor molecules in the plasma membrane. Another potential explanation for reduced expression of 60KDa human P2X4 [K67A, K313A] would be impaired trafficking to the cell membrane as malfunctioning proteins can be detected and retained in the endoplasmic reticulum by a phenomenon called ‘quality control’ (Nicke et al., 1998; Hammond & Helenius, 1995; Sun & Brodsky, 2019). The 120KDa and 180KDa higher molecular weight proteins were also observed at the cell membrane fractions for human P2X4 wild-type subunits, where functional/trimeric P2X4 receptors were expected to form (Nicke et al., 2005; Young et al., 2008; Kawate et al., 2009). An extra band was also detected for human P2X4 [K67A, K313A] dead receptors of just over 250KDa. There are two possibilities to explain these much heavier bands: i) they corresponded most likely to folding and assembly artefacts of the overexpressed protein, or ii) they corresponded to tetrameric interactions. Although further experiments are required for clarification, we hypothesised that artificial protein aggregation occurred and that the resulting mass was retained in the stacking phase of the SDS-PAGE gel over the formation of an unlikely tetrameric P2X4 channel (Nicke et al., 1998).

Overall, we interpreted that a wild-type P2X4 subunit did not completely rescue channel function when co-expressed with a human P2X4 [K67A, K313A] dead subunit, suggesting that the human P2X4 double mutant subunit had a dominant negative effect in channel function. Comparable results were observed when co-expressed with human P2X4 [K67A] and P2X4 [K313A] subunits, suggesting that both lysine residues have equivalent roles. These claims partially agree with the original hypothesis of the dead receptor, where the first lysine was found to be critical for P2X2/3 channel function and the second one slightly less so (Wilkinson et al., 2006). We concluded that the effects of these lysine residues are likely to not be independent and that an interaction occurs between K67 and K313 in order to gate the human P2X4 receptor. Moreover, the particular effects of lysine-to-alanine mutations might differ depending on the P2X receptor subtype.

Finally, human P2X4 wild-type HA-tagged proteins formed interaction complexes with both human P2X4 wild-type FLAG-tagged proteins (Fig 3.31) and human P2X4 [K67A, K313A] FLAG-tagged dead subunits (Fig 3.34). In agreement with this, no human P2X4 wild-type HA-tagged proteins were detected when anti-FLAG purification was performed on samples separately transfected with human P2X4 FLAG-tagged wild-type or dead subunits, or P2X4 HA-tagged wild-type subunits (Fig 3.31A-B and 3.32A-B). Reciprocal co-immunoprecipitation data also showed positive interaction bands for human P2X4 FLAG-tagged wild-type and dead subunits when co-expressed with human P2X4 HA-tagged wild-type subunits but not when transfected individually after anti-HA purification (Fig 3.31C-D and 3.34C-D). The relative amount of human P2X4 HA-tagged wild-type subunits and human P2X4 FLAG-tagged wild-type subunits in the 60KDa protein interaction complex was equivalent using either combination of pull-down and immunoblotting antibodies ($p>0.05$; Fig 3.31). Similarly, comparable amounts of human P2X4 HA-tagged wild-type subunits and human P2X4 [K67A, K313A] FLAG-tagged dead subunits were present in the 60KDa co-immunoprecipitated complex ($p>0.05$; Fig 3.34). Nevertheless, a significant reduction of human P2X4 wild-type HA-tagged proteins in the precipitate complex lane compared to input control was observed ($p<0.05$; Fig 3.34A-B) while co-immunoprecipitated human P2X4 [K67A, K313A] FLAG-

tagged protein levels remained unchanged compared to input control ($p>0.05$; Fig 3.34C-D). We proposed that these differences result from variability in co-transfection efficiency between experiments combined with differences in antigen-antibody affinities and protein expression patterns in our model system. Firstly, our data showed no significant differences between human P2X4 wild-type and human P2X4 dead subunits at whole-cell and cell surface levels (Fig 3.32). Secondly, total cell extracts were used for co-immunoprecipitation studies, so differences in cell surface expression levels would not have affected our results. Thirdly, anti-FLAG antibodies might have a lower affinity for their epitope compared to anti-HA antibodies causing a lower amount of human P2X4 dead subunits to be precipitated, so fewer amounts of human P2X4 wild-type proteins would be present in the interaction complex compared to input control but not vice versa (Fig 3.34). Fourthly, there was an increment in higher molecular weight species in the co-immunoprecipitated lane, possibly accounting for some reduction of the 60KDa monomeric band. These higher interaction complexes observed at 120KDa and 180KDa suggested that the possible formation of dimeric and trimeric receptors also occurred (Bergmann et al., 2019; Glass et al., 2002). Moreover, another study revealed that only one wild-type subunit was required for receptor retention at the plasma membrane, while two wild-type subunits were needed for channel function (Chaumont et al., 2004), possibly justifying some of the higher molecular weight human P2X4 dead subunit species observed at the cell membrane (Fig 3.32). These suggest that some monomeric, dimeric, and trimeric protein interactions between wild-type and dead subunits occurred, aligning with what we observed in Figure 3.34 (Bergmann et al., 2019; Glass et al., 2002). Both functional and biochemical data results indicated the possible formation of homomeric complexes between human P2X4 HA-tagged wild-type and P2X4 FLAG-tagged wild-type subunits, as well as ‘homomeric’ complexes formed by human P2X4 HA-tagged wild-type and P2X4 [K67A, K313A] FLAG-tagged dead subunits.

As discussed before, there is no easy way to interpret these data as the FlexStation 3 instrument measures an average calcium influx response of a confluent well. Human P2X4 receptors assemble as trimers to form a functional ion channel, so transient co-transfection of human P2X4 wild-type subunits and human P2X4 dead subunits could result in different receptor expression profiles. These could be: human P2X4 wild-type homomers, human P2X4 [K67A, K313A] homomers, mixed human P2X4 wild-type and P2X4 [K67A, K313A] homomers, human P2X4 WT/P2X4 [K67A, K313A] receptors, mixed human P2X4 wild-type homomers and P2X4 WT/P2X4 [K67A, K313A] receptors, and inevitably some untransfected cells. Therefore, the present analysis cannot distinguish between different numbers of ligand binding sites and different degrees of intersubunit cooperativity in the heteromeric versus the homomeric channels. However, it gives a solid starting point to elucidate potential human P2X4 functional subunit interactions.

Taken together, these results i) provided a meticulous transient co-transfection protocol for successful heterologous co-expression of purinergic receptors in human astrocytoma cells, ii) supported human 1321N1 parental astrocytoma cells as a better cell line model to study the effects of dead subunits on the human P2X4 wild-type ATP-evoked calcium responses over the human P2X4 stable astrocytoma cell

line, iii) verified the use of dead receptor tools as a well-rounded experimental system to elucidate potential homo- and hetero-oligomeric human P2X subunit interactions.

4 Exploring functional heteromeric interactions of the human P2X4 receptor

4.1 Introduction

P2X receptors have a trimeric structure, where three different subunits assemble around a common pore to form a functional ion channel. These subunits can be the same P2X subtype and form homotrimers, or they can be different and form P2X heterotrimers. Current genetic, biochemical, and physiological evidence indicates that all P2X subtypes can form homotrimers, excluding the P2X6 receptor subtype. Thus, six P2X homotrimeric receptors have been described in mammals (North, 2002; Burnstock, 2018). Initial evidence for the formation of functional P2X heteromers was obtained from the co-expression of the slow desensitising and $\alpha\beta$ -MeATP-insensitive P2X2 receptor with the fast desensitising and $\alpha\beta$ -MeATP-sensitive P2X3 receptor (Lewis et al., 1995). Their combination resulted in a novel P2X receptor pharmacological profile: a slowly desensitising and $\alpha\beta$ -MeATP-sensitive P2X2/3 heteromeric receptor, merging properties from both homomers (Lewis et al., 1995). From here, evidence regarding P2X heteromerisation started to emerge. The first systematic analysis of co-expressed HA- and FLAG-tagged rat P2X subunits in HEK293 cells predicted eleven possible P2X heterotrimeric receptors using co-immunoprecipitation assays (Torres et al., 1999). However, only seven heteromeric receptors have been characterised using electrophysiology techniques in rodent models: P2X1/2, P2X1/4, P2X1/5, P2X2/3, P2X2/5, P2X2/6, and P2X4/6 (Table 4.1; Saul et al., 2013). According to this study, all P2X subtypes can organise as heterotrimeric receptors except the P2X7 receptor subtype. From these, the P2X1/5 and P2X2/3 receptors have been unambiguously characterised as heteromeric P2X receptors in native rodent tissues, and only the P2X2/3 heteromeric receptor has been functionally established in humans and is widely accepted by the research community (Table 4.1; Saul et al., 2013; Burnstock, 2018).

In the following paragraphs, I describe the information in Table 4.1, which summarises current findings involving the most functionally characterised P2X heteromers and the experimental systems employed, specifically which biochemical or functional assays and model organisms were used. Most P2X heteromeric receptors reported so far are defined by the combination of the pharmacological characteristics of each constituent subunit. The slowly desensitising subunit usually dominates the kinetic properties of the heteromer. Whereas the subunit with a higher affinity for the agonist and/or antagonist used greatly influences the ligand-binding sensitivity of the proposed heteromer.

Heterologously expressed P2X1 and P2X2 subunits can generate heteromeric receptors at the plasma membrane with a suggested 2:1 stoichiometry in favour of the P2X1 subunit (Brown et al., 2002; Aschrafi et al., 2004). The heteromeric P2X1/2 receptor followed similar P2X1 homomeric pharmacological characteristics, including a rapid desensitisation phase, but displayed pH sensitivity, resembling the P2X2 homomeric receptor (Aschrafi et al., 2004; Marquez-Klaka et al., 2009). Calvert and Evans contemplated the existence of P2X1/2 heteromeric receptors in mouse superior cervical ganglion neurons given that $\alpha\beta$ -MeATP stimulation showed mixed pharmacological profiles suggestive of a heterogenous P2X receptor population (Calvert & Evans, 2004). Nevertheless, these pharmacological profiles have not been completely characterised, and no definite evidence exists for native P2X1/2 heteromeric assembly.

Initial co-purification experiments failed to show an interaction between rat P2X1 and P2X4 subunits in HEK293 cells (Lê et al., 1998; Torres et al., 1999). However, a P2X1/4 heteromeric interaction was later observed by co-purification and subsequent Blue Native polyacrylamide gel electrophoresis (BN-PAGE) analysis in *Xenopus laevis* oocytes (Nicke et al., 2005). The heteromeric assembly of P2X1 and P2X4 subunits resulted in a functional channel with high sensitivity to $\alpha\beta$ -MeATP and a slow desensitisation profile, properties similar to homomeric P2X1 receptors and homomeric P2X4 receptors, respectively. In addition, heteromeric P2X1/4 receptors were blocked by Suramin and TNP-ATP (Nicke et al., 2005). P2X1 homomeric receptors are sensitive to Suramin inhibition but not P2X4 homomeric receptors. Other studies also presented P2X1/4 functional electrophysiological data in rodent (Kennedy et al., 2007; Harhun et al., 2014) and human (Conant et al., 2008; Nichols et al., 2014) vascular smooth muscle cells. This combination is further discussed later in this chapter (sections 4.2.1.1 and 4.3.1).

Smooth muscle cells and some immune cells express P2X1 and P2X5 receptors, which raises the possibility of a functional heteromeric subunit interaction. Expression of heteromeric P2X1/5 receptors displayed P2X1-like sensitivity to $\alpha\beta$ -MeATP and a non-desensitising phase similar to functional homomeric P2X5 currents (Torres et al., 1998, 1999; Haines et al., 1999; Lê et al., 1999; Surprenant et al., 2000). Cells expressing P2X1/5 receptors were more sensitive to ATP than those only expressing the homomeric receptors (Surprenant et al., 2000). There is pharmacological evidence suggesting the existence of P2X1/5 heteromers in rodent native systems, such as guinea pig mesenteric arteries (Surprenant et al., 2000) and mouse cortical astrocytes (Lalo et al., 2008).

Heteromeric P2X2/3 receptors exhibit pharmacological properties similar to those of P2X3 homomers, including sensitivity to $\alpha\beta$ -MeATP and a similar rank order of agonist potencies (Koshimizu et al., 2002). They can be distinguished from homomeric P2X3 receptors by their slow desensitisation phase (Koshimizu et al., 2002). P2X2/3 receptors are the best-characterised P2X heteromeric receptors to date. There is solid evidence for P2X2/3 receptor expression *in vivo* in sensory neurons and its functional role in sensory neurotransmission (Lewis et al., 1995; Cockayne et al., 2005). Table 4.1 only contains initial and more recent findings that prove the existence of native P2X2/3 heteromeric receptors. This heteromeric combination has been thoroughly discussed in Chapter 3 (sections 3.1, 3.2.3.4, and 3.3.3).

Besides co-immunoprecipitation studies (Torres et al., 1999), biochemical evidence for the possible existence of a rat P2X2/5 heteromeric receptor was provided by an enzyme-linked immunosorbent assay (ELISA) that measured the increase in plasma membrane expression of a trafficking-deficient P2X2 subunit by co-expression with a wild-type P2X5 subunit, and vice versa (Compan et al., 2012). In addition, measured distances in Bioluminescence Resonance Energy Transfer (BRET) and Bimolecular Fluorescence Complementation (BiFC) studies were sufficiently close to suggest P2X2 and P2X5 protein interactions (Compan et al., 2012). However, there is no conclusive data for the existence of P2X2/5 heteromers yet.

No evidence for functional human P2X6 homomeric receptors has been found to date, and it is therefore considered a ‘silent’ subunit in humans (Illes et al., 2021). There is a growing belief that the P2X6 subunit might only contribute to functional channels when other P2X subunits are present,

namely P2X2 and P2X4 (Torres et al., 1999). A flexible expression-dependent P2X2/6 subunit stoichiometry was initially observed by Atomic Force Microscopy (AFM; Barrera et al., 2005). But later, a 2:1 subunit stoichiometry consisting of two P2X2 subunits and one P2X6 subunit was suggested using biochemical and functional analysis of heterologously expressed P2X2/6 receptors (Hausmann et al., 2012). ATP-induced fast activating and slowly desensitising P2X2-like currents when both subunits were co-expressed in *Xenopus laevis* oocytes and showed a more convincing novel P2X2/6 heteromeric phenotype when sensitivity to AP4A was lost and inhibition by Suramin caused biphasic currents at pH 6.5, given that AP4A acts as a full agonist at homomeric P2X2 receptors and P2X6 receptors are insensitive to blockade by Suramin (King et al. 2000). Nevertheless, there is no clear proof for the presence of functional heterotrimeric P2X2/6 assemblies in native cells or tissues.

Rat P2X4 and P2X5 subunits co-immunoprecipitated when heterologously expressed in HEK293 cells (Torres et al., 1999) and in *Xenopus laevis* oocytes (Compan et al., 2012) but have not been further investigated. Functional interactions between human P2X4 and P2X5 subunits are discussed later in this thesis chapter (sections 4.2.1.3 and 4.3.4).

Co-immunoprecipitation of P2X4 and P2X6 subunits was observed in *Xenopus laevis* oocytes and rat hippocampal neurons (Lê et al., 1998; Torres et al., 1999; Khakh et al., 1999). The functional properties of P2X4/6 receptors are difficult to interpret because the differences between homomeric P2X4 receptors and P2X4/6 receptors are minor and the two groups that managed to express a functional P2X6 homotrimer showed controversial data regarding its sensitivity to $\alpha\beta$ -MeATP (Collo et al., 1996; Jones et al., 2004). Similar cellular distribution and internalisation patterns between P2X4 and P2X4/6 receptors in primary cultures of rat neurons were also reported (Bobanovic et al., 2002). Still, it is currently unclear whether native P2X4 and P2X6 channels can exist as heteromers. Sections 4.2.1.1 and 4.3.5 in this thesis chapter examine functional interactions between human P2X4 and P2X6 subunits.

There is controversial data regarding interactions between P2X4 and P2X7 receptors. The original co-immunoprecipitation screening using recombinant HEK293 cells failed to show positive protein interaction between rat P2X4 and P2X7 subunits (Torres et al., 1999). A later study in 2013 also performed in a heterologous system, presented electrophysiological evidence that P2X7 subunits were not able to combine with other P2X subunits (Saul et al., 2013). Thus, P2X7 were the only P2X receptors unable to form heterotrimers (Saul et al., 2013; Burnstock, 2018). The only study that showed a physical interaction between heterologous rat P2X4 and P2X7 proteins was published in 2007 (Guo et al., 2007). Guo et al. also provided initial electrophysiological evidence for a functional heteromeric P2X4/7 receptor by co-expressing dominant-negative and non-dominant-negative P2X4 mutants with P2X7 wild-type receptors. However, the suggested pharmacological properties were only characterised using ivermectin and TNP-ATP, both effectively acting at homomeric P2X4 receptors (Guo et al., 2007). No P2X7-specific pharmacological tools were used to differentiate homomeric P2X7 from heteromeric P2X4/7 receptors in their study. Guo et al. successfully showed co-immunoprecipitation of P2X4 and P2X7 proteins from mice bone marrow-derived macrophages (BMDM) but the combination was not further analysed in such cells (Guo et al., 2007). Similarly, other studies have shown a more likely

physical interaction between P2X4 and P2X7 homotrimers in rodents but none have further investigated the physiological implications of such an arrangement (Nicke, 2008; Boumechache et al., 2009; Antonio et al., 2011). Additional examination of human P2X4 and P2X7 receptor interactions is discussed later in sections 4.2.1.4 and 4.3.6 of this chapter.

Finally, three studies speculated the formation of heterotrimeric P2X receptors formed by the association of P2X2, P2X4, and P2X6 subunits with P2X2 homomer-like electrophysiology properties and with the P2X6 subunit acting as a linker between the other two subunits (Hugel & Schlichter, 2000; Rubio & Soto, 2001; Antonio et al., 2009). Additionally, P2X2, P2X4, and P2X6 subunits colocalised in rat spinal cord dorsal horn neurons, rat Purkinje neurons, and rat Leydig cells (Hugel & Schlichter, 2000; Rubio & Soto, 2001; Antonio et al., 2009). Their conclusions were later confirmed by positive co-purification of P2X2, P2X4, and P2X6 subunits and by Atomic Force Microscopy imaging (Antonio et al., 2014).

Table 4.1. Current biochemical and functional evidence for P2X receptor heteromerisation.

Heteromer	Biochemical evidence	Functional evidence	Model organism	Reference
P2X1/2	CoIP	—	HEK293 (rat), <i>X. laevis</i> (rat)	Torres et al., 1999; Aschrafi et al., 2004
	BN-PAGE	Ephys	<i>X. laevis</i> (rat)	Aschrafi et al., 2004; Marquez-Klaka et al., 2009
	—	Ephys	<i>X. laevis</i> (rat)	Brown et al., 2002
P2X1/4	—	Ephys, Ca ²⁺ imaging	Mice SCG neurons	Calvert & Evans, 2004
	CoIP, BN-PAGE	Ephys	<i>X. laevis</i> (rat)	Rettinger et al., 2000; Nicke et al., 2005
	—	Ephys, Ca ²⁺ imaging	Rat middle cerebral arteries	Harhun et al., 2014
	—	Ephys	Guinea pig urinary bladder and vas deferens SMCs	Kennedy et al., 2007
P2X1/5	—	Ephys	Human coronary arteries	Conant et al., 2008
	—	Ephys	Human omental arteries	Nichols et al., 2014
	CoIP	Ephys	HEK293 (rat), <i>X. laevis</i> (rat)	Torres et al., 1998 and 1999; Lê et al., 1999
P2X2/3	—	Ephys	CHO-K1 (rat), HEK293 (rat)	Haines et al., 1999; Surprenant et al., 2000
	—	Ephys	Guinea pig mesenteric arteries	Surprenant et al., 2000
	—	Ephys	Mouse cortical astrocytes	Lalo et al., 2008
P2X2/5	CoIP	Ephys	HEK293 (rat)	Lewis et al., 1995; Torres et al., 1999
	BN-PAGE	Ephys, Ca ²⁺ mobilisation	HEK293 (human), <i>X. laevis</i> (human)	Hausmann et al., 2012
	—	Ephys	HEK293 (rat)	Jiang et al., 2003; Wilkinson et al., 2006
P2X2/6	—	Ephys	Mice DRG and SCG neurons, urinary bladder nerves and SMCs	Cockayne et al. 2005
	CoIP	—	HEK293 (rat)	Torres et al., 1999
	BN-PAGE	Ephys, Ca ²⁺ mobilisation	HEK293 (human), <i>X. laevis</i> (human)	Hausmann et al., 2012
P2X4/5	AFM	—	HEK293 (rat), NRK (rat)	Barrera et al., 2005
	—	Ephys	<i>X. laevis</i> (rat)	King et al., 2000
	CoIP	—	HEK293 (rat), <i>X. laevis</i> (rat)	Torres et al., 1999; Compan et al., 2012
P2X4/6	CoIP	Ephys	HEK293 (rat), <i>X. laevis</i> (rat)	Lê et al., 1998; Torres et al., 1999
	—	Ephys	HEK293 (rat), <i>X. laevis</i> (rat), rat hippocampal neurons	Khakh et al., 1999
	CoIP (subunits)	Ephys	HEK293 (rat), NRK (rat), mice BMDM	Guo et al. 2007
P2X4/7	CoIP and BN-PAGE (dimeric homotrimers)	—	<i>X. laevis</i> (rat), rat DRG neurons	Nicke, 2008
	CoIP (dimeric homotrimers)	—	Rat microglia, mice BMDM	Boumechache et al., 2009
	CoIP, PLA, and AFM (dimeric homotrimers)	—	HEK293 (rat)	Antonio et al. 2011
P2X2/4/6	—	Ephys	Rat spinal cord dorsal horn neurons, rat Purkinje cells, and rat Leydig cells	Hugel & Schlichter, 2000; Rubio & Soto, 2001; Antonio et al., 2009
	AFM, CoIP	—	HEK293 (rat)	Antonio et al., 2014

AFM, atomic force microscopy; BMDM, bone marrow-derived macrophages; BiFC, bimolecular fluorescence complementation; BN-PAGE, blue native polyacrylamide gel electrophoresis; BRET, bioluminescence resonance energy transfer; CoIP, co-immunoprecipitation; DRG, dorsal root ganglia; ELISA, enzyme-linked immunosorbent assay; Ephys, electrophysiological recordings; PLA, *in situ* proximity ligation assay; SCG, superior cervical ganglion; SMC, smooth muscle cell; VSMC, vascular smooth muscle cell; *X. laevis*, *Xenopus laevis* oocytes.

Other than homomeric and heteromeric subunit interactions to form a functional P2X receptor, transient or permanent interactions with associated proteins can also occur and contribute to the diversity in P2X receptor properties and their signalling roles. As introduced in section 1.3.2.1, P2X receptors undergo protein folding and post-translational modifications before trafficking to the membrane. Proteins involved in P2X receptor synthesis and maturation, such as glycosylation enzymes and chaperones, can transiently interact with P2X receptors. Proteins that participate in the trafficking and stabilisation of the receptor at the cell membrane and other intracellular membranes comprising adaptor, anchoring, and scaffolding proteins, can also transiently interact with P2X receptors. In the case of P2X4 receptors, membrane targeting is mediated by proteins of the SNARE (soluble N-ethylmaleimide-sensitive factor attachment protein receptors) family, and receptor internalisation is dependent on clathrin and dynamin proteins (Kaczmarek-Hájek et al., 2012). The C-term tyrosine motif is crucial for receptor internalisation, as reviewed in section 1.3.2.1. The adapter protein 2 (AP2)-clathrin adapter protein complex interacts with the C-term tyrosine motif and regulates receptor internalisation (Royle et al., 2005). This endocytic motif also appears to be involved in cAMP-dependent P2X4 receptor phosphorylation by protein kinase A, suggesting that receptor internalisation might be regulated by phosphorylation and that a transient interaction between P2X4 receptors and protein kinase A also occurs (Brown & Yule, 2010). Caveolae-associated proteins, such as caveolin-1 (Cav-1), are scaffolding proteins essential for the formation of caveolae in cell membranes, small invaginations formed during endocytosis and membrane trafficking processes (Kong et al., 2021). In a murine preosteoblast-like cell line, P2X7 receptor activation induced Cav-1-dependent caveolae formation and suppression of Cav-1 increased P2X7 receptor-mediated calcium signalling, suggesting that caveolae may be necessary for regulating the expression of membrane proteins involved in bone formation (Gangadharan et al., 2015). However, more research is needed to provide evidence of direct interaction between Cav-1 and P2X receptors.

Once the P2X receptor is fully matured, its properties can be modified by intracellular signalling molecules. For example, a conserved protein kinase C phosphorylation site is found at the N-terminus of P2X receptors and might be indirectly involved in receptor desensitisation properties (Ennion & Evans, 2002b). Furthermore, P2X receptor properties and signalling roles can be modified by interactions between different P2X receptor subtypes, which have been described for P2X2 with P2X4 and P2X6 receptors (Hugel & Schlichter, 2000; Antonio et al., 2009, 2014) and between P2X4 and P2X7 receptors (Nicke, 2008; Boumechache et al., 2009; Antonio et al., 2011; Table 4.1).

In addition, functional and physical interactions between P2X receptors and other ion channels have also been revealed, frequently involving the P2X receptor C-terminus region (Kaczmarek-Hájek et al., 2012). For example, P2X2 receptors co-immunoprecipitated and showed close Fluorescence Resonance Energy Transfer (FRET) proximity signals with GABA receptors in recombinant HEK293 cells and mice spinal cord neurons (Shrivastava et al., 2011). P2X2 receptor activation downregulated the GABA receptor surface expression levels in both systems (Shrivastava et al., 2011). Similar results were obtained for GABA receptors interacting with P2X3 and P2X4 receptors in rat dorsal root ganglia and mice hippocampal neurons, respectively (Toulmé et al., 2007; Jo et al., 2011). In all cases, inhibitory

crosstalk effects were observed when ATP and GABA were co-applied, suggesting that interactions between their respective receptor channels may play a critical role in regulating and shaping synaptic transmission (Toulmé et al., 2007; Jo et al., 2011; Shrivastava et al., 2011). Furthermore, electrophysiological current recordings showed non-additive responses upon co-stimulation of P2X2 and $\alpha 4\beta 2$ nicotinic acetylcholine receptors (nAChR) in HEK293 cells. FRET assays showed proximity signals between P2X2 receptors and $\alpha 4\beta 2$ nAChR heterologously expressed in HEK293 cells and endogenously expressed in rat hippocampal neurons (Khakh et al., 2005). Also, physical and functional evidence for interaction between P2X2 and 5-HT3 serotonin-gated receptors was obtained in recombinant and native systems (Boué-Grabot et al., 2003). Simultaneous activation of both native receptors evoked non-additive currents, suggesting crosstalks between ATP-gated and serotonin-gated ion channel signalling in guinea pig myenteric neurons (Boué-Grabot et al., 2003).

Finally, coupling with other ion channels and membrane proteins can also impact P2X receptor-mediated signalling roles. Epithelial sodium channels (ENaC) are expressed in epithelial cells lining the nephrons and are primarily involved in the reabsorption of sodium ions in the kidney. ENaC channels are structurally the closest proteins to P2X receptors. They are also trimeric, and each subunit is formed by two α -helix transmembrane domains connected by a large extracellular domain with the N- and C-termini located in the cytosol (Noreng et al., 2018). Co-expression of recombinant ENaC channels with various P2X receptors (i.e., P2X2, P2X4, P2X2/6, P2X4/6) resulted in mutual regulation of channel trafficking in *Xenopus laevis* oocytes (Wildman et al., 2005). Applying ATP resulted in a reduction of amiloride-evoked ENaC currents, primarily due to a reduction in surface expression of ENaC channels, demonstrating a functional relation between certain P2X receptors and ENaC channels (Wildman et al., 2005). P2X receptors can also couple with acid-sensing ion channels (ASIC), which belong to the trimeric ENaC channel family and detect changes in pH. For example, ATP stimulation through P2X2, P2X4, and P2X5 receptors mediated the activation of ASIC3 channels in rat dorsal root ganglia sensory neurons (Birdsong et al., 2010). FRET analysis showed that only the P2X5 subtype was close enough to form a molecular complex with ASIC3, which was further confirmed by co-localisation immunoreactivities in rat dorsal root ganglia sensory neurons (Birdsong et al., 2010). These findings suggested a possible signalling interplay between P2X receptors and ASIC3 channels during ischemic pain, caused when blood and oxygen flow are restricted in a part of the body (Birdsong et al., 2010). More recently, physical and functional evidence for a novel protein complex formed by the association of rat P2X3 receptors and rat ASIC3 channels was reported in recombinant CHO (Chinese hamster ovary) cells, *Xenopus laevis* oocytes, and in native rat dorsal root ganglia sensory neurons (Stephan et al., 2018). This P2X3/ASIC3 complex modulated local mechanic hyperalgesia in a pH-dependent manner, as shown in rat paw withdrawal experiments (Stephan et al., 2018).

In conclusion, P2X4 receptors are expressed in many cell types and contribute to physiological and pathophysiological processes, as described in section 1.3.4. Understanding human P2X4 subunit assembly and potential interactions with other associated proteins is crucial for its therapeutic exploitation. Our current knowledge of P2X4 receptor involvement in health and disease is based on its distinct pharmacological properties among other P2X receptor subtypes. However, only a few native

receptors have been identified that exactly resemble the pharmacological characteristics of recombinant homomeric P2X4 receptors, which are relatively insensitive to αβ-MeATP (Coddou et al., 2011). These differences might be justified by unknown receptors formed by the heteromeric assembly of P2X4 subunits with other P2X subunits or with other associated proteins. These differences also raise some concerns and question the current paradigm of ATP signalling pathways and the effects mediated through P2X4 receptors. For example, is the production of nitric oxide (NO) in vascular endothelial cells promoted by homomeric P2X4 receptors or heteromeric P2X4 receptors, i.e., P2X1/4 receptors? Is the observed overall cardioprotective effect due to stimulation of homomeric P2X4 receptors or heteromeric P2X4 receptors, i.e., P2X4/6 receptors? Furthermore, the generation of P2X4 receptor knockout mice helped decipher and confirm its many functions *in vivo* by comparing differences in phenotypical and pharmacological properties with wild-type mice. These studies also draw attention to other research matters. For example, does the P2X4 knockout mice model lack homomeric P2X4 receptors and/or other P2X4-containing heteromeric receptors? A deeper exploration of the human P2X4 subunit stoichiometry and interaction with other proteins can solve these uncertainties.

This chapter reveals potential human P2X4 heteromeric interactions, opening novel investigation lines within the purinergic research field.

4.1.1 Aim and objectives

This chapter aims to thoroughly puzzle out functional human P2X4 subunit interactions using the experimental system established in Chapter 3. The specific objectives to achieve were:

1. To validate whole-cell and membrane expression of dead receptor tools in transiently co-transfected human 1321N1 parental astrocytoma cells.
2. To explore the effects of dead receptor tools on the human P2X4 wild-type ATP-evoked responses using intracellular calcium mobilisation assays.
3. To analyse physical protein-protein interactions by co-immunoprecipitation and Western blotting.
4. To assess any alterations in human P2X4 wild-type surface and total protein expression levels due to transient co-transfection with dead receptor tools.

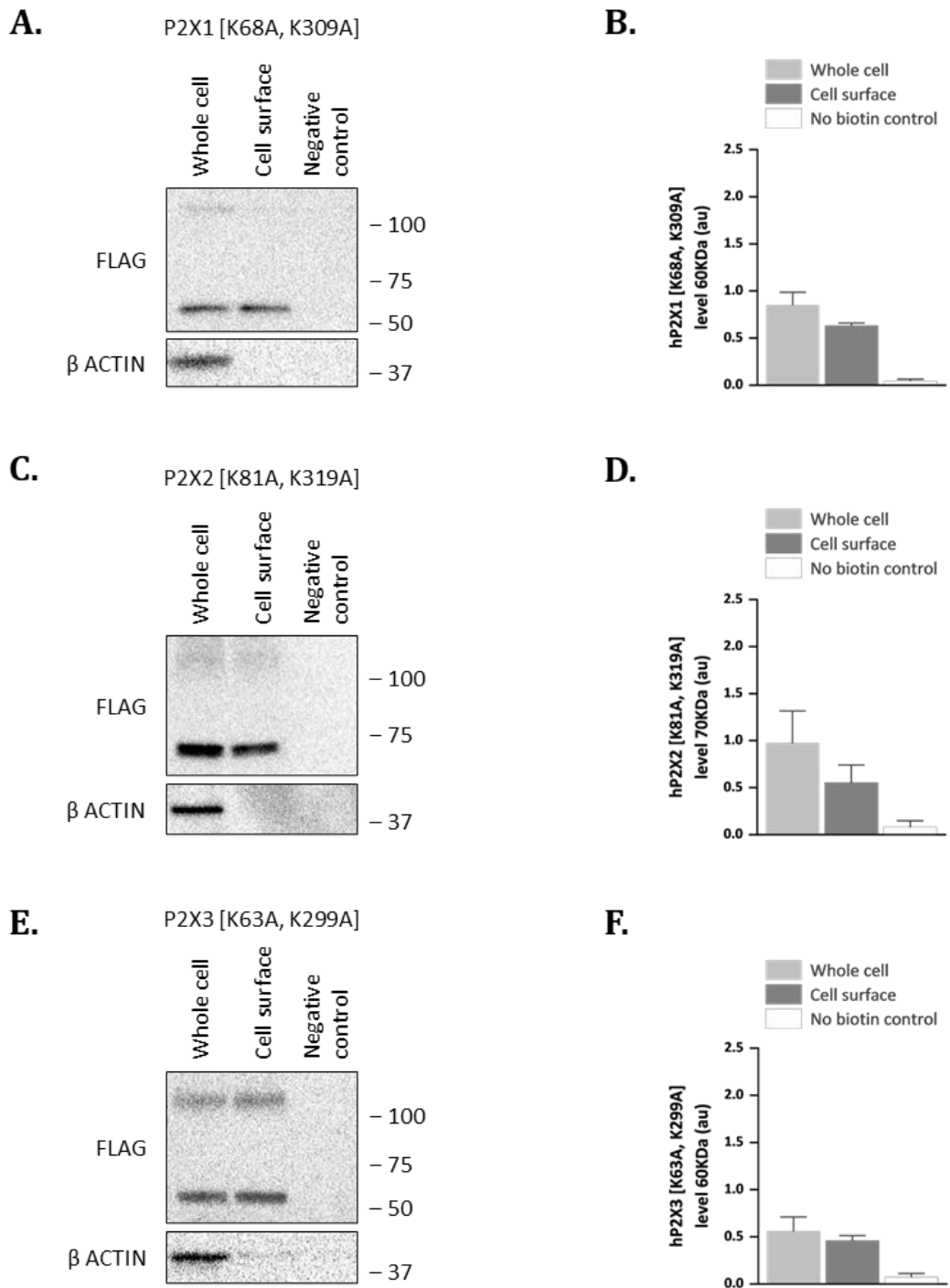
4.2 Results

4.2.1 Probing functional interactions of the human P2X4 receptor for ATP

The use of dead receptor tools proved to be a good experimental system to detect and validate human P2X homo- and heteromeric interactions in transiently co-transfected 1321N1 parental astrocytoma cells. To explore functional human P2X4 heteromeric interactions, intracellular calcium responses from 1321N1 parental astrocytoma cells transiently co-transfected with human P2X4 wild-type subunits and human P2X1-7 double lysine-to-alanine mutant subunits were recorded. Functional data were complemented with whole-cell and cell surface protein expression studies and co-immunoprecipitation assays to unravel potential human P2X4 subunit interactions.

Before screening for functional human P2X4 subunit interactions using ATP, whole-cell and cell membrane expression levels for all human P2X1-7 dead receptor tools were assessed by biotinylation and Western blotting. These results were fundamental to confirm that the presence of C-terminal epitope tags did not alter their functional properties and to interpret both intracellular calcium mobilisation and protein interaction datasets confidently.

Results showed high expression levels for human P2X1 [K68A, K309A] at both whole-cell and cell surface levels (0.85 ± 0.13 au and 0.63 ± 0.02 au, respectively, $p > 0.05$; Fig 4.1A-B). A faint heavier band at approximately 120kDa was once observed at the whole-cell level (0.14au; Fig 4.1A). Human P2X2 [K81A, K319A] subunits were also greatly expressed at a whole-cell level (0.97 ± 0.34 au) and at the cell membrane (0.55 ± 0.19 au, $p > 0.05$; Fig 4.1C-D). Human P2X3 [K63A, K299A] dead subunits were equally expressed at whole-cell (0.55 ± 0.15 au) and cell membrane levels (0.45 ± 0.05 au, $p > 0.05$; Fig 4.1E-F). Heavier bands at 120kDa were detected at both whole-cell and cell membrane lysates, too (0.45 ± 0.04 au and 0.48 ± 0.01 au, respectively, $p > 0.05$; Fig 4.1E). Whole-cell and cell surface expression levels of human P2X5 [K69A, K315A] dead subunits were also comparable (1.08 ± 0.16 au and 0.88 ± 0.16 au, respectively, $p > 0.05$; Fig 4.1G-H). A noticeable band was detected once at the cell surface level of approximately 150kDa (0.68au; Fig 4.1G). Human P2X6 [K78A, K315A] dead subunits were weakly expressed at both whole-cell (0.32 ± 0.17 au) and cell surface levels (0.23 ± 0.10 au, $p > 0.05$; Fig 4.1I-J). Finally, human P2X7 [K64A, K311A] dead subunits were highly expressed at both whole-cell and cell surface levels (1.11 ± 0.28 au and 0.61 ± 0.04 au, respectively, $p > 0.05$; Fig 4.1K-L). 150kDa bands were also detected at whole-cell (0.16 ± 0.06 au) and cell surface levels (0.49 ± 0.18 au, $p > 0.05$; Fig 4.1K).



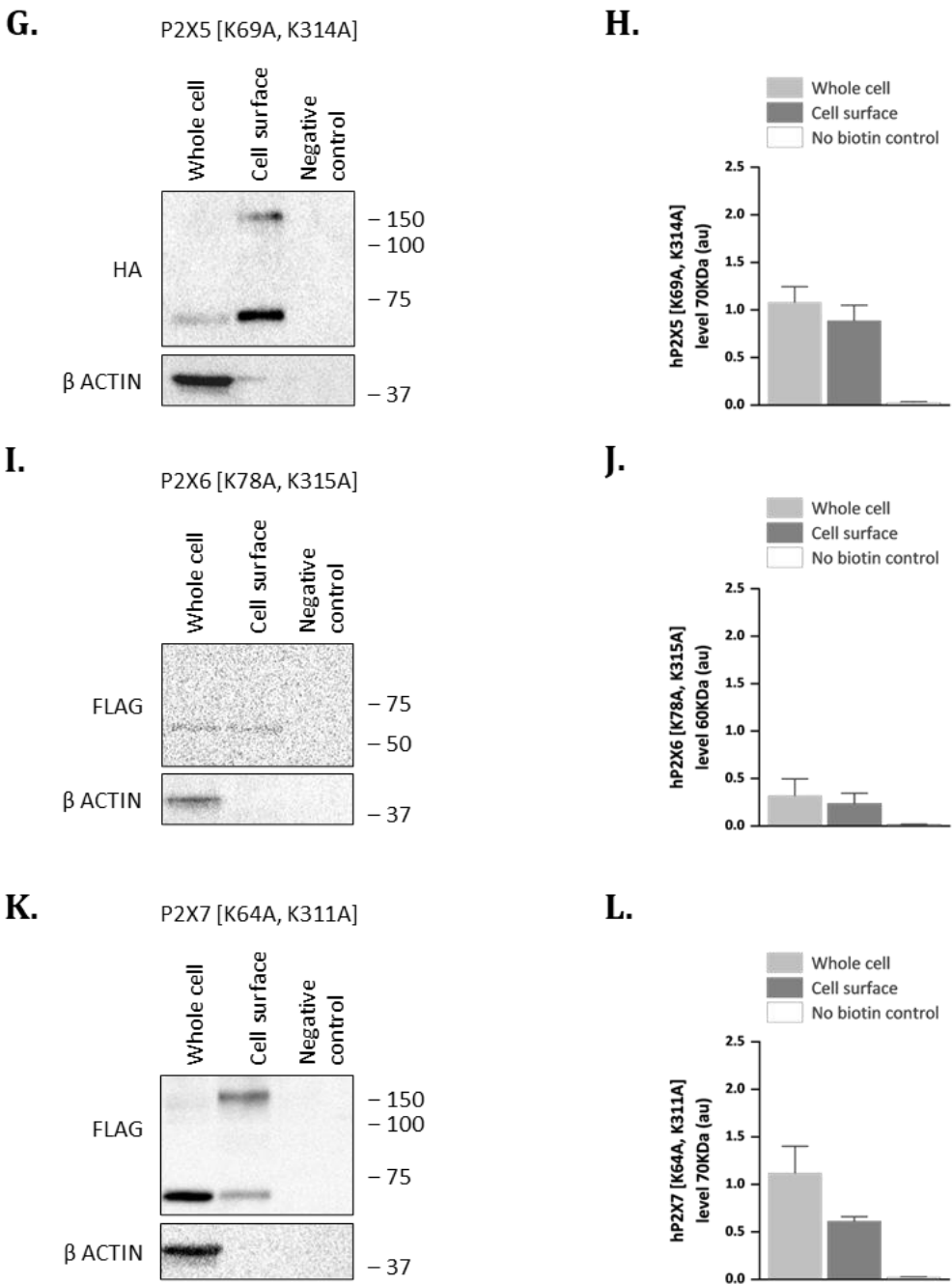


Fig 4.1. Whole-cell and cell surface expression levels of human P2X dead subunits in transiently co-transfected 1321N1 parental astrocytoma cells. (A, C, E, G, I, K) Representative immunoblots for (A) hP2X1 [K68A, K309A], (C) hP2X2 [K81A, K319A], (E) hP2X3 [K63A, K299A], (G) hP2X5 [K69A, K314A], (I) hP2X6 [K78A, K315A], and (K) hP2X7 [K64A, K311A], with corresponding β-actin loading controls. Molecular weight size standards were indicated in kDa. Lanes 1 corresponded to whole-cell samples, lanes 2 to cell surface protein lysates, and lanes 3 were negative controls for biotin labelling. (B, D, F, H, J, L) Comparison of densitometric analysis of (B) hP2X1 [K68A, K309A], (D) hP2X2 [K81A, K319A], (F) hP2X3 [K63A, K299A], (H) hP2X5 [K69A, K314A], (J) hP2X6 [K78A, K315A], and (L) hP2X7 [K64A, K311A] protein levels relative to loading control for whole-cell and cell surface lysates. Data were represented as mean ± SEM ($N=3$).

4.2.1.1 Human P2X4 subunits formed functional interactions with human P2X1 and human P2X6 subunits

Presence of human P2X1 [K68A, K309A] dead subunits had a dominant negative effect on human P2X4 WT ATP-evoked intracellular calcium responses in a concentration-dependent manner. High concentrations of ATP, i.e., 10µM, 30µM, 100µM and 300µM, evoked significantly smaller calcium responses in 1321N1 parental astrocytoma cells transiently co-transfected with human P2X4 wild-type and human P2X1 [K68A, K309A] dead subunits compared to plasmid control ($p<0.01$, $p<0.01$, $p<0.05$, and $p<0.001$, respectively vs corresponding plasmid control responses; Fig 4.2A). The maximal response plateaued at 3µM, 10µM, and 30µM ATP concentrations, but the greatest reduction of ATP efficacy was achieved at 30µM ATP (nearly 50%) compared to respective pcDNA 3.1 control responses ($43.0\pm7.03\%$ vs $82.1\pm1.77\%$, $p<0.01$; Fig 4.2). Human P2X1 receptors are known to be fast desensitising amongst the P2X receptor family (North, 2002). However, the 30µM ATP-evoked calcium response was sustained at 35% above baseline levels over the recorded time, suggesting conservation of the slow desensitisation characteristics of the human P2X4 receptors (Fig 4.2B). A significant reduction was also observed upon stimulation with 0.3µM ATP of about 80% of the equivalent plasmid control response ($3.97\pm3.46\%$ vs $20.1\pm3.99\%$, $p<0.05$; Fig 4.2A). In addition, the ATP potency value was not affected by the presence of human P2X1 [K68A, K309A] dead subunits ($1.58\pm0.26\mu M$, $p>0.05$ vs $2.40\pm0.79\mu M$ for plasmid control; Fig 4.2A).

Whole-cell and cell surface protein expression levels of both human P2X4 WT HA-tagged and human P2X1 [K68A, K309A] FLAG-tagged subunits were assessed to determine any changes associated with subunit co-expression, ensuring a correct interpretation of the calcium mobilisation data. Both human P2X4 WT and human P2X1 [K68A, K309A] dead subunits were highly expressed in transiently co-transfected 1321N1 parental astrocytoma cells with pcDNA 3.1 plasmid control, detecting major whole-cell protein bands at 60KDa corresponding to each subunit monomeric weight ($1.80\pm0.18\text{au}$ for human P2X4 WT vs $1.06\pm0.26\text{au}$ for human P2X1 [K68A, K309A], $p>0.05$; Fig 4.3A and B). Moreover, their whole-cell expression levels did not change when co-expressed together ($1.34\pm0.06\text{au}$ vs human P2X4 WT alone, $p>0.05$; $1.06\pm0.27\text{au}$ vs human P2X1 [K68A, K309A] alone, $p>0.05$; Fig 4.3A and B). Human P2X4 WT subunits were equally expressed at cell surface levels both in combination with pcDNA 3.1 plasmid control ($0.81\pm0.15\text{au}$) and with human P2X1 [K68A, K309A] dead subunits ($0.39\pm0.08\text{au}$, $p>0.05$; Fig 4.3A and B). Human P2X1 [K68A, K309A] dead subunits were also equally detected at the cell membrane both in combination with pcDNA 3.1 plasmid control ($0.59\pm0.13\text{au}$) and with human P2X4 WT subunits ($0.54\pm0.04\text{au}$, $p>0.05$; Fig 4.3A and B). An expected reduction between whole-cell and cell surface expression levels of human P2X4 WT subunits co-expressed with human P2X1 [K68A, K309A] dead subunits was observed ($1.34\pm0.06\text{au}$ vs $0.39\pm0.08\text{au}$, $p<0.01$; Fig 4.3B). However, it did not occur for human P2X1 [K68A, K309A] dead subunit expression levels ($1.06\pm0.27\text{au}$ vs $0.54\pm0.04\text{au}$, $p>0.05$; Fig 4.3B). Expression of human P2X4 WT subunits and P2X1 [K68A, K309A] dead subunits was the same when co-expressed together at the cell membrane ($0.39\pm0.08\text{au}$ vs $0.54\pm0.04\text{au}$, respectively, $p>0.05$) and at whole-cell levels ($1.34\pm0.06\text{au}$ vs $1.06\pm0.27\text{au}$, respectively, $p>0.05$). Higher molecular weight bands were also detected at 120KDa and 180KDa for both human P2X4 WT and human P2X1

[K68A, K309A] dead subunits (Fig 4.3A, C and D). Whole-cell human P2X4 WT subunits showed higher expression levels at 60KDa when combined with human P2X1 [K68A, K309A] dead subunits compared to 120KDa (1.34 ± 0.06 au vs 0.08 ± 0.04 au, respectively, $p < 0.001$) and to 180KDa relative expression levels (0.03 ± 0.01 au vs 60KDa, $p < 0.001$). At the cell surface, expression of human P2X4 WT subunits was similar at 60KDa and 120KDa (0.39 ± 0.08 au vs 0.21 ± 0.03 au, respectively, $p > 0.05$), but only the 60KDa form predominated over the 180KDa relative expression levels (0.08 ± 0.04 au, $p < 0.05$ vs 60KDa; and $p > 0.05$ vs 120KDa). Whole-cell human P2X1 [K68A, K309A] dead subunits were equivalently expressed at 60KDa and 120KDa when combined with human P2X4 WT subunits (1.06 ± 0.27 au vs 0.24 ± 0.13 , respectively, $p > 0.05$) and the 60KDa form predominated over the 180KDa relative protein expression levels (0.14 ± 0.06 au, $p < 0.05$ vs 60KDa; and $p > 0.05$ vs 120KDa). All 60KDa, 120KDa and 180KDa protein bands were equally detected at the cell membrane for human P2X1 [K68A, K309A] (0.54 ± 0.04 au for 60KDa vs 0.23 ± 0.13 au for 120KDa, $p > 0.05$; and 0.19 ± 0.23 au for 180KDa, $p > 0.05$ vs 60KDa and $p > 0.05$ vs 120KDa).

Initial co-immunoprecipitation assays were also carried out to reveal physical protein-protein interactions using human P2X4 WT HA-tagged constructs transiently co-transfected with human P2X1 WT FLAG-tagged dead subunits in 1321N1 parental astrocytoma cells. Following the protocol detailed in Chapter 3, human P2X1 WT subunits were immuno-precipitated using anti-FLAG tag antibodies, and the precipitate was analysed by Western blot using anti-HA antibodies. If an interaction occurred between human P2X4 WT HA-tagged and P2X1 WT FLAG-tagged subunits, a P2X4-specific band would be present in the co-immunoprecipitate lane. Indeed, human P2X4 WT subunits co-immunoprecipitated with human P2X1 WT subunits as a 60KDa band was detected in the immunoprecipitate lane (0.38 ± 0.04 au; Fig 4.4A and B). Whole-cell input controls showed similar human P2X4 WT expression levels when co-transfected with human P2X1 WT subunits (1.13 ± 0.15 au vs 1.41 ± 0.11 au plasmid control, $p > 0.05$; Fig 4.4A and B). The human P2X4 WT relative amount in the co-immunoprecipitate lane was significantly smaller than its input protein co-expression control levels (0.38 ± 0.04 au vs 1.13 ± 0.15 au, respectively, $p < 0.01$; Fig 4.4A and B). The input controls corresponded to whole-cell protein samples prior to protein pull-down and ensured correct sample preparation and Western blotting procedures, as well as adequate interpretation of co-immunoprecipitation data. Higher 180KDa bands were also detected in whole-cell and co-immunoprecipitation lanes (Fig 4.4A). Reciprocate human P2X1 WT FLAG-tagged pull-down using the anti-FLAG antibody, and analysis of protein interaction with anti-HA antibody were also assessed for completeness. A positive protein-protein interaction was also detected at approximately 60KDa corresponding to human P2X1 WT monomeric weight (0.42 ± 0.11 au; Fig 4.4C). Again, whole-cell input controls showed similar human P2X1 WT expression levels when co-transfected with human P2X4 WT subunits (1.06 ± 0.13 au vs 1.64 ± 0.48 au plasmid control, $p > 0.05$; Fig 4.4C and D) and the co-immunoprecipitated expression levels were significantly smaller than the corresponding human P2X1 WT input co-expression control levels (0.42 ± 0.11 au vs 1.06 ± 0.13 au, respectively, $p < 0.05$; Fig 4.4C and D). Both human P2X4 WT and P2X1 WT subunits were equally expressed in the co-immunoprecipitate lane (0.38 ± 0.04 au vs 0.42 ± 0.11 au, respectively, $p > 0.05$; Fig 4.4B and D).

Co-immunoprecipitation assays were also performed to detect protein interaction between human P2X4 wild-type subunits and human P2X1 [K68A, K309A] dead subunits. Figure 4.5 showed a positive interaction between human P2X4 WT and P2X1 [K68A, K309A] dead subunits when either anti-FLAG or anti-HA antibodies were used for protein pull-down (Fig 4.5A and C). A significant reduction in protein expression was detected for human P2X4 WT co-immunoprecipitated complex compared to corresponding co-transfected input control (0.19 ± 0.07 au vs 1.06 ± 0.10 au input control, $p < 0.01$; Fig 4.5A and B). However, no changes in human P2X1 [K68A, K309A] dead subunits were observed compared to co-expression input control (0.38 ± 0.12 au vs 0.64 ± 0.16 au, $p > 0.05$; Fig 4.5C and D). Co-expression of human P2X4 WT subunits with human P2X1 [K68A, K309A] dead subunits did not affect whole-cell input controls compared to co-transfection with pcDNA 3.1 plasmid control (1.06 ± 0.10 au vs 1.35 ± 0.13 au, respectively, $p > 0.05$; Fig 4.5A and B) and vice versa, co-expression of human P2X1 [K68A, K309A] dead subunits with human P2X4 WT subunits did not affect whole-cell input controls compared to co-transfection with pcDNA 3.1 plasmid control (0.64 ± 0.16 au vs 0.48 ± 0.17 au, respectively, $p > 0.05$; Fig 4.5C and D). Co-immunoprecipitated protein levels for human P2X4 WT and human P2X1 [K68A, K309A] dead subunits were statistically the same (0.19 ± 0.07 au and 0.38 ± 0.12 au, respectively, $p > 0.05$; Fig 4.5B and D). Despite the apparently weaker detection of 60KDa interaction bands for human P2X4 WT and P2X1 [K68A, K309A] combinations, the complex expression levels were comparable to the ones obtained for human P2X4 WT and P2X1 WT combinations ($p > 0.05$ for both anti-FLAG and anti-HA immunoprecipitates). Notably, human P2X1 [K68A, K309A] dead subunits were consistently expressed compared to human P2X1 WT subunits when co-transfected with pcDNA 3.1 plasmid control (0.48 ± 0.17 au vs 1.64 ± 0.48 au, respectively, $p > 0.05$) and when co-transfected with human P2X4 WT subunits (0.64 ± 0.16 au vs 1.06 ± 0.13 au, respectively, $p > 0.05$).

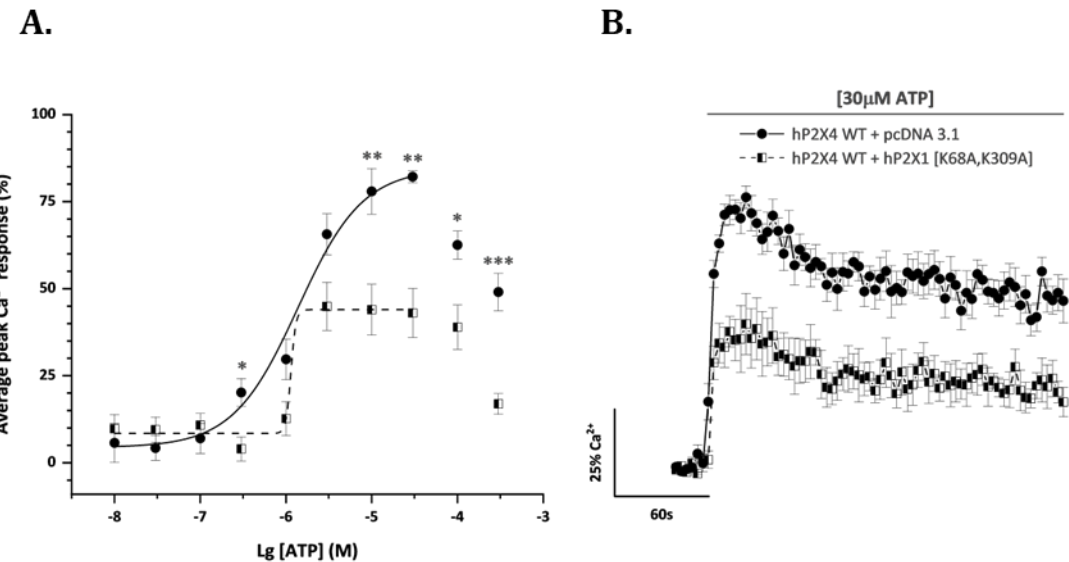


Fig 4.2. The human P2X1 [K68A, K309A] dead subunit had a dominant negative effect on human P2X4 WT ATP-evoked Ca^{2+} responses in transiently co-transfected 1321N1 parental astrocytoma cells. (A) ATP concentration-response curves for the peak magnitude of intracellular Ca^{2+} influx in the presence (half-full squares) and absence (closed circles) of hP2X1 [K68A, K309A]. (B) Averaged time-resolved intracellular Ca^{2+} influx elicited by 30 μM ATP in the presence (half-full squares) and absence (closed circles) of hP2X1 [K68A, K309A]. All data were normalised to respective maximal 100 μM Carbachol responses. Data were represented as mean \pm SEM ($N=5$).

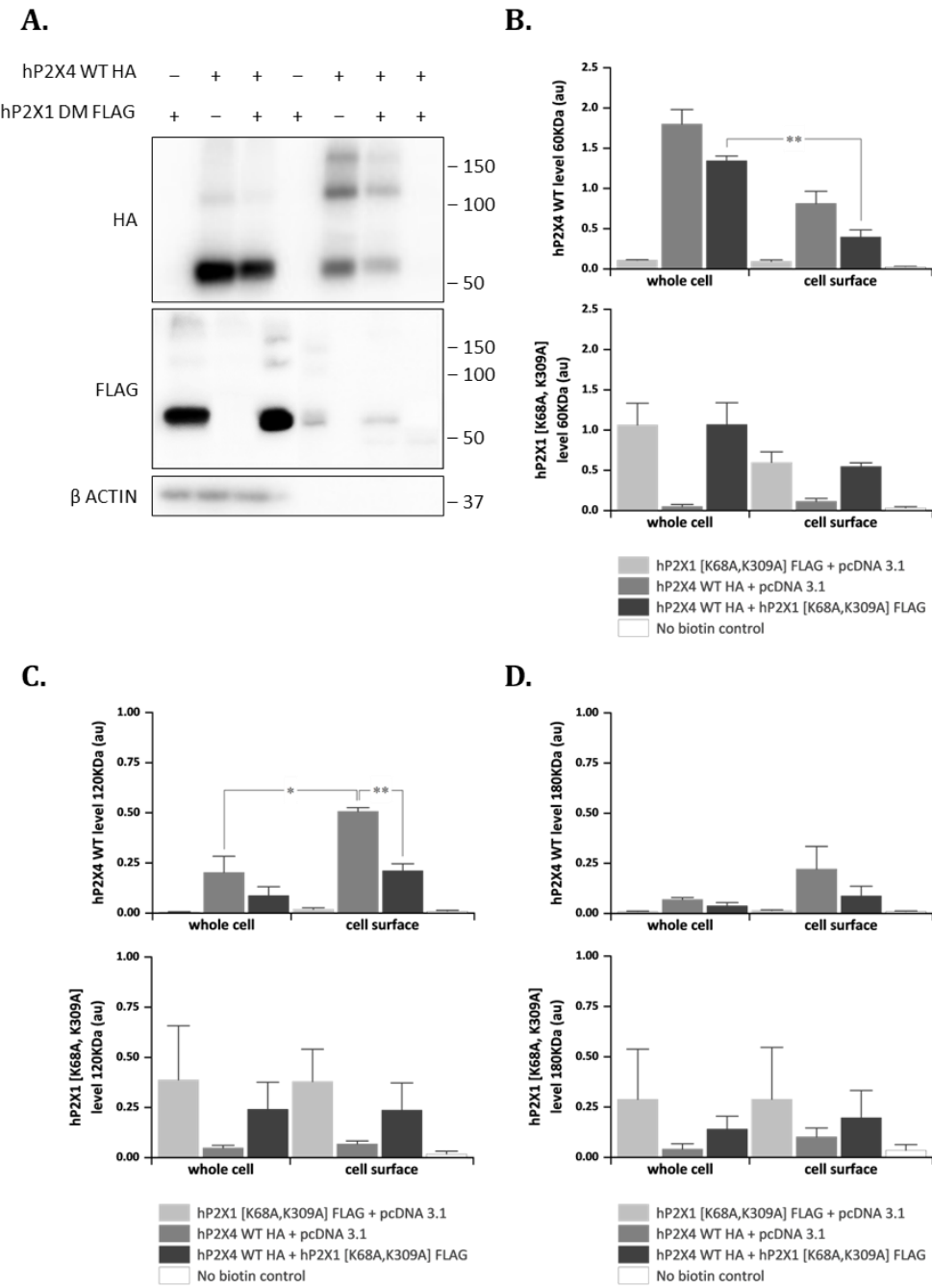


Fig 4.3. Whole-cell and cell surface expression levels of human P2X4 WT and human P2X1 [K68A, K309A] subunits in transiently co-transfected 1321N1 parental astrocytoma cells. (A) Representative immunoblot for hP2X4 WT HA-tagged protein (top), hP2X1 [K68A, K309A] FLAG-tagged protein (middle), and β -actin loading control (bottom). Molecular weight size standards were indicated in kDa. Lanes 1-3 corresponded to whole-cell samples and lanes 4-7 to cell surface protein lysates. Lane 7 was a negative control for biotin labelling. (B – D) Comparison of densitometric analysis for bands at (B) 60kDa, (C) 120kDa, (D) and 180kDa of hP2X4 WT HA-tagged (top) and hP2X1 [K68A, K309A] FLAG-tagged (bottom) protein levels relative to loading control for whole-cell and cell surface lysates. Data were represented as mean \pm SEM ($N=3$).

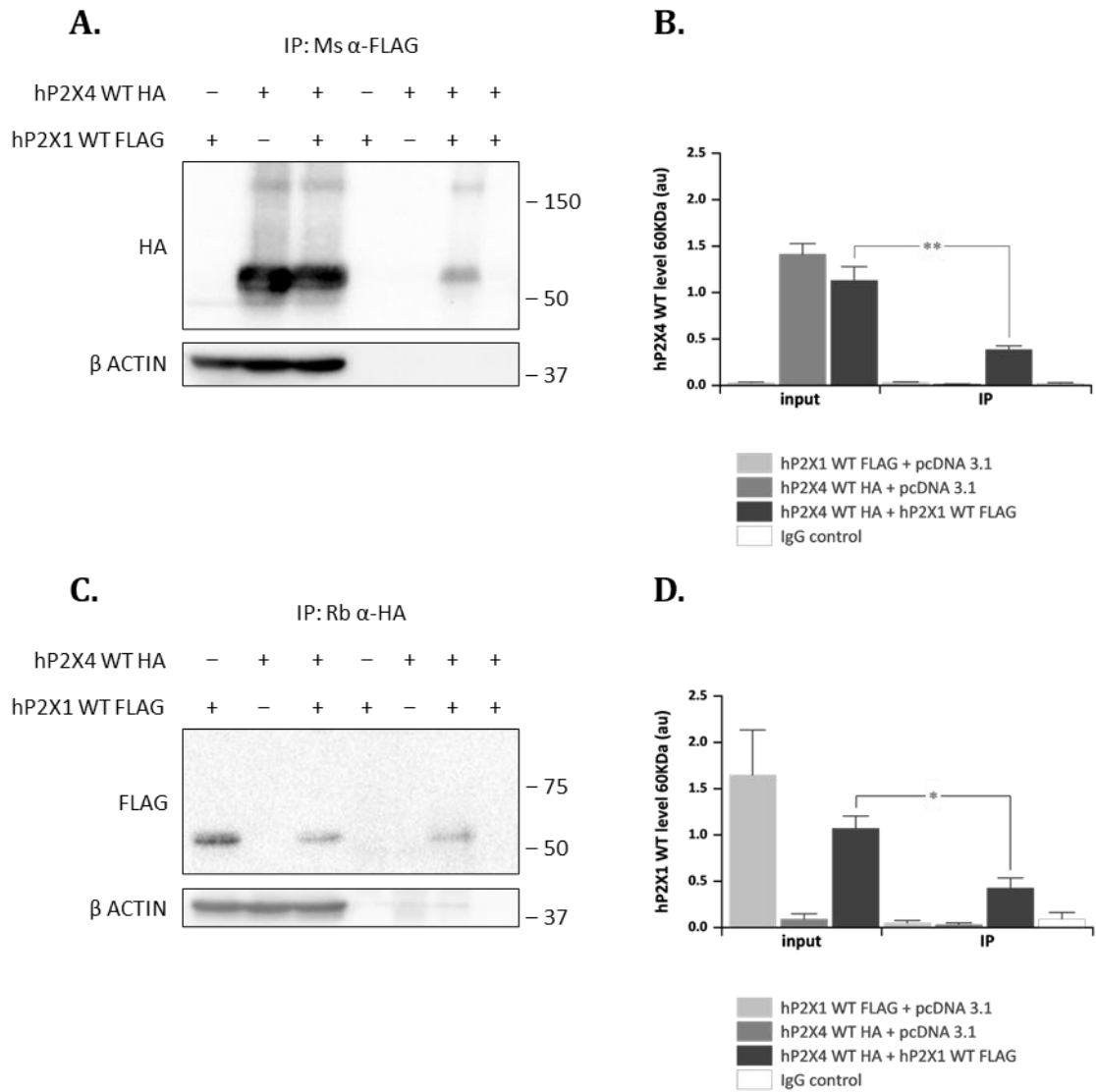


Fig 4.4. Human P2X4 WT subunits co-immunoprecipitated with human P2X1 WT subunits when transiently co-transfected in 1321N1 parental astrocytoma cells. (A) Representative immunoblot for hP2X4 WT HA-tagged protein after immunoprecipitation using anti-FLAG antibody, and for the β -actin loading control. (B) Comparison of densitometric analysis of hP2X4 WT HA-tagged protein level relative to loading control for input and co-immunoprecipitated complexes. (C) Representative immunoblot for hP2X1 WT FLAG-tagged protein after immunoprecipitation using anti-HA antibody, and for the β -actin loading control. (D) Comparison of densitometric analysis of hP2X1 WT FLAG-tagged protein level relative to loading control for input and co-immunoprecipitated complexes. Molecular weight size standards were indicated in kDa. Lanes 1-3 corresponded to whole-cell protein lysates and lanes 4-7 to immunoprecipitated protein complexes. Lane 7 was an IgG negative control for immunoprecipitation without antibody. Data were represented as mean \pm SEM ($N=3$).

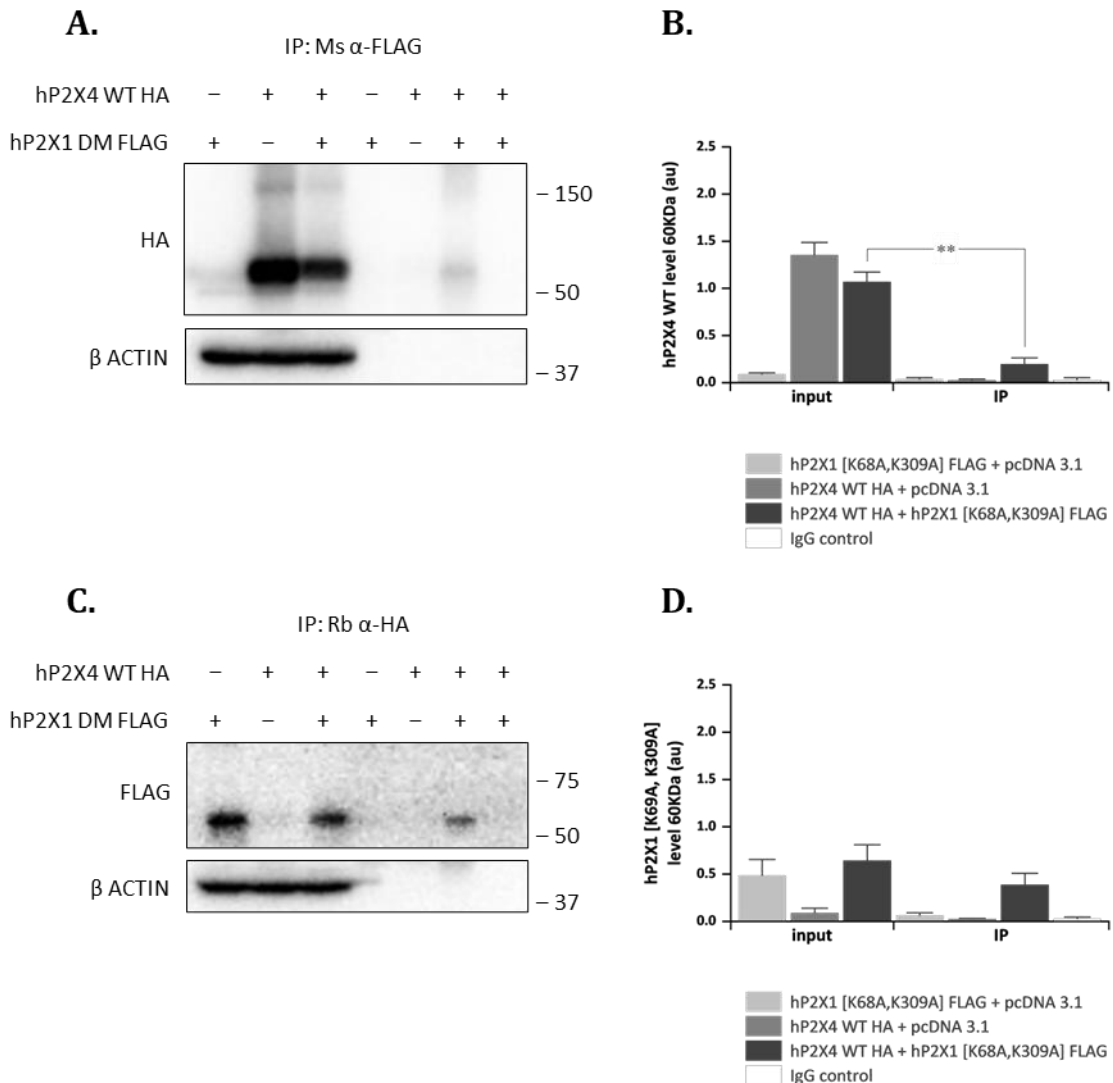


Fig 4.5. Human P2X4 WT subunits co-immunoprecipitated with human P2X1 [K68A, K309A] subunits when transiently co-transfected in 1321N1 parental astrocytoma cells. (A) Representative immunoblot for hP2X4 WT HA-tagged protein after immunoprecipitation using anti-FLAG antibody, and for the β -actin loading control. (B) Comparison of densitometric analysis of hP2X4 WT HA-tagged protein level relative to loading control for input and co-immunoprecipitated complexes. (C) Representative immunoblot for hP2X1 [K68A, K309A] FLAG-tagged protein after immunoprecipitation using anti-HA antibody, and for the β -actin loading control. (D) Comparison of densitometric analysis of hP2X1 [K68A, K309A] FLAG-tagged protein level relative to loading control for input and co-immunoprecipitated complexes. Molecular weight size standards were indicated in kDa. Lanes 1-3 corresponded to whole-cell protein lysates and lanes 4-7 to immunoprecipitated protein complexes. Lane 8 was an IgG negative control for immunoprecipitation without antibody. Data were represented as mean \pm SEM ($N=3$).

As previously described, out of seven different P2X receptor subtypes, only six can form functional homotrimeric receptors in humans (North, 2002). Over the past 30 years, just two groups have been able to express functional rat P2X6 homomeric receptors (Collo et al., 1996; Jones et al., 2004). Both studies showed ATP-evoked current responses with a slow desensitisation phase for the rat P2X6 receptor in transiently transfected HEK293 cells. Jones et al. also demonstrated that rat P2X6 recombinant expression and channel function depended on subunit glycosylation (Jones et al., 2004). There is no functional evidence for human P2X6 homomeric receptors to date. Thus, it is considered a “silent” subunit in humans (Illes et al., 2021).

Human 1321N1 parental astrocytoma cells transiently co-transfected with human P2X4 WT and human P2X6 [K78A, K315A] dead subunits behaved similarly to the ones co-transfected with human P2X1 [K68A, K309A] dead subunits instead. Thereby, the presence of human P2X6 [K78A, K315A] dead subunits had a dominant negative effect on the ATP-evoked intracellular calcium responses at concentrations of 0.3 μ M, 10 μ M, 30 μ M, 100 μ M, and 300 μ M compared to ATP-evoked intracellular calcium responses in cells transiently co-transfected with human P2X4 WT and pcDNA 3.1 plasmid control ($p<0.05$, $p<0.01$, $p<0.01$, $p<0.01$, and $p<0.001$ vs corresponding plasmid control responses; Fig 4.6A). In the same way, 30 μ M ATP evoked the maximal calcium influx of 58.8 \pm 5.80%, which was nearly 30% smaller than the human P2X4 WT with pcDNA 3.1 plasmid control response ($p<0.01$ vs 82.1 \pm 1.77% for plasmid control; Fig 4.6) and that response was also sustained over time at approximately 40% above baseline (Fig 4.6B). However, the biggest reduction effect was observed at 300 μ M ATP, reaching only a 10.7 \pm 4.20% peak calcium response compared to 49.0 \pm 5.36% for the corresponding 300 μ M ATP plasmid control response (approximately 78% reduction, $p<0.001$; Fig 4.6A). Again, the half maximal effective concentration remained the same in the presence and absence of human P2X6 [K78A, K315A] dead subunits (5.20 \pm 2.64 μ M vs 2.40 \pm 0.79 μ M for plasmid control, $p>0.05$; Fig 4.6A).

Co-immunoprecipitation data revealed a positive interaction between human P2X4 WT HA-tagged and human P2X6 WT FLAG-tagged subunits in transiently co-transfected 1321N1 parental astrocytoma cells. When anti-FLAG antibodies were used for protein pull-down, specific human P2X4 WT 60KDa bands were detected in whole-cell input controls (1.58 \pm 0.38au for human P2X4 WT alone and 1.47 \pm 0.34au for human P2X4 WT co-expressed with human P2X6 WT, $p>0.05$; Fig 4.7A and B). The expression levels of human P2X4 WT HA-tagged subunits in the anti-FLAG immunoprecipitation complex lane remained unchanged compared to co-transfected input controls (0.72 \pm 0.22au vs input control, $p>0.05$; Fig 4.7A and B). Human P2X6 WT proteins were also detected at approximately 60KDa for input controls (0.26 \pm 0.07au for human P2X6 WT alone and 0.30 \pm 0.08au for human P2X6 WT co-expressed with human P2X4 WT, $p>0.05$; Fig 4.7C and D). It is important to mention that human P2X6 WT expression levels were significantly lower than human P2X4 WT expression levels in transiently co-transfected 1321N1 parental astrocytoma whole-cell lysates ($p<0.05$; Fig 4.7). Accordingly, when anti-HA antibodies were used for protein pull-down, a 60KDa band corresponding to human P2X6 WT FLAG-tagged subunits was detected in the co-immunoprecipitation lane (0.78 \pm 0.48au, $p>0.05$ vs input control; Fig 4.7C and D). Both human P2X4 WT and human P2X6 WT subunits were equally expressed in the co-immunoprecipitate lane (0.72 \pm 0.22au vs 0.78 \pm 0.48au, respectively, $p>0.05$; Fig 4.7B and D).

Consequent studies of human P2X4 WT surface and total protein expression levels in the presence and absence of human P2X6 [K78A, K315A] dead subunits, as well as co-immunoprecipitation assays of human P2X4 WT HA-tagged subunits with human P2X6 [K78A, K315A] FLAG-tagged dead subunits, still need to be performed as human P2X6 [K78A, K315A] dead subunits showed poor expression levels in 1321N1 parental astrocytoma cells (Fig 4.1I-J and 4.7C-D).

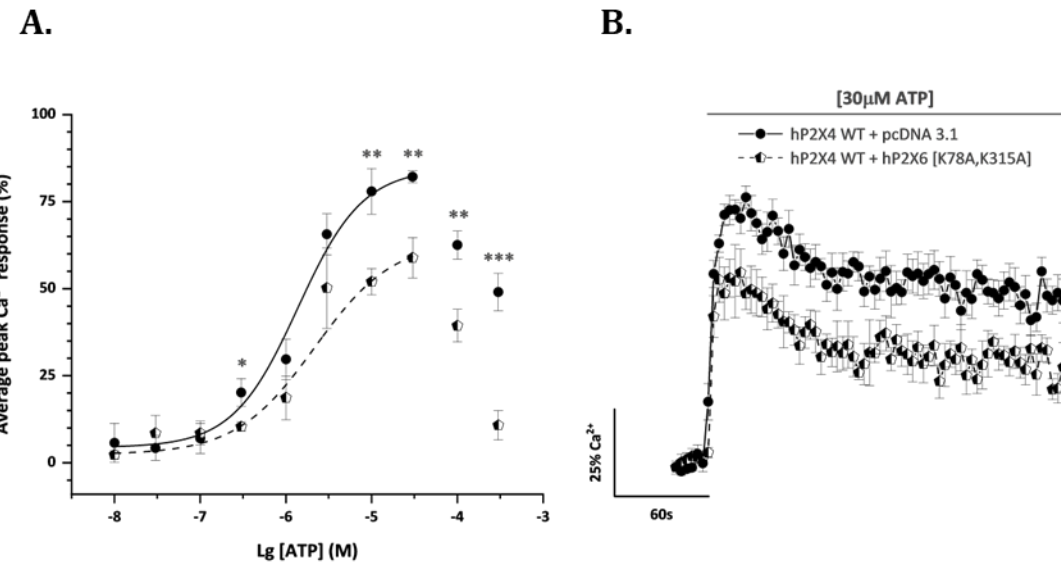


Fig 4.6. The human P2X6 [K78A, K315A] dead subunit had a dominant negative effect on human P2X4 WT ATP-evoked Ca^{2+} responses in transiently co-transfected 1321N1 parental astrocytoma cells. (A) ATP concentration-response curves for the peak magnitude of intracellular Ca^{2+} influx in the presence (half-full pentagons) and absence (closed circles) of hP2X6 [K78A, K315A]. (B) Averaged time-resolved intracellular Ca^{2+} influx elicited by 30 μM ATP in the presence (half-full pentagons) and absence (closed circles) of hP2X6 [K78A, K315A]. All data were normalised to respective maximal 100 μM Carbachol responses. Data were represented as mean \pm SEM ($N=5$).

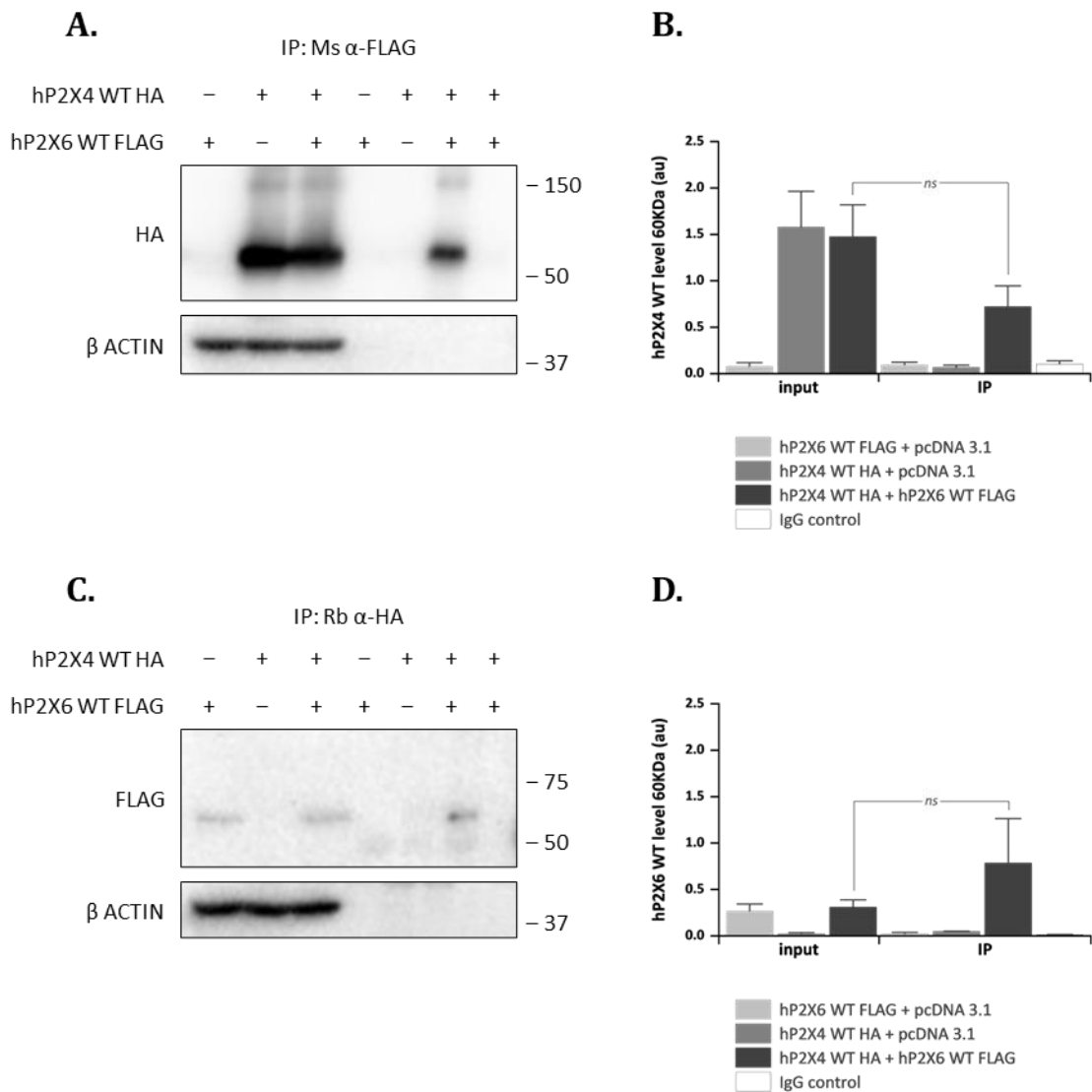


Fig 4.7. Human P2X4 WT subunits co-immunoprecipitated with human P2X6 WT subunits when transiently co-transfected in 1321N1 parental astrocytoma cells. (A) Representative immunoblot for hP2X4 WT HA-tagged protein after immunoprecipitation using anti-FLAG antibody, and for the β -actin loading control. (B) Comparison of densitometric analysis of hP2X4 WT HA-tagged protein level relative to loading control for input and co-immunoprecipitated complexes. (C) Representative immunoblot for hP2X6 WT FLAG-tagged protein after immunoprecipitation using anti-HA antibody, and for the β -actin loading control. (D) Comparison of densitometric analysis of hP2X6 WT FLAG-tagged protein level relative to loading control for input and co-immunoprecipitated complexes. Molecular weight size standards were indicated in kDa. Lanes 1-3 corresponded to whole-cell protein lysates and lanes 4-7 to immunoprecipitated protein complexes. Lane 7 was an IgG negative control for immunoprecipitation without antibody. Data were represented as mean \pm SEM ($N=3$).

4.2.1.2 Human P2X4 subunits did not form functional interactions with human P2X2 or human P2X3 subunits

Transient co-transfection of human P2X2 [K81A, K319A] dead subunits with human P2X4 WT subunits did not affect the ATP-evoked calcium responses at any concentration tested, reaching a maximal intracellular calcium influx at 30 μ M (72.1±5.68% vs 82.1±1.77% for plasmid control, p>0.05; Fig 4.8). The 30 μ M ATP-evoked intracellular calcium response was sustained over time at nearly 60% above the baseline level, which followed the same desensitisation profile as the human P2X4 WT with pcDNA 3.1 plasmid control responses (Fig 4.8B). The ATP potency value for human P2X4 WT transiently co-transfected with human P2X2 [K81A, K319A] remained unchanged compared to plasmid control (1.32±0.03 μ M vs 2.40±0.79 μ M, p>0.05; Fig 4.8A).

Similarly, transient co-transfection of human P2X3 [K63A, K299A] dead subunits with human P2X4 WT subunits did not affect the ATP-evoked calcium responses at concentrations ranging from 10nM up to 100 μ M ATP. The maximal intracellular calcium influx was attained at a concentration of 30 μ M ATP, comparable to the one obtained for human P2X4 WT with pcDNA 3.1 plasmid control (74.5±10.1% vs 82.1±1.77% for plasmid control, p>0.05; Fig 4.9). The response was also sustained over time at approximately 60% above baseline following the desensitisation characteristics of the human P2X4 WT with pcDNA 3.1 plasmid control response (Fig 4.9B). It is important to note that there was a 52% reduction of intracellular calcium responses evoked by 300 μ M ATP compared to human P2X4 WT subunits co-transfected with pcDNA 3.1 plasmid control (24.0±3.13% vs 49.0±5.36%, respectively, p<0.01; Fig 4.9A and 4.10B). However, the ATP potency value was not affected by the presence of human P2X3 [K63A, K299A] dead subunits compared to co-transfection of human P2X4 WT with pcDNA 3.1 plasmid control (1.32±0.03 μ M vs 2.40±0.79 μ M, p>0.05; Fig 4.9A).

As detailed in section 2.13.1 (Chapter 2), peak calcium responses were quantified as the difference between the highest and the lowest y-axis values and represented the maximal response magnitude. The area under the curve (AUC) is another value provided by the FlexStation 3 software. It is defined as the integral of the intracellular calcium response as a function of time. AUC data encompasses both the initial response and the sustained calcium phase over the recorded period of time, representing the net calcium movement upon application of ATP in this case. Consequently, analysis of the area under the curve was performed to detect any possible effects missed by solely analysing peak data. If significant differences in AUC data were found, further analysis of the decay rate (τ) of the calcium responses was quantified for completeness. The decay rate represented the decline in efficacy of the ATP-evoked calcium responses over time and was used as an indicative measure to detect potential effects on the desensitisation phase of the human P2X4 receptor.

The presence of both human P2X2 [K81A, K319A] (AUC 7.83±1.31%) and human P2X3 [K63A, K299A] (AUC 5.13±2.44%) dead subunits significantly reduced the net calcium movement upon 300 μ M ATP application compared to plasmid control (22.7±3.18%, p<0.01 for both vs plasmid control; Fig 4.10). The human P2X4 WT and P2X2 [K81A, K319A] transients showed a 24.59±1.51s decay rate (p>0.05 vs 28.53±1.17s for plasmid control; Fig 4.10A), whereas the human P2X4 WT and human P2X3 [K63A,

K299A] transients presented a 12.82 ± 2.01 s decay rate (approximately 55% faster than plasmid control, $p < 0.001$ vs 28.53 ± 1.17 s for plasmid control; Fig 4.10B). Moreover, both $300\mu\text{M}$ ATP-evoked calcium responses decayed to baseline levels over the recorded period of time (Fig 4.10). P2X2 and P2X4 receptors are characteristic amongst the P2X receptor family for their slow desensitisation phase where the intracellular calcium response is sustained over time, whereas P2X3 receptors are known for having the fastest channel desensitisation along with the P2X1 subtype (North, 2002).

Surprisingly, human P2X4 WT HA-tagged subunits co-immunoprecipitated with human P2X2 WT FLAG-tagged subunits in transiently co-transfected 1321N1 parental astrocytoma cells (Fig 4.11A). Whole-cell input controls showed no significant differences when human P2X4 WT subunits were co-transfected with either pcDNA 3.1 plasmid control or human P2X2 WT subunits ($p > 0.05$, 1.62 ± 0.13 au vs 1.43 ± 0.09 au, respectively; Fig 4.11A and B). However, expression levels of human P2X4 WT in the co-immunoprecipitated complexes were significantly reduced compared to co-transfected input control (0.91 ± 0.01 au, $p < 0.05$ vs input control; Fig 4.11A and B). Reciprocal human P2X4 WT HA-tagged subunit pull-down and immunoblot detection using anti-FLAG antibodies showed positive interaction bands at approximately 70KDa corresponding to the human P2X2 WT subunit protein weight (0.28 ± 0.02 au, $p > 0.05$ vs input control; Fig 4.11C and D). Similarly, there were no differences in whole-cell input control expression levels when human P2X2 WT subunits were transiently co-transfected with pcDNA 3.1 plasmid control or combined with human P2X4 WT subunits ($p > 0.05$, 1.16 ± 0.36 au vs 0.46 ± 0.15 au, respectively; Fig 4.11C and D). The human P2X4 WT subunit expression levels were three times larger than the amount of human P2X2 WT subunits in the co-immunoprecipitated complexes ($p < 0.001$), and the same occurred for whole-cell input controls when both subunits were co-expressed ($p < 0.01$).

In contrast, human P2X4 WT subunits did not co-immunoprecipitate with human P2X3 WT subunits in transiently co-transfected 1321N1 parental astrocytoma cells (0.16 ± 0.04 au, $p < 0.001$ vs input control; Fig 4.12A and B) and vice versa, human P2X3 WT subunits did not form a co-immunoprecipitate complex with human P2X4 WT subunits (0.12 ± 0.05 au, $p > 0.05$ vs input control, Fig 4.12C and D). Although a faint 60KDa band could be perceived in the co-immunoprecipitate lane for human P2X4 WT HA-tagged subunits, its expression levels were the same as the anti-FLAG immunoprecipitation controls for samples containing only human P2X3 WT FLAG-tagged subunits with pcDNA 3.1 plasmid (0.02 ± 0.01 au vs 0.16 ± 0.04 au, $p > 0.05$) and as the IgG negative control samples where no antibody was added during immunoprecipitation (0.01 ± 0.00 vs 0.16 ± 0.04 au, $p > 0.05$; Fig 4.12A and B). Correspondingly, a dim human P2X3 WT FLAG-tagged specific band was also noticeable at 60KDa in the co-immunoprecipitate lane, but its expression was equal to the anti-HA immunoprecipitation control for samples containing only human P2X4 WT HA-tagged subunits with pcDNA 3.1 plasmid (0.02 ± 0.00 au vs 0.12 ± 0.05 au, $p > 0.05$) and to the IgG negative control samples where no antibody was added during immunoprecipitation (0.03 ± 0.03 vs 0.12 ± 0.05 au, $p > 0.05$; Fig 4.12C and D). Human P2X4 WT subunit whole-cell expression levels were equivalent in the presence and absence of human P2X3 WT subunits (0.96 ± 0.08 au vs 1.16 ± 0.09 , respectively, $p > 0.05$; Fig 4.12A and B). Similarly, there were no differences in whole-cell expression levels when human P2X3 WT subunits were co-expressed with pcDNA 3.1

plasmid control or with human P2X4 WT subunits (0.73 ± 0.14 au vs 0.47 ± 0.07 au, respectively, $p>0.05$; Fig 4.12C and D). In co-transfected samples, human P2X3 WT subunits were two times less expressed than human P2X4 WT subunits at a whole-cell level ($p<0.01$).

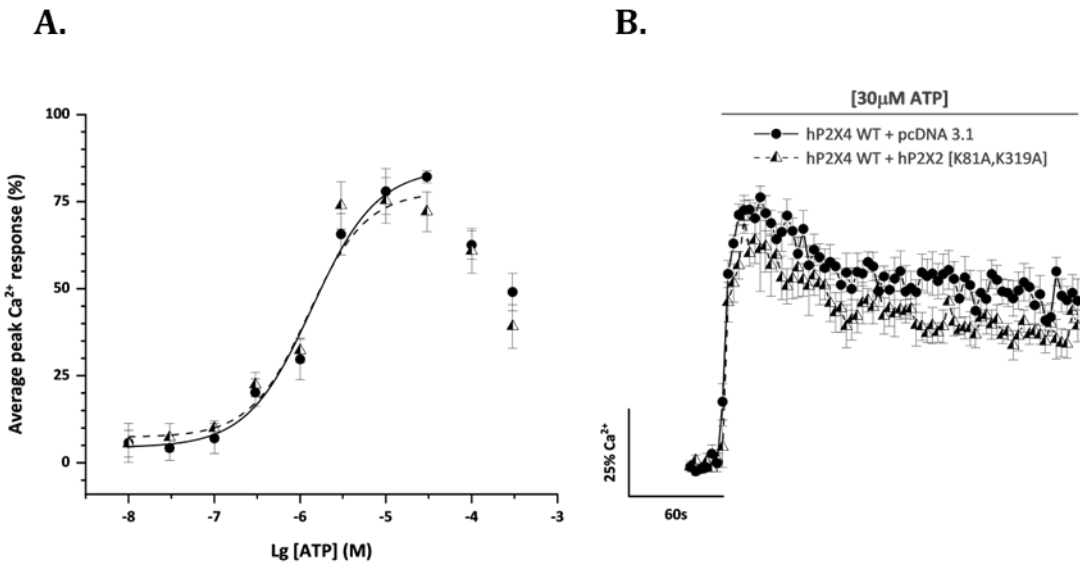


Fig 4.8. The human P2X2 [K81A, K319A] dead subunit did not affect the human P2X4 WT ATP-evoked Ca^{2+} responses in transiently co-transfected 1321N1 parental astrocytoma cells. (A) ATP concentration-response curves for the peak magnitude of intracellular Ca^{2+} influx in the presence (half-full triangles) and absence (closed circles) of hP2X2 [K81A, K319A]. (B) Averaged time-resolved intracellular Ca^{2+} influx elicited by 30 μM ATP in the presence (half-full triangles) and absence (closed circles) of hP2X2 [K81A, K319A]. All data were normalised to respective maximal 100 μM Carbachol responses. Data were represented as mean \pm SEM ($N=5$).

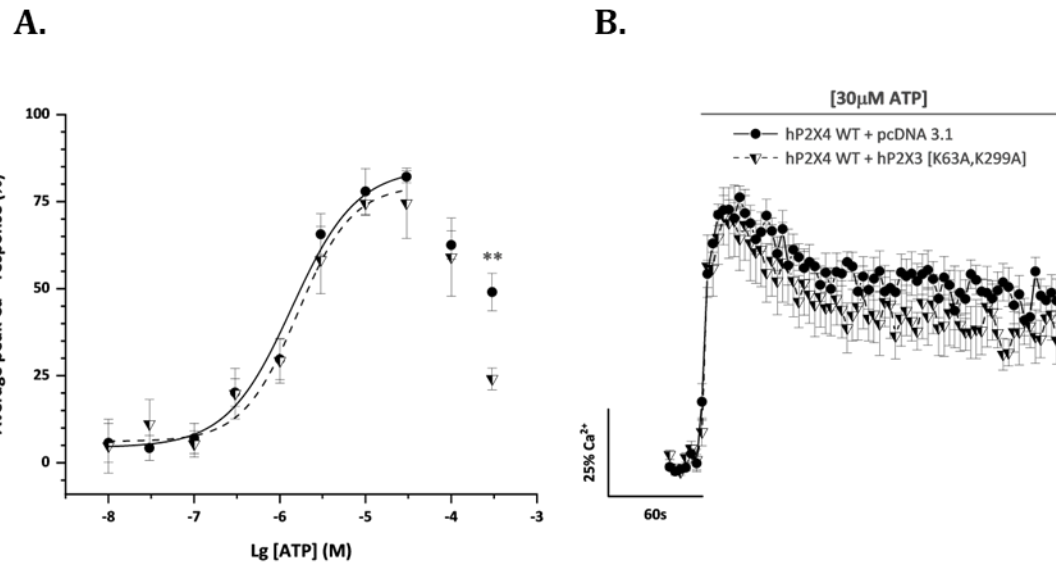


Fig 4.9. The human P2X3 [K63A, K299A] dead subunit did not affect the human P2X4 WT ATP-evoked Ca^{2+} responses in transiently co-transfected 1321N1 parental astrocytoma cells. (A) ATP concentration-response curves for the peak magnitude of intracellular Ca^{2+} influx in the presence (half-full triangles) and absence (closed circles) of hP2X3 [K63A, K299A]. (B) Averaged time-resolved intracellular Ca^{2+} influx elicited by $30\mu\text{M}$ ATP in the presence (half-full triangles) and absence (closed circles) of hP2X3 [K63A, K299A]. All data were normalised to respective maximal $100\mu\text{M}$ Carbachol responses. Data were represented as mean \pm SEM ($N=5$).

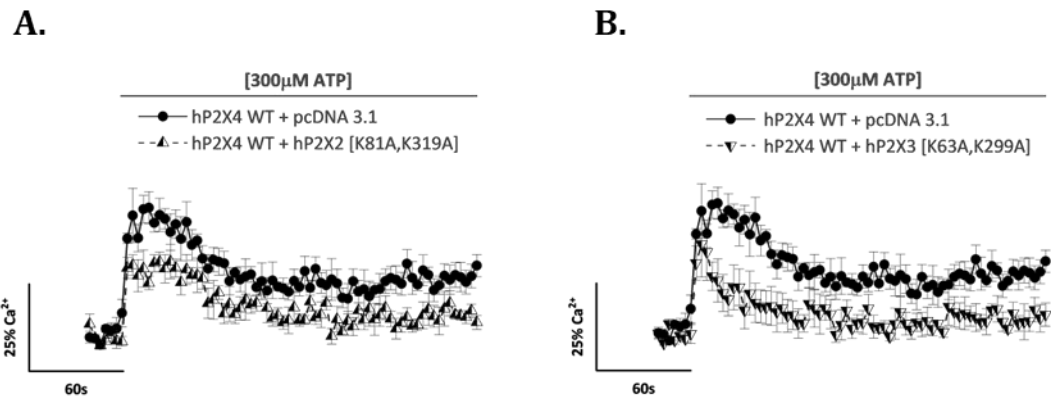


Fig 4.10. Effects of human P2X2 [K81A, K319A] and human P2X3 [K63A, K299A] dead subunits on the human P2X4 WT desensitisation phase in transiently co-transfected 1321N1 parental astrocytoma cells. Pairs of averaged time-resolved intracellular Ca^{2+} influx responses elicited by 300 μM ATP in the presence (half-full triangles) and absence (closed circles) of (A) hP2X2 [K81A, K319A] or (B) hP2X3 [K63A, K299A] dead subunits. All data were normalised to respective maximal 100 μM Carbachol responses. Data were represented as mean \pm SEM ($N=5$).

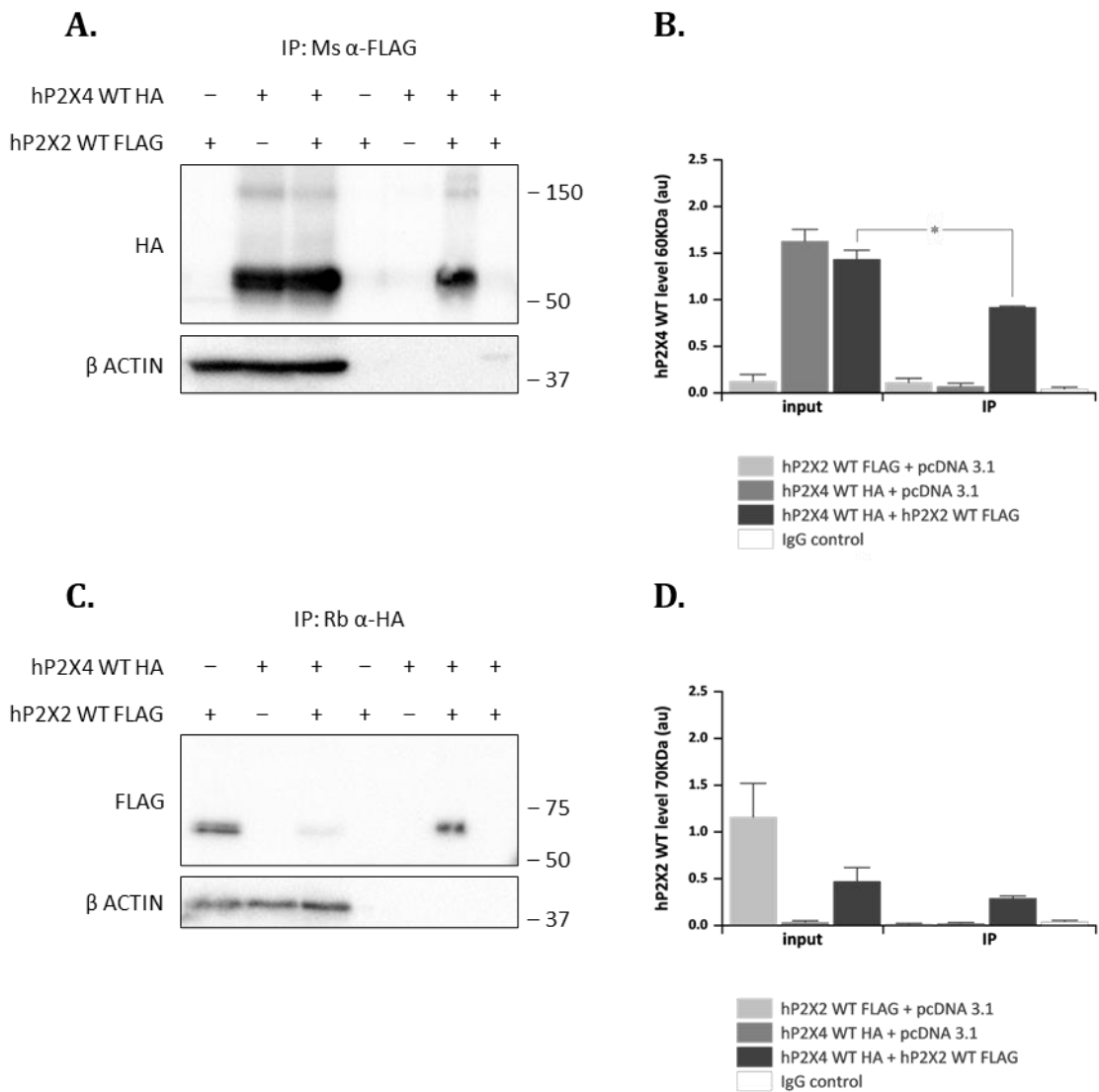


Fig 4.11. Human P2X4 WT subunits co-immunoprecipitated with human P2X2 WT subunits when transiently co-transfected in 1321N1 parental astrocytoma cells. (A) Representative immunoblot for hP2X4 WT HA-tagged protein after immunoprecipitation using anti-FLAG antibody, and for the β -actin loading control. (B) Comparison of densitometric analysis of hP2X4 WT HA-tagged protein level relative to loading control for input and co-immunoprecipitated complexes. (C) Representative immunoblot for hP2X2 WT FLAG-tagged protein after immunoprecipitation using anti-HA antibody, and for the β -actin loading control. (D) Comparison of densitometric analysis of hP2X2 WT FLAG-tagged protein level relative to loading control for input and co-immunoprecipitated complexes. Molecular weight size standards were indicated in kDa. Lanes 1-3 corresponded to whole-cell protein lysates and lanes 4-7 to immunoprecipitated protein complexes. Lane 7 was an IgG negative control for immunoprecipitation without antibody. Data were represented as mean \pm SEM ($N=3$).

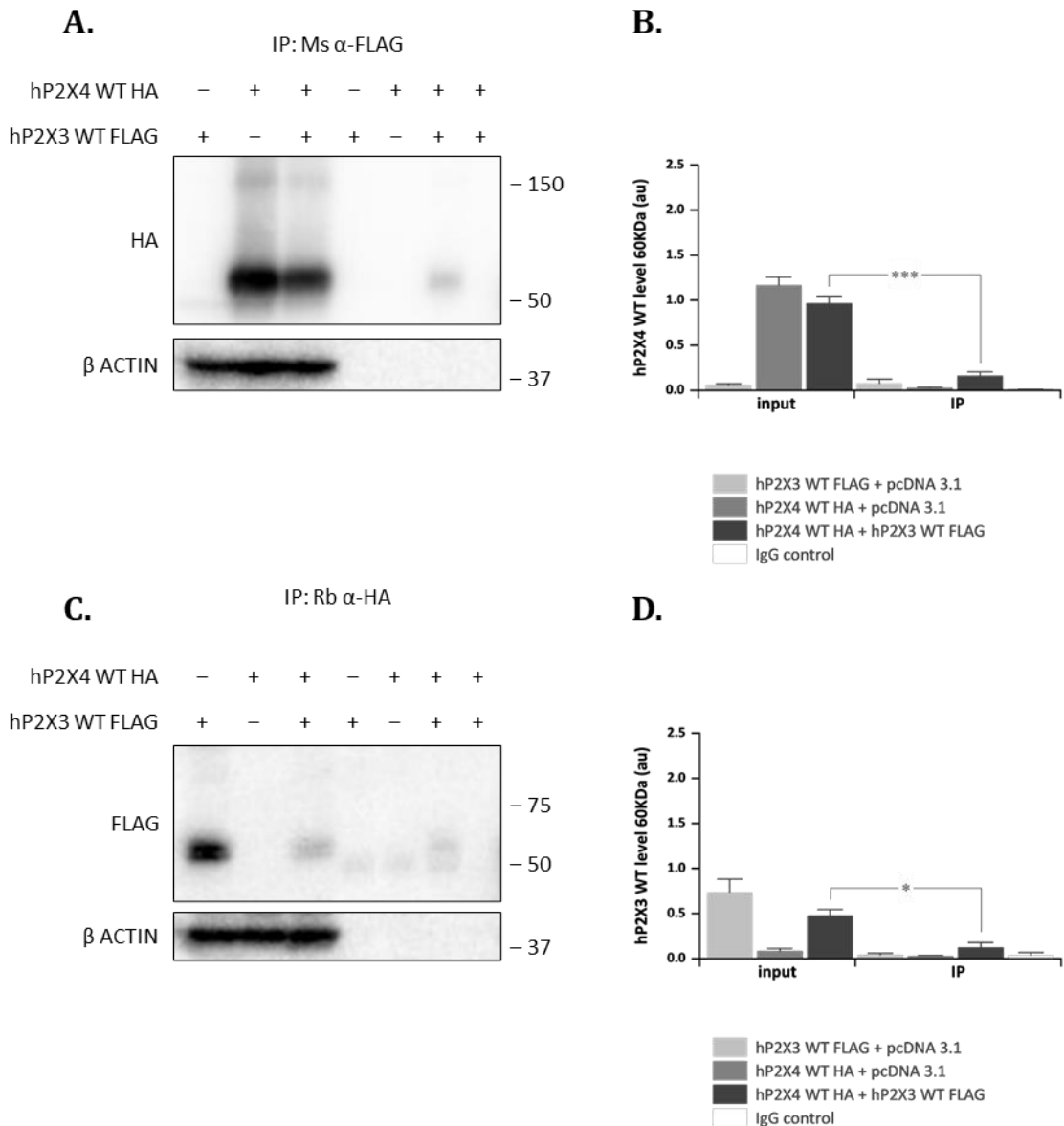


Fig 4.12. Human P2X4 WT subunits did not co-immunoprecipitate with human P2X3 WT subunits when transiently co-transfected in 1321N1 parental astrocytoma cells. (A) Representative immunoblot for hP2X4 WT HA-tagged protein after immunoprecipitation using anti-FLAG antibody, and for the β -actin loading control. (B) Comparison of densitometric analysis of hP2X4 WT HA-tagged protein level relative to loading control for input and co-immunoprecipitated complexes. (C) Representative immunoblot for hP2X3 WT FLAG-tagged protein after immunoprecipitation using anti-HA antibody, and for the β -actin loading control. (D) Comparison of densitometric analysis of hP2X3 WT FLAG-tagged protein level relative to loading control for input and co-immunoprecipitated complexes. Molecular weight size standards were indicated in kDa. Lanes 1-3 corresponded to whole-cell protein lysates and lanes 4-7 to immunoprecipitated protein complexes. Lane 7 was an IgG negative control for immunoprecipitation without antibody. Note the immunoblots shown here showed poor interaction bands. The other blots showed no co-immunoprecipitated bands (not shown). Data were represented as mean \pm SEM ($N=3$).

4.2.1.3 Human P2X4 subunits formed functional interactions with human P2X5 subunits containing exon 10

Homotrimeric P2X5 receptors have been previously reported to have limited roles in humans, with only 14% of individuals likely to form functional homomeric channels (Bo et al., 2003). The only human P2X5 cDNAs reported are missing exon 10 (human P2X5a) or exons 3 and 10 (human P2X5b), both non-functional channels (North, 2002). Analysis of the human genome showed a G>T polymorphism in the gene encoding the P2X5 receptor. Sequences with thymidine (T) will be recognised during mRNA processing and will be translated to a ‘full-length’ P2X5 receptor. However, sequences with a guanine (G) at this position will be read as a consensus for RNA splicing during mRNA processing and will be translated to a P2X5 receptor that does not include exon 10. Exon 10 is 22 amino acids long toward the C-terminus from the inner end of the second transmembrane domain. Human P2X5 receptors containing all exons showed high expression levels in HEK293 cells and produced robust currents upon application of ATP (Bo et al., 2003). Because our experimental system was based on functional and biochemical evidence of P2X heteromerisation, we used the full-length human P2X5 receptor cloned in a pcDNA 3.1 backbone vector. The wild-type sequence was used as a template for generating the human P2X5 dead receptor tool.

Calcium mobilisation data showed a significant reduction of ATP-evoked peak calcium responses in 1321N1 parental astrocytoma cells co-transfected with human P2X4 WT and human P2X5 [K69A, K314A] dead subunits at high ATP concentrations of 30 μ M, 100 μ M, and 300 μ M ($p<0.001$, $p<0.01$, and $p<0.001$ vs corresponding plasmid control responses; Fig 4.13A). The calcium response plateaued at 3 μ M, 10 μ M, and 30 μ M ATP concentrations, with the maximal calcium response being 60.8 \pm 4.69% at 10 μ M ATP ($p>0.05$ vs 77.9 \pm 6.54% for plasmid control; Fig 4.13A). The greatest difference was observed at 300 μ M of nearly 80% calcium response reduction compared to human P2X4 WT with pcDNA 3.1 plasmid control responses (10.3 \pm 3.10% vs 49.0 \pm 5.36%, respectively, $p<0.001$; Fig 4.13). For comparison with the other P2X dead receptor tools, Figure 4.13B showed a 45% reduction of the 30 μ M ATP-evoked peak calcium response in the presence of human P2X5 [K69A, K314A] dead subunits (48.1 \pm 3.83% vs 82.1 \pm 1.77% plasmid control response, $p<0.001$) and a low sustained desensitisation phase over time (approximately 30% above baseline level). Similarly, co-transfection of human P2X5 [K69A, K314A] dead subunits did not change the ATP potency value compared to human P2X4 WT subunits co-transfected with pcDNA 3.1 plasmid control (1.76 \pm 0.43 μ M, $p>0.05$; Fig 4.13A).

The presence of human P2X5 [K69A, K314A] dead subunits significantly reduced the amount of human P2X4 WT at the cell surface by approximately 43% compared to human P2X4 WT transiently co-transfected with pcDNA 3.1 plasmid control (0.45 \pm 0.05au vs 0.79 \pm 0.02au, respectively, $p<0.01$; Fig 4.14A and B). In contrast, whole-cell expression levels remained unchanged (1.28 \pm 0.15au vs 1.46 \pm 0.24au, respectively, $p>0.05$; Fig 4.14A and B). Human P2X5 [K69A, K314A] dead subunits were equally expressed at the cell surface when transiently co-transfected with human P2X4 WT subunits compared to plasmid control (0.22 \pm 0.01au vs 0.30 \pm 0.05au, respectively, $p>0.05$; Fig 4.14A and B). However, whole-cell expression levels of human P2X5 [K69A, K314A] dead subunits were reduced by

approximately 46% when co-expressed with human P2X4 WT subunits compared to plasmid control (0.98 ± 0.10 au vs 1.80 ± 0.20 au, respectively, $p<0.05$; Fig 4.14A and B). As expected, both human P2X4 WT and human P2X5 [K69A, K314A] subunits were less expressed at the cell membrane compared to whole-cell controls when co-expressed together ($p<0.01$ for both vs respective controls; Fig 4.14A and B). Expression of human P2X4 WT subunits was double that of human P2X5 [K69A, K314A] dead subunits when co-expressed together at the cell membrane (0.45 ± 0.05 au vs 0.22 ± 0.01 au, respectively, $p<0.05$) but comparable at whole-cell levels (1.28 ± 0.15 au vs 0.98 ± 0.10 au, respectively, $p>0.05$). Higher bands were also detected at approximately 120KDa and 180KDa for human P2X4 WT subunits and 150KDa and just over 250KDa for human P2X5 [K67A, K314A] dead subunits (Fig 4.14A, C and D). Whole-cell human P2X4 WT subunits showed higher expression levels at 60KDa when combined with human P2X5 [K67A, K314A] dead subunits compared to 120KDa (0.45 ± 0.05 au vs 0.23 ± 0.04 au, respectively, $p<0.05$) and to 180KDa relative expression levels (0.11 ± 0.01 au vs 60KDa, $p<0.01$). Comparable results were obtained for human P2X4 WT subunits expression at the cell surface where bands at 60KDa predominated over 120KDa (1.28 ± 0.15 au vs 0.16 ± 0.02 au, respectively, $p<0.01$) and 180KDa relative expression levels (0.14 ± 0.01 au vs 60KDa, $p<0.05$). Whole-cell human P2X5 [K69A, K314A] dead subunits were also more expressed at 70KDa when combined with human P2X4 WT subunits (0.98 ± 0.10 au for 70KDa vs 0.04 ± 0.01 for 150KDa, $p<0.05$; and 0.15 ± 0.08 au for 250KDa vs 70KDa, $p<0.01$). However, both human P2X5 [K69A, K314A] expression levels at 70KDa and 250KDa were higher at the cell surface (0.22 ± 0.01 au for 70KDa vs 0.05 ± 0.04 au for 150KDa, $p<0.01$; and 0.18 ± 0.10 au for 250KDa vs 70KDa, $p>0.05$).

Co-immunoprecipitation assays showed positive interactions between human P2X4 WT HA-tagged and human P2X5 WT FLAG-tagged subunits. There were no significant changes in human P2X4 WT whole-cell expression levels when transiently co-transfected with human P2X5 WT subunits compared to plasmid control (0.99 ± 0.03 au vs 1.24 ± 0.09 au, respectively, $p>0.05$; Fig 4.15A and B). Human P2X5 WT subunits were equally expressed at whole-cell input levels in combination with human P2X4 WT subunits compared to pcDNA 3.1 plasmid control (0.59 ± 0.09 au vs 0.78 ± 0.12 au, respectively, $p>0.05$; Fig 4.15C and D). Human P2X4 WT subunits were equally expressed in the co-immunoprecipitate lane compared to co-transfected input controls (0.68 ± 0.11 au vs 0.99 ± 0.03 au, $p>0.05$; Fig 4.15A and B) as well as human P2X5 WT subunits (0.71 ± 0.05 au vs 0.59 ± 0.09 au input control, $p>0.05$; Fig 4.15B and D). Relative expression levels of human P2X4 WT and human P2X5 WT subunits were the same in co-immunoprecipitated bands (0.68 ± 0.11 au vs 0.71 ± 0.05 au, respectively, $p>0.05$; Fig 4.15B and D).

Co-immunoprecipitation assays using 1321N1 parental astrocytoma cells transiently co-transfected with human P2X4 WT HA-tagged subunits and human P2X5 [K69A, K314A] FLAG-tagged dead subunits were also performed. Human P2X4 WT subunits co-immunoprecipitated with human P2X5 [K69A, K314A] dead subunits when anti-FLAG antibodies were used for protein pull-down (Fig 4.16A). Whole-cell input controls showed a reduction in human P2X4 WT expression levels when co-transfected with human P2X5 [K69A, K314A] dead subunits (0.81 ± 0.03 au vs 1.10 ± 0.08 au plasmid control, $p<0.05$; Fig 4.16A and B). The relative amount of co-immunoprecipitated human P2X4 WT protein was significantly reduced by approximately 62% compared to co-transfected input control (0.31 ± 0.01 vs 0.81 ± 0.03 au,

$p<0.001$; Fig 4.16A and B). A reduction in protein expression levels was also observed for whole-cell human P2X5 [K69A, K314A] dead subunit levels compared to pcDNA 3.1 plasmid control (0.92 ± 0.05 au vs 1.41 ± 0.12 au, respectively, $p<0.05$; Fig 4.16C and D). Co-immunoprecipitated human P2X5 [K69A, K314A] protein expression levels after anti-HA antibody pull-down were significantly smaller compared to co-transfected input control (about 47% reduction, 0.49 ± 0.08 au vs 0.92 ± 0.05 au, respectively, $p<0.05$; Fig 4.16C and D). As per human P2X4 WT and P2X5 WT co-immunoprecipitation studies, no differences in protein expression levels were registered between co-immunoprecipitated human P2X4 WT subunits and P2X5 [K69A, K314A] dead subunits ($p>0.05$; Fig 4.16B and D). The detection of a strong interaction band was consistent, and the complex expression levels were comparable to the ones obtained for human P2X4 WT and P2X5 WT combinations ($p>0.05$ for both anti-FLAG and anti-HA immunoprecipitates). It is also important to mention that human P2X5 [K69A, K314A] dead subunits were more expressed than human P2X5 WT subunits when co-transfected with pcDNA 3.1 plasmid control (1.41 ± 0.12 au vs 0.78 ± 0.12 au, respectively, $p<0.05$) and when co-transfected with human P2X4 WT subunits (0.92 ± 0.05 au vs 0.59 ± 0.09 au, respectively, $p<0.05$).

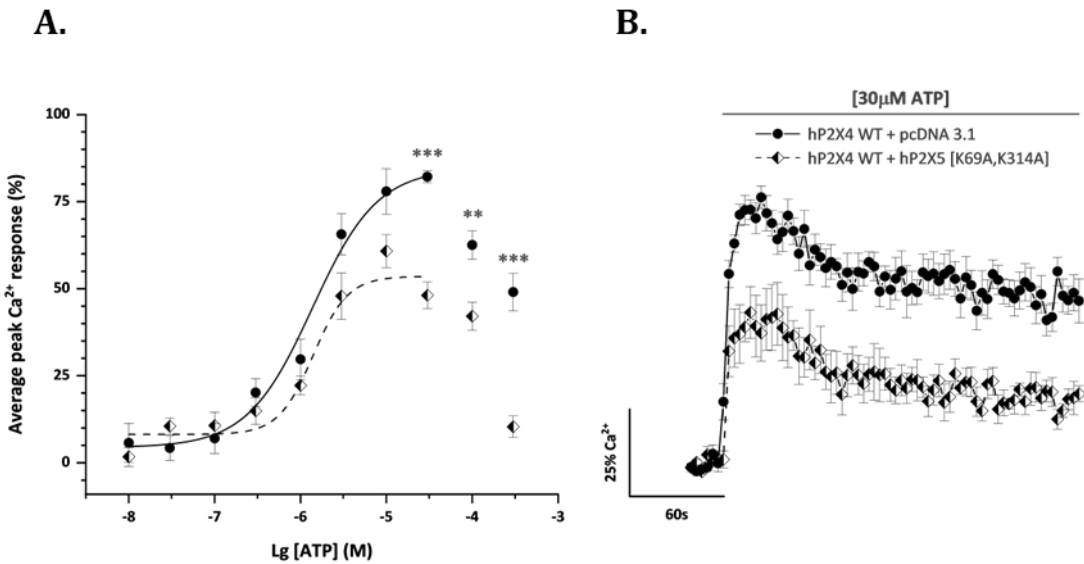


Fig 4.13. The human P2X5 [K69A, K314A] dead subunit had a dominant negative effect on human P2X4 WT ATP-evoked Ca^{2+} responses in transiently co-transfected 1321N1 parental astrocytoma cells. (A) ATP concentration-response curves for the peak magnitude of intracellular Ca^{2+} influx in the presence (half-full diamonds) and absence (closed circles) of hP2X5 [K69A, K314A]. (B) Averaged time-resolved intracellular Ca^{2+} influx elicited by 30 μM ATP in the presence (half-full diamonds) and absence (closed circles) of hP2X5 [K69A, K314A]. All data were normalised to respective maximal 100 μM Carbachol responses. Data were represented as mean \pm SEM ($N=5$).

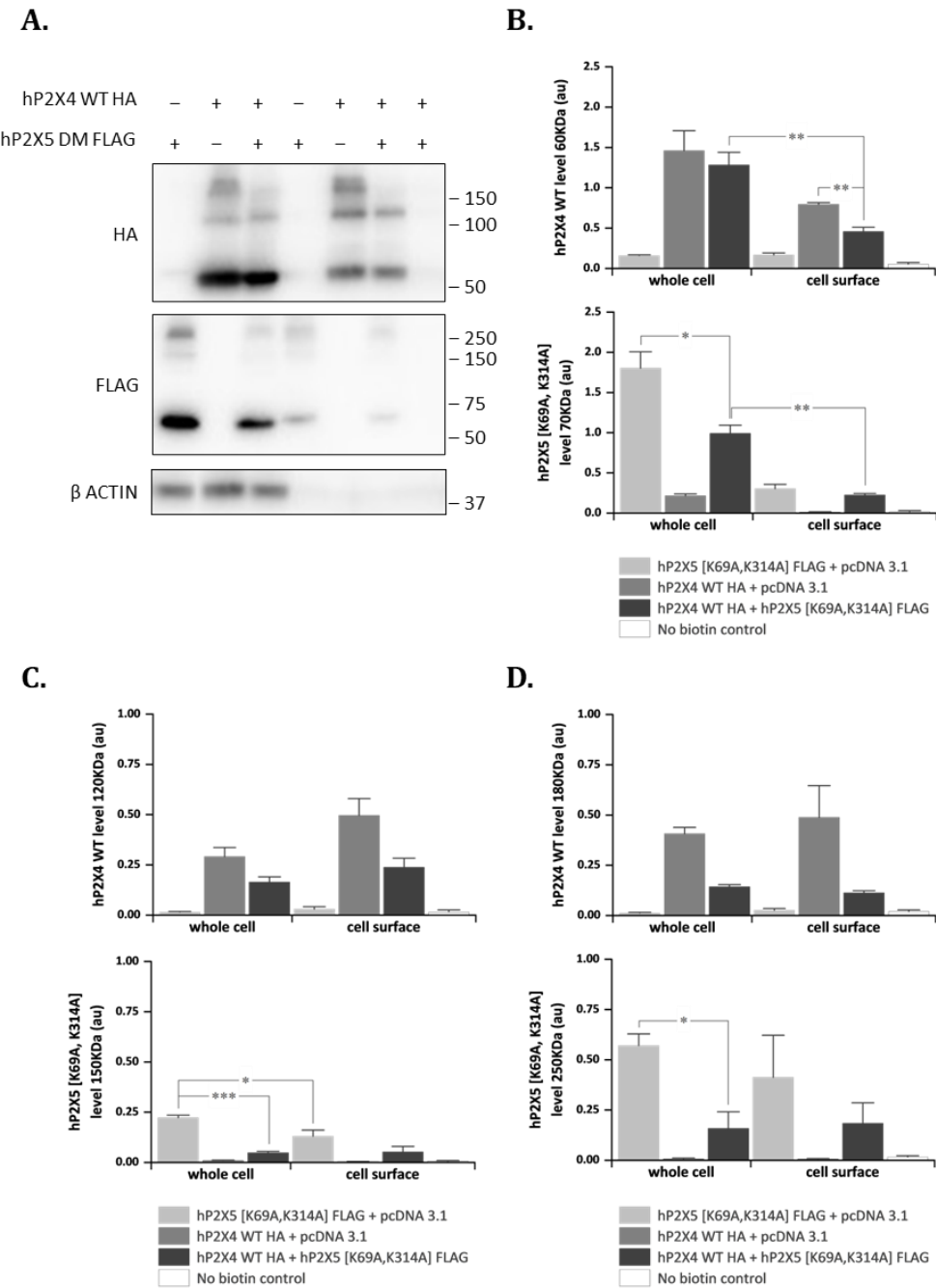


Fig 4.14. Whole-cell and cell surface expression levels of human P2X4 WT and human P2X5 [K69A, K314A] subunits in transiently co-transfected 1321N1 parental astrocytoma cells. (A) Representative immunoblot for hP2X4 WT HA-tagged protein (top), hP2X5 [K69A, K314A] FLAG-tagged protein (middle), and β -actin loading control (bottom). Molecular weight size standards were indicated in KDa. Lanes 1-3 corresponded to whole-cell samples and lanes 4-7 to cell surface protein lysates. Lane 7 was a negative control for biotin labelling. (B – D) Comparison of densitometric analysis for bands at (B) 60kDa, (C) 120kDa, (D) and 180kDa of hP2X4 WT HA-tagged (top) and hP2X5 [K69A, K314A] FLAG-tagged (bottom) protein levels relative to loading control for whole-cell and cell surface lysates. Data were represented as mean \pm SEM ($N=3$).

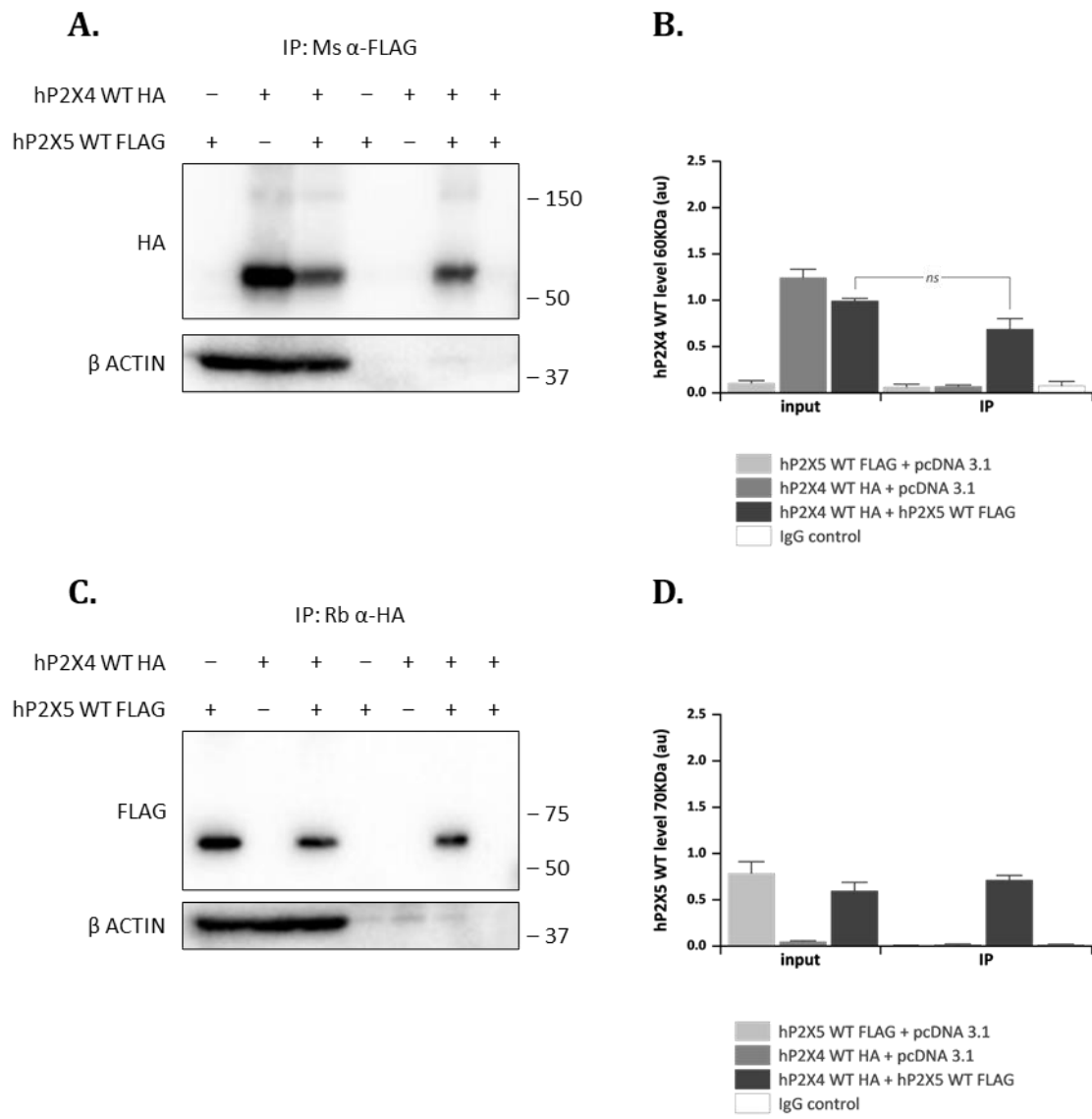


Fig 4.15. Human P2X4 WT subunits co-immunoprecipitated with human P2X5 WT subunits when transiently co-transfected in 1321N1 parental astrocytoma cells. (A) Representative immunoblot for hP2X4 WT HA-tagged protein after immunoprecipitation using anti-FLAG antibody, and for the β -actin loading control. (B) Comparison of densitometric analysis of hP2X4 WT HA-tagged protein level relative to loading control for input and co-immunoprecipitated complexes. (C) Representative immunoblot for hP2X5 WT FLAG-tagged protein after immunoprecipitation using anti-HA antibody, and for the β -actin loading control. (D) Comparison of densitometric analysis of hP2X5 WT FLAG-tagged protein level relative to loading control for input and co-immunoprecipitated complexes. Molecular weight size standards were indicated in KDa. Lanes 1-3 corresponded to whole-cell protein lysates and lanes 4-7 to immunoprecipitated protein complexes. Lane 7 was an IgG negative control for immunoprecipitation without antibody. Data were represented as mean \pm SEM ($N=3$).

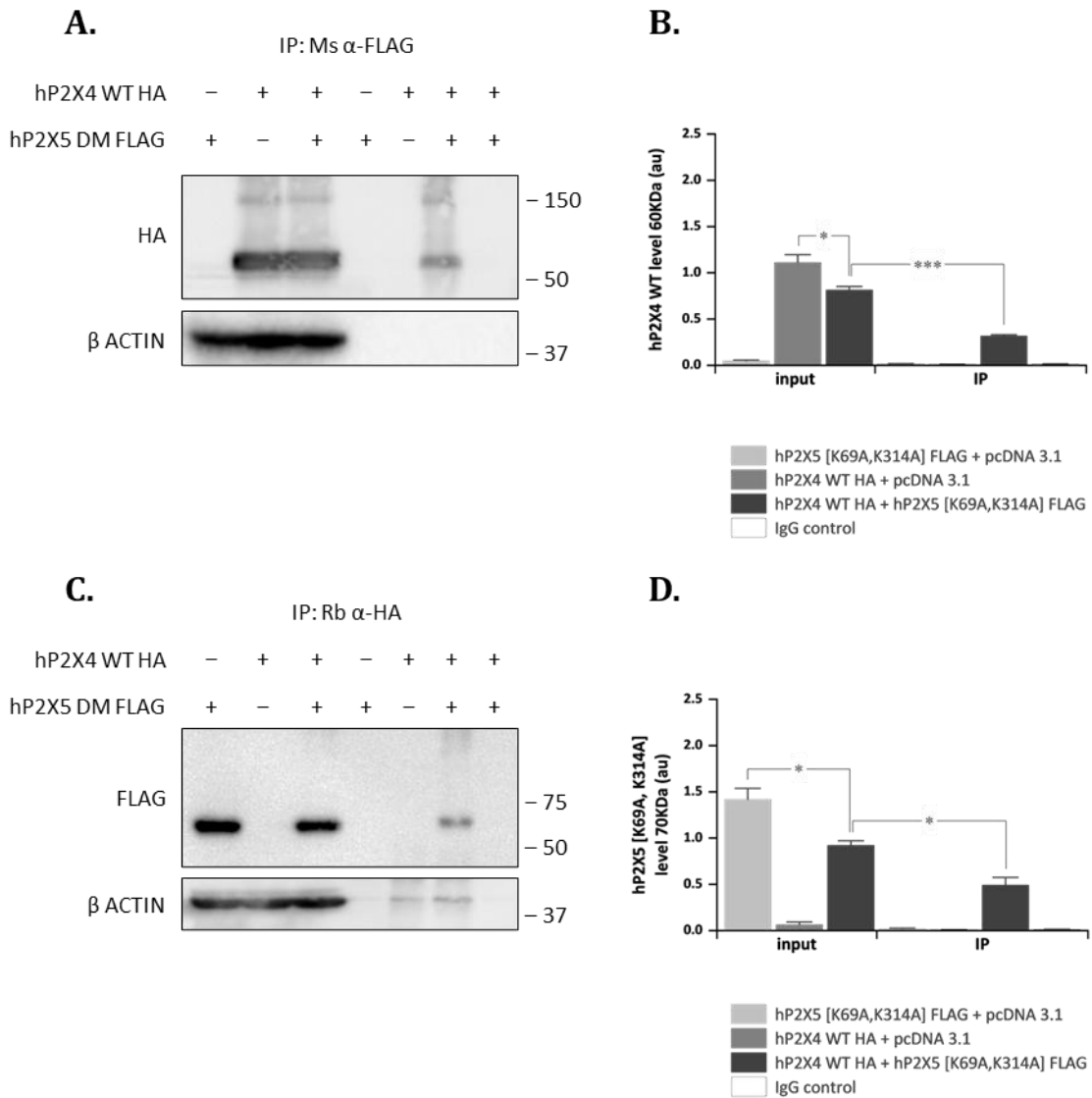


Fig 4.16. Human P2X4 WT subunits co-immunoprecipitated with human P2X5 [K69A, K314A] subunits when transiently co-transfected in 1321N1 parental astrocytoma cells. (A) Representative immunoblot for hP2X4 WT HA-tagged protein after immunoprecipitation using anti-FLAG antibody, and for the β -actin loading control. (B) Comparison of densitometric analysis of hP2X4 WT HA-tagged protein level relative to loading control for input and co-immunoprecipitated complexes. (C) Representative immunoblot for hP2X5 [K69A, K314A] FLAG-tagged protein after immunoprecipitation using anti-HA antibody, and for the β -actin loading control. (D) Comparison of densitometric analysis of hP2X5 [K69A, K314A] FLAG-tagged protein level relative to loading control for input and co-immunoprecipitated complexes. Molecular weight size standards were indicated in kDa. Lanes 1-3 corresponded to whole-cell protein lysates and lanes 4-7 to immunoprecipitated protein complexes. Lane 7 was an IgG negative control for immunoprecipitation without antibody. Data were represented as mean \pm SEM ($N=3$).

4.2.1.4 Human P2X7 subunits altered human P2X4 receptor function but did not form interaction complexes with human P2X4 subunits

Human 1321N1 parental astrocytoma cells transiently co-transfected with human P2X4 WT and human P2X7 [K64A, K311A] dead subunits behaved similarly to the ones co-transfected with human P2X4 [K67A, K313A] dead subunits instead. Thereby, the presence of human P2X7 [K64A, K311A] dead subunits had a dominant negative effect on the ATP-evoked intracellular calcium influx transiently co-transfected 1321N1 parental astrocytoma cells. This 70-80% reduction occurred in a concentration-dependent manner within a 0.3 μ M to 300 μ M concentration range compared to human P2X4 WT with pcDNA 3.1 plasmid control responses ($p<0.05$ and $p<0.001$ vs corresponding plasmid control responses, respectively; Fig 4.17A). The maximal calcium influx response was observed at 10 μ M ATP, reaching a peak magnitude of 41.3 \pm 8.62%, which was nearly 50% smaller than the corresponding calcium responses evoked in 1321N1 parental astrocytoma cells transiently co-transfected with human P2X4 WT and pcDNA 3.1 plasmid control (77.9 \pm 6.54%, $p<0.05$; Fig 4.17). Figure 4.17B showed a representative calcium response upon application of 30 μ M over time in the presence and absence of human P2X7 [K64A, K311A] dead subunits. ATP evoked a peak calcium response of only 36.7 \pm 6.76%, which was approximately 60% lower than the corresponding human P2X4 WT with pcDNA 3.1 plasmid control response ($p<0.001$; Fig 4.17), yet it was slowly desensitising and sustained over time at a 25% above baseline level (Fig 4.17B). These data were comparable to the effects seen for human P2X4 [K67A, K313A] dead subunits (24.2 \pm 1.58% 30 μ M ATP-evoked maximal response, $p>0.05$; Fig 3.33) with a slowly desensitising phase over time at about 20% above baseline (Fig 3.33B). As with the other human P2X1-6 dead receptor tools, co-transfection of human P2X7 [K64A, K311A] dead subunits did not change the ATP potency value compared to human P2X4 WT co-transfected with pcDNA 3.1 plasmid control (3.96 \pm 1.02 μ M vs 2.40 \pm 0.79 μ M, $p>0.05$; Fig 4.17A).

To accurately interpret the calcium mobilisation data, the protein expression levels of both human P2X4 WT subunits and human P2X7 [K64A, K311A] dead subunits were assessed when co-expressed with a pcDNA 3.1 plasmid control or in combination with each other. Data showed the presence of human P2X7 [K64A, K311A] dead subunits significantly reduced the amount of human P2X4 WT subunits at the cell surface by approximately 60% compared to human P2X4 WT transiently co-transfected with pcDNA 3.1 plasmid control (0.42 \pm 0.06au vs 1.02 \pm 0.12au, respectively, $p<0.01$; Fig 4.18A and B). In contrast, whole-cell expression levels remained unchanged (1.01 \pm 0.10au vs 1.48 \pm 0.16au, respectively, $p>0.05$; Fig 4.18A and B). On the other hand, 70kDa human P2X7 [K64A, K311A] dead subunits were equally expressed at the cell surface when transiently co-transfected with human P2X4 WT subunits compared to plasmid control (0.52 \pm 0.04au vs 0.34 \pm 0.12au, respectively, $p>0.05$; Fig 4.18A and B) as well as at whole-cell levels (0.64 \pm 0.18au vs 0.91 \pm 0.12au, respectively, $p>0.05$; Fig 4.18A and B). The relative amount of human P2X4 WT subunits was smaller at the cell membrane when combined with human P2X7 [K64A, K311A] compared to whole-cell co-expression levels ($p<0.01$ vs respective control; Fig 4.18A and B). The combination of the two did not affect the human P2X7 [K64A, K311A] protein amount at the cell surface compared to whole-cell co-expression levels ($p>0.05$ vs respective control; Fig 4.18A and B). Expression of human P2X4 WT subunits and human P2X7 [K64A, K311A] dead subunits was the

same when co-expressed together at the cell membrane (0.42 ± 0.06 au vs 0.52 ± 0.04 au, respectively, $p>0.05$) and at whole-cell level (1.01 ± 0.10 au vs 0.91 ± 0.12 au, respectively, $p>0.05$). Higher bands were faintly detected at approximately 120KDa and 180KDa when using anti-HA antibodies for protein detection (Fig 4.18A, C and D). Whole-cell human P2X4 WT subunits showed higher expression levels at 60KDa when combined with human P2X7 [K64A, K311A] dead subunits compared to 120KDa (1.01 ± 0.10 au vs 0.16 ± 0.07 au, respectively, $p<0.01$) and to 180KDa relative expression levels (0.06 ± 0.00 au vs 60KDa, $p<0.05$). Comparable results were obtained for human P2X4 WT subunits expression at the cell surface where bands at 60KDa predominated over 120KDa (0.42 ± 0.06 au vs 0.15 ± 0.00 au, respectively, $p<0.05$) and 180KDa relative expression levels (0.05 ± 0.02 au vs 60KDa, $p<0.01$). Higher bands were also detected at approximately 150KDa and just over 250KDa when immunoblotting with anti-FLAG antibodies (Fig 4.18A, C and D). Whole-cell human P2X7 [K64A, K311A] dead subunits were equally expressed at 70KDa, 150KDa and 250KDa when combined with human P2X4 WT subunits (0.64 ± 0.18 au for 70KDa vs 0.15 ± 0.04 for 150KDa, $p>0.05$; and 0.14 ± 0.07 au for 250KDa vs 70KDa, $p>0.05$). At the cell surface, both human P2X7 [K64A, K311A] expression levels at 70KDa and 250KDa were higher compared to expression levels at 150KDa (0.52 ± 0.04 au for 70KDa vs 0.04 ± 0.02 au for 150KDa, $p<0.001$; and 0.28 ± 0.12 au for 250KDa vs 70KDa, $p>0.05$).

Subsequently, co-immunoprecipitation assays using 1321N1 parental astrocytoma cells transiently co-transfected with human P2X4 WT HA-tagged subunits and human P2X7 WT FLAG-tagged dead subunits were performed. Remarkably, human P2X4 WT subunits did not co-immunoprecipitate with human P2X7 WT subunits when anti-FLAG antibodies were used for protein pull-down (0.05 ± 0.03 au vs input control, $p<0.01$; Fig 4.19A and B). Whole-cell input controls showed similar human P2X4 WT expression levels when co-transfected with human P2X7 WT subunits (0.86 ± 0.11 au vs 1.02 ± 0.04 au plasmid control, $p>0.05$; Fig 4.19A and B). In parallel, human P2X7 WT subunits did not co-immunoprecipitate with human P2X4 WT subunits when anti-HA antibodies were used for protein pull-down (0.02 ± 0.00 au vs input control, $p<0.05$; Fig 4.19C and D). Conversely, human P2X7 WT subunit expression levels were reduced by about 47% when transiently co-transfected with human P2X4 WT subunits compared to pcDNA 3.1 plasmid control (0.57 ± 0.07 au vs 1.06 ± 0.08 au, respectively, $p<0.05$; Fig 4.19C and D).

Accordingly, human P2X4 WT HA-tagged subunits did not co-immunoprecipitate with human P2X7 [K64A, K311A] FLAG-tagged dead subunits (0.01 ± 0.00 au vs input control, $p<0.01$; Fig 4.20A and B). There were no significant changes in human P2X4 WT whole-cell expression levels when transiently co-transfected with human P2X7 [K64A, K311A] dead subunits compared to plasmid control (1.23 ± 0.14 au vs 1.20 ± 0.11 au, respectively, $p>0.05$; Fig 4.20A and B). Reciprocal immunoprecipitation assays showed that human P2X7 WT FLAG-tagged subunits did not co-immunoprecipitate with human P2X4 WT HA-tagged subunits either (0.02 ± 0.02 au vs input control, $p<0.01$; Fig 4.20C and D). However, the relative expression levels of human P2X7 [K64A, K311A] dead subunits were significantly lower when transiently co-transfected with human P2X4 WT subunits compared to plasmid control (0.20 ± 0.01 au vs 0.34 ± 0.02 au, respectively, $p<0.01$; Fig 4.20C and D). Expression levels of human P2X7 [K64A, K311A] dead subunits were about six times smaller compared to human P2X4 WT subunits when co-transfected together ($p<0.05$; Fig 4.20). It is also important to note that human P2X7 [K64A, K311A] dead subunits

were significantly less expressed than human P2X7 WT subunits when co-transfected with pcDNA 3.1 plasmid control (0.34 ± 0.02 au vs 1.06 ± 0.08 au, respectively, $p<0.01$) and when co-transfected with human P2X4 WT subunits (0.20 ± 0.01 au vs 0.57 ± 0.07 au, respectively, $p<0.01$).

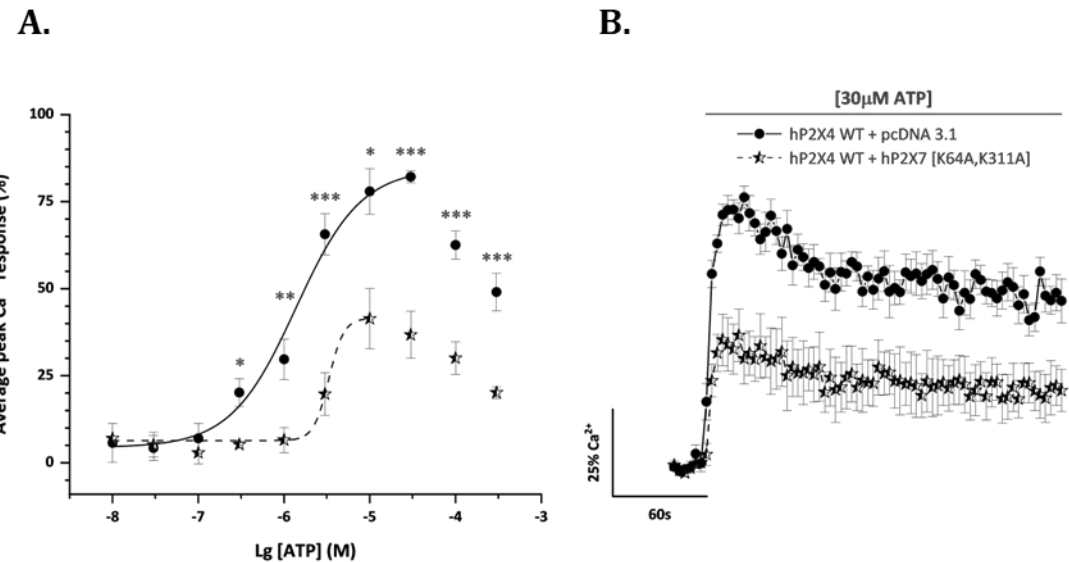


Fig 4.17. The human P2X7 [K64A, K311A] dead subunit had a dominant negative effect on human P2X4 WT ATP-evoked Ca^{2+} responses in transiently co-transfected 1321N1 parental astrocytoma cells. (A) ATP concentration-response curves for the peak magnitude of intracellular Ca^{2+} influx in the presence (half-full stars) and absence (closed circles) of hP2X7 [K64A, K311A]. (B) Averaged time-resolved intracellular Ca^{2+} influx elicited by 30 $\mu\text{M ATP}$ in the presence (half-full stars) and absence (closed circles) of hP2X7 [K64A, K311A]. All data were normalised to respective maximal 100 μM Carbachol responses. Data were represented as mean \pm SEM ($N=5$).

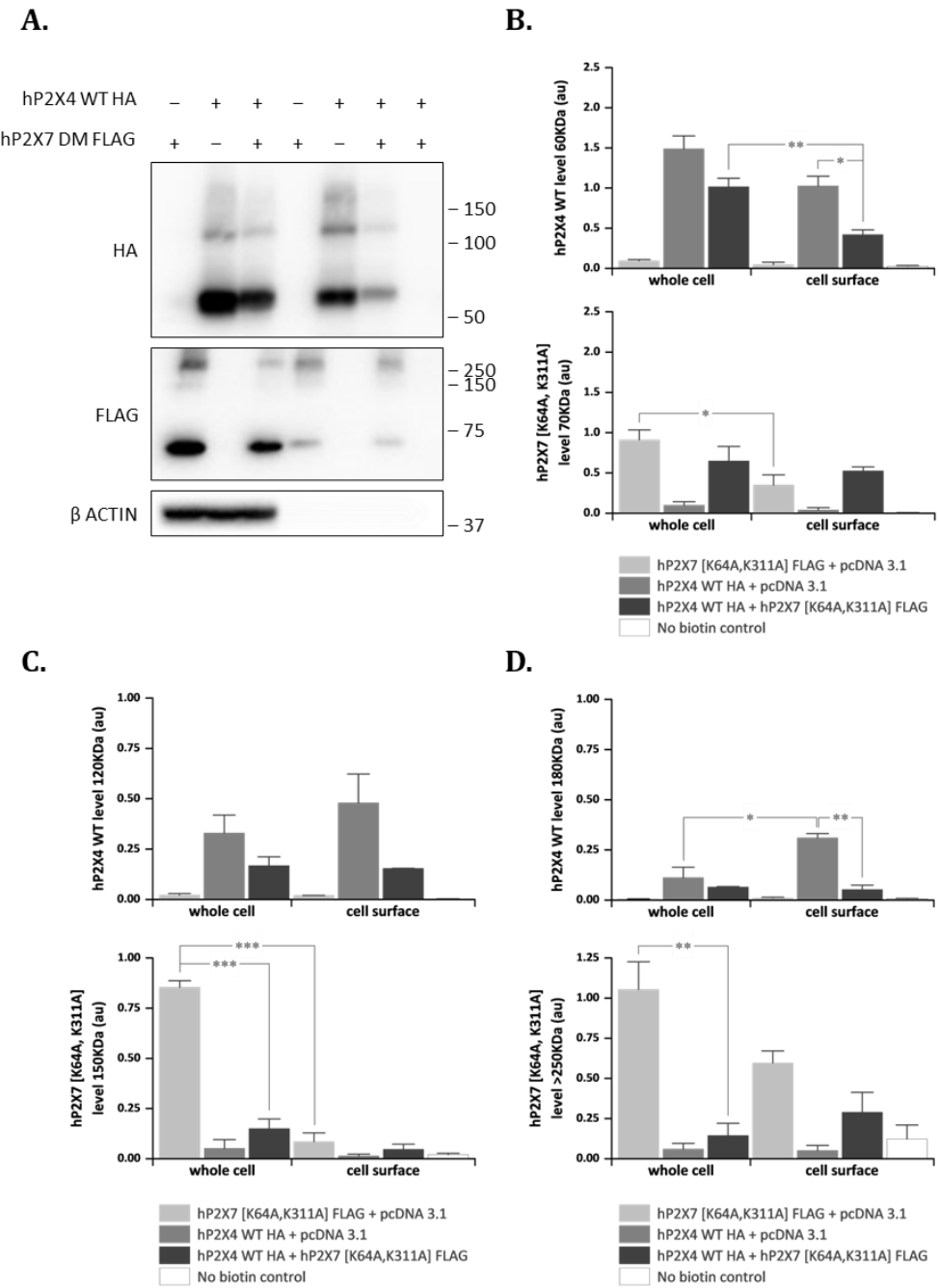


Fig 4.18. Whole-cell and cell surface expression levels of human P2X4 WT and human P2X7 [K64A, K311A] subunits in transiently co-transfected 1321N1 parental astrocytoma cells. (A) Representative immunoblot for hP2X4 WT HA-tagged protein (top), hP2X7 [K64A, K311A] FLAG-tagged protein (middle), and β-actin loading control (bottom). Molecular weight size standards were indicated in KDa. Lanes 1-3 corresponded to whole-cell samples and lanes 4-7 to cell surface protein lysates. Lane 7 was a negative control for biotin labelling. (B – D) Comparison of densitometric analysis for bands at (B) 60KDa and 70KDa, (C) 120KDa and 150KDa, (D) and 180KDa and >250KDa for hP2X4 WT HA-tagged (top) and hP2X7 [K64A, K311A] FLAG-tagged (bottom) protein levels relative to loading control for whole-cell and cell surface lysates, respectively. Data were represented as mean ± SEM ($N=3$).

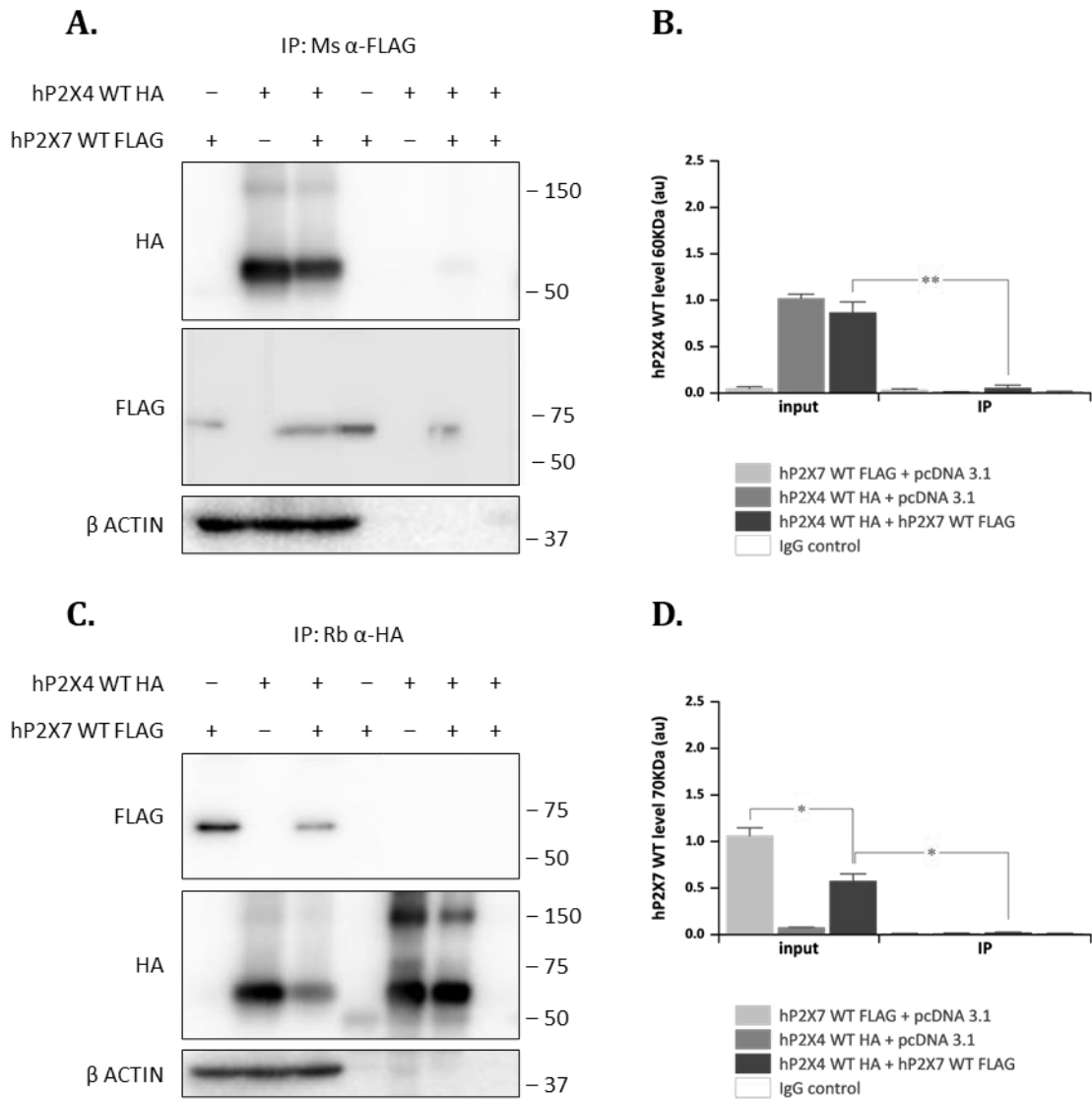


Fig 4.19. Human P2X4 WT subunits did not co-immunoprecipitate with human P2X7 WT subunits when transiently co-transfected in 1321N1 parental astrocytoma cells. (A) Representative immunoblot for hP2X4 WT HA-tagged protein after immunoprecipitation using anti-FLAG antibody (top), for hP2X7 WT FLAG-tagged anti-FLAG immunoprecipitation control (middle), and for the β -actin loading control. (B) Comparison of densitometric analysis of hP2X4 WT HA-tagged protein level relative to loading control for input and co-immunoprecipitated complexes. (C) Representative immunoblot for hP2X7 WT FLAG-tagged protein after immunoprecipitation using anti-HA antibody (top), for hP2X4 WT HA-tagged anti-HA immunoprecipitation control (middle), and for the β -actin loading control (bottom). (D) Comparison of densitometric analysis of hP2X7 WT FLAG-tagged protein level relative to loading control for input and co-immunoprecipitated complexes. Molecular weight size standards were indicated in kDa. Lanes 1-3 corresponded to whole-cell protein lysates and lanes 4-7 to immunoprecipitated protein complexes. Lane 7 was an IgG negative control for immunoprecipitation without antibody. Data were represented as mean \pm SEM ($N=3$).

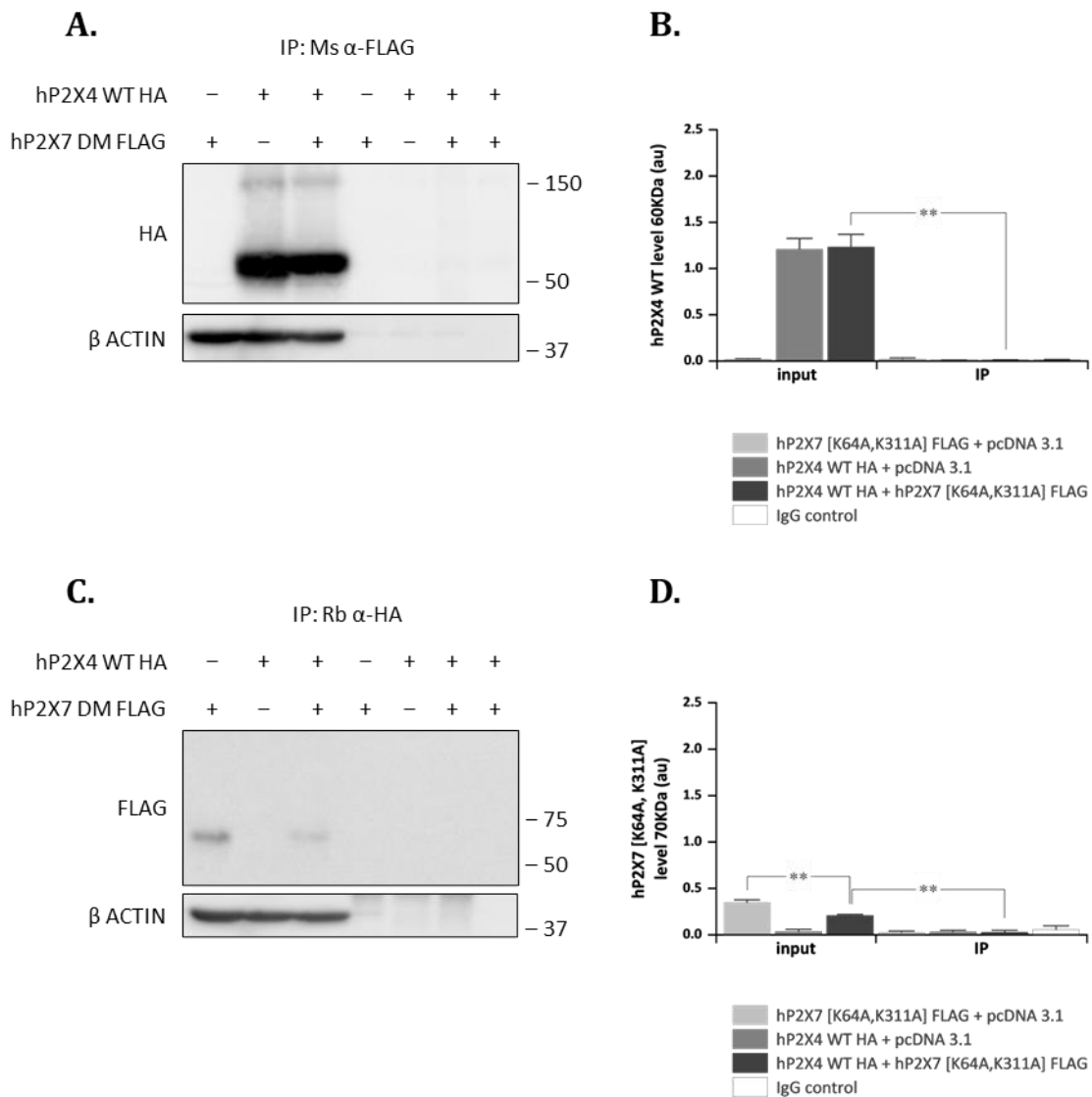


Fig 4.20. Human P2X4 WT subunits did not co-immunoprecipitate with human P2X7 [K64A, K311A] subunits when transiently co-transfected in 1321N1 parental astrocytoma cells. (A) Representative immunoblot for hP2X4 WT HA-tagged protein after immunoprecipitation using anti-FLAG antibody, and for the β-actin loading control. (B) Comparison of densitometric analysis of hP2X4 WT HA-tagged protein level relative to loading control for input and co-immunoprecipitated complexes. (C) Representative immunoblot for hP2X7 [K64A, K311A] FLAG-tagged protein after immunoprecipitation using anti-HA antibody, and for the β-actin loading control. (D) Comparison of densitometric analysis of hP2X7 [K64A, K311A] FLAG-tagged protein level relative to loading control for input and co-immunoprecipitated complexes. Molecular weight size standards were indicated in kDa. Lanes 1-3 corresponded to whole-cell protein lysates and lanes 4-7 to immunoprecipitated protein complexes. Lane 7 was an IgG negative control for immunoprecipitation without antibody. Data were represented as mean ± SEM ($N=3$).

4.2.2 Potential impacts of co-expressing human P2X4 wild-type subunits with other P2X wild-type subunits on its pharmacological properties

We hypothesised that receptor multimerisation increases the number of functional P2X receptor subtypes and the diversity of ATP signalling pathways. Besides, heteromerisation can impact the ATP binding interface between adjacent subunits and consequently change pharmacological properties and channel projection. Once the human P2X4 functional heteromeric screening for ATP was finished, I started analysing potential effects on the human P2X4 WT HA-tagged ATP concentration-response data caused by the presence of other human P2X1-7 WT FLAG-tagged subunits.

At first, whole-cell expression of all human P2X1-7 subunits transiently co-transfected with human P2X4 WT subunits was analysed. Figure 4.21 showed high expression levels for all subunits in 1321N1 parental astrocytoma cells. The human P2X4 WT specific band at 60kDa is visually thicker than the other subunits, most likely because the experimental system was optimised for human P2X4 WT responses. Complementary biotinylation experiments to check the membrane expression of each P2X subunit were not completed due to time constraints.

The reader must know that this was a pilot study, and only one biological repeat was done. Thus, the resulting data was preliminary. The analysis was assessed using the technical repeats within the same experiment tested in triplicate ($n=3$). However, more biological repeats are required to support the following information.

Calcium mobilisation assays were performed on 1321N1 parental astrocytoma cells transiently co-transfected with human P2X4 WT HA-tagged and human P2X4 FLAG-tagged subunits. Figure 4.22 showed no significant differences in the ATP-evoked concentration-response data in cells transiently co-transfected with human P2X4 WT HA-tagged and either pcDNA3.1 plasmid control or human P2X4 FLAG-tagged subunits. The maximal ATP-evoked calcium response was obtained at $3\mu\text{M}$ ATP ($89.0\pm7.86\%$ vs $65.6\pm5.89\%$ for plasmid control, $p>0.05$; Fig 4.22A). The ATP potency value remained unchanged compared to plasmid control ($1.00\pm0.25\mu\text{M}$ vs $2.40\pm0.79\mu\text{M}$ for plasmid control, $p>0.05$; Fig 4.22A). Figure 4.22B represented an averaged calcium response upon application of $30\mu\text{M}$ ATP, which reached a maximal amplitude of response of $73.7\pm11.7\%$ ($p>0.05$ vs $82.1\pm1.77\%$ for plasmid control) and slowly decayed over time, sustaining the response at approximately 60% above the baseline level.

Similarly occurred in 1321N1 parental astrocytoma cells transiently co-transfected with human P2X4 WT subunits and either human P2X1 WT, P2X3 WT or P2X5 WT subunits (Fig 4.23). Co-transfection with human P2X1 WT subunits had no effect on the human P2X4 WT ATP-evoked intracellular calcium responses, and the ATP potency value obtained was close to the one for plasmid control ($1.55\pm0.58\mu\text{M}$; Fig 4.23A and B). The maximal response was obtained at $30\mu\text{M}$ ATP ($80.3\pm14.0\%$ vs plasmid control, $p>0.05$; Fig 4.23A and B), which decayed to approximately 35% above baseline. For human P2X3 WT with human P2X4 WT co-transfected cells, the ATP-evoked calcium responses did not change at any concentrations tested compared to plasmid control with an ATP potency value of $2.39\pm1.57\mu\text{M}$ (Fig

4.23C and D). The maximal calcium response was also attained upon application of 30 μ M ATP (85.7 \pm 9.10% vs plasmid control, p>0.05; Fig 4.23C and D), sustaining the response at approximately 43% above baseline (Fig 4.23D). Likewise, the presence of human P2X5 WT subunits did not affect the human P2X4 WT ATP-evoked calcium responses, and the ATP potency value calculated was comparable to the one for plasmid control (0.78 \pm 0.30 μ M; Fig 4.23E). The maximal response was obtained at 3 μ M ATP (81.1 \pm 9.31% vs 65.6 \pm 5.89% for plasmid control, p>0.05; Fig 4.23E). A representative calcium response over time after stimulation with 30 μ M ATP is shown in Figure 4.23F, reaching a 69.3 \pm 18.8% peak response (p>0.05 vs 82.1 \pm 1.77% for plasmid control; Fig 4.23E and F) and decaying to a sustained phase over the recorded period (about 37% above baseline). A preliminary analysis of net calcium movement derived from the area under the curve data was performed to complement peak data information as detailed in sections 2.13.1 (Chapter 2) and 4.2.1.2 (Chapter 4). The AUC values obtained for human P2X1 WT and human P2X3 WT appeared smaller than the plasmid control data. The decay rates obtained upon 30 μ M ATP application were 31.7 \pm 5.50s and 43.4 \pm 7.00s for human P2X4 WT transiently co-transfected with human P2X1 WT and human P2X3 WT subunits, respectively (p>0.05 for both vs 154.4 \pm 42.4s for plasmid control). Moreover, no significant differences were detected for the area under the curve data for human P2X4 WT and human P2X5 WT transients at any concentrations tested. The decay rate value obtained after 30 μ M ATP application was 103.7 \pm 41.9s (p>0.05 vs 154.4 \pm 42.4s for plasmid control).

The presence of human P2X2 WT subunits altered the human P2X4 WT ATP-evoked calcium response in a concentration-dependent manner (Fig 4.24). Intracellular calcium responses caused by ATP concentrations ranging from 3 μ M (110.1 \pm 15.4% vs 65.6 \pm 5.89% for plasmid control, p<0.05) to 300 μ M (95.9 \pm 15.8% vs 49.0 \pm 5.36% for plasmid control, p<0.05) were significantly larger compared to corresponding plasmid control responses (Fig 4.24A). The ATP potency value obtained was 1.86 \pm 0.48 μ M (Fig 4.24A). The maximal ATP-evoked calcium response was also reached at 30 μ M ATP and was approximately two times greater than the plasmid control response (160.0 \pm 11.3% vs 82.1 \pm 1.77% for plasmid control, p<0.001; Fig 4.24). Figure 4.24B also showed a slow desensitisation phase which decayed to approximately 80% above baseline over the recorded period of time. As expected, net calcium movement analysis showed a significant increase of the ATP-evoked calcium responses in a concentration-dependent manner compared to plasmid control (e.g., AUC 312.2 \pm 16.2% vs AUC 157.3 \pm 26.7% for 30 μ M ATP, p<0.01). The decay rate upon application of 30 μ M ATP was 363.1 \pm 162.1s (p>0.05 vs 154.4 \pm 42.4s for plasmid control).

Finally, human P2X6 WT and P2X7 WT subunits inhibited human P2X4 WT ATP-evoked calcium responses (Fig 4.25). The presence of human P2X6 WT subunits significantly reduced the ATP-evoked calcium responses at concentrations of 0.3 μ M, 10 μ M, 30 μ M and 300 μ M (p<0.05, p<0.05, p<0.001, and p<0.01 vs corresponding plasmid control responses, respectively; Fig 4.25A). The ATP EC₅₀ value obtained was 1.61 \pm 0.21 μ M. The maximal calcium response was obtained upon application of 30 μ M ATP and was approximately 33% smaller than the plasmid control response (55.5 \pm 3.39% vs plasmid control, p<0.001; Fig 4.25A and B). The reduction caused by co-transfection of human P2X6 WT subunits was comparable to the reduction observed in the presence of human P2X6 [K78A, K315A] dead subunits

on human P2X4 WT ATP-evoked calcium responses. Co-transfection of human P2X7 WT subunits also reduced the ATP-evoked calcium response at concentrations of 3 μ M, 10 μ M, 30 μ M, and 300 μ M ($p<0.01$, $p<0.05$, $p<0.001$, and $p<0.01$ vs corresponding plasmid control responses, respectively; Fig 4.25C). The ATP EC₅₀ value obtained was $1.09\pm0.71\mu$ M. A 45% reduction of the peak calcium response was observed at 30 μ M ATP ($45.9\pm4.41\%$ vs plasmid control, $p<0.001$; Fig 4.25C and D). Figure 4.25D also showed a slow desensitisation phase that decayed to approximately 25% above the baseline level over the recorded time. Comparison between the effects of human P2X7 WT and P2X7 [K64A, K311A] dead subunits on the human P2X4 WT ATP-evoked calcium responses were similar at high concentrations of ATP (i.e., from 3 μ M to 300 μ M). However, the presence of human P2X7 [K64A, K311A] dead subunits caused a greater reduction of the calcium response at ATP concentrations of 1 μ M ($26.6\pm2.31\%$ vs $6.55\pm3.64\%$, $p<0.01$) and 0.3 μ M ($17.3\pm3.43\%$ vs $5.21\pm0.94\%$, $p<0.01$). Net calcium movement analysis showed similar results as the intracellular calcium peak responses for human P2X4 WT subunits transiently co-transfected with either human P2X6 WT or P2X7 WT subunits.

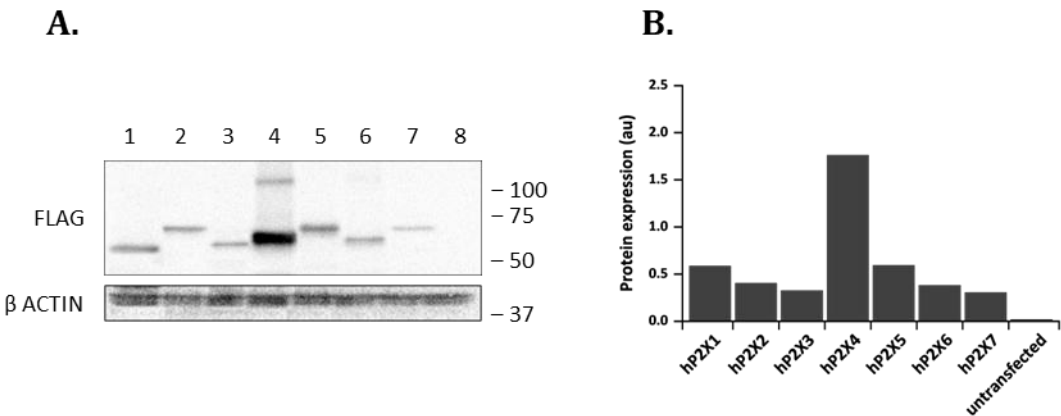


Fig 4.21. Whole-cell expression levels of human P2X1-7 WT subunits in transiently co-transfected 1321N1 parental astrocytoma cells. (A) Whole-cell immunoblot for hP2X1-7 WT FLAG-tagged subunits (lanes 1-7, respectively) and untransfected 1321N1 parental astrocytoma cells as a negative control (lane 8), with corresponding β -actin loading controls. Molecular weight size standards were indicated in KDa. (B) Comparison of densitometric analysis of hP2X1-7 WT FLAG-tagged protein levels relative to loading control for whole-cell lysates. Data were represented as mean \pm SEM ($N=1$).

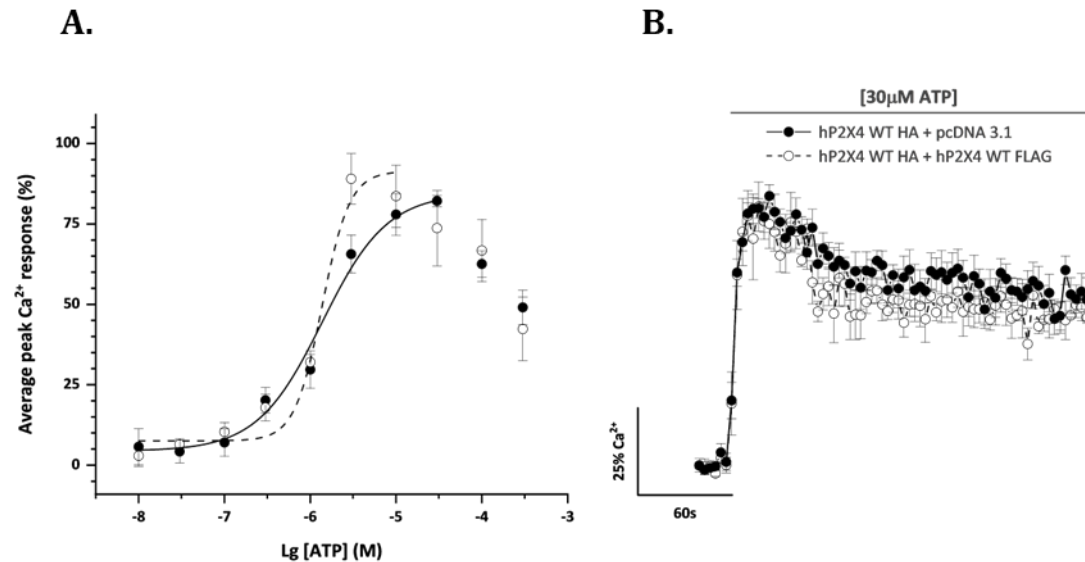


Fig 4.22. The human P2X4 WT FLAG-tagged subunit had no effect on human P2X4 WT HA-tagged ATP-evoked Ca^{2+} responses in transiently co-transfected 1321N1 parental astrocytoma cells. (A) ATP concentration-response curves for the peak magnitude of intracellular Ca^{2+} influx in the presence (open circles) and absence (closed circles) of hP2X4 WT FLAG. (B) Averaged time-resolved intracellular Ca^{2+} influx elicited by 30 μM ATP in the presence (open circles) and absence (closed circles) of hP2X4 WT FLAG. All data were normalised to respective maximal 100 μM Carbachol responses. Data were represented as mean \pm SEM ($N=3$).

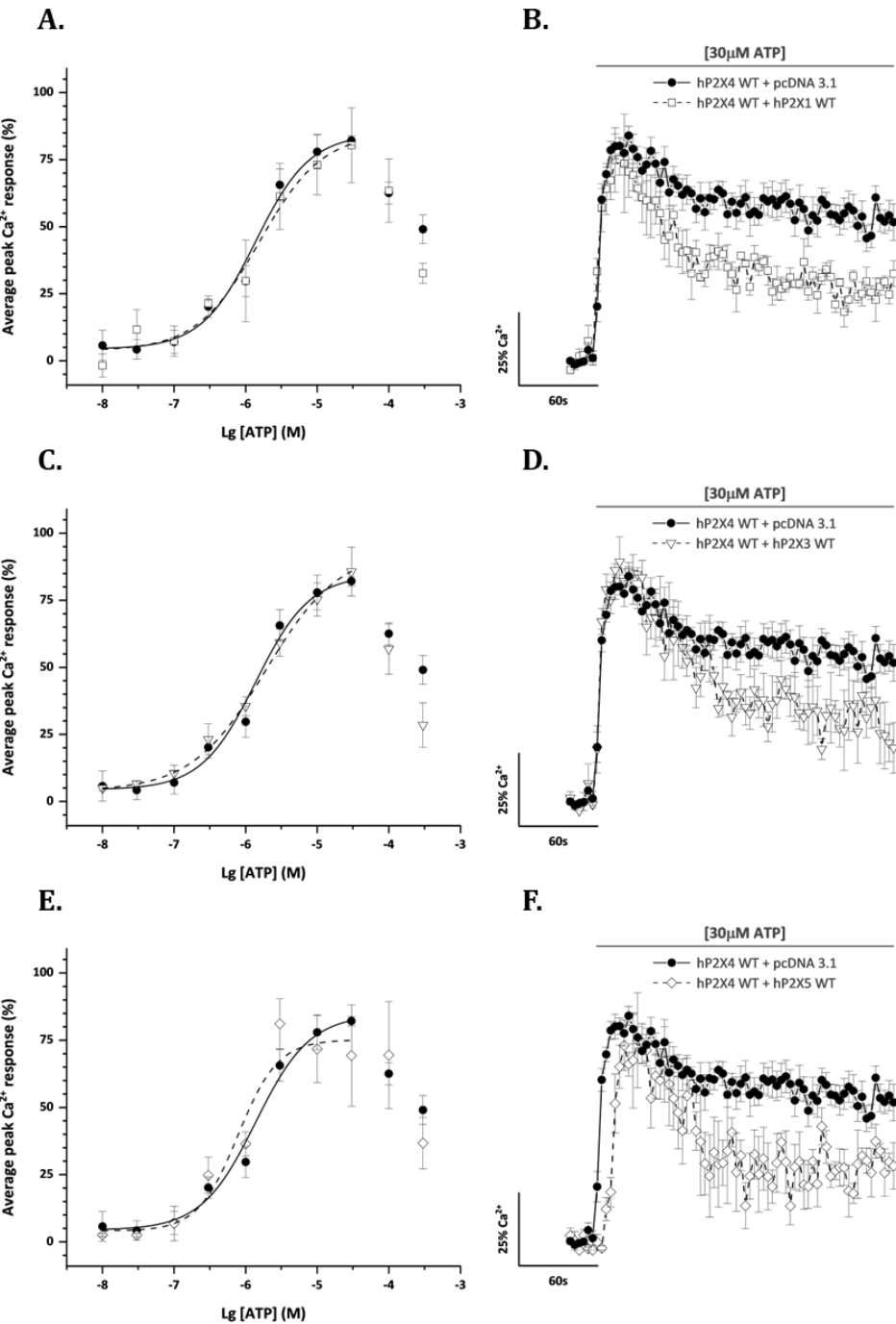


Fig 4.23. Human P2X1, P2X3 and P2X5 WT subunits had no effect on human P2X4 WT ATP-evoked Ca^{2+} responses in transiently co-transfected 1321N1 parental astrocytoma cells. (A, C, E) ATP concentration-response curves for the peak magnitude of intracellular Ca^{2+} influx in the presence (open shapes) and absence (closed circles) of (A) hP2X1 WT, (C) hP2X3 WT, and (E) hP2X5 WT. (B, D, F) Averaged time-resolved intracellular Ca^{2+} influx elicited by $30\mu\text{M ATP}$ in the presence (open shapes) and absence (closed circles) of (B) hP2X1 WT, (D) hP2X3 WT, and (F) hP2X5 WT. All data were normalised to respective maximal $100\mu\text{M Carbachol}$ responses. Data were represented as mean \pm SEM ($N=1$ in triplicate).

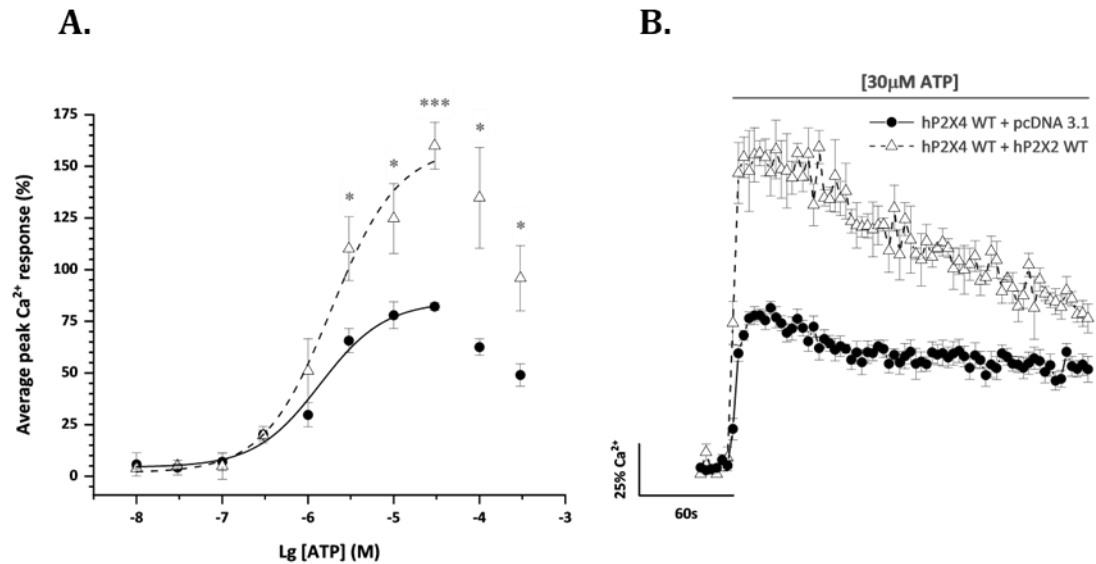


Fig 4.24. Effects of human P2X2 WT subunit co-transfection on the human P2X4 WT ATP-evoked Ca^{2+} responses in transiently co-transfected 1321N1 parental astrocytoma cells. (A) ATP concentration-response curves for the peak magnitude of intracellular Ca^{2+} influx in the presence (open triangles) and absence (closed circles) of hP2X2 WT subunits. (B) Averaged time-resolved intracellular Ca^{2+} influx elicited by $30\mu\text{M}$ ATP in the presence (open circles) and absence (closed circles) of hP2X2 WT subunits. All data were normalised to respective maximal $100\mu\text{M}$ Carbachol responses. Data were represented as mean \pm SEM ($N=1$ in triplicate).

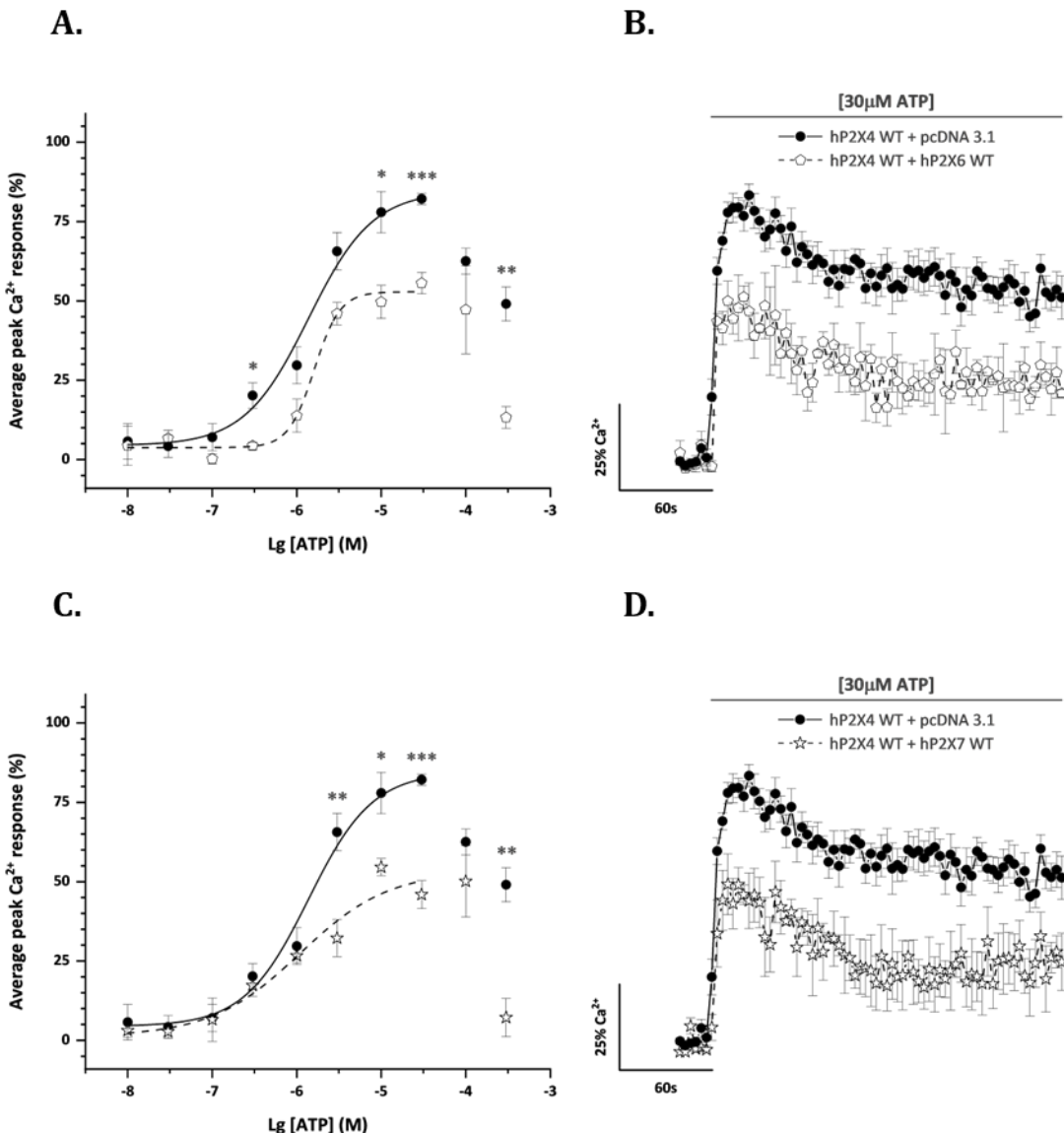


Fig 4.25. Human P2X6 and P2X7 WT subunits had an inhibitory effect on human P2X4 WT ATP-evoked Ca^{2+} responses in transiently co-transfected 1321N1 parental astrocytoma cells. (A, C) ATP concentration-response curves for the peak magnitude of intracellular Ca^{2+} influx in the presence (open shapes) and absence (closed circles) of (A) hP2X6 WT and (C) hP2X7 WT. (B, D) Averaged time-resolved intracellular Ca^{2+} influx elicited by $30\mu\text{M ATP}$ in the presence (open shapes) and absence (closed circles) of (B) hP2X6 WT and (D) hP2X7 WT. All data were normalised to respective maximal $100\mu\text{M Carbachol}$ responses. Data were represented as mean \pm SEM ($N=1$ in triplicate).

4.3 Discussion

In this chapter, we systematically examined functional interactions of the human P2X4 wild-type subunit following the experimental methodology determined in Chapter 3. The process of identification of potential human P2X4 heteromers began with the establishment and validation of the dead receptor experimental system in transiently co-transfected human 1321N1 parental astrocytoma cells. After its characterisation, a thorough functional and biochemical interaction screening was carried out. We discovered some functional and non-functional human P2X subunits that interacted with human P2X4 wild-type subunits. These are thoroughly discussed in the following pages and Table 4.2 provides a summary of the effects of human P2X dead subunits on the human P2X4 WT 30 μ M ATP-evoked calcium responses and includes positive and negative co-immunoprecipitation data to visually guide the reader through each combination.

The reader should keep in mind that the present analysis cannot distinguish between different numbers of ligand binding sites and different subunit arrangements. As a reminder, the FlexStation 3 instrument measures an average calcium influx response of a confluent well and transient co-transfection of human P2X4 wild-type subunits and human P2X dead subunits could result in different receptor expression profiles. These apply to all human P2X4 and P2X dead subunit combinations and might include: human P2X4 wild-type homomers, human P2X dead homomers, mixed human P2X4 wild-type and P2X dead homomers, human P2X4 WT/P2X dead receptors, mixed human P2X4 wild-type homomers and P2X4 WT/P2X dead receptors, and certainly some untransfected cells. Besides, if any heteromeric receptors formed, we could not discern between potential subunit combinations, i.e., two human P2X4 wild-type subunits and one P2X dead subunit or one human P2X4 wild-type with two dead P2X subunits. Considering these limitations, we could not make any assumptions about the formation of heteromeric human P2X4 channels and their stoichiometry using this experimental system.

Table 4.2. Summary of the effects of human P2X dead subunits on the human P2X4 WT 30μM ATP-evoked calcium responses and co-immunoprecipitation data.

Human P2X4 WT +	EC ₅₀ (μM)	P value	E _{max} (μM)	Efficacy (%)	P value	WT-WT CoIP	WT-DM CoIP
pcDNA 3.1	2.40±0.79		30	82.1±1.77			
P2X4 [K67A, K313A]	1.11±0.30	ns	30	24.2±1.58	<0.01	Yes	Yes
P2X1 [K68A, K309A]	1.58±0.26	ns	30	43.0±7.03	<0.01	Yes	Yes
P2X2 [K81A, K319A]	1.32±0.03	ns	30	72.1±5.68	ns	Yes	/
P2X3 [K63A, K299A]	1.32±0.03	ns	30	74.5±10.1	ns	No	/
P2X5 [K69A, K314A]	1.76±0.43	ns	30	48.1±3.83	<0.001	Yes	Yes
P2X6 [K78A, K315A]	5.20±2.64	ns	30	58.8±5.80	<0.01	Yes	/
P2X7 [K64A, K311A]	3.96±1.02	ns	30	36.7±6.76	<0.01	No	No

CoIP, co-immunoprecipitation; ns, non-significant. Statistical analysis was performed against the respective EC₅₀ and efficacy values obtained for cells transiently co-transfected with human P2X4 WT and pcDNA 3.1 plasmid control.

4.3.1 Human P2X4 subunits functionally interacted with human P2X1 subunits

The P2X1 receptor is the predominant P2X subunit in most smooth muscle cells lining the arteries, vas deferens, and urinary bladder. It is also found in platelets, megakaryocytes, and other immune cells, contributing to platelet development, coagulation, and inflammatory responses (Burnstock & Knight, 2004; Bennetts et al., 2022).

In this study, substitutions of K68 and K309 of the human P2X1 receptor by alanine residues caused a significant reduction in human P2X4 wild-type ATP-evoked intracellular calcium responses in a concentration-dependent manner (Fig 4.2). These results inferred that a wild-type P2X4 subunit did not rescue channel function when co-expressed with a human P2X1 [K68A, K309A] dead subunit, suggesting that human P2X1 double mutant subunits had a dominant negative effect in channel function. Human P2X1 receptors are known to be fast desensitising amongst the P2X receptor family (North, 2002). The 30 μ M ATP-evoked calcium response was reduced by approximately 50% when human P2X1 dead subunits were present, but it was sustained at 35% above baseline levels over the recorded time, suggesting conservation of the slow desensitisation characteristics of the human P2X4 receptors (Fig 4.2B). The affinity for ATP remained unchanged by the presence of human P2X1 [K68A, K309A] dead subunits ($1.58 \pm 0.26\%$ vs $2.40 \pm 0.79\mu$ M for plasmid control, $p>0.05$; Fig 4.2A), indicating that the number of functional human P2X4 wild-type receptors at the cell membrane was not affected by co-transfection with human P2X1 [K68A, K309A] dead subunits. A smaller amount of 60KDa human P2X4 wild-type subunits was detected at the cell membrane when co-expressed with human P2X1 dead subunits (Fig 4.1 and 4.3A-B). This reduction could be explained by an increment in the expression of human P2X4 wild-type 120KDa and 180KDa bands corresponding to dimeric and trimeric molecular weight species at the cell membrane where functional receptors are presumed to form (Fig 4.3; Nicke et al., 2005). Moreover, physical subunit interactions were observed for human P2X4 wild-type with human P2X1 [K68A, K309A] dead subunits (Fig 4.5). The co-immunoprecipitated human P2X4 wild-type protein levels were significantly reduced from the whole-cell input control when co-expressed with human P2X1 [K68A, K309A] dead subunits. This had three possible explanations: i) some interaction complex was retained in higher phases of the SDS-PAGE gel electrophoresis as fainter 180KDa bands were detected, ii) anti-FLAG antibodies might have a lower affinity for their epitope as previously reported, so a smaller amount of human P2X1 dead subunits would be purified affecting the detection of human P2X4 wild-type, or iii) not all human P2X4 subunits interacted with human P2X1 dead subunits. Co-immunoprecipitation experiments using human P2X1 wild-type subunits confirmed physical interaction between human P2X4 and P2X1 subunits (Fig 4.4). Similarly, co-immunoprecipitated levels of human P2X4 wild-type subunits were significantly reduced compared to input control, but this time the amount of human P2X1 wild-type precipitate was also smaller (Fig 4.4). The reported monomeric weight for glycosylated P2X1 subunits is 58KDa (Rettinger et al., 2000) which aligns with what we observed. Higher molecular species for either human P2X1 wild-type or dead subunits were observed in co-immunoprecipitated lanes. The reduction in human P2X1 protein expression could be due to low antigen-antibody affinity to detect FLAG-tagged proteins, although this was not an issue for immunoblot detection as it was for protein purification in our experimental system.

Another probable explanation would be that not all human P2X1 wild-type subunits interacted with human P2X4 wild-type subunits. Pilot data showed that the presence of human P2X1 wild-type subunits did not affect the efficacy and potency values of the human P2X4 wild-type ATP-evoked intracellular calcium responses (Fig 4.23A-B). At 30 μ M ATP, the calcium response seemed to desensitise slightly faster whilst maintaining a lower sustained response over time compared to homomeric human P2X4 receptor populations (Fig 4.23A-B), suggestive of a mixed pharmacological profile. In this pilot study, the reading settings were set to 3-second sampling, so we potentially missed some effects caused by the co-expression of human P2X1 wild-type subunits as they are fast desensitising (North, 2002).

In summary, both functional and biochemical data results insinuated that the formation of heteromeric complexes between human P2X4 wild-type and P2X1 [K68A, K319A] dead subunits and between human P2X4 and P2X1 wild-type subunits possibly occurred. We confirmed that both ectodomain lysines K69 and K319 were also important for ATP recognition and human P2X1 receptor activation. Using the FlexStation 3 device and ATP to assess the functional properties of potential heteromeric P2X1/4 receptors had many limitations. Taking advantage of the distinct characteristics of homomeric P2X1 and P2X4 receptors would be more suitable in the future. For example, P2X1 receptors are fast desensitising, activated by $\alpha\beta$ -MeATP and highly sensitive to the antagonists Suramin and TNP-ATP, whereas P2X4 receptors are slowly desensitising and relatively insensitive to both $\alpha\beta$ -MeATP and such antagonists (North, 2002).

We evidenced that functional subunit interaction between human P2X4 and P2X1 subunits probably occurred in our recombinant system. We hypothesised that these interactions could occur at both intracellular and cell membrane levels. Initially, co-purification experiments failed to show an interaction between rat P2X1 and P2X4 subunits in HEK293 cells (Lê et al., 1998; Torres et al., 1999) but was later found by co-purification and subsequent Blue Native polyacrylamide gel electrophoresis (BN-PAGE) analysis in *Xenopus laevis* oocytes (Nicke et al., 2005). Whilst P2X1 subunits show overlapping distribution with P2X4 subunits in several tissues, little evidence for a P2X1/4 heteromer in native tissues has been provided so far. In vascular smooth muscle cells, both P2X1 and P2X4 receptors modulate arterial vasoconstriction and some functional studies suggested the presence of P2X1/4 heteromers with mixed electrophysiological properties (Conant et al., 2008; Harhun et al., 2014; Nichols et al., 2014). Thus, investigation of whether P2X1 and P2X4 subunits form heteromeric receptors is critical for understanding their physiological roles and for the development of more selective therapeutics to treat hypertension and other symptoms associated with cardiovascular disease. Previous studies reported a role for P2X1 homomers and possibly P2X1/4 heteromeric receptors in urinary bladder contraction (Kennedy et al., 2007). Both subtypes also participate in the modulation of inflammation (Burnstock, 2016).

Human P2X4 wild-type receptor expression was reduced at the cell membrane when co-expressed with human P2X1 dead subunits, suggestive of interaction during protein formation and trafficking to the cell membrane. The lack of high molecular weight species for human P2X4 wild-type subunits, human P2X1 wild-type and dead subunits in co-immunoprecipitated complexes are suggestive of monomeric

interactions over dimeric and trimeric interactions, which are more likely to occur at the cell membrane and where functional receptors exert their extracellular signalling roles. Besides, the combination of human P2X1 and P2X4 wild-type subunits did not reflect on a different ATP pharmacological profile in our pilot data. P2X1 and P2X4 subtypes have been reported as highly mobile proteins at the cell membrane, so an intracellular interaction during trafficking might also be possible (Ennion & Evans, 2002; Bobanovik et al., 2002).

4.3.2 Human P2X2 subunits formed interaction complexes with human P2X4 subunits but did not alter their receptor function

P2X2 receptors are widely expressed in the Central Nervous System (CNS) and, together with P2X3 receptors, account for practically all sensory nerve excitation mediated by ATP (Lewis et al., 1995; Cockayne et al., 2005). They are also expressed in the carotid body contributing to detecting oxygen, carbon dioxide, and blood pH levels, and stimulating afferent nerves in case of hypoxia (Rong et al., 2003). Thus, P2X2 receptors might play a role in cardiovascular and respiratory function. The P2X2 receptors are found in various parts of the inner ear, such as the cochlea, sensory hairs, and spiral ganglion neurons, where they process ATP signals regulating hearing sensitivity (George et al., 2019). Co-localisation with P2X4 receptors was reported in some CNS neurons where both subtypes play a role in ATP-mediated synapses (Rubio & Soto, 2001).

Our results showed no significant effects on human P2X4 wild-type ATP-evoked intracellular calcium responses when co-transfected with human P2X2 [K81A, K319A] dead subunits (Fig 4.8). The sensitivity to ATP also remained unchanged ($1.32 \pm 0.03 \mu\text{M}$ vs $2.40 \pm 0.79 \mu\text{M}$ for plasmid control, $p > 0.05$; Fig 4.8A), suggesting the number of functional human P2X4 wild-type receptors at the cell membrane was not affected. Whole-cell and cell surface expression levels for human P2X2 [K81A, K379A] were high (Fig 4.1C-D). However, potential differences in expression levels when co-transfected with human P2X4 wild-type subunits have not been investigated yet. Co-expression of human P2X4 wild-type and P2X2 wild-type subunits in human astrocytoma cells caused a 2-fold increase in ATP-evoked intracellular calcium responses while the ATP potency remained the same (Fig 4.24). A representative time-resolved calcium response upon application of $30 \mu\text{M}$ ATP showed a slightly faster activation of the overexpressed receptors with a much slower desensitisation phase over the recorded time (4.24B). In cells co-expressing these receptors, the summation of the response produced by each receptor expressed individually would suggest two independent pools of homomeric receptors. Although these data suggested that ATP-evoked calcium responses resulted from the addition of homomeric human P2X2 wild-type responses and homomeric P2X4 wild-type responses, we should also test the ATP-evoked calcium response in astrocytoma cells only expressing human P2X2 wild-type receptors for completeness. Interestingly, co-immunoprecipitation assays showed reciprocal interaction complexes formed between human P2X2 and human P2X4 wild-type subunits (Fig 4.11). Whole-cell input lanes showed a fainter but not significantly different human P2X2 wild-type band when co-expressed with human P2X4 wild-type subunits compared to plasmid control, while human P2X4 wild-type subunit expression levels remained unchanged (Fig 4.11). Differences in cell membrane expression levels, when

human P2X2 and P2X4 wild-type subunits are co-expressed, remain to be assessed. The co-immunoprecipitated human P2X4 wild-type protein levels were significantly reduced from the whole-cell input control when co-expressed with human P2X2 wild-type subunits (Fig 4.11). This had three possible explanations: i) some interaction complex was retained in higher phases of the SDS-PAGE gel electrophoresis as weaker 180KDa bands were detected (Fig 4.11A), ii) anti-FLAG antibodies might have a lower affinity for their epitope as previously described, or iii) not all human P2X4 subunits interacted with human P2X2 wild-type subunits. Curiously, the human P2X4 wild-type subunit expression levels were three times larger than the amount of human P2X2 wild-type subunits in the co-immunoprecipitated complexes ($p<0.001$) and the same occurred for whole-cell input controls when both subunits were co-expressed ($p<0.01$). These results are suggestive of potential interactions in the form of homotrimers rather than receptor heteromers. However, due to limitations in our experimental system, we cannot draw any conclusions on possible subunit/receptor arrangements. Another group reported homomeric interactions between P2X2 and P2X4 receptors using co-immunoprecipitation approaches, *in situ* proximity ligation assays, and Atomic Force Microscopy imaging (Antonio et al., 2011, 2014). Despite this, intracellular calcium measurements evoked by ATP failed to show evidence for potential functional human P2X4 wild-type and P2X2 [K81A, K319A] dead subunit interactions, even if they occurred in the form of homotrimeric dimers. We determined that using $\alpha\beta$ -MeATP or Ivermectin might be better tools to investigate possibly missed effects of human P2X2 [K81A, K319A] dead subunits on the human P2X4 wild-type receptor pharmacological profile since they only affect human P2X4 receptors (Fig 3.13E-F and 3.36E-F; Priel & Silberberg, 2004). On the other hand, ATP- γ -S acted as a full agonist at human P2X2 wild-type receptors (Lynch et al., 1999) but did not evoke any responses via human P2X4 receptors (Fig 3.14A-B) in our system, thus it could also be used to detect any functional interactions between human P2X4 wild-type and P2X2 [K81A, K319A] dead subunits. Similarly, human P2X2 receptors are more sensitive to blockade by PPADS than human P2X4 receptors (Lynch et al., 1999).

Previous studies evidenced no interaction between rat P2X4 and rat P2X2 subunits using co-immunoprecipitation studies (Torres et al., 1999), Fluorescence Resonance Energy Transfer (FRET) and Bioluminescence Resonance Energy Transfer (BRET) assays that determinate the approach between two molecules within several nanometres, a distance sufficiently close for protein interactions to occur, as well as using Bimolecular Fluorescence Complementation (BiFC) assays which enable visualisation of protein interactions in living cells (Compan et al., 2012). Our results were more consistent with a strong functional and biochemical study that evidenced the formation of dimeric homotrimers between rat P2X2 and rat P2X4 receptors with P2X2-like pharmacology (Hugel & Schlichter, 2000; Rubio & Soto, 2001; Antonio et al., 2009) because a higher 180KDa band corresponding to the trimeric human P2X4 wild-type receptor co-immunoprecipitated with human P2X2 wild-type subunits in our experimental system (Fig 4.11A; Nicke et al., 2005). These conclusions were later confirmed by co-purification of P2X2, P2X4 and P2X6 subunits and by Atomic Force Microscopy imaging (Antonio et al., 2014).

4.3.3 Human P2X4 subunits did not functionally interact with human P2X3 subunits

P2X3 receptors are found in the Central Nervous System, mainly in sensory neurons of the dorsal root ganglia. P2X2 and P2X3 account for virtually all sensory nerve excitation mediated by ATP (Lewis et al., 1995; Cockayne et al., 2005). P2X3 receptors regulate inflammatory and neuropathic pain transmission and perception. They are also expressed in the urinary tract, modulating urinary bladder reflexes (Cockayne et al., 2005). Gefapixant is a novel drug for the treatment of chronic refractory cough or unexplained cough, which antagonises P2X3 and P2X2/3 receptors found in afferent neurons innervating the respiratory lining (Richards et al., 2019; Smith et al., 2020). Together with P2X2/3 heteromeric receptors, they are also involved in taste perception (Smith et al., 2020; Taruno et al., 2021).

Even though human P2X3 [K63A, K299A] dead subunits showed good protein expression levels at whole-cell and cell membrane lysates (Fig 4.1C-D), our study showed no significant effects of human P2X4 wild-type ATP-evoked intracellular calcium responses when co-transfected with human P2X3 [K63A, K299A] dead subunits (Fig 4.9). A significant reduction of ATP-evoked calcium responses was only evident upon application of 300 μ M ATP. At 300 μ M ATP, the decline in efficacy of the ATP-evoked calcium responses over time was significantly faster compared to plasmid control and decayed to baseline levels. These reflected potential effects of P2X3 [K63A, K299A] dead subunit co-transfection on the desensitisation phase of the human P2X4 wild-type receptor but only at high concentrations of ATP (τ 12.82 \pm 2.01s vs τ 28.53 \pm 1.17s, p<0.001; Fig 4.10B). Accordingly, no human P2X4 and P2X3 wild-type interaction complexes were observed in our co-immunoprecipitation data (Fig 4.12). A fainter 60kDa human P2X4 wild-type specific band was detected once, but its relative protein expression amount was not statistically significant from that of negative controls (Fig 4.12A-B). Similarly, a fainter 60kDa human P2X3 wild-type specific band was observed once in the co-immunoprecipitated lane, but its expression was not significantly different to the immunoprecipitation negative controls (Fig 4.12C-D). These results emphasise the importance of performing several experimental repeats ‘N’ and including individually and combined co-transfected samples for input and immunoprecipitation protein expression controls, as well as antibody IgG-beads specific binding controls. All these measures contributed to ensure the correct interpretation of the protein interaction data. We expected that co-expression of human P2X4 and P2X3 wild-type subunits would produce a cumulative calcium response produced by homomeric receptor but, co-expression of human P2X3 wild-type subunits did not affect the human P2X4 wild-type ATP-evoked maximal calcium responses or ATP potency (Fig 4.23C-D). Although these results were obtained from an N=1 pilot study, the most reasonable explanation was that the reading settings were not set to the fastest 1-second sampling but to the standard 3-second, so we possibly missed the real effects caused by human P2X3 wild-type subunits.

In conclusion, human P2X3 [K63A, K299A] dead subunits did not have dominant negative effects on ATP-evoked human P2X4 wild-type channel function. While co-immunoprecipitation data to discard functional interactions between human P2X4 wild-type and human P2X3 [K63A, K299A] dead subunits still needs to be addressed, no physical interaction occurred between human P2X4 and P2X3 wild-type

subunits which aligns with previous co-purification studies in HEK293 cells (Torres, et al., 1999). No other studies have reported functional evidence of whether P2X3/4 heterotrimers exist or not. Using Gefapixant to block human P2X3 receptors or analysing the desensitisation phase upon $\alpha\beta$ -MeATP application would complement our functional studies to confirm these results.

4.3.4 Human P2X4 subunits functionally interacted with human P2X5 subunits containing exon 10

Analysis of the human genome showed that the P2X5 gene occurs as two alleles, namely G and T. Sequences with thymidine (T) will be recognised during mRNA processing and will be translated to a ‘full-length’ P2X5 receptor; however, sequences with a guanine (G) at this position will be read as the consensus for RNA splicing during mRNA processing and will be translated to a truncated P2X5 receptor that does not include exon 10. Exon 10 is 22 amino acids long toward the C-terminus from the inner end of the second transmembrane domain (TM2). Truncation of the TM2 leads to the misfolding of P2X5 subunits and their retention in the cytoplasm by the endoplasmic reticulum (Duckwitz et al., 2006). The common isoform of human P2X5 receptors is the truncated non-functional channel, with only 14% of individuals estimated to form functional homomeric P2X5 receptors (Bo et al., 2003; King, 2022), although this percentage may grow as more humans are screened.

The number of functional studies of human P2X5 receptors is limited, mainly because a functional receptor was initially thought to not exist in humans. Recombinant human P2X5 receptors containing all exons produced robust and slowly desensitising currents upon application of ATP in HEK293, 1321N1 human astrocytoma cells and *Xenopus laevis* oocytes (Bo et al., 2003; Schiller et al. 2022). Unlike other P2X receptors, the P2X5 receptor is also permeable to chloride ions (Bo et al., 2003; Schiller et al., 2022). P2X5 mRNA is well expressed by developing skeletal muscle cells, so P2X5 receptors might be involved in the development, growth, and remodelling of bones (Meyer et al., 1999; Ruppelt et al., 2001). Functional P2X5 receptors may also play a secondary role in inflammation since high expression levels were also found in lymphocytes (Kotnis et al., 2010).

Human P2X5 K69A, K314A] dead subunits caused a significant reduction of the human P2X4 wild-type ATP-evoked calcium responses while its ATP potency remained unaltered ($1.76 \pm 0.43 \mu\text{M}$ vs $2.40 \pm 0.79 \mu\text{M}$ for plasmid control, $p > 0.05$; Fig 4.13). The 60kDa human P2X4 wild-type cell membrane expression levels were reduced when co-transfected with human P2X5 [K69A, K314A] dead subunits (Fig 4.14A-B). Although human P2X5 [K69A, K314A] dead subunits showed high protein expression for whole-cell and cell surface lysates, their expression levels were significantly reduced when co-transfected with human P2X4 wild-type subunits (Fig 4.1G-H and 4.14). These results suggested that some reduction of the ATP-evoked intracellular calcium influx might have been due to a reduction of human P2X4 wild-type receptors at the cell membrane, which was also supported by a reduction of the dimeric and trimeric human P2X4 wild-type protein species at 120kDa and 180kDa when human P2X5 [K69A, K314A] dead subunits were present (Fig 4.14; Nicke et al., 2005). If the human P2X5 [K69A, K314A] dead subunits did not express well at the cell membrane, their full dominant-negative effects might have been missed. Interestingly, co-immunoprecipitation complexes were formed between

human P2X4 wild-type and human P2X5 [K69A, K314A] dead subunits (Fig 4.16). Whole-cell input controls were consistent with the observed reduction of protein expression levels when both subunits were co-transfected together compared to individually transfected samples (Fig 4.16). Co-transfection of human P2X4 and P2X5 wild-type subunits did not alter the human P2X4 wild-type receptor ATP-evoked intracellular calcium responses (4.23E-F). The presence of human P2X5 wild-type subunits might have delayed the human P2X4 receptor onset upon application of ATP (Fig 4.23F). Human P2X4 and P2X5 wild-type subunits also co-immunoprecipitated (Fig 4.15). In this case, no major protein expression differences were observed in whole-cell input control when both subunits were co-transfected together or individually (Fig 4.15). These are consistent with a previous discussion point, where the amount of P2X5 dead subunits expressed at the cell membrane might have been restricted by a protein expression quality control mechanism, retaining supposedly mal-functioning human P2X5 dead subunits in the endoplasmic reticulum but not functional human P2X5 wild-type subunits (Hammond & Helenius, 1995; Duckwitz et al., 2006; Sun & Brodsky 2019). Analysis of cell membrane protein levels when both human P2X4 and P2X5 wild-type subunits are co-expressed might clarify this.

Taken together, we cannot conclude that human P2X5 [K69A, K314A] dead subunits had an actual dominant-negative effect on the human P2X4 wild-type ATP-evoked calcium responses. However, positive protein-protein interaction was observed for human P2X4 wild-type subunits with both human P2X5 wild-type and dead subunits, implying that our functional study was limited. Further pharmacological studies are required to establish if a functional interaction occurred, possibly using α,β -MeATP which caused large human P2X5 currents or TNP-ATP, which effectively blocked them (Surprenant et al., 2000) but had little effects on human P2X4 receptors. Looking at reverse potential currents might be useful to determine any changes in chloride permeability when human P2X4 wild-type subunits are co-expressed with human P2X5 wild-type subunits. Original co-immunoprecipitation studies also showed that P2X4 subunits participated in heteromeric assemblies containing P2X5 subunits in HEK293 cells (Torres et al., 1999). An ELISA assay suggested a possible heteromerisation between P2X4 and P2X5 subunits in which the surface expression of a trafficking-deficient P2X5 mutant was strongly increased by co-expression with P2X4 subunits, which correlates to our protein expression observations (Compan et al., 2012; Fig 4.14). However, this heteromer has not been further characterised. Both P2X4 and P2X5 receptors are involved in inflammasome activation (Han et al., 2020; Jeong et al., 2020; Kanellopoulos et al., 2021). Thus, we speculated that possible functional interactions might occur there.

4.3.5 Human P2X4 subunits functionally interacted with human P2X6 subunits

P2X6 receptors are expressed in the Central Nervous System (CNS), skeletal muscle cells, thymocytes, and urinary bladder (Collo et al., 1996; Jones et al., 2004; Illes et al., 2021). They may have a role in the progression of renal cell cancer as P2X6 receptors are also expressed in the kidney (Gong et al., 2019). While no functional evidence for the human P2X6 homomeric receptor has been found to date, and it is therefore considered a ‘silent’ subunit in humans (Illes et al., 2021), there is a growing belief that the

P2X6 subunit might only contribute to functional channels when other P2X subunits are present (Torres et al., 1999).

Human P2X6 wild-type subunits showed low expression levels when transiently transfected in human astrocytoma cells at approximately 60KDa (Fig 4.7 and 4.21). Similarly, low expression levels were reported for human P2X6 [K78A, K315A] dead subunits transiently transfected in human astrocytoma cells at 55-60KDa (Fig 4.1I-J). These data raised the possibility that the receptor was not sufficiently glycosylated in our heterologous expression system compared to fully glycosylated P2X6 subunits reported in native cells with an approximated weight of 70KDa (North, 2002; Jones et al., 2004). Jones et al. also demonstrated that rat P2X6 recombinant expression and channel function depended on subunit glycosylation (Jones et al., 2004). Transient co-expression of human P2X6 wild-type subunits had an inhibitory effect on the human P2X4 wild-type ATP-evoked calcium responses without affecting its sensitivity (Fig 4.25A-B). A similar reduction of the human P2X4 wild-type ATP-evoked intracellular calcium responses was obtained when using human P2X6 [K78A, K315A] dead receptor tools instead (EC_{50} of $5.20 \pm 2.64 \mu M$ vs $2.40 \pm 0.79 \mu M$ for plasmid control, $p > 0.05$; Fig 4.6). The interpretation of whether these dominant-negative effects were due to a functional interaction between subunits or a reduction of human P2X4 wild-type receptors at the cell membrane in the presence of human P2X6 [K78A, K315A] dead subunits cannot be determined without further biotinylation experiments. We observed the formation of interaction complexes between human P2X4 and P2X6 wild-type subunits (Fig 4.7), but confirmation of protein interaction between human P2X4 wild-type and human P2X6 [K78A, K315A] dead subunits still needs to be addressed. It is important to note that higher molecular weight species for human P2X6 wild-type proteins were not detected for either whole-cell lysates or co-immunoprecipitates (Fig 4.7 and 4.21). These might indicate the lack of dimeric and trimeric P2X6 receptor expression in this recombinant system.

We concluded that a potential functional interaction occurred between human P2X4 and P2X6 subunits in our heterologous system, however further studies are required to confirm true dominant-negative effects of P2X6 [K78A, K315A] dead subunits on the human P2X4 wild-type receptor activity and to elucidate possible pharmacological effects of co-expression of human P2X4 and P2X6 wild-type subunits. Previous studies reported the formation of heteromeric P2X4/6 receptors using co-immunoprecipitation assays in HEK293 cells (Torres et al., 1999) and *Xenopus laevis* oocytes (Lê et al., 1998) and showed similar cellular distribution between P2X4 and P2X4/6 receptors in primary cultures of rat neurons (Bobanovic et al., 2002). The internalisation of P2X4/6 heterodimers was also observed, suggesting that one or two P2X4 subunits were sufficient to regulate the trafficking properties of the receptor (Bobanovic et al., 2002). Unique pharmacological phenotypes were observed in *Xenopus laevis* oocytes and rat brain cells supporting a possible heteromeric receptor composed of P2X4 and P2X6 subunits sensitive to Suramin, PPADS, and α, β -MeATP (Lê et al., 1998; Khakh et al., 1999). Three studies speculated the formation of heterotrimeric P2X receptors formed by the association of P2X2, P2X4 and P2X6 subunits where the P2X6 subunit might act as a linker between the other two and with an electrophysiological and pharmacological phenotype characteristic of the P2X2 subunit in rat spinal cord dorsal horn neurons, rat Purkinje neurons, and rat Leydig cells (Hugel & Schlichter 2000; Rubio &

Soto, 2001; Antonio et al., 2009). Their conclusions were later confirmed by co-purification of P2X2, P2X4 and P2X6 subunits and by Atomic Force Microscopy imaging (Antonio et al., 2014). The lack of information regarding human P2X receptor assembly becomes more evident as only two studies proposed possible roles for human P2X4/6 heteromeric receptors but did not investigate direct protein interaction between the two subtypes. One showed that human P2X4 and P2X6 receptors were closely associated with VE-cadherin and suggested a role in modulating cell-cell adhesion in HUVECs (Glass et al., 2002). And the second supposed that the ATP released as a result of radiotherapy contributed to cell death by binding and activating human P2X4/6 heteromers in T24 cells, a human urinary bladder cancer model (Dietrich et al., 2022).

4.3.6 Human P2X7 subunits did not form interaction complexes with human P2X4 subunits but altered their receptor function

P2X7 receptors are ubiquitously expressed throughout the body. They are well established in immune cells, including neutrophils, macrophages, microglial cells, dendritic cells and, to a lesser extent, platelets. P2X7 receptors are involved in the modulation of inflammatory responses and neuropathic pain signalling (Illes et al., 2021). P2X7 receptors are also expressed in vascular endothelial cells, vascular smooth muscle cells, skeletal muscle cells, hepatocytes, and epithelial cells of the airway tract (Illes et al., 2021). Due to similar expression patterns and overlapping roles in neuroinflammatory pain signalling with P2X4 receptors, it is relevant to investigate if these P2X subtypes can form functional interactions.

Transient co-transfection of human P2X7 [K64A, K311A] dead subunits with human P2X4 wild-type subunits significantly reduced the ATP-evoked intracellular calcium responses in a concentration-dependent manner identical to the one observed when human P2X4 [K67A, K313A] dead subunits were co-transfected with human P2X4 wild-type subunits (Fig 4.17 and 3.30). Thus, we initially thought that human P2X7 [K67A, K313A] might play a dominant-negative effect on human P2X4 wild-type sensitivity for ATP according to the hypothesis of the dead receptor. However, no physical interaction was observed in co-immunoprecipitation assays. Moreover, when human P2X4 and P2X7 wild-type subunits were co-expressed, there was a significant reduction in the ATP-evoked calcium responses, while the ATP potency remained the same compared to plasmid control (Fig 4.25C-D). Similarly, no interaction complexes were formed between wild-type subunits when co-expressed in human astrocytoma cells (Fig 4.19). Both functional and biochemical results showed a reduction of human P2X4-mediated calcium responses but no physical interaction between the two proteins. These initially suggested that interactions between P2X4 and P2X7 proteins were either only transient, did not resist the process of solubilisation or Western blotting analysis, or the complex levels were just below the detection limit for co-immunoprecipitation, as P2X7 receptors seemed to give a generally weaker signal. In agreement with previous statements and according to the dead receptor hypothesis, dead subunits would analogously be acting like non-competitive inhibitors of the human P2X4 wild-type receptor suppressing its activity by restricting the number of available ATP binding sites without altering the number of functional human P2X4 wild-type receptors at the cell membrane. Nevertheless, analysis of

whole-cell and membrane expression levels for human P2X4 wild-type and human P2X7 [K64A, K311A] dead subunits demonstrated that the presence of P2X7 dead subunits significantly reduced the amount of human P2X4 wild-type receptors expressed at the cell surface (Fig 4.18). Significant reductions of cell surface dimeric and trimeric forms of human P2X4 receptors were also spotted when human P2X7 [K64A, K311A] dead subunits were present (Fig 4.18). It is important to note that smaller amounts of both human P2X7 wild-type and [K64A, K311A] dead subunits were observed when co-expressed with human P2X4 wild-type subunits in respective whole-cell input controls (Fig 4.20 and 4.19]. Some studies also reported changes in cell surface expression levels under inflammatory conditions depending on which subtype was activated (Wilson et al., 2007). Interestingly, the P2X4 and P2X7 receptor genes are located on chromosome 12 within 130Kb of each other (Illes et al., 2021). Certainly, it can be possible that they share common promoter elements explaining how their expression levels appear to be closely intertwined and their co-localisation in various cell types.

Finally, we proposed that the observed reductions of intracellular calcium responses upon application of ATP were due to a reduction of functional human P2X4 receptors expressed at the cell membrane rather than an interaction between the two. Thus, we concluded that no functional interactions occurred between human P2X4 and P2X7 subunits in this experimental system. Our results are in agreement with many other studies: i) the extended P2X immunoprecipitation original study, which revealed that P2X7 subunits formed exclusively homotrimeric receptors (Torres et al., 1999), ii) a later study performed in native tissues which did not detect heteromeric P2X4/7 complexes using subtype-specific antibodies and BN-PAGE (Nicke, 2008), and iii) a more recent functional approach evidenced that P2X4 and P2X7 receptors were activated independently from each other in BV-2 mice microglial cells and no functional interaction occurred between the two P2X receptor subtypes (Trang et al., 2020). In contrast, a 2007 study provided evidence of recombinant rat P2X4/7 heteromers in Normal Rat Kidney cells (NRK) and HEK293 cells and endogenous mouse P2X4/7 heteromers in bone marrow-derived macrophages (Guo et al., 2007). A disparity between Guo et al. and our data was the difference in surface expression levels when both subunits were co-expressed. Our study is more consistent with other findings that showed a correlation between subtype expression levels (Wilson et al., 2007; Craigie et al., 2013) along with functional evidence that P2X4 receptor modulated P2X7 receptor-dependent inflammatory functions when co-expressed in mouse macrophage RAW264.7 cells (Kawano et al., 2012a) and was involved in P2X7 receptor-mediated cell death, but not pore formation (Kawano et al., b). There is a growing body of evidence suggesting that the roles of P2X4 and P2X7 receptors can be influenced when they are co-expressed (Adamiak et al., 2022). Nicke (2008) and two other studies might clarify the differences observed over the last two decades (Boumechache et al., 2009; Antonio et al., 2011). These indicated that the preferred assembly pathway for both receptors is the formation of homotrimers. Homotrimers of P2X7 were able to co-immunoprecipitate with P2X4 homotrimers, suggesting that an interaction occurred between rather than within receptor complexes (Nicke, 2008; Boumechache et al., 2009; Antonio et al., 2011). Further studies are needed to discriminate between these three possibilities.

Due to the limitations of our experimental system, we could not rule out the possibility that P2X4/7 homotrimeric receptor interactions might occur. Finally, we hypothesised these might be transient intracellular interactions possibly occurring during receptor trafficking or during the formation of mature phagolysosomes. Besides, P2X4 receptors are involved in the fusion of late endosomes and lysosomes via the activation of calmodulin and promote vesicle fusion (Cao et al., 2015; Kanellopoulos et al., 2021), while P2X7 receptors facilitate the formation of phagosomes when activated by high concentrations of ATP (Kuehnel et al., 2009), both potentially supporting our statement.

5 General discussion

Key findings and future directions

5.1 Key findings and concluding remarks

P2X ligand-gated ion channels are responsible for many of the physiological effects of ATP in both central and peripheral nervous systems. P2X receptor activation via ATP binding causes the opening of an ionic pore and the movement of small cations across cell membranes. This ionic movement underpins a multitude of biological processes in health and disease. Over the past fifteen years, there has been a growing interest in how P2X subunits arrange to form functional channels. While the existence of heterotrimeric P2X_{2/3} receptors is well established, the composition of other P2X heteromers and/or the interaction between distinct trimeric receptors remains controversial.

The P2X₄ receptor subtype is widely distributed in human tissues and cells. They are one of the predominant receptors found in immune cells and have been linked to the regulation of immune responses and inflammation (Burnstock, 2016; Antonioli et al., 2019). In the peripheral and central nervous systems, P2X₄ receptors are expressed in neurons and glial cells such as microglia found in the spinal cord, and they are linked to the transmission of neuropathic pain (Tsuda et al., 2013; Stokes et al., 2017). Furthermore, P2X₄ receptors are abundantly expressed in human vascular endothelial cells and are recognised for their role in regulating vascular tone (Yamamoto et al., 2006; Stokes et al., 2011). P2X₄ receptors have particular membrane trafficking patterns and are also located in lysosomes and other acidic intracellular compartments (Xu et al., 2014; Murrell-Lagnado & Frick, 2019). Its varied distribution in human tissues and its involvement in both physiological and pathophysiological processes make it a promising target for the development of new therapeutic agents. As previously described, P2X receptors are trimeric, and P2X₄ subunits can form a functional homotrimer. But can a P2X₄ subunit combine with other P2X subunits to form a functional receptor?

The principal aim of this thesis was to disclose potential human P2X₄ functional subunit interactions through the compilation of biochemical and functional evidence, contributing original knowledge to the current literature. Deciphering P2X subunit-subunit association is an arduous task and usually requires the combination of multiple approaches before a heteromer is established and accepted by the research community. Our experimental strategy encompassed i) molecular biology techniques to generate human P2X dead receptor tools by site-directed mutagenesis and to transiently co-transfect human astrocytoma cells, ii) biochemical methods such as Western blotting and immunoprecipitation to assess protein expression patterns and demonstrate physical protein interactions, and iii) pharmacological tools to investigate P2X channel function by intracellular calcium mobilisation assays. We proposed human 1321N1 astrocytoma cells and human P2X dead receptor tools as a well-rounded experimental system to identify human P2X₄ heteromeric candidates.

In the first part of this thesis, we provided a reliable and reproducible method for the study of human P2X₄ subunit assembly, determining both physical and functional interactions. Initially, we explored how to transfet human P2X₄ wild-type receptors into 1321N1 astrocytoma cells successfully. The ideal approach was determined empirically and was selected for high transfection efficiency, low cell toxicity, accessibility and convenience, and reproducibility. Our results evidenced that successful and reproducible transient transfection of human 1321N1 astrocytoma cells is possible, overcoming a major

problem related to the investigation of P2X receptor properties. HEK293 cells have been the most frequent cell model used to assess the role of recombinant P2X receptors but endogenously express other P2 receptor subtypes, namely P2Y1, P2Y2, and P2Y4, which also respond to ATP and other extracellular nucleotides (Fischer et al., 2003, 2005), causing large intracellular calcium changes and potentially interfering with P2X receptor-mediated calcium signals (He et al., 2003). Therefore, the human 1321N1 astrocytoma cell model was a more suitable heterologous system to provide new insights into the human P2X heteromerisation matter. Once this technique was mastered, we then demonstrated that a heterologously expressed human P2X4 receptor accurately represented its characteristic pharmacological profile. To do so, intracellular calcium influx experiments were performed by application of ATP and different agonists into 1321N1 astrocytoma cells stably expressing human P2X4 receptors. The effects of broad-spectrum and human P2X4 selective antagonists on its activity were also investigated for completeness. In summary, recombinant human P2X4 receptors were distinguished for their partial activation with nucleotide analogues other than ATP and their complete inhibition by the competitive inhibitor TNP-ATP and the negative allosteric modulators PPADS, BAY-1797, PSB-12062, BX-430, 5-BDBD, and Taspine. While heterologously expressed P2X4 receptors were efficiently expressed in the plasma membrane, formed functional homomeric interactions, and showed a distinct pharmacological profile, only a few native receptors have been identified that resemble exactly the recombinant homomeric P2X4 receptors (Coddou et al., 2011). These differences might be justified by unknown receptors formed by a heteromeric assembly comprising P2X4 with P2X subunits or other associated proteins. As with other ligand-gated ion channels, the subunit composition of P2X receptors defines not only their pharmacological profile properties but also their functional roles in physiological processes, which can ultimately lead to the development of more selective therapeutics. Finally, evidence that human P2X4 wild-type subunits interact to form a functional ATP-gated channel was obtained successfully by intracellular calcium measurements and protein expression and interaction studies. Following the hypothesis proposed by Wilkinson et al. (2006), dead receptor proof-of-concept was performed and thoroughly optimised to provide a reliable and consistent base to explore human P2X4 heteromeric interactions whilst avoiding significant data biases. Dominant negative effects of human P2X4 [K67A, K313A] dead subunits on the human P2X4 wild-type ATP-evoked calcium responses and co-immunoprecipitation assays proved that mutations on key ectodomain lysine residues caused a significant loss of channel function and that a homo-oligomeric interaction occurred between human P2X4 wild-type and P2X4 double mutant subunits. In addition, this experimental system revealed functional interactions between human P2X2 and human P2X3 subunits, an exclusively recognised P2X heteromeric receptor by the purinergic community. Overall, using human 1321N1 parental astrocytoma cells and dead receptor tools is a well-rounded experimental system to systematically screen for functional human P2X4 heteromeric candidates.

In the second part of this thesis, functional human P2X4 interactions were scrutinised using our novel experimental approach (Table 4.2). Taking experimental biases and limitations into account, as well as current literature knowledge, solid evidence for human P2X4 wild-type subunits functionally interacting

with human P2X1 [K68A, K309A], human P2X5 [K69A, K314A], and human P2X6 [K78A, K315A] dead subunits was obtained, which compromised the ATP binding pocket according to the dead receptor hypothesis. In the same way, human P2X4 wild-type subunits formed interaction complexes with respective human P2X1, human P2X5, and human P2X6 wild-type subunits. These data revealed that functional human P2X1/4, P2X4/5, and P2X4/6 heteromeric receptors can exist in this heterologous system. No functional interaction was observed for human P2X4 wild-type subunits transiently co-transfected with human P2X2 [K81A, K319A] dead subunits, but the co-immunoprecipitation data showed a positive interaction between human P2X4 wild-type and human P2X2 wild-type subunits. Furthermore, the human P2X4 wild-type ATP-evoked calcium responses were significantly increased by the presence of human P2X2 wild-type subunits. Taken together, these results supported interaction between homomeric P2X2 and P2X4 receptors rather than between subunits. No functional interaction was determined between human P2X4 wild-type subunits and human P2X3 [K63A, K299A] dead subunits and no interaction complexes were detected between human P2X4 wild-type and human P2X3 wild-type subunits. These suggested that a heteromeric P2X3/4 receptor is unlikely in this heterologous system. Lastly, human P2X7 [K64A, K311A] dead subunits compromised the human P2X4 wild-type ATP-evoked calcium responses due to a reduction in P2X4 receptor cell surface expression. Furthermore, human P2X4 and P2X7 subunits did not co-immunoprecipitate. These data indicate that a functional human P2X4/7 heteromer is unlikely, although their expression patterns seem to be intertwined.

While this thesis has enabled the interpretation of previous and current P2X4 heteromerisation studies, it also highlights the great deal of work that still has to be done. Current views and our results raise the important general point that co-localization, co-immunoprecipitation, and functional evidence can be used as templates for elucidating the molecular identities of native P2X receptor channels. However, we must be cautious when concluding whether P2X receptor heteromers, involving the co-assembly of different subunits around a common pore, are being formed or not. Instead, it is still essential to provide direct structural evidence for P2X heteromerisation. We hopefully will not have to wait long before possible P2X heteromeric structures are available, providing information on the subunit interaction mechanisms of this fascinating family of ligand-gated ion channels.

Our future goals in investigating human P2X subunit assembly should lead to the clear determination of the nature of functional P2X interactions, i.e., between subunits and/or receptors, to the exact definition of the stoichiometry of these interactions, and ultimately to demonstrate their existence in native conditions.

5.2 Future directions

This thesis has enabled the interpretation of previous and current P2X4 heteromerisation studies and successfully contributed original knowledge to the field. We discovered some functional and non-functional human P2X subunits that interacted with human P2X4 wild-type subunits. Nevertheless, there are limitations in our experimental system and analysis, and we emphasise the amount of work that still needs to be done to establish the existence of novel human P2X4 heteromeric receptors.

Firstly, we could not make any assumptions about the formation of heteromeric human P2X4 channels and their stoichiometry. I believe using P2X dead receptor tools might provide clarity in this matter by using the FlexStation 3 device to initially flesh out interesting leads and then using patch-clamp electrophysiology to confirm those results in manually selected cells. We could exploit our human P2X mutants and complement our hypothesis of the dead receptor data by co-transfected P2X4 wild-type subunits with human P2X single mutants instead and analyse if channel activity can be rescued or not, as demonstrated by Wilkinson et al. (Wilkinson et al. 2006). The reciprocal combination of human P2X4 single or double dead subunits with other P2X wild-type subunits would make the functional studies more comprehensive. We could also use these human P2X single and double dead receptor tools to provide insight into the surface and total protein expression patterns when co-expressed with human P2X wild-type subunits. Finally, we could extend this experimental approach to other P2X receptor subtypes and decipher potential human P2X heteromers that do not contain human P2X4 subunits. This combined approach might be applicable to determine the arrangement of subunits in those channels, but it is important not to over-interpret it in any structural sense.

Secondly, any functional and biochemical interaction data disclosed here comes from a heterologous system. Thus, all candidates must be tested in a native setting too. For example, candidates found to interact in our cell model could be found endogenously in human primary cell cultures (HUVEC or THP-1 as human vascular endothelium and human monocyte/macrophage cell models, respectively) or in human tissue samples obtained from collaborations with the Norfolk and Norwich University Hospital (arteries found in breast adipose tissue could be starting points). Moreover, we could use the human P2X dead receptors as experimental tools to investigate the functional roles of P2X4 and other P2X receptors in these native settings. For example, does the expression of a dead P2X4 receptor affect the role of other P2X receptors in vascular endothelium cells?

Electrophysiology techniques would help define the pharmacological properties of potential heterotrimeric candidates, which might become useful for future investigations in native systems and for developing small molecules that could selectively target either the homomeric or the heteromeric receptors. These would ultimately lead to a deeper understanding of ATP signalling pathways and the physiological and pathophysiological roles of each receptor subtype. However, the factors regulating P2X subunit-subunit association and trimer stability remain to be elucidated but could prove important in designing stable constructs for electrophysiology and structure studies. We could investigate physiological protein partners associated with human P2X4 receptors and other receptor subtypes found in these human primary cell models or tissue samples by immunoprecipitation and mass

spectrometry analyses, Blue native PAGE (BN-PAGE) assays, or SMALPS. The SMALPS technique is a revolutionary membrane solubilisation method that produces vesicles containing membrane proteins in their surrounding lipid environment (Teo et al., 2019).

Finally, we cannot draw any final conclusions on the existence of human P2X4 heteromers without any structural evidence. Although protein crystallography data for the human P2X4 receptor has not been released yet, we can use artificial intelligence programs such as AlphaFold to generate protein structure models of projected human P2X4 heteromeric candidates (Fig 5.1). These accurate structure predictions might enable highly focused structure-function studies to unravel which residues are involved in heteromeric subunit interactions and changes on the agonist-binding interfaces, for example. The data derived from these studies, combined with our experimental approach and current views in the literature, will be more readily interpreted and will hopefully provide a wide range of testable hypotheses in the future.

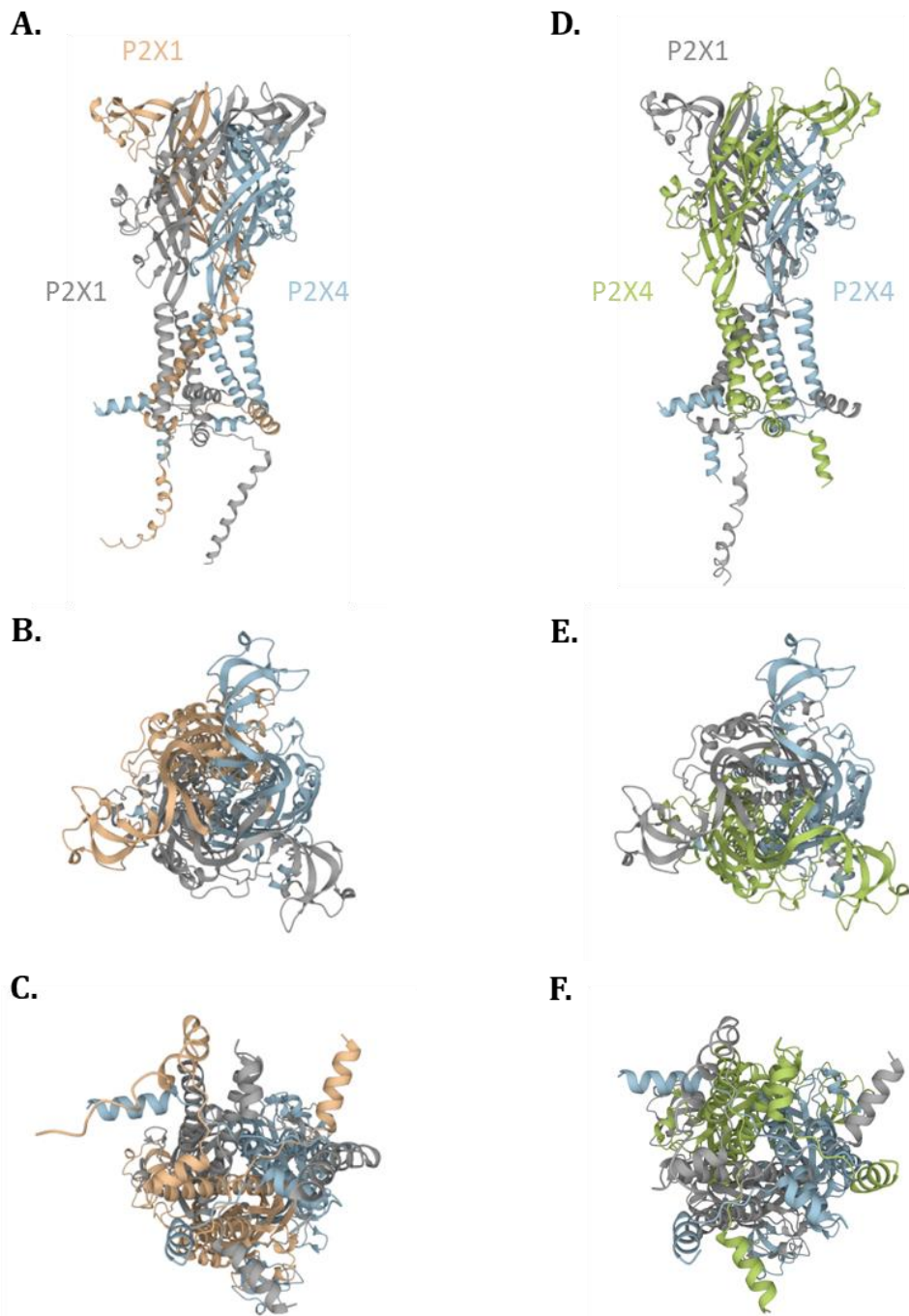


Fig 5.1. Structure modelling of a potential human P2X1/4 heteromeric receptor in the apo state. (A-C) Front (A), top (B), and bottom (C) views of the structure of a potential human P2X1/4 receptor formed by two P2X1 (orange and grey) and one P2X4 (blue) subunits. (D-F) Front (D), top (E), and bottom (F) views of the structure of a potential human P2X1/4 receptor formed by one P2X1 (grey) and two P2X4 (blue and green) subunits. Each subunit is shown in a cartoon representation and a different colour. The sequences used for these models do not contain any C-terminus epitopes. These structures were obtained using the ColabFold modelling software from AlphaFold: (<https://colab.research.google.com/github/sokrypton/ColabFold/blob/main/AlphaFold2.ipynb>).

References

- Abbracchio, M. P., Burnstock, G., Boeynaems, J., Barnard, E. A., Boyer, J. L., Kennedy, C., Knight, G. E., Fumagalli, M., Gachet, C., Jacobson, K. A., & Weisman, G. A. (2006). International Union of Pharmacology LVIII: Update on the P2Y G-protein-coupled nucleotide receptors: From molecular mechanisms and pathophysiology to therapy. *Pharmacological Reviews*, 58(3), 281–341. <https://doi.org/10.1124/pr.58.3.3>
- Abbracchio, M. P., Burnstock, G., Verkhratsky, A., & Zimmermann, H. (2008). Purinergic signalling in the nervous system: an overview. *Trends in Neurosciences*, 32(1), 19–29. <https://doi.org/10.1016/j.tins.2008.10.001>
- Abdelrahman, A., Namasivayam, V., Hinz, S., Schiedel, A. C., Köse, M., Burton, M., El-Tayeb, A., Gillard, M., Bajorath, J., de Ryck, M., & Müller, C. E. (2017). Characterization of P2X4 receptor agonists and antagonists by calcium influx and radioligand binding studies. *Biochemical Pharmacology*, 125, 41–54. <https://doi.org/10.1016/j.bcp.2016.11.016>
- Acuña-Castillo, C., Morales, B., & Huidobro-Toro, J. P. (2002). Zinc and Copper modulate differentially the P2X4 receptor. *Journal of Neurochemistry*, 74(4), 1529–1537. <https://doi.org/10.1046/j.1471-4159.2000.0741529.x>
- Adamiak, M., Bujko, K., Thapa, A., Pensato, V., Brzezniakiewicz-Janus, K., Ratajczak, J., Davies, D. L., Ulrich, H., Kucia, M., & Ratajczak, M. Z. (2022). The P2X4 purinergic receptor has emerged as a potent regulator of hematopoietic stem/progenitor cell mobilization and homing - a novel view of P2X4 and P2X7 receptor interaction in orchestrating stem cell trafficking. *Leukemia*, 36(1), 248–256. <https://doi.org/10.1038/s41375-021-01352-9>
- Alberts, B., Johnson, A., Lewis, J., Morgan, D., Raff, M., Roberts, K., & Walter, P. (2017). Molecular biology of the cell. In *Molecular Biology of the Cell* (6th ed.). Garland Science. <https://doi.org/10.1201/9781315735368>
- Alexander, S. P. H., Mathie, A., & Peters, J. A. (2011). Guide to receptors and channels. *British Journal of Pharmacology*, 164, S1–S320. https://doi.org/10.1111/j.1476-5381.2011.01649_1.x
- Antonio, L. S., Costa, R. R., Gomes, M. D., & Varanda, W. A. (2009). Mouse Leydig cells express multiple P2X receptor subunits. *Purinergic Signalling*, 5(3), 277–287. <https://doi.org/10.1007/s11302-008-9128-9>
- Antonio, L. S., Stewart, A. P., Varanda, W. A., & Edwardson, J. M. (2014). Identification of P2X2/P2X4/P2X6 heterotrimeric receptors using atomic force microscopy (AFM) imaging. *FEBS Letters*, 588(12), 2125–2128. <https://doi.org/10.1016/j.febslet.2014.04.048>
- Antonio, L., Stewart, A., Xu, X., Varanda, W., Murrell-Lagnado, R., & Edwardson, J. (2011). P2X4 receptors interact with both P2X2 and P2X7 receptors in the form of homotrimers. *British Journal of Pharmacology*, 163(5), 1069–1077. <https://doi.org/10.1111/j.1476-5381.2011.01303.x>

Antonioli, L., Blandizzi, C., Fornai, M., Pacher, P., Lee, H. T., & Haskó, G. (2019). P2X4 receptors, immunity, and sepsis. *Current Opinion in Pharmacology*, 47, 65–74. <https://doi.org/10.1016/j.coph.2019.02.011>

Aschrafi, A., Sadtler, S., Niculescu, C., Rettinger, J., & Schmalzing, G. (2004). Trimeric architecture of homomeric P2X2 and heteromeric P2X1+2 receptor subtypes. *Journal of Molecular Biology*, 342(1), 333–343. <https://doi.org/10.1016/j.jmb.2004.06.092>

Ase, A. R., Honson, N. S., Zaghdane, H., Pfeifer, T. A., & Seguela, P. (2015). Identification and Characterization of a Selective Allosteric Antagonist of Human P2X4 Receptor Channels. *Molecular Pharmacology*, 87(4), 606–616. <https://doi.org/10.1124/mol.114.096222>

Ase, A. R., Therrien, É., & Séguéla, P. (2019). An allosteric inhibitory site conserved in the ectodomain of P2X Receptor channels. *Frontiers in Cellular Neuroscience*, 13(121), 1–11. <https://doi.org/10.3389/fncel.2019.00121>

Balázs, B., Dankó, T., Kovács, G., Köles, L., Hediger, M. A., & Zsembery, Á. (2013). Investigation of the inhibitory effects of the benzodiazepine derivative, 5-BDBD on P2X4 purinergic receptors by two complementary methods. *Cellular Physiology and Biochemistry*, 32(1), 11–24. <https://doi.org/10.1159/000350119>

Barrera, N. P., Ormond, S. J., Henderson, R. M., Murrell-Lagnado, R. D., & Edwardson, J. M. (2005). Atomic Force Microscopy imaging demonstrates that P2X2 receptors are trimers but that P2X6 receptor subunits do not oligomerize. *Journal of Biological Chemistry*, 280(11), 10759–10765. <https://doi.org/10.1074/jbc.M412265200>

Bayon, Y., Hernandez, M., Alonso, A., Nunez, L., Garcia-Sancho, J., Leslie, C., Crespo, M. S., & Nieto, M. L. (1997). Cytosolic phospholipase A2 is coupled to muscarinic receptors in the human astrocytoma cell line 1321N1: characterization of the transducing mechanism. *Biochemical Journal*, 323, 281–287.

Beamer, E., Gölöncsér, F., Horváth, G., Beko, K., Otrokoci, L., Koványi, B., & Sperlágh, B. (2016). Purinergic mechanisms in neuroinflammation: An update from molecules to behaviour. *Neuropharmacology*, 104, 94–104. <https://doi.org/10.1016/j.neuropharm.2015.09.019>

Bean, B. (1990). ATP-activated channels in rat and bullfrog sensory neurons: concentration dependence and kinetics. *The Journal of Neuroscience*, 10(1), 1–10. <https://doi.org/10.1523/JNEUROSCI.10-01-00001.1990>

Bennetts, F. M., Mobbs, J. I., Ventura, S., & Thal, D. M. (2022). The P2X1 receptor as a therapeutic target. *Purinergic Signalling*, 12(5), 647–661. <https://doi.org/10.1007/s11302-022-09880-4>

Bergmann, P., Garcia de Paco, E., Rissiek, B., Menzel, S., Dubberke, G., Hua, J., Rassendren, F., Ullmann, L., & Koch-Nolte, F. (2019). Generation and Characterization of Specific Monoclonal Antibodies and Nanobodies Directed Against the ATP-Gated Channel P2X4. *Frontiers in Cellular Neuroscience*, 13(November), 1–12. <https://doi.org/10.3389/fncel.2019.00498>

Besnard, A., Gautherot, J., Julien, B., Tebbi, A., Garcin, I., Doignon, I., Péan, N., Gonzales, E., Cassio, D., Grosse, B., Liu, B., Safya, H., Cauchois, F., Humbert, L., Rainteau, D., & Tordjmann, T. (2016). The P2X4 purinergic receptor impacts liver regeneration after partial hepatectomy in mice through the regulation of biliary homeostasis. *Hepatology*, 64(3), 941–953. <https://doi.org/10.1002/hep.28675>

Bianchi, B. R., Lynch, K. J., Touma, E., Niforatos, W., Burgard, E. C., Alexander, K. M., Park, H. S., Yu, H., Metzger, R., Kowaluk, E., Jarvis, M. F., & van Biesen, T. (1999). Pharmacological characterization of recombinant human and rat P2X receptor subtypes. *European Journal of Pharmacology*, 376(1–2), 127–138. [https://doi.org/10.1016/S0014-2999\(99\)00350-7](https://doi.org/10.1016/S0014-2999(99)00350-7)

Bidula, S., Nadzirin, I. bin, Cominetti, M., Hickey, H., Cullum, S. A., Searcey, M., Schmid, R., & Fountain, S. J. (2022). Structural basis of the Negative Allosteric Modulation of 5-BDBD at human P2X4 receptors. *Molecular Pharmacology*, 101(1), 33–44. <https://doi.org/10.1124/MOLPHARM.121.000402>

bin Nadzirin, I. bin, Fortuny-Gomez, A., Ngum, N., Richards, D., Ali, S., Searcey, M., & Fountain, S. J. (2021). Taspine is a natural product that suppresses P2X4 receptor activity via phosphoinositide 3-kinase inhibition. *British Journal of Pharmacology*, July, 1–14. <https://doi.org/10.1111/bph.15663>

Birdsong, W. T., Fierro, L., Williams, F. G., Spelta, V., Naves, L. A., Knowles, M., Marsh-Haffner, J., Adelman, J. P., Almers, W., Elde, R. P., & McCleskey, E. W. (2010). Sensing muscle ischemia: Coincident detection of acid and ATP via interplay of two ion channels. *Neuron*, 68(4), 739–749. <https://doi.org/10.1016/j.neuron.2010.09.029>

Bo, X., Jiang, L. H., Wilson, H. L., Kim, M., Burnstock, G., Surprenant, A., & North, R. A. (2003). Pharmacological and biophysical properties of the human P2X5 receptor. *Molecular Pharmacology*, 63(6), 1407–1416. <https://doi.org/10.1124/mol.63.6.1407>

Bobanovic, L. K., Royle, S. J., & Murrell-Lagnado, R. D. (2002). P2X receptor trafficking in neurons is subunit-specific. *The Journal of Neuroscience*, 22(12), 4814–4824. <https://doi.org/10.1523/JNEUROSCI.22-12-04814.2002>

Boué-Grabot, É., Barajas-López, C., Chakfe, Y., Blais, D., Bélanger, D., Émerit, M. B., & Séguéla, P. (2003). Intracellular cross talk and physical interaction between two classes of neurotransmitter-gated channels. *The Journal of Neuroscience*, 23(4), 1246–1253. <https://doi.org/10.1523/JNEUROSCI.23-04-01246.2003>

Boumechache, M., Masin, M., Edwardson, J. M., Górecki, D. C., & Murrell-Lagnado, R. (2009). Analysis of assembly and trafficking of native P2X4 and P2X7 receptor complexes in rodent immune cells. *Journal of Biological Chemistry*, 284(20), 13446–13454. <https://doi.org/10.1074/jbc.M901255200>

Brake, A. J., Wagenbach, M. J., & Julius, D. (1994). New structural motif for ligand-gated ion channels defined by an ionotropic ATP receptor. *Nature*, 371(6497), 519–523. doi: 10.1038/371519a0

- Brown, D. A., & Yule, D. I. (2010). Protein kinase A regulation of P2X4 receptors: requirement for a specific motif in the C-terminus. *Biochimica et Biophysica Acta (BBA) - Molecular Cell Research*, 1803(2), 275–287. <https://doi.org/10.1016/j.bbamcr.2009.12.002>
- Brown, S. G., Townsend-Nicholson, A., Jacobson, K. A., Burnstock, G., & King, B. F. (2002). Heteromultimeric P2X1/2 receptors show a novel sensitivity to extracellular pH. *Journal of Pharmacology and Experimental Therapeutics*, 300(2), 673–680. <https://doi.org/10.1124/jpet.300.2.673>
- Burnett, E., Lydford, S., Fellows, D., Taylor, J., & Cooper, J. (2011). *Molecular identification and pharmacological characterisation of the co-expression of M3 and M5 muscarinic receptors on the human astrocytoma cell line 1321N1*.
- Burnstock, G. (1972). Purinergic nerves. *Pharmacological Reviews*, 24(3), 509–581. [https://doi.org/10.1016/S0140-6736\(77\)90373-7](https://doi.org/10.1016/S0140-6736(77)90373-7)
- Burnstock, G. (1990). This week's citation classic: Burnstock, 1978. *ISI Current Contents*, 40, 18.
- Burnstock, G. (2007). Physiology and pathophysiology of purinergic neurotransmission. *Physiological Reviews*, 87, 659–797. <https://doi.org/10.1152/physrev.00043.2006>
- Burnstock, G. (2016a). An introduction to the roles of purinergic signalling in neurodegeneration, neuroprotection and neuroregeneration. *Neuropharmacology*, 104, 4–17. <https://doi.org/10.1016/j.neuropharm.2015.05.031>
- Burnstock, G. (2016b). P2X ion channel receptors and inflammation. *Purinergic Signalling*, 12(1), 59–67. <https://doi.org/10.1007/s11302-015-9493-0>
- Burnstock, G. (2018). Purine and purinergic receptors. *Brain and Neuroscience Advances*, 2, 239821281881749. <https://doi.org/10.1177/2398212818817494>
- Burnstock, G., Campbell, G., Satchell, D., & Smythe, A. (1970). Evidence that adenosine triphosphate or a related nucleotide is the transmitter substance released by non-adrenergic inhibitory nerves in the gut. *British Journal of Pharmacology*, 40, 668–688. <https://doi.org/10.1111/j.1476-5381.1970.tb10646.x>
- Burnstock, G., & Kennedy, C. (1985). Is there a basis for distinguishing two types of P2-purinoceptor? *General Pharmacology*, 16(5), 433–440. [https://doi.org/10.1016/0306-3623\(85\)90001-1%0A](https://doi.org/10.1016/0306-3623(85)90001-1%0A)
- Burnstock, G., & Kennedy, C. (2011). P2X receptors in health and disease. In K. A. Jacobson & J. Linden (Eds.), *Pharmacology of purine and pyrimidine receptors* (Vol. 61, pp. 333–372). Advances in pharmacology. <https://doi.org/10.1016/B978-0-12-385526-8.00011-4>
- Burnstock, G., & Knight, G. E. (2004). Cellular distribution and functions of P2 receptor subtypes in different systems. *International Review of Cytology*, 240, 31–304. [https://doi.org/10.1016/S0074-7696\(04\)40002-3](https://doi.org/10.1016/S0074-7696(04)40002-3)

Cao, Q., Zhong, X. Z., Zou, Y., Murrell-Lagnado, R., Zhu, M. X., & Dong, X.-P. (2015). Calcium release through P2X4 activates calmodulin to promote endolysosomal membrane fusion. *The Journal of Cell Biology*, 209(6), 879–894. <https://doi.org/10.1083/jcb.201409071>

Chataigneau, T., Lemoine, D., & Grutter, T. (2013). Exploring the ATP-binding site of P2X receptors. *Frontiers in Cellular Neuroscience*, 7(December), 1–12. <https://doi.org/10.3389/fncel.2013.00273>

Chaumont, S., Jiang, L.-H., Penna, A., North, R. A., & Rassendren, F. (2004). Identification of a trafficking motif involved in the stabilization and polarization of P2X receptors. *The Journal of Biological Chemistry*, 279(28), 29628–29638. <https://doi.org/10.1074/jbc.M403940200>

Chen, H., Xia, Q., Feng, X., Cao, F., Yu, H., Song, Y., & Ni, X. (2016). Effect of P2X4R on airway inflammation and airway remodelling in allergic airway challenge in mice. *Molecular Medicine Reports*, 13(1), 697–704. <https://doi.org/10.3892/mmr.2015.4622>

Chen, I.-S., & Kubo, Y. (2018). Ivermectin and its target molecules: shared and unique modulation mechanisms of ion channels and receptors by ivermectin. *The Journal of Physiology*, 596(10), 1833–1845. <https://doi.org/10.1113/JP275236>

Cockayne, D. A., Dunn, P. M., Zhong, Y., Rong, W., Hamilton, S. G., Knight, G. E., Ruan, H.-Z., Ma, B., Yip, P., Nunn, P., McMahon, S. B., Burnstock, G., & Ford, A. P. D. W. (2005). P2X2 knockout mice and P2X2/P2X3 double knockout mice reveal a role for the P2X2 receptor subunit in mediating multiple sensory effects of ATP. *The Journal of Physiology*, 567(2), 621–639. <https://doi.org/10.1113/jphysiol.2005.088435>

Coddou, C., Sandoval, R., Hevia, M. J., & Stojilkovic, S. S. (2019). Characterization of the antagonist actions of 5-BDBD at the rat P2X4 receptor. *Neuroscience Letters*, 690, 219–224. <https://doi.org/10.1016/j.neulet.2018.10.047>

Coddou, C., Yan, Z., Obsil, T., Huidobro-Toro, J. P., & Stojilkovic, S. S. (2011). Activation and regulation of purinergic P2X receptor channels. *Pharmacological Reviews*, 63(3), 641–683. <https://doi.org/10.1124/pr.110.003129>

Collo, G., North, R., Kawashima, E., Merlo-Pich, E., Neidhart, S., Surprenant, A., & Buell, G. (1996). Cloning OF P2X5 and P2X6 receptors and the distribution and properties of an extended family of ATP-gated ion channels. *The Journal of Neuroscience*, 16(8), 2495–2507. <https://doi.org/10.1523/JNEUROSCI.16-08-02495.1996>

Compan, V., Ulmann, L., Stelmashenko, O., Chemin, J., Chaumont, S., & Rassendren, F. (2012). P2X2 and P2X5 subunits define a new heteromeric receptor with P2X7-like properties. *Journal of Neuroscience*, 32(12), 4284–4296. <https://doi.org/10.1523/JNEUROSCI.6332-11.2012>

Conant, A. R., Theologou, T., Dihmis, W. C., & Simpson, A. W. M. (2008). Diadenosine polyphosphates are selective vasoconstrictors in human coronary artery bypass grafts. *Vascular Pharmacology*, 48(4–6), 157–164. <https://doi.org/10.1016/j.vph.2008.01.005>

Cook, S. P., & McCleskey, E. W. (2002). Cell damage excites nociceptors through release of cytosolic ATP. *Pain*, 95(1–2), 41–47. [https://doi.org/10.1016/S0304-3959\(01\)00372-4](https://doi.org/10.1016/S0304-3959(01)00372-4)

Craigie, E., Birch, R. E., Unwin, R. J., & Wildman, S. S. (2013). The relationship between P2X4 and P2X7: a physiologically important interaction? *Frontiers in Physiology*, 4, 1–6. <https://doi.org/10.3389/fphys.2013.00216>

Csóka, B., Németh, Z. H., Szabó, I., Davies, D. L., Varga, Z. v., Pálóczi, J., Falzoni, S., di Virgilio, F., Muramatsu, R., Yamashita, T., Pacher, P., & Haskó, G. (2018). Macrophage P2X4 receptors augment bacterial killing and protect against sepsis. *JCI Insight*, 3(11). <https://doi.org/10.1172/jci.insight.99431>

D'Antongiovanni, V., Pellegrini, C., Benvenuti, L., Fornai, M., di Salvo, C., Natale, G., Ryskalin, L., Bertani, L., Lucarini, E., di Cesare Mannelli, L., Ghelardini, C., Nemeth, Z. H., Haskó, G., & Antonioli, L. (2022). Anti-inflammatory Effects of Novel P2X4 Receptor Antagonists, NC-2600 and NP-1815-PX, in a Murine Model of Colitis. *Inflammation*, 45(4), 1829–1847. <https://doi.org/10.1007/s10753-022-01663-8>

di Virgilio, F., Sarti, A. C., Falzoni, S., de Marchi, E., & Adinolfi, E. (2018). Extracellular ATP and P2 purinergic signalling in the tumour microenvironment. *Nature Reviews Cancer*, 18(10), 601–618. <https://doi.org/10.1038/s41568-018-0037-0>

Dietrich, F., Cappellari, A. R., Filippi-Chiela, E. C., de Paula, P. B., de Souza, J. B., Agatti, S. W., Andrejew, R., Roesler, R., Morrone, F. B., & Battastini, A. M. O. (2022). High P2X6 receptor expression in human bladder cancer predicts good survival prognosis. *Molecular and Cellular Biochemistry*, 477(8), 2047–2057. <https://doi.org/10.1007/s11010-022-04425-0>

Donnelly-Roberts, D., McGaraughty, S., Shieh, C.-C., Honore, P., & Jarvis, M. F. (2007). Painful Purinergic Receptors. *Journal of Pharmacology and Experimental Therapeutics*, 324(2), 409–415. <https://doi.org/10.1124/jpet.106.105890>

Drury, A. N., & Szent-Györgyi, A. (1929). The physiological activity of adenine compounds with special reference to their action upon the mammalian heart. *The Journal of Physiology*, 14, 213–237. <http://erj.ersjournals.com/lookup/doi/10.1183/09031936.00137511>

Duckwitz, W., Hausmann, R., Aschrafi, A., & Schmalzing, G. (2006). P2X5 subunit assembly requires scaffolding by the second transmembrane domain and a conserved aspartate. *Journal of Biological Chemistry*, 281(51), 39561–39572. <https://doi.org/10.1074/jbc.M606113200>

Dunton, C. L., Purves, J. T., Hughes, F. M., Jin, H., & Nagatomi, J. (2018). Elevated hydrostatic pressure stimulates ATP release which mediates activation of the NLRP3 inflammasome via P2X4 in rat urothelial cells. *International Urology and Nephrology*, 50(9), 1607–1617. <https://doi.org/10.1007/s11255-018-1948-0>

Emmelin, N., & Feldberg, W. (1948). Systemic effects of adenosine triphosphate. *British Journal of Pharmacology and Chemotherapy*, 3, 273–284. <https://doi.org/10.1111/j.1476-5381.1948.tb00387.x>

Ennion, S. J., & Evans, R. J. (2002a). Conserved cysteine residues in the extracellular loop of the human P2X1 receptor form disulfide bonds and are involved in receptor trafficking to the cell surface. *Molecular Pharmacology*, 61(2), 303–311. <https://doi.org/10.1124/mol.61.2.303>

Ennion, S. J., & Evans, R. J. (2002b). P2X1 receptor subunit contribution to gating revealed by a dominant negative PKC mutant. *Biochemical and Biophysical Research Communications*, 291(3), 611–616. <https://doi.org/10.1006/bbrc.2002.6488>

Fischer, R., Kalthof, B., Grützmann, R., Woltering, E., Stelte-Ludwig, B., & Wuttke, M. (2004). *Benzofuro-1,4-diazepin-2-one derivatives* (Patent No. WO2004085440A1).

Fischer, W., Franke, H., Gröger-Arndt, H., & Illes, P. (2005). Evidence for the existence of P2Y1,2,4 receptor subtypes in HEK-293 cells: reactivation of P2Y1 receptors after repetitive agonist application. *Naunyn-Schmiedeberg's Archives of Pharmacology*, 371(6), 466–472. <https://doi.org/10.1007/s00210-005-1070-6>

Fischer, W., Wirkner, K., Weber, M., Eberts, C., Köles, L., Reinhardt, R., Franke, H., Allgaier, C., Gillen, C., & Illes, P. (2003). Characterization of P2X3, P2Y1 and P2Y4 receptors in cultured HEK293-hP2X3 cells and their inhibition by ethanol and trichloroethanol. *Journal of Neurochemistry*, 85(3), 779–790. <https://doi.org/10.1046/j.1471-4159.2003.01716.x>

Fois, G., Föhr, K. J., Kling, C., Fauler, M., Wittekindt, O. H., Dietl, P., & Frick, M. (2018). P2X4 receptor resensitization depends on a protonation/deprotonation cycle mediated by receptor internalization and recycling. *The Journal of Physiology*, 596(20), 4893–4907. <https://doi.org/10.1113/JP275448>

Fois, G., Winkelmann, V. E., Bareis, L., Staudenmaier, L., Hecht, E., Ziller, C., Ehinger, K., Schymeinsky, J., Kranz, C., & Frick, M. (2018). ATP is stored in lamellar bodies to activate vesicular P2X4 in an autocrine fashion upon exocytosis. *Journal of General Physiology*, 150(2), 277–291. <https://doi.org/10.1085/jgp.201711870>

Fountain, S. J., Parkinson, K., Young, M. T., Cao, L., Thompson, C. R. L., & North, R. A. (2007). An intracellular P2X receptor required for osmoregulation in Dictyostelium discoideum. *Nature*, 448(7150), 200–203. <https://doi.org/10.1038/nature05926>

Franklin, K. M., Asatryan, L., Jakowec, M. W., Trudell, J. R., Bell, R. L., & Davies, D. L. (2014). P2X4 receptors (P2X4Rs) represent a novel target for the development of drugs to prevent and/or treat alcohol use disorders. *Frontiers in Neuroscience*, 8(8 JUN), 1–12. <https://doi.org/10.3389/fnins.2014.00176>

Fuller, S. J., Stokes, L., Skarratt, K. K., Gu, B. J., & Wiley, J. S. (2009). Genetics of the P2X7 receptor and human disease. *Purinergic Signalling*, 5(2), 257–262. <https://doi.org/10.1007/s11302-009-9136-4>

Gangadharan, V., Nohe, A., Caplan, J., Czymbmek, K., & Duncan, R. L. (2015). Caveolin-1 regulates P2X7 receptor signalling in osteoblasts. *American Journal of Physiology-Cell Physiology*, 308(1), C41–C50. <https://doi.org/10.1152/ajpcell.00037.2014>

- Gao, Z.-G., & Jacobson, K. A. (2017). Distinct signalling patterns of allosteric antagonism at the P2Y1 receptor. *Molecular Pharmacology*, 92(5), 613–626. <https://doi.org/10.1124/mol.117.109660>
- Garcia-Guzman, M., Soto, F., Gomez-Hernandez, J. M., Lund, P.-E., & Stühmer, W. (1997). Characterization of recombinant human P2X4 receptor reveals pharmacological differences to the rat homologue. *Molecular Pharmacology*, 51, 109–118. <https://doi.org/10.1124/mol.51.1.109>
- Garcia-Guzman, M., Stühmer, W., & Soto, F. (1997). Molecular characterization and pharmacological properties of the human P2X3 purinoceptor. *Molecular Brain Research*, 47(1–2), 59–66. [https://doi.org/10.1016/S0169-328X\(97\)00036-3](https://doi.org/10.1016/S0169-328X(97)00036-3)
- George, B., Swartz, K. J., & Li, M. (2019). Hearing loss mutations alter the functional properties of human P2X2 receptor channels through distinct mechanisms. *Proceedings of the National Academy of Sciences*, 116(45), 22862–22871. <https://doi.org/10.1073/pnas.1912156116>
- George, J., Cunha, R. A., Mulle, C., & Amédée, T. (2016). Microglia-derived purines modulate mossy fibre synaptic transmission and plasticity through P2X4 and A1 receptors. *European Journal of Neuroscience*, 43(10), 1366–1378. <https://doi.org/10.1111/ejn.13191>
- Glass, R., Loesch, A., Bodin, P., & Burnstock, G. (2002). P2X4 and P2X6 receptors associate with VE-cadherin in human endothelial cells. *Cellular and Molecular Life Sciences*, 59(5), 870–881. <http://www.springerlink.com/index/xu6dejv2xpn1fvpn.pdf>
- Gofman, L., Cenna, J. M., & Potula, R. (2014). P2X4 receptor regulates alcohol-induced responses in microglia. *Journal of Neuroimmune Pharmacology*, 9(5), 668–678. <https://doi.org/10.1007/s11481-014-9559-8>
- Gong, D., Zhang, J., Chen, Y., Xu, Y., Ma, J., Hu, G., Huang, Y., Zheng, J., Zhai, W., & Xue, W. (2019). The m6A-suppressed P2RX6 activation promotes renal cancer cell migration and invasion through ATP-induced Ca²⁺ influx modulating ERK1/2 phosphorylation and MMP9 signalling pathway. *Journal of Experimental and Clinical Cancer Research*, 38(1), 1–16. <https://doi.org/10.1186/s13046-019-1223-y>
- Gong, Y., Jiang, J. H., & Li, S. T. (2016). Functional expression of human α 7 nicotinic acetylcholine receptor in human embryonic kidney 293 cells. *Molecular Medicine Reports*, 14(3), 2257–2263. <https://doi.org/10.3892/mmr.2016.5493>
- Gonzales, E., Julien, B., Serrière-Lanneau, V., Nicou, A., Doignon, I., Lagoudakis, L., Garcin, I., Azoulay, D., Duclos-Vallée, J.-C., Castaing, D., Didier, S., Hernandez-Garcia, A., Awad, S. S., Combettes, L., Thevananther, S., & Tordjmann, T. (2010). ATP release after partial hepatectomy regulates liver regeneration in the rat. *Journal of Hepatology*, 52(1), 54–62. <https://doi.org/10.1016/j.jhep.2009.10.005>
- Grynkiewicz, G., Poenie, M., & Tsien, R. Y. (1985). A new generation of Calcium indicators with greatly improved fluorescence properties. *Journal of Biological Chemistry*, 260(6), 3440–3450. [https://doi.org/10.1016/S0021-9258\(19\)83641-4](https://doi.org/10.1016/S0021-9258(19)83641-4)

Guo, C., Masin, M., Qureshi, O. S., & Murrell-Lagnado, R. D. (2007). Evidence for functional P2X4 /P2X7 heteromeric receptors. *Molecular Pharmacology*, 72(6), 1447–1456. <https://doi.org/10.1124/mol.107.035980>

Guo, L. H., Trautmann, K., & Schluesener, H. J. (2004). Expression of P2X4 receptor in rat C6 glioma by tumour-associated macrophages and activated microglia. *Journal of Neuroimmunology*, 152(1–2), 67–72. <https://doi.org/10.1016/j.jneuroim.2004.04.005>

Habermacher, C., Dunning, K., Chataigneau, T., & Grutter, T. (2016). Molecular structure and function of P2X receptors. *Neuropharmacology*, 104, 18–30. <https://doi.org/10.1016/j.neuropharm.2015.07.032>

Haines, W. R., Torres, G. E., Voigt, M. M., & Egan, T. M. (1999). Properties of the novel ATP-gated ionotropic receptor composed of the P2X1 and P2X5 isoforms. *Molecular Pharmacology*, 56(4), 720–727. <http://www.ncbi.nlm.nih.gov/pubmed/10496954>

Hammond, C., & Helenius, A. (1995). Quality control in the secretory pathway. *Current Opinion in Cell Biology*, 7(4), 523–529. [https://doi.org/10.1016/0955-0674\(95\)80009-3](https://doi.org/10.1016/0955-0674(95)80009-3)

Han, S. J., Lovaszi, M., Kim, M., D'Agati, V., Haskó, G., & Lee, H. T. (2020). P2X4 receptor exacerbates ischemic AKI and induces renal proximal tubular NLRP3 inflammasome signalling. *The FASEB Journal*, 34(4), 5465–5482. <https://doi.org/10.1096/fj.201903287R>

Harhun, M. I., Povstyan, O. v., Albert, A. P., & Nichols, C. M. (2014). ATP-evoked sustained vasoconstrictions mediated by heteromeric P2X1/4 receptors in cerebral arteries. *Stroke*, 45(8), 2444–2450. <https://doi.org/10.1161/STROKEAHA.114.005544>

Hattori, M., & Gouaux, E. (2012). Molecular mechanism of ATP binding and ion channel activation in P2X receptors. *Nature*, 485(7397), 207–212. <https://doi.org/10.1038/nature11010>

Hausmann, R., Bodnar, M., Woltersdorf, R., Wang, H., Fuchs, M., Messemer, N., Qin, Y., Günther, J., Riedel, T., Grohmann, M., Nieber, K., Schmalzing, G., Rubini, P., & Illes, P. (2012). ATP binding site mutagenesis reveals different subunit stoichiometry of functional P2X2/3 and P2X2/6 receptors. *Journal of Biological Chemistry*, 287(17), 13930–13943. <https://doi.org/10.1074/jbc.M112.345207>

He, M. L., Zemkova, H., Koshimizu, T. aki, Tomić, M., & Stojilkovic, S. S. (2003). Intracellular calcium measurements as a method in studies on activity of purinergic P2X receptor channels. *American Journal of Physiology - Cell Physiology*, 285, 467–479. <https://doi.org/10.1152/ajpcell.00042.2003>

Hernandez-Olmos, V., Abdelrahman, A., El-Tayeb, A., Freudendahl, D., Weinhausen, S., & Müller, C. E. (2012). N-substituted phenoxazine and acridone derivatives: Structure-activity relationships of potent P2X4 receptor antagonists. *Journal of Medicinal Chemistry*, 55(22), 9576–9588. <https://doi.org/10.1021/jm300845v>

Hille, B. (2001). *Ionic channels of excitable membranes* (3rd ed.). Sinauer Associates.

Holton, P. (1959). The liberation of adenosine triphosphate on antidromic stimulation of sensory nerves. *The Journal of Physiology*, 145, 494–504. <https://doi.org/10.1113/jphysiol.1959.sp006157>

Hu, B., Senkler, C., Yang, A., Soto, F., & Liang, B. T. (2002). P2X4 receptor is a glycosylated cardiac receptor mediating a positive ionotropic response to ATP. *Journal of Biological Chemistry*, 277(18), 15752–15757. <https://doi.org/10.1074/jbc.M112097200>

Hugel, S., & Schlichter, R. (2000). Presynaptic P2X receptors facilitate inhibitory GABAergic transmission between cultured rat spinal cord dorsal horn neurons. *The Journal of Neuroscience*, 20(6), 2121–2130. <https://doi.org/10.1523/JNEUROSCI.20-06-02121.2000>

Illes, P., Müller, C. E., Jacobson, K. A., Grutter, T., Nicke, A., Fountain, S. J., Kennedy, C., Schmalzing, G., Jarvis, M. F., Stojilkovic, S. S., King, B. F., & di Virgilio, F. (2021). Update of P2X receptor properties and their pharmacology: IUPHAR Review 30. *British Journal of Pharmacology*, 178(3), 489–514. <https://doi.org/10.1111/bph.15299>

Immadisetti, K., Alenciks, J., & Kekenes-Huskey, P. M. (2022). Modulation of P2X4 pore closure by magnesium, potassium, and ATP. *Biophysical Journal*, 121(7), 1134–1142. <https://doi.org/10.1016/j.bpj.2022.02.038>

Inoue, K. (2021). Nociceptive signalling of P2X receptors in chronic pain states. *Purinergic Signalling*, 17(1), 41–47. <https://doi.org/10.1007/s11302-020-09743-w>

Jeong, Y. H., Walsh, M. C., Yu, J., Shen, H., Wherry, E. J., & Choi, Y. (2020). Mice lacking the purinergic receptor P2X5 exhibit defective inflammasome activation and early susceptibility to Listeria monocytogenes. *The Journal of Immunology*, 205(3), 760–766. <https://doi.org/10.4049/jimmunol.1901423>

Jiang, L.-H., Kim, M., Spelta, V., Bo, X., Surprenant, A., & North, R. A. (2003). Subunit arrangement in P2X receptors. *The Journal of Neuroscience*, 23(26), 8903–8910. <https://doi.org/10.1523/JNEUROSCI.23-26-08903.2003>

Jiang, L.-H., Rassendren, F., Surprenant, A., & North, R. A. (2000). Identification of amino acid residues contributing to the ATP-binding site of a purinergic P2X receptor. *The Journal of Biological Chemistry*, 275(44), 34190–34196. <https://doi.org/10.1074/jbc.M005481200>

Jin, P., Jan, L. Y., & Jan, Y.-N. (2020). Mechanosensitive ion channels: structural features relevant to mechanotransduction mechanisms. *Annual Review of Neuroscience*, 43(1), 207–229. <https://doi.org/10.1146/annurev-neuro-070918-050509>

Jin, S., Fu, Q., Wuyun, G., & Wuyun, T. (2013). Management of post-hepatectomy complications. *World Journal of Gastroenterology*, 19(44), 7983–7991. doi: 10.3748/wjg.v19.i44.7983

Jo, Y.-H., Donier, E., Martinez, A., Garret, M., Toulmé, E., & Boué-Grabot, E. (2011). Cross-talk between P2X4 and γ -aminobutyric acid, type A receptors determines synaptic efficacy at a central synapse. *Journal of Biological Chemistry*, 286(22), 19993–20004. <https://doi.org/10.1074/jbc.M111.231324>

Johnsen, B., Kaschubowski, K. E., Nader, S., Schneider, E., Nicola, J. A., Fliegert, R., Wolf, I. M. A., Guse, A. H., Nikolaev, V. O., Koch-Nolte, F., & Haag, F. (2019). P2X7-mediated ATP secretion is accompanied by depletion of cytosolic ATP. *Purinergic Signalling*, 15(2), 155–166. <https://doi.org/10.1007/s11302-019-09654-5>

Jones, C. A., Chessell, I. P., Simon, J., Barnard, E. A., Miller, K. J., Michel, A. D., & Humphrey, P. P. A. (2000). Functional characterization of the P2X4 receptor orthologues. *British Journal of Pharmacology*, 129(2), 388–394. <https://doi.org/10.1038/sj.bjp.0703059>

Jones, C. A., Vial, C., Sellers, L. A., Humphrey, P. P. A., Evans, R. J., & Chessell, I. P. (2004). Functional Regulation of P2X6 Receptors by N-Linked Glycosylation: Identification of a Novel αβ-Methylene ATP-Sensitive Phenotype. *Molecular Pharmacology*, 65(4), 979–985. <https://doi.org/10.1124/mol.65.4.979>

Kaczmarek-Hájek, K., Lörinczi, É., Hausmann, R., & Nicke, A. (2012). Molecular and functional properties of P2X receptors - recent progress and persisting challenges. *Purinergic Signalling*, 8(3), 375–417. <https://doi.org/10.1007/s11302-012-9314-7>

Kanellopoulos, J. M., Almeida-da-Silva, C. L. C., Rüütel Boudinot, S., & Ojcius, D. M. (2021). Structural and functional features of the P2X4 receptor: an immunological perspective. *Frontiers in Immunology*, 12(March), 1–21. <https://doi.org/10.3389/fimmu.2021.645834>

Kawano, A., Tsukimoto, M., Mori, D., Noguchi, T., Harada, H., Takenouchi, T., Kitani, H., & Kojima, S. (2012). Regulation of P2X7-dependent inflammatory functions by P2X4 receptor in mouse macrophages. *Biochemical and Biophysical Research Communications*, 420(1), 102–107. <https://doi.org/10.1016/j.bbrc.2012.02.122>

Kawano, A., Tsukimoto, M., Noguchi, T., Hotta, N., Harada, H., Takenouchi, T., Kitani, H., & Kojima, S. (2012). Involvement of P2X4 receptor in P2X7 receptor-dependent cell death of mouse macrophages. *Biochemical and Biophysical Research Communications*, 419(2), 374–380. <https://doi.org/10.1016/j.bbrc.2012.01.156>

Kawate, T., Michel, J. C., Birdsong, W. T., & Gouaux, E. (2009). Crystal structure of the ATP-gated P2X4 ion channel in the closed state. *Nature*, 460(7255), 592–598. <https://doi.org/10.1038/nature08198>

Kawate, T., Robertson, J. L., Li, M., Silberberg, S. D., & Swartz, K. J. (2011). Ion access pathway to the transmembrane pore in P2X receptor channels. *The Journal of General Physiology*, 137(6), 579–590. <https://doi.org/10.1085/jgp.201010593>

Kennedy, C., Tasker, P. N., Gallacher, G., & Westfall, T. D. (2007). Identification of atropine- and P2X1 receptor antagonist-resistant, neurogenic contractions of the urinary bladder. *Journal of Neuroscience*, 27(4), 845–851. <https://doi.org/10.1523/JNEUROSCI.3115-06.2007>

Khakh, B. S., Fisher, J. A., Nashmi, R., Bowser, D. N., & Lester, H. A. (2005). An Angstrom scale interaction between plasma membrane ATP-gated P2X2 and 4 2 nicotinic channels measured with Fluorescence

Resonance Energy Transfer and Total Internal Reflection Fluorescence microscopy. *Journal of Neuroscience*, 25(29), 6911–6920. <https://doi.org/10.1523/JNEUROSCI.0561-05.2005>

Khakh, B. S., Proctor, W. R., Dunwiddie, T. v, Labarca, C., & Lester, H. A. (1999). Allosteric control of gating and kinetics at P2X4 receptor channels. *The Journal of Neuroscience*, 19(17), 7289–7299.

Khoja, S., Shah, V., Garcia, D., Asatryan, L., Jakowec, M. W., & Davies, D. L. (2016). Role of purinergic P2X4 receptors in regulating striatal dopamine homeostasis and dependent behaviours. *Journal of Neurochemistry*, 139(1), 134–148. <https://doi.org/10.1111/jnc.13734>

King, B. F. (2022). Rehabilitation of the P2X5 receptor: a re-evaluation of structure and function. *Purinergic Signalling*. <https://doi.org/10.1007/s11302-022-09903-0>

King, B. F., Townsend-Nicholson, A., Wildman, S. S., Thomas, T., Spyer, K. M., & Burnstock, G. (2000). Coexpression of rat P2X2 and P2X6 subunits in Xenopus Oocytes. *The Journal of Neuroscience*, 20(13), 4871–4877. <https://doi.org/10.1523/JNEUROSCI.20-13-04871.2000>

Kong, Q., Quan, Y., Tian, G., Zhou, J., & Liu, X. (2021). Purinergic P2 receptors: novel mediators of mechanotransduction. *Frontiers in Pharmacology*, 12, 1–7. <https://doi.org/10.3389/fphar.2021.671809>

Koshimizu, T. A., Tomic, M., van Goor, F., & Stojilkovic, S. S. (1998). Functional role of alternative splicing in pituitary P2X2 receptor-channel activation and desensitization. *Molecular Endocrinology*, 12(7), 901–913. <https://doi.org/10.1210/mend.12.7.0129>

Koshimizu, T., Ueno, S., Tanoue, A., Yanagihara, N., Stojilkovic, S. S., & Tsujimoto, G. (2002). Heteromultimerization modulates P2X receptor functions through participating extracellular and C-terminal subdomains. *The Journal of Biological Chemistry*, 277(49), 46891–46899. <https://doi.org/10.1074/jbc.M205274200>

Kotnis, S., Bingham, B., Vasilyev, D. v., Miller, S. W., Bai, Y., Yeola, S., Chanda, P. K., Bowlby, M. R., Kaftan, E. J., Samad, T. A., & Whiteside, G. T. (2010). Genetic and functional analysis of human P2X5 reveals a distinct pattern of exon 10 polymorphism with predominant expression of the nonfunctional receptor isoform. *Molecular Pharmacology*, 77(6), 953–960. <https://doi.org/10.1124/mol.110.063636>

Kowalski, M., Hausmann, R., Schmid, J., Dopychaj, A., Stephan, G., Tang, Y., Schmalzing, G., Illes, P., & Rubini, P. (2015). Flexible subunit stoichiometry of functional human P2X2/3 heteromeric receptors. *Neuropharmacology*, 99, 115–130. <https://doi.org/10.1016/j.neuropharm.2015.07.008>

Kuehnel, M. P., Rybin, V., Anand, P. K., Anes, E., & Griffiths, G. (2009). Lipids regulate P2X7-receptor-dependent actin assembly by phagosomes via ADP translocation and ATP synthesis in the phagosome lumen. *Journal of Cell Science*, 122(4), 499–504. <https://doi.org/10.1242/jcs.034199>

Lalo, U., Pankratov, Y., Wichert, S. P., Rossner, M. J., North, R. A., Kirchhoff, F., & Verkhratsky, A. (2008). P2X1 and P2X5 subunits form the functional P2X receptor in mouse cortical astrocytes. *The Journal of Neuroscience*, 28(21), 5473–5480. <https://doi.org/10.1523/JNEUROSCI.1149-08.2008>

Latapiat, V., Rodríguez, F. E., Godoy, F., Montenegro, F. A., Barrera, N. P., & Huidobro-Toro, J. P. (2017). P2X4 receptor in silico and electrophysiological approaches reveal insights of Ivermectin and zinc allosteric modulation. *Frontiers in Pharmacology*, 8(918), 1–13. <https://doi.org/10.3389/fphar.2017.00918>

Layhadi, J. A., Turner, J., Crossman, D., & Fountain, S. J. (2018). ATP evokes Ca²⁺ responses and CXCL5 secretion via P2X4 receptor activation in human monocyte-derived macrophages. *The Journal of Immunology*, 200(3), 1159–1168. <https://doi.org/10.4049/jimmunol.1700965>

Lazarowski, E. R., Boucher, R. C., & Harden, T. K. (2000). Constitutive release of ATP and evidence for major contribution of ecto-nucleotide pyrophosphatase and nucleoside diphosphokinase to extracellular nucleotide concentrations. *Journal of Biological Chemistry*, 275(40), 31061–31068. <https://doi.org/10.1074/jbc.M003255200>

Lê, K., Boué-Grabot, É., Archambault, V., & Séguéla, P. (1999). Functional and biochemical evidence for heteromeric ATP-gated channels composed of P2X1 and P2X5 subunits. *The Journal of Biological Chemistry*, 274(22), 15415–15419. <https://doi.org/10.1074/jbc.274.22.15415>

Lê, K.-T., Babinski, K., & Séguéla, P. (1998). Central P2X 4 and P2X 6 Channel Subunits Coassemble into a Novel Heteromeric ATP Receptor. *The Journal of Neuroscience*, 18(18), 7152–7159. <https://doi.org/10.1523/JNEUROSCI.18-18-07152.1998>

Lewis, C., Neldhart, S., Holy, C., North, R. A., Buell, G., & Surprenant, A. (1995). Coexpression of P2X2 and P2X3 receptor subunits can account for ATP-gated currents in sensory neurons. *Nature*, 377(October), 432–435. doi: 10.1038/377432a0

Li, F., Guo, N., Ma, Y., Ning, B., Wang, Y., & Kou, L. (2014). Inhibition of P2X4 suppresses joint inflammation and damage in collagen-induced arthritis. *Inflammation*, 37(1), 146–153. <https://doi.org/10.1007/s10753-013-9723-y>

Li, J., & Fountain, S. J. (2012). Fluvastatin suppresses native and recombinant human P2X4 receptor function. *Purinergic Signalling*, 8(2), 311–316. <https://doi.org/10.1007/s11302-011-9289-9>

Li, M., Silberberg, S. D., & Swartz, K. J. (2013). Subtype-specific control of P2X receptor channel signalling by ATP and Mg²⁺. *Proceedings of the National Academy of Sciences*, 110(36), E3455–E3463. <https://doi.org/10.1073/pnas.1308088110>

Li, M., Toombes, G. E. S., Silberberg, S. D., & Swartz, K. J. (2015). Physical basis of apparent pore dilation of ATP-activated P2X receptor channels. *Nature Neuroscience*, 18(11), 1577–1583. <https://doi.org/10.1038/nn.4120>

Lowe, P. P., Morel, C., Ambade, A., Iracheta-Vellve, A., Kwiatkowski, E., Satishchandran, A., Furi, I., Cho, Y., Gyongyosi, B., Catalano, D., Lefebvre, E., Fischer, L., Seyedkazemi, S., Schafer, D. P., & Szabo, G. (2020). Chronic alcohol-induced neuroinflammation involves CCR2/5-dependent peripheral macrophage infiltration and microglia alterations. *Journal of Neuroinflammation*, 17(1), 296. <https://doi.org/10.1186/s12974-020-01972-5>

Lynch, K. J., Touma, E., Niforatos, W., Kage, K. L., Burgard, E. C., van Biesen, T., Kowaluk, E. A., & Jarvis, M. F. (1999). Molecular and functional characterization of human P2X(2) receptors. *Molecular Pharmacology*, 56(6), 1171–1181. <http://www.ncbi.nlm.nih.gov/pubmed/10570044>

Macintyre, E. H., Pontén, J., & Vatter, A. E. (1972). The ultrastructure of human and murine astrocytes and of human fibroblasts in culture. *Acta Pathologica Microbiologica Scandinavica Section A Pathology*, 80(2), 267–283. <https://doi.org/10.1111/j.1699-0463.1972.tb02176.x>

Mansoor, S. E., Lü, W., Oosterheert, W., Shekhar, M., Tajkhorshid, E., & Gouaux, E. (2016). X-ray structures define human P2X3 receptor gating cycle and antagonist action. *Nature*, 538(7623), 66–71. <https://doi.org/10.1038/nature19367>

Marquez-Klaka, B., Rettinger, J., & Nicke, A. (2009). Inter-subunit disulfide cross-linking in homomeric and heteromeric P2X receptors. *European Biophysics Journal*, 38(3), 329–338. <https://doi.org/10.1007/s00249-008-0325-9>

Marucci, G., Lammi, C., Buccioni, M., Dal Ben, D., Lambertucci, C., Amantini, C., Santoni, G., Kandhavelu, M., Abbracchio, M. P., Lecca, D., Volpini, R., & Cristalli, G. (2011). Comparison and optimization of transient transfection methods at human astrocytoma cell line 1321N1. *Analytical Biochemistry*, 414(2), 300–302. <https://doi.org/10.1016/j.ab.2011.02.028>

Meyer, M. P., Gröschel-Stewart, U., Robson, T., & Burnstock, G. (1999). Expression of two ATP-gated ion channels, P2X5 and P2X6, in developing chick skeletal muscle. *Developmental Dynamics*, 216(4–5), 442–449. [https://doi.org/10.1002/\(sici\)1097-0177\(199912\)216:4/5<442::aid-dvdy12>3.0.co;2-z](https://doi.org/10.1002/(sici)1097-0177(199912)216:4/5<442::aid-dvdy12>3.0.co;2-z)

Michel, A. D., Miller, K. J., Lundström, K., Buell, G. N., & Humphrey, P. P. A. (1997). Radiolabeling of the rat P2X4 purinoceptor: evidence for allosteric interactions of purinoceptor antagonists and monovalent cations with P2X purinoceptors. *Molecular Pharmacology*, 51(3), 524–532. <http://www.ncbi.nlm.nih.gov/pubmed/9058609>

Murrell-Lagnado, R. D., & Frick, M. (2019). P2X4 and lysosome fusion. *Current Opinion in Pharmacology*, 47, 126–132. <https://doi.org/10.1016/j.coph.2019.03.002>

Nagata, K., Imai, T., Yamashita, T., Tsuda, M., Tozaki-Saitoh, H., & Inoue, K. (2009). Antidepressants Inhibit P2X 4 Receptor Function: a Possible Involvement in Neuropathic Pain Relief. *Molecular Pain*, 5, 1744-8069-5–20. <https://doi.org/10.1186/1744-8069-5-20>

Nichols, C. M., Povstyan, O. v., Albert, A. P., Gordienko, D. v., Khan, O., Vasilikostas, G., Khong, T. K., Wan, A., Reddy, M., & Harhun, M. I. (2014). Vascular smooth muscle cells from small human omental arteries express P2X1 and P2X4 receptor subunits. *Purinergic Signalling*, 10(4), 565–572. <https://doi.org/10.1007/s11302-014-9415-6>

Nicke, A. (2008). Homotrimeric complexes are the dominant assembly state of native P2X7 subunits. *Biochemical and Biophysical Research Communications*, 377(3), 803–808. <https://doi.org/10.1016/j.bbrc.2008.10.042>

- Nicke, A., Bäumert, H. G., Rettinger, J., Eichele, A., Lambrecht, G., Mutschler, E., & Schmalzing, G. (1998). P2X1 and P2X3 receptors form stable trimers: a novel structural motif of ligand-gated ion channels. *The EMBO Journal*, 17(11), 3016–3028. <https://doi.org/10.1093/emboj/17.11.3016>
- Nicke, A., Kerschensteiner, D., & Soto, F. (2005). Biochemical and functional evidence for heteromeric assembly of P2X1 and P2X4 subunits. *Journal of Neurochemistry*, 92(4), 925–933. <https://doi.org/10.1111/j.1471-4159.2004.02939.x>
- North, R. A. (2002). Molecular Physiology of P2X Receptors. *Physiological Reviews*, 82(4), 1013–1067. <https://doi.org/10.1152/physrev.00015.2002>
- North, R. A. (2016). P2X receptors. *Philosophical Transactions of the Royal Society B: Biological Sciences*, 371(1700), 20150427. <https://doi.org/10.1098/rstb.2015.0427>
- North, R. A., & Surprenant, A. (2000). Pharmacology of cloned P2X receptors. *Annual Review of Pharmacology and Toxicology*, 40, 563–580. <https://doi.org/10.1146/annurev.pharmtox.40.1.563>
- Öjemalm, K., Watson, H. R., Roboti, P., Cross, B. C. S., Warwicker, J., von Heijne, G., & High, S. (2013). Positional editing of transmembrane domains during ion channel assembly. *Journal of Cell Science*, 126(2), 464–472. <https://doi.org/10.1242/jcs.111773>
- Pasqualetto, G., Brancale, A., & Young, M. T. (2018). The molecular determinants of small-molecule ligand binding at P2X receptors. *Frontiers in Pharmacology*, 9(58), 1–13. <https://doi.org/10.3389/fphar.2018.00058>
- Paton, W. D. M., & Vane, J. R. (1963). An analysis of the responses of the isolated stomach to electrical stimulation and to drugs. *Journal of Physiology*, 165, 10–46.
- Pelegrín, P. (ed.). (2020). Purinergic signalling: methods and protocols. In P. Pelegrín (Ed.), *Methods in Molecular Biology* (Vol. 2041). Springer Science+Business Media, LLC, part of Springer Nature 2020. <https://doi.org/10.1007/978-1-4939-9717-6>
- Peverini, L., Beudez, J., Dunning, K., Chataignneau, T., & Grutter, T. (2018). New Insights Into Permeation of Large Cations Through ATP-Gated P2X Receptors. *Frontiers in Molecular Neuroscience*, 11(July), 1–12. <https://doi.org/10.3389/fnmol.2018.00265>
- Pintor, J., King, B. F., Miras-Portugal, M. T., & Burnstock, G. (1996). Selectivity and activity of adenine dinucleotides at recombinant P2X2 and P2Y1 purinoceptors. *British Journal of Pharmacology*, 119(5), 1006–1012. <https://doi.org/10.1111/j.1476-5381.1996.tb15771.x>
- Pintor, J., Puche, J. A., Gualix, J., Hoyle, C. H. V., & Miras-Portugal, M. T. (1997). Diadenosine polyphosphates evoke calcium transients in guinea-pig brain via receptors distinct from those for ATP. *Journal of Physiology*, 504(2), 327–335. <https://doi.org/10.1111/j.1469-7793.1997.327be.x>
- Priel, A., & Silberberg, S. D. (2004). Mechanism of ivermectin facilitation of human P2X4 receptor channels. *The Journal of General Physiology*, 123(3), 281–293. <https://doi.org/10.1085/jgp.200308986>

Qureshi, O. S., Paramasivam, A., Yu, J. C. H., & Murrell-Lagnado, R. D. (2007). Regulation of P2X4 receptors by lysosomal targeting, glycan protection and exocytosis. *Journal of Cell Science*, 120(21), 3838–3849. <https://doi.org/10.1242/jcs.010348>

Ralevic, V., & Burnstock, G. (1998). Receptors for purines and pyrimidines. *Pharmacological Reviews*, 50(3), 413–492. <http://www.ncbi.nlm.nih.gov/pubmed/9755289>

Ranade, S. S., Syeda, R., & Patapoutian, A. (2015). Mechanically activated ion channels. *Neuron*, 87(6), 1162–1179. <https://doi.org/10.1016/j.neuron.2015.08.032>

Rettinger, J., Aschrafi, A., & Schmalzing, G. (2000). Roles of individual N-glycans for ATP potency and expression of the rat P2X1 receptor. *Journal of Biological Chemistry*, 275(43), 33542–33547. <https://doi.org/10.1074/jbc.M002918200>

Richards, D., Gever, J. R., Ford, A. P., & Fountain, S. J. (2019). Action of MK-7264 (Gefapixant) at human P2X3 and P2X2/3 receptors and in vivo efficacy in models of sensitisation. *British Journal of Pharmacology*, 1–13. <https://doi.org/10.1111/bph.14677>

Robinson, L. E., & Murrell-Lagnado, R. D. (2013). The trafficking and targeting of P2X receptors. *Frontiers in Cellular Neuroscience*, 7(233), 1–6. <https://doi.org/10.3389/fncel.2013.00233>

Rong, W., Gourine, A. v., Cockayne, D. A., Xiang, Z., Ford, A. P. D. W., Spyer, K. M., & Burnstock, G. (2003). Pivotal role of nucleotide P2X2 receptor subunit of the ATP-gated ion channel mediating ventilatory responses to hypoxia. *Journal of Neuroscience*, 23(36), 11315–11321. <https://doi.org/10.1523/jneurosci.23-36-11315.2003>

Royle, S. J., Qureshi, O. S., Bobanovic, L. K., Evans, P. R., Owen, D. J., & Murrell-Lagnado, R. D. (2005). Non-canonical YXXG endocytic motifs: recognition by AP2 and preferential utilization in P2X4 receptors. *Journal of Cell Science*, 118(14), 3073–3080. <https://doi.org/10.1242/jcs.02451>

Rubio, M. E., & Soto, F. (2001). Distinct localization of P2X receptors at excitatory postsynaptic specializations. *Journal of Neuroscience*, 21(2), 641–653. <https://doi.org/10.1523/jneurosci.21-02-00641.2001>

Samways, D. S. K., Khakh, B. S., Dutertre, S., & Egan, T. M. (2011). Preferential use of unobstructed lateral portals as the access route to the pore of human ATP-gated ion channels (P2X receptors). *Proceedings of the National Academy of Sciences*, 108(33), 13800–13805. <https://doi.org/10.1073/pnas.1017550108>

Samways, D. S. K., Khakh, B. S., & Egan, T. M. (2012). Allosteric modulation of Ca²⁺ flux in ligand-gated cation channel (P2X4) by actions on lateral portals. *The Journal of Biological Chemistry*, 287(10), 7594–7602. <https://doi.org/10.1074/jbc.M111.322461>

Samways, D. S. K., Li, Z., & Egan, T. M. (2014). Principles and properties of ion flow in P2X receptors. *Frontiers in Cellular Neuroscience*, 8(February), 1–18. <https://doi.org/10.3389/fncel.2014.00006>

Saul, A., Hausmann, R., Kless, A., & Nicke, A. (2013). Heteromeric assembly of P2X subunits. *Frontiers in Cellular Neuroscience*, 7(250), 1–20. <https://doi.org/10.3389/fncel.2013.00250>

Schiller, I. C., Jacobson, K. A., Wen, Z., Malisetty, A., Schmalzing, G., & Markwardt, F. (2022). Dihydropyridines potentiate ATP-induced currents mediated by the full-length human P2X5 receptor. *Molecules*, 27(6). <https://doi.org/10.3390/molecules27061846>

Shrivastava, A. N., Triller, A., Sieghart, W., & Sarto-Jackson, I. (2011). Regulation of GABA-A receptor dynamics by interaction with purinergic P2X2 receptors. *Journal of Biological Chemistry*, 286(16), 14455–14468. <https://doi.org/10.1074/jbc.M110.165282>

Silberberg, S. D., Li, M., & Swartz, K. J. (2007). Ivermectin interaction with transmembrane helices reveals widespread rearrangements during opening of P2X receptor channels. *Neuron*, 54(2), 263–274. <https://doi.org/10.1016/j.neuron.2007.03.020>

Sine, S. M., & Engel, A. G. (2006). Recent advances in Cys-loop receptor structure and function. *Nature*, 440, 448–455. doi:10.1038/nature04708

Smith, J. A., Kitt, M. M., Butera, P., Smith, S. A., Li, Y., Xu, Z. J., Holt, K., Sen, S., Sher, M. R., & Ford, A. P. (2020). Gefapixant in two randomised dose-escalation studies in chronic cough. *European Respiratory Journal*, 55(3), 1901615. <https://doi.org/10.1183/13993003.01615-2019>

Sonnenreich, P. (2021). *Nippon Chemiphar Presents Promising Data on Novel Prescription Cough Medicine, Representing Possibly Second New Rx Cough Drug to Enter Market Since 1950s*. BioSpace. <https://www.biospace.com/article/nippon-chemiphar-presents-promising-data-on-novel-prescription-cough-medicine-representing-possibly-second-new-rx-cough-drug-to-enter-market-since-1950s/#:~:text=NC-2600> is the only receptor on the respiratory tract.

Sophocleous, R. A., Berg, T., Finol-Urdaneta, R. K., Sluyter, V., Keshiya, S., Bell, L., Curtis, S. J., Curtis, B. L., Seavers, A., Bartlett, R., Dowton, M., Stokes, L., Ooi, L., & Sluyter, R. (2020). Pharmacological and genetic characterisation of the canine P2X4 receptor. *British Journal of Pharmacology*, 177(12), 2812–2829. <https://doi.org/10.1111/bph.15009>

Soto, F., Garcia-Guzman, M., Gomez-Hernandez, J. M., Hollmann, M., Karschin, C., & Stühmer, W. (1996). P2X4: an ATP-activated ionotropic receptor cloned from rat brain. *Proceedings of the National Academy of Sciences*, 93(8), 3684–3688. <https://doi.org/10.1073/pnas.93.8.3684>

Stephan, G., Huang, L., Tang, Y., Vilotti, S., Fabbretti, E., Yu, Y., Nörenberg, W., Franke, H., Göröncsér, F., Sperlágh, B., Dopychaj, A., Hausmann, R., Schmalzing, G., Rubini, P., & Illes, P. (2018). The ASIC3/P2X3 cognate receptor is a pain-relevant and ligand-gated cationic channel. *Nature Communications*, 9(1). <https://doi.org/10.1038/s41467-018-03728-5>

Stokes, L., Layhadi, J. A., Bibic, L., Dhuna, K., & Fountain, S. J. (2017). P2X4 receptor function in the nervous system and current breakthroughs in pharmacology. *Frontiers in Pharmacology*, 8(291), 1–15. <https://doi.org/10.3389/fphar.2017.00291>

- Stokes, L., Scurrah, K., Ellis, J. A., Cromer, B. A., Skarratt, K. K., Gu, B. J., Harrap, S. B., & Wiley, J. S. (2011). A loss-of-function polymorphism in the human P2X4 receptor is associated with increased pulse pressure. *Hypertension*, 58(6), 1086–1092. <https://doi.org/10.1161/HYPERTENSIONAHA.111.176180>
- Sun, Z., & Brodsky, J. L. (2019). Protein quality control in the secretory pathway. *Journal of Cell Biology*, 218(10), 3171–3187. <https://doi.org/10.1083/jcb.201906047>
- Surprenant, A., Schneider, D. A., Wilson, H. L., Galligan, J. J., & North, R. A. (2000). Functional properties of heteromeric P2X1/5 receptors expressed in HEK cells and excitatory junction potentials in guinea-pig submucosal arterioles. *Journal of the Autonomic Nervous System*, 81(1–3), 249–263. [https://doi.org/10.1016/S0165-1838\(00\)00123-5](https://doi.org/10.1016/S0165-1838(00)00123-5)
- Suurväli, J., Boudinot, P., Kanellopoulos, J., & Rüütel Boudinot, S. (2017). P2X4: A fast and sensitive purinergic receptor. *Biomedical Journal*, 40(5), 245–256. <https://doi.org/10.1016/j.bj.2017.06.010>
- Taruno, A. (2018). ATP Release Channels. *International Journal of Molecular Sciences*, 19(808), 1–26. <https://doi.org/10.3390/ijms19030808>
- Taruno, A., Nomura, K., Kusakizako, T., Ma, Z., Nureki, O., & Foskett, J. K. (2021). Taste transduction and channel synapses in taste buds. *Pflugers Archiv European Journal of Physiology*, 473(1), 3–13. <https://doi.org/10.1007/s00424-020-02464-4>
- Teo, A. C. K., Lee, S. C., Pollock, N. L., Stroud, Z., Hall, S., Thakker, A., Pitt, A. R., Dafforn, T. R., Spickett, C. M., & Roper, D. I. (2019). Analysis of SMALP co-extracted phospholipids shows distinct membrane environments for three classes of bacterial membrane protein. *Scientific Reports*, 9(1), 1813. <https://doi.org/10.1038/s41598-018-37962-0>
- Torres, G. E., Egan, T. M., & Voigt, M. M. (1999). Hetero-oligomeric assembly of P2X receptor subunits. *Journal of Biological Chemistry*, 274(10), 6653–6659. <https://doi.org/10.1074/jbc.274.10.6653>
- Torres, G. E., Haines, W. R., Egan, T. M., & Voigt, M. M. (1998). Co-expression of P2X1 and P2X5 receptor subunits reveals a novel ATP-gated ion channel. *Molecular Pharmacology*, 54(6), 989–993. <https://doi.org/10.1124/mol.54.6.989>
- Toulmé, E., Blais, D., Léger, C., Landry, M., Garret, M., Séguéla, P., & Boué-Grabot, E. (2007). An intracellular motif of P2X3 receptors is required for functional cross-talk with GABA_A receptors in nociceptive DRG neurons. *Journal of Neurochemistry*, 102(4), 1357–1368. <https://doi.org/10.1111/j.1471-4159.2007.04640.x>
- Trang, M., Schmalzing, G., Müller, C. E., & Markwardt, F. (2020). Dissection of P2X4 and P2X7 receptor current components in BV-2 microglia. *International Journal of Molecular Sciences*, 21(22), 1–20. <https://doi.org/10.3390/ijms21228489>
- Tsuda, M., Masuda, T., Tozaki-Saitoh, H., & Inoue, K. (2013). P2X4 receptors and neuropathic pain. *Frontiers in Cellular Neuroscience*, 7(191), 1–6. <https://doi.org/10.3389/fncel.2013.00191>

- Tsuda, M., Shigemoto-Mogami, Y., Koizumi, S., Mizokoshi, A., Kohsaka, S., Salter, M. W., & Inoue, K. (2003). P2X4 receptors induced in spinal microglia gate tactile allodynia after nerve injury. *Nature*, 424(6950), 778–783. <https://doi.org/10.1038/nature01786>
- Valera, S., Hussy, N., Evans, R. J., Adami, N., North, R. A., Surprenant, A., & Buell, G. (1994). A new class of ligand-gated ion channel defined by P2X receptor for extracellular ATP. *Nature*, 371, 516–519.
- von Kügelgen, I., & Hoffmann, K. (2016). Pharmacology and structure of P2Y receptors. *Neuropharmacology*, 104, 50–61. <https://doi.org/10.1016/j.neuropharm.2015.10.030>
- Webb, T. E., Simon, J., Krishek, B. J., Bateson, A. N., Smart, T. G., King, B. F., Burnstock, G., & Barnard, E. A. (1993). Cloning and functional expression of a brain G-protein-coupled ATP receptor. *Federation of European Biochemical Societies*, 324(2), 219–225. [https://doi.org/10.1016/0014-5793\(93\)81397-I](https://doi.org/10.1016/0014-5793(93)81397-I)
- Weinhausen, S., Nagel, J., Namasivayam, V., Spanier, C., Abdelrahman, A., Hanck, T., Hausmann, R., & Müller, C. E. (2022). Extracellular binding sites of positive and negative allosteric P2X4 receptor modulators. *Life Sciences*, 311(121143), 1–18. <https://doi.org/10.1016/j.lfs.2022.121143>
- Werner, S., Mesch, S., Hillig, R. C., ter Laak, A., Klint, J., Neagoe, I., Laux-Biehlmann, A., Dahllof, H., Brauer, N., Puetter, V., Nubbemeyer, R., Schulz, S., Bairlein, M., Zollner, T. M., & Steinmeyer, A. (2019). Discovery and characterization of the potent and selective P2X4 inhibitor N-[4-(3-Chlorophenoxy)-3-sulfamoylphenyl]-2-phenylacetamide (BAY-1797) and structure-guided amelioration of its CYP3A4 induction profile. *Journal of Medicinal Chemistry*, 62, 11194–11217.
- Wildman, S. S., Marks, J., Churchill, L. J., Peppiatt, C. M., Chraibi, A., Shirley, D. G., Horisberger, J. D., King, B. F., & Unwin, R. J. (2005). Regulatory interdependence of cloned epithelial Na⁺ channels and P2X receptors. *Journal of the American Society of Nephrology*, 16(9), 2586–2597. <https://doi.org/10.1681/ASN.2005020130>
- Wilkinson, W. J., Jiang, L.-H., Surprenant, A., & North, R. A. (2006). Role of ectodomain lysines in the subunits of the heteromeric P2X2/3 receptor. *Molecular Pharmacology*, 70(4), 1159–1163. <https://doi.org/10.1124/mol.106.026658>
- Wilson, H. L., Varcoe, R. W., Stokes, L., Holland, K. L., Francis, S. E., Dower, S. K., Surprenant, A., & Crossman, D. C. (2007). P2X receptor characterization and IL-1/IL-1Ra release from human endothelial cells. *British Journal of Pharmacology*, 151(1), 96–108. <https://doi.org/10.1038/sj.bjp.0707213>
- Wirsching, E., Fauler, M., Fois, G., & Frick, M. (2020). P2 purinergic signalling in the distal lung in health and disease. *International Journal of Molecular Sciences*, 21(14), 1–25. <https://doi.org/10.3390/ijms21144973>
- Xia, G., Cai, J., Wu, X., Fang, Q., Zhao, N., & Lv, X. (2022). The mechanism by which ATP regulates alcoholic steatohepatitis through P2X4 and CD39. *European Journal of Pharmacology*, 916(August 2021), 174729. <https://doi.org/10.1016/j.ejphar.2021.174729>

Xu, J., Chai, H., Ehinger, K., Egan, T. M., Srinivasan, R., Frick, M., & Khakh S., B. (2014). Imaging P2X4 receptor subcellular distribution, trafficking, and regulation using P2X4-pHluorin. *The Journal of General Physiology*, 144(1), 81–104. <https://doi.org/10.1085/jgp.201411169>

Yamamoto, K., Korenaga, R., Kamiya, A., & Ando, J. (2000). Fluid shear stress activates Ca²⁺ influx into human endothelial cells via P2X4 purinoceptors. *Circulation Research*, 87(5), 385–391. <https://doi.org/10.1161/01.RES.87.5.385>

Yamamoto, K., Korenaga, R., Kamiya, A., Qi, Z., Sokabe, M., & Ando, J. (2000). P2X4 receptors mediate ATP-induced calcium influx in human vascular endothelial cells. *American Journal of Physiology-Heart and Circulatory Physiology*, 279, 285–292. <https://doi.org/10.1152/ajpheart.2000.279.1.H285>

Yamamoto, K., Sokabe, T., Matsumoto, T., Yoshimura, K., Shibata, M., Ohura, N., Fukuda, T., Sato, T., Sekine, K., Kato, S., Isshiki, M., Fujita, T., Kobayashi, M., Kawamura, K., Masuda, H., Kamiya, A., & Ando, J. (2006). Impaired flow-dependent control of vascular tone and remodelling in P2X4-deficient mice. *Nature Medicine*, 12(1), 133–137. <https://doi.org/10.1038/nm1338>

Yang, R., & Liang, B. T. (2012). Cardiac P2X4 Receptors: Targets in Ischemia and Heart Failure? *Circulation Research*, 111(4), 397–401. <https://doi.org/10.1161/CIRCRESAHA.112.265959>

Yang, T., Shen, J., Yang, R., Redden, J., Dodge-Kafka, K., Grady, J., Jacobson, K. A., & Liang, B. T. (2014). Novel protective role of endogenous cardiac myocyte P2X4 receptors in heart failure. *Circulation: Heart Failure*, 7(3), 510–518. <https://doi.org/10.1161/CIRCHEARTFAILURE.113.001023>

Yegutkin, G. G. (2008). Nucleotide- and nucleoside-converting ectoenzymes: Important modulators of purinergic signalling cascade. *Biochimica et Biophysica Acta (BBA) - Molecular Cell Research*, 1783(5), 673–694. <https://doi.org/10.1016/j.bbamcr.2008.01.024>

Yegutkin, G. G. (2014). Enzymes involved in metabolism of extracellular nucleotides and nucleosides: Functional implications and measurement of activities. *Critical Reviews in Biochemistry and Molecular Biology*, 49(6), 473–497. <https://doi.org/10.3109/10409238.2014.953627>

Young, M. T. (2010). P2X receptors: dawn of the post-structure era. *Trends in Biochemical Sciences*, 35(2), 83–90. <https://doi.org/10.1016/j.tibs.2009.09.006>

Young, M. T., Fisher, J. A., Fountain, S. J., Ford, R. C., North, R. A., & Khakh, B. S. (2008). Molecular shape, architecture, and size of P2X4 receptors determined using fluorescence resonance energy transfer and electron microscopy. *Journal of Biological Chemistry*, 283(38), 26241–26251. <https://doi.org/10.1074/jbc.M804458200>

Zabala, A., Vazquez-Villoldo, N., Rissiek, B., Gejo, J., Martin, A., Palomino, A., Perez-Samartín, A., Pulagam, K. R., Lukowiak, M., Capetillo-Zarate, E., Llop, J., Magnus, T., Koch-Nolte, F., Rassendren, F., Matute, C., & Domercq, M. (2018). P2X4 receptor controls microglia activation and favours remyelination in autoimmune encephalitis. *EMBO Molecular Medicine*, 10(8), 1–20. <https://doi.org/10.15252/emmm.201708743>

Zech, A., Wiesler, B., Ayata, C. K., Schlaich, T., Dürk, T., Hoßfeld, M., Ehrat, N., Cicko, S., & Idzko, M. (2016). P2RX4 deficiency in mice alleviates allergen-induced airway inflammation. *Oncotarget*, 7(49), 80288–80297. <https://doi.org/10.18632/oncotarget.13375>

Zhang, D., Gao, Z.-G., Zhang, K., Kiselev, E., Crane, S., Wang, J., Paoletta, S., Yi, C., Ma, L., Zhang, W., Han, G. W., Liu, H., Cherezov, V., Katritch, V., Jiang, H., Stevens, R. C., Jacobson, K. A., Zhao, Q., & Wu, B. (2015). Two disparate ligand-binding sites in the human P2Y1 receptor. *Nature*, 520(7547), 317–321. <https://doi.org/10.1038/nature14287>

Appendix 1

A. Nucleotide (nts) and peptide (aa) sequences for human $\alpha 7$ nAChR and human P2X1-7 receptors with a C-terminus HA tag. ‘ATG’ corresponds to the start codon and codes for a Methionine (M), and both ‘TAA’ and ‘TGA’ are stop codons (*) which terminate the translation process of the protein. Human P2X1-7 receptor sequences contain a C-term HA epitope (highlighted in grey) as an example.

> $\alpha 7$ nAChR_nts

```
ATGCCTGCTGCCGGAGCGTCTGGCTGGCGCTGCCCGTCGCTCCTGCACGTGTCCCTGCAAGG  
CGAGTTCCAGAGGAAGCTTACAAGGAGCTGGTCAAGAACTACAATCCCCTGGAGAGGCCGTGGCCA  
ATGACTCGAACCACTCACCGTCACTCTCCCTGAGCCTCCTGCAGATCATGGACGTGGATGAGAAG  
AACCAAGTTAACCAACATTGGCTGCAAATGTCTGGACAGATCACTATTACAGTGGAAATGT  
GTCAGAATATCCAGGGTGAAGACTGTTCTCCAGATGCCAGATTGGAAACCAGACATTCTC  
TCTATAACAGTGCTGATGAGCGCTTGACGCCACATTCCACACTAACGTGTTGGTAATTCTCTGG  
CATTGCCAGTACCTGCCTCCAGGCATATTCAAGAGTCTGCTACATCGATGTACGCTGGTTCCCT  
TGATGTGCAGCACTGCAAAGTTGGCTCTGGTCTTACGGAGGCTGGCCTGGATCTGCAGA  
TGCAGGAGGCAGATATCAGTGGCTATATCCCCAATGGAGAATGGACCTAGTGGAAATCCCCGGCAAG  
AGGAGTGAAAGGTTCTATGAGTGCTGCAAAGAGCCCTACCCCTGATGTCACCTCACAGTGACCATGCG  
CCGCAGGACACTCTACTATGCCCTAACCTGCTGATCCCTGTGCTCATCTCCGCCCTGCCCTGC  
TGGTGTCTGCTCCTGCAGATTCCGGGAGAAGATTCCCTGGGATAACAGTCTTACTCTCT  
ACCGTCTTCATGCTGCTCGTGGCTGAGATCATGCCGAAACATCCGATTGGTACCATGATAGCCA  
GTACTCGCCAGCACCATGATCATCGTGGCCTCTCGGTGGTGACGGTGATCGTGCAGTAC  
ACCACCAACGACCCGACGGGGCAAGATGCCAAGTGGACCAGAGTCATCCTCTGAACGGTGC  
TGGTCTGCAATGAAGAGGCCGGGGAGGACAAGGTGCGCCGCCAGCACAGCAGCG  
CTGCAGCCTGCCAGTGTGGAGATGAGCGCCGTGGCGCCGCCAGCAACGGAACCTGCTGT  
ACATCGGCTTCCGCGGCCCTGGACGGCGTGCAGTGTCTCCGACCCCCGACTCTGGGTAGTGTGG  
CGCATGGCCTGCTCCCCACGCACGATGAGCACCTCCTGCACGGTGGCAACCCCCGAGGGGACCC  
GGACTTGGCCAAGATCCTGGAGGAGGTCCGCTACATTGCCAACCGCTCCGCTGCCAGGAC  
AGGCGGTCTGCAGCGAGTGGAAAGTTGCCGCTGTGTGGACCGCCTGTGCCTCATGCCCTCTCG  
GTCTTCACCATCATGCAACCATGGCATCCTGATGTCGGCTCCAACTCGTGGAGGCCGTGTCAA  
AGACTTTGCGTATAA
```

> $\alpha 7$ nAChR_aa

```
MRCSPGGVWLALAASLLHVSIQGEFQRKLYKELVKYNPLERPVANDSQPLTVYFSLSLIQIMDVDEK  
NQVLTTNIWLQMSWTDHYLQWNVSEYPGVKTVRFPDGQIWKPDILLYNSADERFDATFHTNVLVNSSG  
HCQYLPPGIFKSSCYIDVRWFPFDVQHCKLKFGWSYGGWSDLQMQEADISGYIPNGEWDLVGIPGK  
RSERFYECCKEPYPDVTFTVTMRRRTLYYGLNLLIPCVLISALALLVFLLPADSGEKISLGITVLLSL  
TVFMLLVAEIMPATSDSVPLIAQYFASTMIIIVGLSVVVTIVLQYHHDPGGKMPKWTRVILLNWCA  
WFLRMKRPGEDKVRPACQHKQRRCSLASVEMSAVAPPASNGNLLYIGFRGLDGVHCVPDGVCG  
RMACSPTHDELLHGGQPPEGDPDLAKILEEVRYIANRFRCQDESEAVCSEWKFAACVVDRCLMAFS  
VFTIICITIGILMSAPNFVEAVSKDFA*
```

>hP2X1WT_nts

ATGGCCAGGAGATTCCAGGAGGAGCTGGCCGCCTTCTGTTGAGTACGACACCCCCAGAATGGTGCT
GGTAGGAACAAGAAGGTGGCGTGATCTCAGACTGATCCAGCTGGTGGTGTGGTACGTGATCG
GCTGGGTGTTCCCTGTACGAGAAGGGCTACCAGACCTCCTCCGGCTGATCTCCTCCGTGTCGTGAAG
CTGAAGGGCCTGGCGTGACCCAGCTGCCCGACTGGGACCACAGGTGTGGATGTGGCGATTACGT
GTTTCCCAGGGCAGAACATAGCTTCGTGGTATGACCAACTCATCGTACCCCTAACGAGACAC
AGGGCTACTGTGCCGAGCACCCCTGAGGGCGCATCTGTAAGGAGGATTCCGGCTGTACCCCGGCAAG
GCCAAGAGAAAGGCCAGGGCATCAGGACCGCAAGTGCCTGGCCTTAATGATAACGTGAAGACATG
CGAGATCTTGGCTGGTGTCCCGTGGAGGTGGATGACATCCCCAGACCTGCCCTGCTGAGAGAGG
CCGAGAATTCACCCCTGTTATCAAGAATAGCATCTCCTCCCCAGATTCAAAGTGAACAGAAGAAC
CTGGTGGAGGAGGTGAACGCCAACATGAAGACCTGCCCTGTTACAGACCCCTGCACCCCTGTG
TCCTGTGTTCCAGCTGGCTACGTGGCAGGAGTCCGGCAGAATTTCCACCCCTGGCGAGAAGG
GCGCGTGGTGGGAATCACAATCGATTGGCACTGTGATCTGGATTGGCACGTGAGGCAGTCAGACCT
ATCTACGAGTTCCACGGCCTGTACGAGGAGAAGAATCTGTCCTGGCTTCAATTCAAGATTTGCCAG
ACACTTTGGAGAACGGCACAAATTACAGGCACCTGTTAAGGTGTTGGCATCAGGTCGATATCC
TGGTGGACGGCAAGGCCAGTTCGATATCATCCCCACCATGACCACAATGGCTCCGGCATCGC
ATCTTCGGCGTGGCCACCGTGTGCGATCTGCTGCTGCACATCCTGCCATAAGAGGCACTACTA
CAAGCAGAAGAAGTTCAAGTACGCCAGGGATATGGGCCCTGGCGCCGAAAGAGACCTGGCTGCCA
CCAGCAGCACACTGGCCTGCAGGAGAATATGAGGACATCCTACCCCTACGACGTGCCGATTACGCC
TGA

>hP2X1WT_aa

MARRFQEELAAFLFEYDTPRMVLVRNKKVGVIFRLIQLVVLVYVIGWVFLYEKGYQTSSGLISSVSK
LKGLAVTQLPGLGPQVWDVADYVFPAQGDNSFVVMNTFIVTPKQTQGYCAEHPEGGICKEDSGCTPGK
AKRKAQGIRTGKCVAFNDTVKTCEIFGWCPVEVDDIPRPALLREAENFTLFIKNSISFPRFKVNRRN
LVEEVNAAHMKTCLFHKLHPLCPVQLGYVVQESQNFSLAEKGGVVGITIDWHCDLDWHVRHCRP
IYEFHGLYEEKNLSPGFNFRFARHFVENGTNYRHLFKVFGIRFDILVDGKAGKFDIIPMTTIGSGIG
IFGVATVLC DLLLHILPKRHYYKQKKFKYAEDMGP GAAERDLAATSSLQENMRTSYPYDVPDYA
*

>hP2X2WT_nts

ATGGCCGCTGCCAGCCTAAGTACCCCGCCGGAGCCACAGCCAGAAGGCTGGCTAGAGGCTGCTGGAG
CGCCCTGTGGACTACGAGACCCCAAGGTATTGTGGTGGAAATAGAAGGCTGGCGTGTAC
GAGCCGTGCAGCTGCTGATCCTGCTGTACTCGTGTGGTACGTGTTATCGTCAGAACCTACCA
GAGAGCGAGACAGGCCAGAGAGCTCCATCATCACAAAGGTGAAGGGCATCACCACCTCCGAGCACAA
GGTGTGGATGTGGAGGAGTACGTGAAGCCTCCGAGGGCGCTCCGTGTTACGCATCATCACAGAG
TGGAGGCCACACACAGCCAGACCCAGGGCACCTGTCCTGAGTCATCAGGGTCACAATGCCACCTGC
CTGTCGATGCCATTGCGTGGCGGAGCTGGACATGCTGGCAACGGCCTGAGGACAGGCAGGTG
CGTGCCTACTACCAGGGCCCTCCAAGACATGTGAGGTGTTGGCTGGGCCGTGGAGGACGGCG
CCTCTGTCCCAGTTCTGGCACCATGGCCCCAATTTACCATCCTGATCAAGAACTCCATCCAC
TACCCCTAAGTTCCACTTCAGCAAGGGCAACATGCCGACAGGACCGACGGCTACCTGAAGAGATGTAC
CTTCCACGAGGCCAGCGACCTGACTGCCCTATCTCAAGCTGGCTCATCGTGGAGAAGGCCGGCG

AGTCCTCACAGAGCTGGCCCACAAGGGCGCGTGATCGCGTGATCATCAATTGGGATTGCGACCTG
GACCTGCCTGCCTCCGAGTGCATGCCAAGTACTCCTCAGAAGGCTGGATCCAAGCACGTGCCGC
CTCCTCCGGCTACAACCTCAGATTCGCCAAGTACTACAAGATCAACGGCACAACCACCAGGACACTGA
TCAAGGCCTACGGCATCAGAATCGATGTGATCGTCACGCCAGGCCAGGCCAGGTTCTCCCTGATCCCC
ACCATCATCAATCTGCCACCGCCCTGACCAGCGTGGCGTGGATCCTTCTGTGTGACTGGATCCT
GCTGACCTTCATGAACAAGAATAAGGTGTACTCCCACAAGAAGTCGATAAGGTGTGACCCCTAGCC
ACCCCAGCGGCAGCTGGCCTGTGACCCCTGGCTAGAGTGCTGGGCCAGGCCAGGCCAGGCCAGGACAT
AGGTCCGAGGATCAGCACCCAGCCCTCCAGCGGCCAGGAAGGACAGCAGGGCGCTGAGTGTGGCC
CGCTTCCCTCCTCTGAGGCCCTGTCCTATCAGGCCCTAGCGAGCAGATGGTGGATACACCGCCA
GCGAGCCTGCCAGGCCTACACCTACCGATCCAAGGGCTGGCCAGCTGTACCCCTACGATGTG
CCCGATTACGCCTGA

>hp2x2wt_aa

MAAAQPKYPAGATARRLARGCWSALWDYETPKVIVVRNRLGVLYRAVQLLILLYFVWYVFIVQKSYQ
ESETGPESSIITVKKGITTSEHKVWDVEEYVKPPEGGSVFSIITRVEATHSQTQGTCPESIRVHNATC
LSDADCVAGELDMLGNGLRTGRCPVYYQGPSKTCEVFGWPVEDASVSQFLGTMAPNFTILIKNSIH
YPKFHFSGNIADRTDGYLKRCTFHEASDLYCPIFKLGFiveKAGESFTELAHKGGVIGVIINWDCDL
DLPASECNPKYSFRRLDPKHVPASSGYNFRFAKYKINGTTTRTLIKAYGIRIDVIVHGQAGKFSLIP
TIINLATALTSGVGSSLCDWILLTFMNKNKVYSHKKFDKVCTPSHPSWPVTLARVLGQAPPEPGH
RSEDQHPSPPSGQEGQQGAECGPAFPPLRPCPISAPSEQMVDTPASEPAQASTPTDPKGLAQLYPYDV
PDYA*

>hp2x3wt_nts

ATGAACTGCATCTCCGACTTCTTACCTACGAGACCACCAAGTCCGTGGTGGTAAGAGACTGGACAAT
CGGCATCATCAACAGGGTGGTGCAGCTGCTGATCATCTCCTACTTCGTGGCTGGTGTTCCTGCACG
AGAAGGCCTACCAGGTGAGGGATACCGCCATCGAGTCCTCCGTGGTACAAAGGTGAAGGGCAGCGGC
CTGTACGCCAATAGGGTCATGGACGTGTCCGACTACGTGACCCCTCCCCAGGGCACCTCCGTGTTGT
GATCATCACCAAGATGATCGTACAGAGAATCAGATGCAGGGCTTCTGTCCCGAGTCCGAGGAGAAGT
ACAGGTGCGTGTCCGACTCCAGTGCAGGCCAGAGAGACTGCCGGAGGAGGAATCCTGACCGGCAGG
TGCCTGAATTACAGCAGCGTGCTGAGGACCTGTGAGATCCAGGGCTGGTGTCTACCGAGGTGGACAC
AGTGGAGACCCCCATCATGATGGAGGCCAGAATTTCACAATCTTCAAGAACCTCCATCAGATTCC
CCCTGTTAACTTGAGAAGGGCAACCTGCTGCCTAACCTGACCGCCAGAGATATGAAGACCTGTAGA
TTCCACCCCTGATAAGGATCCCTCTGCCCATCCTGAGAGTGGCGATGTGGTAAGTCGCCGCCA
GGACTTTGCCAAGCTGCCAGAACCGCCGGCGTGGCATCAAGATCGCTGGGTGCGACCTGG
ATAAGGCCTGGGATCAGTGTATCCCTAAGTACTCCTTACCAAGACTGGATAGCGTGTCCGAGAAGTCC
TCCGTGAGCCCTGGCTACAATTAGGTTGCCAAGTACTACAAGATGGAGAATGGCTCCGAGTACAG
GACCCGTGAAGGCCCTTGGCATCAGATTTGATGTGCTGGTACGGCAATGCCGGCAAGTTCAATA
TCATCCCTACCATCATCAGCAGCGTGGCCGCTTCACATCCGTGGCGTGGCACCGTGTGCGAC
ATCATCCTGCTGAATTCTGAAGGGCGCCGATCAGTACAAGGCCAAGAAGTTGAGGAGGTGAACGA
GACAACCCCTGAAGATGCCGCCCTGACCAACCCGTGTACCCAGCGATCAGACCACAGCCAGAAC
AGAGCACCGATAGCGGCCCTTCCATCGGCCACTACCCCTACGATGTGCCTGATTACGCCTGA

>hP2X3WT_aa

MNCISDFFTYETTKSVVVKSWTIGIINRVVQLLIISYFVGWVFLHEKAYQVRDTAIESVVTKVKSGSLYANRVMVDVSDYVTPPQGTSVFVIITKMIVTENMQGFCPESEEKYRCVSDSQCGPERLPGGILTGRCVNYSSVLRTCEIQGWCPTEVDTVETPIMMEAENFTIFIKNSIRFPLFNFEKGPNLLPNTARDMKTCRFHPDKDPFCPILRGVGVFKAGQDFAKLARTGGVLGIKIGWVCDLDKAWDQCIPKYSFTRLDSVSEKS SVSPGYNFRFAKYYKMENGSEYRTLKLAFGIRFDVLVYGNAGKFNIPTIISSSVAFTSVGVTLCDIILLNFLKGADQYKAKKFEEVNETTLKIAALTNPVYPSDQTTAEKQSTDGAFSIGHYPYDVPDYA*

>hP2X4WT_nts

ATGGCCGGATGCTGCGCTGCTCTGCCGTTCTGAGTACGACACCCCACGCATTGTGCTCATTAGGTCCCGCAAGGTGGGCTCATGAACAGAGCTGTGCAGCTCCTGATTCTCGCTTACGTGATCGGATGGGTGTCGTGTGGAGAAGGGATAACCAGGAGACCGACTCCGTGGTGTCTAGCGTGACCACAAAGGTGAAGGGAGTGCTGTGACCAACACATCTAACGCTCGGTTCAGAATTGGGACGTGGCTGACTACGTGATCCCCGCTCAGGAGGAACTCTCTGTTGTGATGACAAACGTGATTCTCACCATGAACCAAGACCCAGGGCTCTGCCCCGAGATCCCTGACGCCACACAGTGTGCAAGTCTGACGCTTCTGCACAGCCGGTCCGCCGGCACCCACTCTAACGGGGTGTCCACCAGGAGATCGTGGCTTCAACGGCAGCGTTAACGACATGCGAGGTGGCTGCTGGTGCCTAGTGGAGGACGACACCCACGTGCCTCAGCCAGCTCCTCAAGGCCGCTGAGAACATTCAACTCCTGCCAACATCACCACAAACCTACCTCAAGTCTGCATTACGACGCCAAGACCGACCCCTTCTGCCCTATTTCAGACTCGGCAAGATTGTGGAAGACGCCGGCACTCTTCCAGGACATGCCGTGGAGGGCGGAATTATGGGAATCCAGGTGAACGGACTGCAACCTGGACCGCGCCGCCTCCCTGTGCCCTCCCTAGATACTCCTCAGGCCCTGGACACACGCGACGTGGACACAACGTCGATCCCGATACAACCTCCGGTTCGCTAACGTAAGTACTACAGAGACCTCGCTGGAAACGAGCAAGCAGCACACTGATTAAGGCTTACGGAATTAGATTGACATTATTGTGTTGGAAAGGCCGGAAAGTTGACATCCTGACATTTCATCCCTACAATGATTAACATCGGGTCCGGCTGCCCTCTGGCATGGCTACAGTGTGCTGCGACATTATTGTGCTGACTGCATGAAGAAGCGGCTGTACTACCGCGAGAAGAAGTACAAGTACGTGGAGGACTACGAGCAGGGGCTCGCCTCTGAACCTGACCAGTACCCCTACGATGTGCCTGATTACGCCCTGA

>hP2X4WT_aa

MAGCCAALAAFLFEYDTPRIVLIRS RKVGLMNRAVQLLILAYVIGWVFWEKGYQETDSVVSSVTTKVKGVAVTNTSKLGFRIVDADYVIPAQEENS FVMTNVILTMNOTQGLCPEIPDATTVCKSDASCTAGSAGTHSNGVSTGRCAVNGSVKTCEVAAWCPVEDDTHVPQPAFLKAAENFTLLVKNNIWYPKFNF SKRNILPNITTLYKSCIYDAKTDPCPIFRLGKIVENAGHSFQDMAVEGGIMGIQVNWDCNLDRAASLCLPRYSFRLLDTRDVEHNVSPGYNFRFAKYYRDLAGNEQRTLIKAYGIRFDIIVFGKAGKFDIIPMINIGSGLALLGMATVLCDIIVLYCMKKRLYYREKKYKYVEDYEQGLASELDQYPYDVPDYA*

>hP2X5WT_nts

ATGGGCCAGGCCGGATGCAAGGGCTGTGCCTGTCCTGTTGATTACAAGACCGAGAAGTACGTGATGCCAAGAACAAAGAAGGTGGGCTGCTGTACAGACTGCTGCAGGCCAGCATCCTGCCCTACCTGGTGGTGTGGTGTCTGATCAAGAAGGGCTACCAGGACGTGGACACATCCCTGCAGTCCGCCGTGATCACAAGGTGAAGGGCGTGGCCTTACCAACACCTCCGATCTGGCCAGAGGATCTGGACGTGGCCGATTA CGTGATCCCTGCCAGGGCGAGAACGTGTTCTTGTGGTACAAACCTGATCGTGCAGCACCTAACATCAGAGACAGAATGTGTGCCCGAGAACGAGGGCATCCCCGACGGCGTTGCAGCAAGGATAGCGACTGTCACGCCGGCGAGGCCGTGACAGCCGGAAACGGAGTGAAGACCGGCAGATGCCCTGAGAAGAGAGAACCTGGC

CAGAGGCACCTGTGAGATCTTGCCTGGTGCCCTGGAGACAAGCTCCAGGCCTGAGGAGCCTTCC
TGAAGGAGGCCGAGGACTTCACCATCTTCATCAAGAACATCACATCAGGTTCCCTAAGTTAATTAGC
AAGTCCAACGTGATGGATGTGAAGGATAGAAGCTCCTGAAGAGCTGTCACTCGGCCCAAGAACATCA
CTACTGTCTATCTCAGGCTGGCTCCGTGATCAGGTGGGCCGGCAGCGACTTCCAGGACATGCC
TGGAGGGCGCGTGATCGGCATCAATATCGAGTGGAACTGCGATCTGGACAAGGCCGCTCCGAGTGT
CACCCCCACTACTCCTTAGCAGACTGGACAATAAGCTGCTCAAGTCCGTGAGCAGCGCTACAATTT
CAGATTGCCAGATACTACAGAGACGCCGCCGGCTGGAGTTAGAACACTGATGAAGGCCAACGGCA
TCAGGTTCGATGTGATGGTGAACGGCAAGGCCGGCAAGTTCTCCATCATCCCTACAATCATCAACGTG
GGCAGCGCGTGGCCCTGATGGCGCTGGAGCTTCTGTGACCTGGTGATCTACCTGATCAA
GAAAAGGGAGTTCTACAGGGATAAGAACAGTACGAGGAGGTGAGGGCCTGGAGGACTCCAGCCAGGAGG
CCGAGGATGAGGCCTCCGGCTGGACTGTCCGAGCAGCTGACCTCCGCCCTGGCCTGCTGGATG
CCCGAGCAGCAGGAGCTGCAGGAGCCCTGAGGCCAAGAGGGCAGCAGCAGCCAGAACAGGCAATGG
CTCCGTGTGTCCTCAGCTGCTGGAGCCTCACAGGAGCACATACCCTACGACGTGCCTGATTACGCCT
GA

>hP2X5WT_aa

MGQAGCKGLCLSLFDYKTEKYVIAKNKKVGLLYRLLQASILAYLVVVVFlikGYQDVDTSLQSAVIT
KVKGVAFTNTSDLQRIWDVADYVIPAQGENVFFVVTNLIVTPNQRQNVCAENEGIPDGACSKDSDCH
AGEAVTAGNGVKTRGRCLRRENLARGTCEIFAWCPLETSSRPEEPFLKEAEDFTIFIKNHIRFPKFNF
KSNVMDVKDRSFLKSCHFGPKNHCPIFRLGSVIRWAGSDFQDIALEGGVIGINIEWNCDLDKAASEC
HPHYSFSRLDNKLSKVSSGYNFRFARYYRDAAGVEFRTLMKAYGIRFDVMVNGKAGKFSIIPTIINV
GSGVALMGAGAFFCDLVLILYLIKREFYRDKKYEEVRGLEDSQEAEDEASGLGLSEQLTSGPGLGM
PEQQELQEPPEAKRGSSSQKGNGSVCQLLEPHRSTYPYDVPDYA*

>hP2X6WT_nts

ATGTGCCCCCAGCTGGCCGGAGCCGGAAGCATGGATCCCCTGGGCCACCACAGGCTGGGACTGCT
GGATTACAAGACAGAGAAGTACGTGATGACAAGAAACTGGAGGGTGGCGCCCTGCAGAGGCTGCTGC
AGTTCGGCATCGTGGTGTACGTGGTGGCTGGCCCTGCTGCCAAGAACGGCTACCAGGAGAGGGAC
CTGGAGCCCCAGTTCTCCATCATCACAAAGCTGAAGGGCGTGAGCGTGACCCAGATCAAGGAGCTGG
CAACAGGCTGTGGACGTGGCGACTTGTGAAGCCCCCTCAGGGCGAGAACGTGTTTCCTGGTGA
CCAACCTCCTGGTGACACCTGCCAGGTGCAGGGCAGATGCCCTGAGCACCCCTCCGTGCCTCTGGCC
AACTGCTGGTGGACGAGGATTGCCCGAGGGCGAGGGCGAACCCACTCTCACGGCGTGAAGACCGG
CCAGTGTGGTGTCAATGGCACCCACAGAACCTGTGAGATCTGGCCTGGTGGCCCGTGGAGTCCG
GCGTGGTGCCTAGCAGGCCTCTGCTGGCCAGGCCAGAACCTCACACTGTTCATCAAGAACACAGTG
ACCTTTCCAAGTTAACCTCCAAGAGCAACGCCCTGGAGACATGGATCCCACATACTTTAACGA
CTGTAGGTACGAGCCCCAGTTCCCTTAAGTGTGCTGTTCAGAACATGGCACCTGGTGGCCAAGG
CCGGCGGAACATTGAGGACCTGCCCTGCTGGCGGCTCCGTTGAATCAGAGTGCAGTGGACTGC
GATCTGGATACAGGCAGCGCTGCTGGCCCACTACAGCTTCCAGCTGCAGGAGAACGTCTACAA
TTTTAGGACAGCCACCCACTGGTGGAGCAGCCTGGCGTGGAGGCCAGGACACTGCTGAAGCTGTACG
GCATCAGATTGACATCCTGGTGACAGGCCAGGCCAGCAAGTCCGCTGATCCCTACCGCGTGACA
CTGGGCACCGCGCTGCTGGCTGGCGTTGTGACCTTTCTGCGATCTGCTGCTGTACGTGGA
CAGAGAGGCCACTTCACTGGAGGACCAAGTACGAGGAGGCCAAGGCCCAAGGCCACCGCTAATA
GCGTGTGGAGGGAGCTGCCCTGGCCTCCAGGCTAGACTGCCAGTGCCTGAGGAGGAGCAGCGCC

CCTGCCCTACAGCCACCGCTGCTGGAAGCCAGACACAGACCCCCGGCTGGCCTGCCCTCTGA
TACACACCTGCCTACACACTCCGGCTCCCTGTACCCTACGACGTGCCTGACTACGCCTGA

>hP2X6WT_aa

MCPQLAGAGSMGSPGATTGWGLDYKTEKYVMTRNWRVGAHQRLQFGIVVVVVGWALLAKKGYQERD
LEPQFSIITKLKGVSVTQIKELGNRLWDVADFVKPPQGENVFFLVTNFLVTPAQVQGRCPHEPSVPLA
NCWVDEDCEPEGEGGTHSHGVKTGQCVVFNGTHRTEIWSWCPVESGVVPSRPLLAQAOQNFTLFIKNTV
TFSKFNFSKSNALETWDPTYFKHCRYEPQFSPYCPVFRIGDLVAKAGGTLEDALLGGSVGIRVHWDC
DLDTGDSGCWPHYSFQLQEKSYNFRATWWEQPGVEARTLLKLYGIRFDILVTGQAGKFGLIPTAVT
LGTGAAWLGVVTFFCDLLLLYVDREAHFYWRTKYEEAKAPKATANSVWRELALASQARLAECLRRSSA
PAPTATAAGSQTQTPGPCPSSDTHLPTHSGSLYPYDVPDYA*

>hP2X7WT_nts

ATGCCTGCCTGCTGTAGCTGTTCCGATGTGTTCACTACGAGACAAATAAGGTGACAAGGATCCAGAG
CATGAATTACGGCACCATCAAGTGGTTCTTCACGTGATCATCTTCAGCTACGTGTGTTGCCCTGG
TGAGCGATAAGCTGTACCAAGAGGAAGGAGCCTGTGATCAGCAGCGTGCACACAAAGGTGAAGGGCATHC
GCCGAGGTGAAGGAGGAGATCGTGGAGAACGGCGTAAGAAGCTGGTGACAGCGTGTGTTGATACCGC
CGATTACACATTCCCCCTGCAGGGCAACAGCTTCTCGTGTGACAAAATTCTCTGAAGACAGAGGGCC
AGGAGCAGAGACTGTGTCCTGAGTACCCCTACAAGAAGGACCTGTGCAGCAGCGACAGGGCTGTAAG
AAGGGCTGGATGGACCCCTCAGAGCAAGGGCATCCAGACCGGCAGGTGTGTTGACAGAGGGCAACCA
GAAGACATGCGAGGTGAGCGCCTGGTGCCTATCGAGGCCGTGGAGGAGGCCAGGCCAGCTCTGC
TGAACCTCCGCGAGAAATTACCGTGCTGATCAAGAACATATCGACTTCCCTGGCCACAATTACACC
ACAAGAAATATCCTGCCTGGCCTGAACATCACATGCACATTCAAGACCCAGAACCCCCAGTGCCT
TATCTTAGACTGGCGACATCTCAGGGAGACCGCGACAATTCAAGCGACGTGGCCATCCAGGGCG
GCATCATGGCATCGAGATCTACTGGATTGTAATCTGGACAGATGTTCCACCACTGTAGACCCAAG
TACTCCTTAGAGGCTGGATGACAAGACCACAAACGTGAGCCTGTACCCCTGGCTACAACATTAGATA
CGCCAAGTACTACAAGGAGAACACAGTGGAGAAGAGGACACTGATCAAGGTGTTGGCATCAGGTTG
ACATCCTGGTGTTCGGCACCGCGCAAGTTGATATCATCCAGCTGGTGGTACATGGCAGCACC
CTGTCCTACTTGGCCTGGCCCGTGTTCATCGATTTCTGATCGACACCTACAGCAGCAACTGTTG
TAGGAGCCACATCTACCCCTGGTCAAGTGTGTCAGCCCTGCGTGGTGAATGAGTACTACTACAGGA
AGAAGTGTGAGAGCATCGTGGAGCCAAAGCCCACACTGAAGTACGTGAGCTCGTGGACGAGTCCCAC
ATCAGAATGGTAATCAGCAGCTGCTGGCAGGAGCCTGCAGGATGTGAAGGCCAGGAGGTGCCAG
GCCTGCCATGGACTTACCGATCTGTCCAGGCTGCCCTGGCCCTGCACGATACACCTCTATCCCTG
GCCAGCCCAGGAGATCCAGCTGCTGAGAAAGGAGGCCACACCCAGAACAGCAGAGACAGCCCTGTGTTG
TGCCAGTGGCAGCTGCCTGCCCTCCAGCTGCCCTGAGTCCCACAGGTGTGCTGGAGGAGCTGTGCTG
TAGAAAGAAGCCGGCGCCTGCATCACCAACCTCCAGCTGTTAGGAAGCTGGTGTGTCAGGCACG
TGCTGCAGTTCTGCTGCTGTACCAAGGAGCCCTGCTGGCCCTGGATGTGGACTCCACCAATAGCAGG
CTGAGGCAGTGCCTACAGGTGTTACGCCACCTGGAGATTGGCTCCAGGACATGGCAGCTTCG
CATCCTGCCCTCTGTTAGGTGGAGAATCAGAAAGGAGTTCTAAAGAGCGAGGGCCAGTACAGCG
GCTTCAAGAGCCCTACTACCCCTACGACGTGCCTGATTACGCCTGA

>hP2X7WT_aa

MPACCSCSDVFQYETNKVTRIQLSMNYGTIKWFFHVIIFSYVCFALVSDKLYQRKEPVISSVHTKVKGIAEVKEEIVENGKKLVHSVFDTADYTFPLQGNSFFVMTNFLKTEGQEQRRLCPEYPTRRTLSSDRGCKKGWMDPQSKGIQTGRCVVYEGNQKTCEVSAWCPIEAVEEAPRALLNSAENFTVLIKNNIDFPGHNYTTRNILPGLNITCTFHKTQNPQCPIFRLGDIFRETGDNFSDVAIQGGIMGIEIYWDCNLDRWFHHCRPKYSFRLDDDKTTNVSLYPGYNFRYAKYYKENNEKRTLIKVFGIRFDILVFGTGGKFDIIQLVVYIGSTLSYFGLAAVFIDFLIDTYSSNCCRSHIYPWCKCCQPCVVNEYYYRKCESIVEPKPTLKYSFVDESHIRMVNQQLLGRSLQDVKGQEVPBPAMDFTDLSRLPLALHDTPIPQPEEIQLLRKEATPRSRDSPVWCQCGSCLPSQLPESHRCLLEELCCRKKPGACITTSELFRKLVLSRHVLQFLLLQEPPLLALDVDSTNSRLRHCAHYRCYATWRFGSQDMADFAILPSCCRWRIRKEFPKSEGQYSGFKSPYYPYDVPDYA*

B. Nucleotide and peptide sequences for EE, FLAG, and HA C-terminus epitope tags.

Tag	Nucleotide sequence (5' – 3')	Amino acid sequence
EE	GAATATATGCCGATGGAA	EYMPME
FLAG	GACTACAAGGACGACGACGACAAG	DYKDDDDK
HA	TACCCCTACGACGTGCCTGATTACGCC	YPYDVPDYA

Appendix 2

Clustal-Omega Multiple Sequence Alignment of rat P2X2 and human P2X1-7 receptors. Residues in bold are the key lysines in positions K69 and K308 (rP2X2 numbering) that were mutated to generate hP2X1-7 dead receptor tools. Residues highlighted in grey are conserved charged and polar amino acids K69, K71, Q108, T184, K188, N288, R290, R304, and K308 (rP2X2 numbering), and underlined residues correspond to strongly conserved amino acid properties S65 and T336 (rP2X2 numbering). These particular residues were chosen based on the ATP-binding scrutiny performed by site-directed mutagenesis and electrophysiology techniques (Jiang et al., 2000).

hP2X1WT	GLYE---EKNLSPGFNFRFARHFVE-NGTNYRHLF KVFGIRFDILVDGKAGKFDIIPMTMT	333
hP2X2WT	RLDPKH--VPASSGYNFRFAKYYKINGTT-TRTLI KAYGIRIDVIVHGQAGKFSLIPTII	343
rP2X2WT	RLDPKY--DPASSGYNFRFAKYYKINGTTTTRTLI KAYGIRIDVIVHGQAGKFSLIPTII	332
hP2X3WT	RLDSVSEKSSVSPGYNFRFAKYYKMENGSEYRTLL KAFGIRFDVLVYGNAGKFNIIPTI	323
hP2X4WT	RLDTRDVEHNVSPGYNFRFAKYYRDLAGNEQRTLI KAYGIRFDIIVFGKAGKFDIIPMI	337
hP2X5WT	RLDNK-LSKS VSSGYNFRFARYYRDAAGVEFRTLM KAYGIRFDVMVNGKAGKFSIIPTI	338
hP2X6WT	LQE-----KSYNFRTATHWWEQPGVEARTLL KLYGIRFDILVTGQAGKFGLIPTAV	339
hP2X7WT	RLDDKTTNVSLYPGYNFRYAKYYKE-NNVEKRTLI KVFGIRFDILVFGTGGKFDIQLVV	335
	. :*** * : : * * :* :* :* * . ***. :*	
hP2X1WT	TIGSGIGIFGVATVLC DLLLHIL-----PKRHYYKQKKFKYAEDMG	375
hP2X2WT	NLATALTSGVGVSFLCDWILLTFM-----NKNKVYSHKKFDKVCTPS	385
rP2X2WT	NLATALT SIGVGVSFLCDWILLTFM -----NKNKLYSHKKFDKVRTPK	374
hP2X3WT	SSVAAFTSVGVTLC DIILNFL-----KGADQYKAKKFEEVNETT	365
hP2X4WT	NIGSGLALLGMATVLC DIIVLYCM-----KKRLYYREKKYKYVEDYE	379
hP2X5WT	NVGS GVALMGAGAFFCDLVLIYLI-----KKREFYRDKYEEVRGLE	380
hP2X6WT	TLGTGAALGVVTFFCD LLLL VD-----REAHFYWR TKYEEAKAPK	381
hP2X7WT	YIGSTLSYFGLAAVFIDLITYSSNCCRSHIY PWCKCCQPCVVNEYYYRKCESIVEPK	395
	* . * : : * : :	
hP2X1WT	PGAAERDLA-ATSSTLGLQ-----ENMRTS----	399
hP2X2WT	HPSG SWPVTLAR--V-----LGQAPPEP	406
rP2X2WT	HPSS RWPVTLAL--V-----LGQIPPPP	395
hP2X3WT	LKIAA-----L-----T--NPVYP	377
hP2X4WT	QGLASELDQ-----	388
hP2X5WT	DSSQEAEDE-A--SGLGLS-----EQLTSGPGLL	406
hP2X6WT	ATANSVWRELALASQARLA-----ECLRRSSA--	408
hP2X7WT	PTLK YVSFV--DESHIRMVNQQLLGRSLQDVKGQEVPRPAMDF TDLSRLPLALHDTPPIP	453
hP2X1WT	-----	399
hP2X2WT	GHRSEDQHPSPPSG--QEGQQG--A-ECGPAFPPLRPCPISAPSEQMVDT PASE-----	455
rP2X2WT	SHYSQDQPPSPPSG--EGPTLGEA-ELPLAVQSPRPCSISALTEQVVDTLGQHM QRP	451
hP2X3WT	SDQTTAEKQSTD SG-----AFSIGH-----	397
hP2X4WT	-----	388
hP2X5WT	GMPEQQELQEPPEAKRGSSSQKGNGSV-CPQL-LEP---HRST-----	444
hP2X6WT	-----PAP TATAAGSQT QTPGWP-CPSS-DTHLP THSGSL-----	441
hP2X7WT	GQPEEIQLLRKEA---TPRS RDSPVWCQCGSCLPSQLPESHR CLEELCCR K-----	501
hP2X1WT	-----	399
hP2X2WT	-----PAQASTPTDP-----KGLAQL-----	471
rP2X2WT	PVPEPSQQDSTSTDP-----KGLAQL-----	472
hP2X3WT	-----	397
hP2X4WT	-----	388
hP2X5WT	-----	444
hP2X6WT	-----	441
hP2X7WT	---KPGACIT TSELFRKLVL SRHV LQFILL YQEPLL ALDVD STNS RLRCAYRCY ATWRF	558
hP2X1WT	-----	399
hP2X2WT	-----	471
rP2X2WT	-----	472
hP2X3WT	-----	397
hP2X4WT	-----	388
hP2X5WT	-----	444
hP2X6WT	-----	441
hP2X7WT	GSQDMADFAILPSCCRWRIRKEFPKSEGQYSGFKSPY	595